



Libraries and Learning Services

University of Auckland Research Repository, ResearchSpace

Copyright Statement

The digital copy of this thesis is protected by the Copyright Act 1994 (New Zealand).

This thesis may be consulted by you, provided you comply with the provisions of the Act and the following conditions of use:

- Any use you make of these documents or images must be for research or private study purposes only, and you may not make them available to any other person.
- Authors control the copyright of their thesis. You will recognize the author's right to be identified as the author of this thesis, and due acknowledgement will be made to the author where appropriate.
- You will obtain the author's permission before publishing any material from their thesis.

General copyright and disclaimer

In addition to the above conditions, authors give their consent for the digital copy of their work to be used subject to the conditions specified on the [Library Thesis Consent Form](#) and [Deposit Licence](#).

Towards an Effective EMG-based Neuromuscular Interface for Human-robot Interaction

Ran Tao

A thesis submitted in fulfilment of the requirements for the degree of Doctor of Philosophy in
Mechanical Engineering, The University of Auckland, 2016

Abstract

In recent years, the requirements of individual assistant systems for elderly and disabled people are daily increasing, as well as the function expansion of prosthetic control, military, residential and commercial robots. In this case, human-robot interactions have become a popular research area. Since these robots are directly interacted with the users, there are several challenges in the design and control of such human-robot interaction technology. Electromyography (EMG) signal is the electrical signals of the human body, which contains a wealth of information on human action and can be used to determine the user's intent. The purpose of this thesis is to develop an EMG-based human-robot interface, which can identify the body's response by signal processing and model calculations, and can also transform the response into the motion control instructions, and control the robot to complete the body movement intentions.

The existing physiological models have provided a continuous motion prediction method. This method of the 'simplified musculoskeletal model' took the mechanical revolute instead of human joint, the straight line instead of skeleton, and the straight segment between the muscle starting point and adhesion point instead of the muscle. During the complex motion of human body, the prediction accuracy of this model is greatly reduced since it is not close to the human actual physiological structure. Also, it cannot be used for the calculation when the muscular force line crosses the joint center. Currently, the studies of the impact of physiological model parameters to the sensitivity of interface have three problems: the amount of assessed parameters was few, the evaluation method was single, and the results of different researches had disagreement. Especially, the analysis of overall parameters in the neuromuscular model was less. The existing sensitivity evaluation was focused on the impact of musculotendon parameters sensitivity to the model.

Through two cases study of elbow flexion/extension and forearm pronation/supination, this thesis overviews the new progresses that aim to address the existing gaps in this research field. The elbow joint was selected to implement a new method of muscle modeling, which could improve the accuracy of model during the complex motion of the elbow, while ensuring the real-time processing of the interface. The forearm rotation was chosen because of the weak EMG of forearm muscles, the short moving time and small changes in muscle length. The interface for forearm rotation has its particularity.

A new EMG-driven elbow physiological model has been developed to predict the elbow flexion and extension. In the process of modeling, this thesis made assumptions based on the physiological properties of muscle. Through the elbow experiments from a plurality of subjects and a variety of

movements, the model's ability of accurately predicting different moving trajectories was verified. The model was also implemented and verified by a single degree of freedom (DOF) exoskeleton.

A new EMG-driven physiological model for forearm pronation/supination has been established. It can predict the forearm continuous rotation movement by the EMG activations from the superficial part of three muscles. The model contained a unique physiology musculoskeletal model. The experiments from four subjects showed the effectiveness of this method. The establishment of this forearm physiological model has opened up a new way for the prediction of complex joint system with small amplitude motions.

A new sensitivity assessment method of model parameters, three-step layered approach, has been established. By using this method, this thesis analyzed the characteristics of the model parameters. A relatively small subset of the parameters was generated for parameter tuning. This method provided a new way of thinking for the parameters sensitivity analysis. The purpose of parameter tuning is to make the model can precisely match every subject. This thesis programmed two kinds of evolutionary algorithm - Differential Evolution (DE) and Genetic Algorithm (GA), and experimentally compared their performances in three aspects. Because of the high accuracy and fast convergence capability, DE can be used for fast online tuning. And GA can only be used in offline tuning.

A controller based on the fusion of EMG and force information has been proposed to validate the proposed models in real time control environment. A 5-DOF upper limb exoskeleton was developed by the Medical and Rehabilitation Research Group at the University of Auckland, the exoskeleton was used to evaluate the effectiveness of the EMG based controller (EBC). The results showed that the dynamic auxiliary effect of the exoskeleton is obvious (the decrease of muscle activation could be ensured above 52% when the assistance works), and the physiological model based EBC can adapt to different individuals. This also showed the effectiveness and online adaptability of the EMG-based Neuromuscular Interface proposed by this thesis.

Acknowledgements

This thesis would not have been completed without the support and encouragement that I have received from all the people around over these years.

Firstly, I would like to express my sincere appreciation and thanks to my supervisor Prof. Shane Xie, who gave me a chance to start my PhD study and supported me all the time. I am grateful for you providing me with the freedom to explore my own ideas, guiding me the path, and helping me whenever I got the difficulties. Thanks for all the comments, encouragements, and helps you offered not only in my study, but also for my daily life.

I wish to acknowledge my co-supervisor Dr. Yanxin Zhang for your valuable input. You offered me some new ideas and providing me with a fresh perspective in my research.

I would also like to thank the people who have helped me with my research. James Pau offered me a start of my study, Ho Shing Lo helped me to make my research more practical, and Mingming Zhang assisted me a lot with my final paper writings. Also, to all the people in my research group, thanks for the comments and discussions between our research and thank you for being a pleasure to work with.

Lastly, to my family and friends, thank you for not disappointing me, but always supported and encouraged me to move on.

This study was not only a challenge, but also a very precious journey in my life. Thanks for all the people who accompanied me, and you are very dear to me.

This form is to accompany the submission of any PhD that contains published or unpublished co-authored work. **Please include one copy of this form for each co-authored work.** Completed forms should be included in all copies of your thesis submitted for examination and library deposit (including digital deposit), following your thesis Acknowledgements. Co-authored works may be included in a thesis if the candidate has written all or the majority of the text and had their contribution confirmed by all co-authors as not less than 65%.

Please indicate the chapter/section/pages of this thesis that are extracted from a co-authored work and give the title and publication details or details of submission of the co-authored work.

Tao, R., Xie S. Q., and Zhang Y. X., "Review of EMG-based Neuromuscular Interface for Upper Limb Control", 19th International conference on Mechatronics and Machine Vision in Practice, Auckland, New Zealand, November 28-30 2012.

Content is the basis of Chapter 2.

Nature of contribution by PhD candidate	Performed review of the literature and analysis. Drafted and revised paper.
---	---

Extent of contribution by PhD candidate (%)	90
---	----


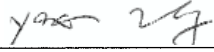
CO-AUTHORS

Name	Nature of Contribution
Shengquan (Shane) Xie	Manuscript revision
Yanxin Zhang	Manuscript revision

Certification by Co-Authors

The undersigned hereby certify that:

- ❖ the above statement correctly reflects the nature and extent of the PhD candidate's contribution to this work, and the nature of the contribution of each of the co-authors; and
- ❖ that the candidate wrote all or the majority of the text.

Name	Signature	Date
Shengquan (Shane) Xie		14/11/2016
Yanxin Zhang		14/11/2016

This form is to accompany the submission of any PhD that contains published or unpublished co-authored work. **Please include one copy of this form for each co-authored work.** Completed forms should be included in all copies of your thesis submitted for examination and library deposit (including digital deposit), following your thesis Acknowledgements. Co-authored works may be included in a thesis if the candidate has written all or the majority of the text and had their contribution confirmed by all co-authors as not less than 65%.

Please indicate the chapter/section/pages of this thesis that are extracted from a co-authored work and give the title and publication details or details of submission of the co-authored work.

R. Tao, S. Xie, Y. Zhang et al., "Review of EMG-based neuromuscular interfaces for rehabilitation: elbow joint as an example," International Journal of Biomechanics and Biomedical Robotics, vol. 2, no. 2, pp. 184-194, 2013.

Content is the basis of Chapter 2 and part of Chapter 1. It is the extension of the first review paper.

Nature of contribution by PhD candidate	Performed review and analysis. Drafted and revised paper.
Extent of contribution by PhD candidate (%)	95


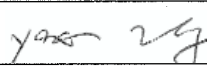
CO-AUTHORS

Name	Nature of Contribution
Shengquan (Shane) Xie	Manuscript revision
Yanxin Zhang	Manuscript revision

Certification by Co-Authors

The undersigned hereby certify that:

- ❖ the above statement correctly reflects the nature and extent of the PhD candidate's contribution to this work, and the nature of the contribution of each of the co-authors; and
- ❖ that the candidate wrote all or the majority of the text.

Name	Signature	Date
Shengquan (Shane) Xie		14/11/2016
Yanxin Zhang		14/11/2016

Co-Authorship Form

This form is to accompany the submission of any PhD that contains published or unpublished co-authored work. **Please include one copy of this form for each co-authored work.** Completed forms should be included in all copies of your thesis submitted for examination and library deposit (including digital deposit), following your thesis Acknowledgements. Co-authored works may be included in a thesis if the candidate has written all or the majority of the text and had their contribution confirmed by all co-authors as not less than 65%.

Please indicate the chapter/section/pages of this thesis that are extracted from a co-authored work and give the title and publication details or details of submission of the co-authored work.

Tao, R., Xie, S. Q., Zhang Y. X. and Pau, J., "sEMG-based Neural-musculoskeletal Model for Human-robot Interface", The 9th IEEE Conference on Industrial Electronics and Applications (ICIEA 2014), 2014, Hangzhou, China.

Content covers the initial model developments in Chapter 3 and one of the initial experimental result in Chapter 4

Nature of contribution by PhD candidate	Performed model development and data analysis. Drafted and revised paper.
Extent of contribution by PhD candidate (%)	85

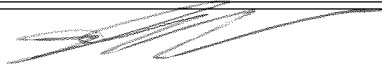
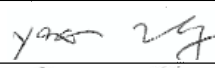
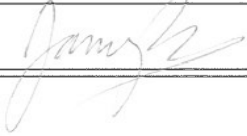
CO-AUTHORS

Name	Nature of Contribution
Shengquan (Shane) Xie	Manuscript revision
Yanxin Zhang	Manuscript revision
James W.L. Pau	Data collection and manuscript revision

Certification by Co-Authors

The undersigned hereby certify that:

- ❖ the above statement correctly reflects the nature and extent of the PhD candidate's contribution to this work, and the nature of the contribution of each of the co-authors; and
- ❖ that the candidate wrote all or the majority of the text.

Name	Signature	Date
Shengquan (Shane) Xie		14/11/2016
Yanxin Zhang		14/11/2016
James W.L. Pau		21/11/2016

Co-Authorship Form

This form is to accompany the submission of any PhD that contains published or unpublished co-authored work. **Please include one copy of this form for each co-authored work.** Completed forms should be included in all copies of your thesis submitted for examination and library deposit (including digital deposit), following your thesis Acknowledgements. Co-authored works may be included in a thesis if the candidate has written all or the majority of the text and had their contribution confirmed by all co-authors as not less than 65%.

Please indicate the chapter/section/pages of this thesis that are extracted from a co-authored work and give the title and publication details or details of submission of the co-authored work.

R. Tao, S. Xie, J. Pau, "A Study of EMG-based Neuromuscular Interface for Elbow Joint", the 7th International Conference on Intelligent Robotics and Application (ICIRA 2014), 2014, Guangzhou, China

It is a practical application of model in Chapter 3, achieves model real-time processing and wireless transferring.

Nature of contribution by PhD candidate	Performed model and software development, results analysis. Drafted paper.
Extent of contribution by PhD candidate (%)	70


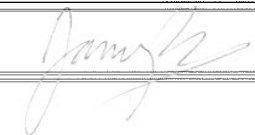
CO-AUTHORS

Name	Nature of Contribution
Shengquan (Shane) Xie	Manuscript revision
James W.L. Pau	Hardware development and data collection

Certification by Co-Authors

The undersigned hereby certify that:

- ❖ the above statement correctly reflects the nature and extent of the PhD candidate's contribution to this work, and the nature of the contribution of each of the co-authors; and
- ❖ that the candidate wrote all or the majority of the text.

Name	Signature	Date
Shengquan (Shane) Xie		14/11/2016
James W.L. Pau		21/11/2016

Co-Authorship Form

This form is to accompany the submission of any PhD that contains published or unpublished co-authored work. **Please include one copy of this form for each co-authored work.** Completed forms should be included in all copies of your thesis submitted for examination and library deposit (including digital deposit), following your thesis Acknowledgements. Co-authored works may be included in a thesis if the candidate has written all or the majority of the text and had their contribution confirmed by all co-authors as not less than 65%.

Please indicate the chapter/section/pages of this thesis that are extracted from a co-authored work and give the title and publication details or details of submission of the co-authored work.

"A new musculoskeletal model in predicting forearm pronation and supination for use in human-robot interaction" has been submitted to the Journal of Biomechanics, and is currently under review.

Content is the basis of Chapter 5.

Nature of contribution by PhD candidate	Performed model development, data collection and analysis. Drafted and revised paper.
Extent of contribution by PhD candidate (%)	95

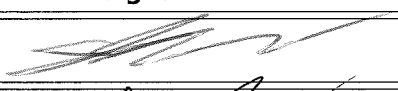
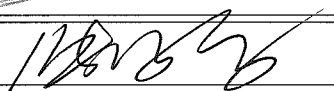
CO-AUTHORS

Name	Nature of Contribution
Shengquan (Shane) Xie	Manuscript revision
Mingming Zhang	Manuscript revision

Certification by Co-Authors

The undersigned hereby certify that:

- ❖ the above statement correctly reflects the nature and extent of the PhD candidate's contribution to this work, and the nature of the contribution of each of the co-authors; and
- ❖ that the candidate wrote all or the majority of the text.

Name	Signature	Date
Shengquan (Shane) Xie		14/11/2016
Mingming Zhang		14/11/2016

Contents

Chapter 1 Introduction	1
1.1 EMG-based Human-Robot Interface.....	1
1.1.1 Research Area.....	2
1.1.2 Challenges of the EMG-based Neuromusculoskeletal Interface.....	3
1.2 Electromyography (EMG).....	4
1.2.1 Advances of EMG.....	4
1.2.2 Characteristics of EMG-based Human-robot Interface.....	5
1.3 Upper Limb Exoskeleton.....	6
1.3.1 Advances of Upper Limb Exoskeleton.....	7
1.3.2 Current Limitations.....	8
1.4 Research Objectives.....	9
1.5 Thesis Outline and Contributions.....	11
1.6 Chapter Summary.....	12
Chapter 2 Literature Review	13
2.1 Input of Interface.....	13
2.1.1 Mechanical Movement of the Human Body.....	13
2.1.2 Voice of the Human Body.....	15
2.1.3 Electroencephalogram (EEG).....	15
2.1.4 Electromyography (EMG).....	16
2.2 Current Applications of EMG.....	17
2.3 EMG-based Neuromuscular Interface.....	22
2.4 Challenges.....	23
2.4.1 Quality of Signal Processing.....	23
2.4.2 Contradictions between Running Time and Number of Muscles.....	24
2.4.3 Accuracy of Model.....	26
2.4.4 Parameters Tuning and Individual Differences.....	26
2.4.5 Impact of Fatigue.....	27
2.5 Chapter Summary.....	27
Chapter 3 A Neuromusculoskeletal Model for the Elbow Joint	29
3.1 Background.....	29
3.2 Musculoskeletal Geometry Model.....	32

3.3	Musculotendon Model.....	38
3.4	Kinematic Model.....	41
3.5	Preliminary Verification of the Neuromuscular Elbow Interface.....	42
3.5.1	A Prototype of Elbow Neuromuscular Interface	43
3.5.2	Preliminary Verification of Elbow Neuromuscular Interface	45
3.6	Model Parameters.....	48
3.7	Chapter Summary.....	50
Chapter 4 Feasibility Analysis and Validation of the Elbow Model		52
4.1	Parameter Sensitivity.....	52
4.1.1	Background	52
4.1.2	Experimental Setup for Sensitivity Analysis.....	54
4.1.3	Sensitivity Analysis Method.....	54
4.1.4	Sensitivity Analysis Results	56
4.1.5	Discussion	60
4.2	The Elbow Physiological Model Validation	67
4.2.1	Experimental Setup for Model Validation.....	67
4.2.2	EMG Signal Processing and Muscle Activation	70
4.2.3	Model Validation.....	71
4.3	Chapter Summary.....	78
Chapter 5 A Neuromusculoskeletal Model for the Forearm Pronation and Supination.....		79
5.1	Physiological Structure of the Forearm Rotation	79
5.1.1	Physiological Skeleton Structure of the Forearm.....	80
5.1.2	Forearm Rotation Axis and Rotation Center of the Distal Radioulnar Joint.....	82
5.1.3	Forearm Muscles	83
5.2	Development of the Forearm Musculoskeletal Model	85
5.2.1	Assumptions of the Forearm Modeling.....	85
5.2.2	Musculoskeletal Model of Forearm Rotation.....	88
5.3	Model Validation.....	95
5.3.1	Test procedures.....	95
5.3.2	Results	95
5.3.3	Discussion	102
5.4	Chapter Summary.....	103
Chapter 6 A Neuromuscular Interface for Motion Prediction of the Upper Limb.....		104
6.1	Interface Design	104

6.2	Tuning Methods to Model Parameters	106
6.2.1	Genetic Algorithm (GA).....	107
6.2.2	Differential Evolution (DE).....	111
6.3	Chapter Summary	114
Chapter 7 A GUI Design to Facilitate the NI Validation		115
7.1	Introduction of a 5-DOF Upper Limb Exoskeleton.....	115
7.1.1	Range of Exoskeleton Joint Motion	117
7.1.2	Joint Alignment	117
7.1.3	Actuators and Sensors	118
7.1.4	Safety Features	118
7.2	System Architecture and Graphical User Interface	119
7.2.1	The Operating Procedures of the Interface.....	119
7.2.2	Graphical User Interface (GUI).....	119
7.3	Chapter Summary	125
Chapter 8 NI Validation through Exoskeleton Control.....		126
8.1	Control Strategies of the 5-DOF Exoskeleton.....	127
8.1.1	Overall Design of the Control System.....	127
8.1.2	EMG Based Controller (EBC).....	128
8.1.3	Force Based Controller (FBC).....	130
8.1.4	Motor Driver Settings.....	130
8.2	Validation of the Elbow Neuromuscular Interface.....	133
8.2.1	Experimental Setup	133
8.2.2	Experimental Results and Analysis	134
8.3	Chapter Summary	138
Chapter 9 Conclusions.....		140
9.1	Main Achievements and Contributions	140
9.2	Future Work	145
9.3	Chapter Summary	147
Appendix I.....		148
Appendix II		152
References		153

List of Figures

Figure 1.1: The concept of an EMG-based interface	2
Figure 1.2: EMG-based control mechanism of neuromuscular system	5
Figure 1.3: The MIT-MANUS end-effector rehabilitation robot [12]	7
Figure 1.4: ARMin rehabilitation device [11].....	7
Figure 1.5: CADEN-7 rehabilitation robot [13]	8
Figure 1.6: Armeo Spring rehabilitation robot [14]	8
Figure 2.1: Photos of real input technology for interface [34-36]	17
Figure 2.2: HALL(Hybrid Assistive Limb, HAL) system [42]	19
Figure 2.3: The University of Michigan rehabilitation robot [43].....	20
Figure 2.4: Prosthetic hand from Otto bock Company [44, 45]	21
Figure 2.5: Virtual joystick based on sEMG gesture recognition [49, 50]	21
Figure 2.6: The function of number of muscles and TET [70].	25
Figure 3.1: Flowchart of EMG-based neuromuscular interface	31
Figure 3.2: Simplified elbow model by Murray [98].....	33
Figure 3.3: Coordinate system of elbow joint model.....	34
Figure 3.4: musculoskeletal model of elbow joint.	35
Figure 3.5: Geometry of the musculoskeletal model	36
Figure 3.6: Musculotendon model [68]	40
Figure 3.7: Stages in hardware to create a linear envelope from raw EMG signals [102].	43
Figure 3.8: The neuromuscular interface hardware system [102].....	44
Figure 3.9: Single degree of freedom representation of the elbow joint [102].	45
Figure 3.10: Neuromuscular interface and single degree of freedom joint in a closed loop system.	45
Figure 3.11: Preliminary result of elbow single cycle flexion and extension	47
Figure 3.12: Preliminary result of elbow continues cycle flexion and extension	47
Figure 3.13: Preliminary result of elbow random movement	48
Figure 4.1: Model sensitivity evaluation methods	56
Figure 4.2: Single cycle flexion and extension movement angle with different parameter value.	58
Figure 4.3: The sensitivity of $Loptbi$	61
Figure 4.4: The sensitivity of $Lopttr$	61
Figure 4.5: The sensitivity of Hum	62
Figure 4.6: The sensitivity of $Cpassbi$	62
Figure 4.7: The changes of sensitivity of Ubi during NSQL test over time and parameter.	63
Figure 4.8: The sensitivity of Utr	63
Figure 4.9: The sensitivity of Rbi	64

Figure 4.10: The sensitivity of F_{maxbi} in NSQL test.....	65
Figure 4.11: (a) The sensitivity of m in NSQL test. (b) The sensitivity of L_{Arm} in NSQL test.....	65
Figure 4.12: Result of a single cycle test with RMSE of 4.42°	74
Figure 4.13: Result of a Continuous cycle full range test with RMSE of 12.97°	74
Figure 4.14: Result of a Continuous cycle half range test with RMSE of 12.71°	75
Figure 4.15: Result of a Continuous cycle increasing range test with RMSE of 9.86°	76
Figure 4.16: Result of a Random movement test with RMSE of 11.57°	76
Figure 5.1: The forearm skeleton.....	80
Figure 5.2: The forearm interosseous membrane.....	81
Figure 5.3: The axis of the forearm rotation [135-137]	83
Figure 5.4: Muscles for forearm pronation and supination.....	84
Figure 5.5: Definition of forearm rotation and the relative position of the radius and ulna	86
Figure 5.6: Measured skeleton.....	88
Figure 5.7: Coordinate system of forearm rotation model.....	88
Figure 5.8: The musculoskeletal model of supinator	89
Figure 5.9: The musculoskeletal model of pronator teres.....	90
Figure 5.10: The musculoskeletal model of pronator quadratus.....	92
Figure 5.11: Musculoskeletal geometry model of three muscles in neutral position.....	94
Figure 5.12: Musculoskeletal geometry model of three muscles in any position.....	94
Figure 5.13: Flowchart of model simulation for forearm rotation.....	96
Figure 5.14: The sEMG signal and activation of pronator teres (PT) in Sup-Pro	98
Figure 5.15: The sEMG signal and activation of PT with a 0.5kg weight in Sup-Pro.....	99
Figure 5.16: The sEMG signal and activation of biceps (Bi) in flexion-extension	99
Figure 5.17: (a) The changes of muscle length of PT, PQ and SUP (in Sup-Pro) . (b) The changes of moment arm of PT,PQ and SUP (in Sup-Pro)	100
Figure 5.18: A result of the basic Sup-Pro Test. (RMSE= 5.10°)	101
Figure 5.19: A result of the basic Sup-Pro Test.....	101
Figure 5.20: Result of the Forearm Continuous Cycles Test.	101
Figure 5.21 A result of the Random movement test.....	101
Figure 6.1 2-DOF interface of the elbow flexion/extension and forearm pronation/supination.....	105
Figure 6.2: The Flowchart of Genetic Algorithm	107
Figure 6.3: The optimal solution of 14 tunable parameters	110
Figure 6.4: The change of the optimal solution and the change of population mean	110
Figure 6.5: The flowchart of basic differential evolution algorithm.....	112
Figure 6.6: The optimal solution of 14 tunable parameters	113
Figure 6.7: The changes of the optimal solution.....	113
Figure 7.1: CAD model of the 5-DOF upper limb exoskeleton [148].....	116

Figure 7.2: The 5-DOF exoskeleton used by a healthy person [148].	116
Figure 7.3: The human-robot interface operating procedures.	120
Figure 7.4: The main interface of this GUI.	121
Figure 7.5: Signal Acquisition and Processing System interface.	122
Figure 7.6: Joint Angle Prediction System program	123
Figure 7.7: Joint Angle Prediction System interface	123
Figure 7.8: Physiological Parameters Tuning interface	124
Figure 7.9: EMG Based Controller Module (EBC) interface	125
Figure 8.1: Schematic diagram of the controller	129
Figure 8.2: Desired torque for Single cycle test.	131
Figure 8.3 Desired torque for Continuous cycles starting with a small amplitude that gradually increases test	131
Figure 8.4: Desired torque for Random movement test.	132
Figure 8.5 Desired torque for Continuous cycles test.	132
Figure 8.6: Desired torque for elbow flexion motion for Continuous cycles at half the range of capable motion	132
Figure 8.7: The flowchart of motor control calculation.	133
Figure 8.8: Single cycle test results (Channel 1) for elbow flexion motion with Subject A	135
Figure 8.9: Random movement test results (Channel 1) for elbow flexion motion with Subject A	135
Figure 8.10: Random movement test results (Channel 1) for elbow flexion motion with Subject B	136
Figure 8.11: Continuous cycles test results (Channel 1) for elbow flexion motion with Subject A	136
Figure 8.12: Continuous cycles at half the range of capable motion test results (Channel 1) for elbow flexion motion with Subject A	137
Figure 8.13: Continuous cycles starting with a small amplitude that gradually increases test results (Channel 1) for elbow flexion motion with Subject A	137
Figure 8.14: Continuous cycles starting with a small amplitude that gradually increases test results (Channel 1) for elbow flexion motion with Subject B	138

List of Table

Table 3.1 The summary of all the tunable parameters in neuromusculoskeletal model.	50
Table 4.1 Sensitivity rates and layer of 19 tunable parameters.....	57
Table 4.2 Sensitivity rates of 19 tunable parameters in different actions	59
Table 4.3 Sensitivity rates of 19 tunable parameters in different subjects.....	60
Table 4.4 Property, layer and processing method of 19 tunable parameters.....	66
Table 4.5 Tuning parameters.....	72
Table 4.6 Accuracy comparison of the models of James Pau and this thesis.....	78
Table 5.1 The size of ulna and radius of a cadaveric forearm.....	87
Table 5.2 Tuning parameters in forearm pronation and supination model	96
Table 5.3 Fixed parameters in forearm pronation and supination model.....	97
Table 5.4 Summary of forearm experimental results (RMSE in Degrees)	102
Table 6.1 The optimal solution of 14 tunable parameters.....	109
Table 7.1 Range of motion of exoskeleton joints	117
Table 7.2 Dimensions of upper limb and exoskeleton segments	117
Table 7.3 Specifications of the motor-gearbox units	118

Nomenclature

ADA	Action Difference Analysis
BCI	Brain-computer interface
Bi	Biceps
DE	Differential Evolution
DOF	Degree of freedom
DSP	Digital processing technology
EBC	EMG based controller
EEG	Electroencephalogram
EMG	Electromyography
FBC	Force Sensors Based Controller
FCE	Contractile force element
FPE	Passive elastic force
FVE	Viscous force
GA	Genetic Algorithm
GSR	Galvanic skin response
GUI	Graphical User Interface
HRI	Human-robot interface
ICOR	Instantaneous Center of Rotation
IDA	Individual Difference Analysis
LE	Linear envelope
MF	Median frequency
MPF	Mean power frequency
MUAP	Motor Unit Action Potential
MVC	Maximum voluntary contraction
NDI	Northern Digital Incorporated
NI	Neuromusculoskeletal Interface
NSQL	Non-Signal Quantization Layer
PCB	Printed circuit board
PCSA	Physiological cross-sectional area
PQ	Pronator Quadratus

PT	Pronator Teres
RMS	Root mean square
RMSE	Root mean square error
ROM	Range of motion
SAA	Simulate Anneal Arithmetic
SDOF	Single degree of freedom
sEMG	Surface Electromyography
SUP	Supinator
TET	Task execution time
UAHPEC	University of Auckland Human Participants Ethics Committee

Chapter 1 Introduction

Electromyography (EMG) signal is the electrical signal accompanied by human muscle contraction. It contains a wealth of information on human action. In recent years, with the increasing requirements of individual assistant system for the elderly or disabled people, and the extensible needs of the prosthetic control, military robots, household robots and commercial robot [1], EMG-based human-robot interactive technology has become a very popular research field. However, the development of this human-robot interaction technology is facing great challenges in its design and control parts, because it is a direct interaction between the external device and users. The purport of this thesis is to develop an EMG-based human-robot interface and to assist the human upper limb movement as an example. This chapter summarizes the current researches of EMG-based human-robot interface and the existing gaps. It also presents the main purpose and outline of this thesis.

1.1 EMG-based Human-Robot Interface

The EMG-based human-robot interface is the study of interactions between humans and robots based on the input information from the EMG signal of human muscles. It achieves the function of transmitting the collected EMG signal to the action control instruction of the external device. Figure 1.1 shows a superficial concept of the EMG-based human-robot interface. In the figure, EMG signals from users' muscles are firstly collected and processed. Then based on the information of EMG, some models or algorithms (such as human physiological models, pattern recognition or neural networks) are used to identify the body's response to external stimulus. The output of these models or algorithms are normally the predicted human movement and they can be used to control the external devices (such as robots or prosthetic arms) through a specific controller. Till then, the human's movement intention is conveyed to the devices through the interface. Since the EMG-based human-robot interface has the characteristics of simple structure, convenient operation, real time, natural harmony, and compliance with human behaviors, it has a wide range of applications in military, medicine, sports and family applications area.

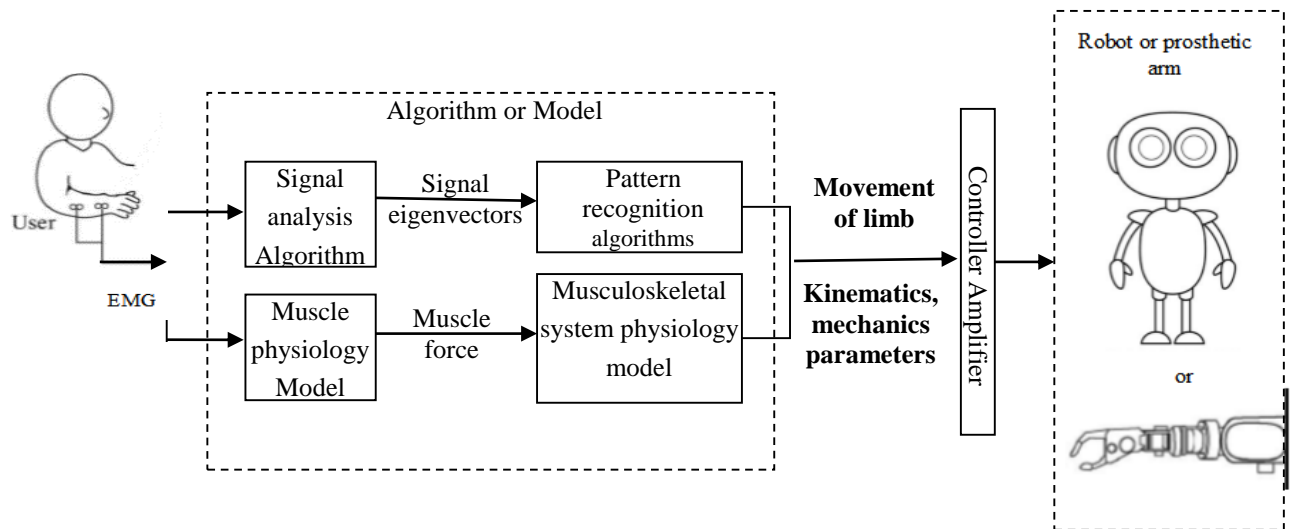


Figure 1.1: The concept of an EMG-based interface

1.1.1 Research Area

Currently, the researches of EMG-based human-robot interface mainly focus on the following two aspects:

1. Provide input to the controller by identifying limb movement patterns.

The key technologies of this aspect are the signal analysis algorithms and human motion pattern recognition algorithms. In recent years, neural network is used widely for the signal classification and pattern recognition. The model based on neural network is a relationship model between the EMG signal and kinematic data. The complex relationship between EMG, kinematic data and dynamics data is modeled by the nonlinear relationship of neural network. The neural network model simplifies the modeling computation, and the influence between systems is considered. So it is more simple, easy to solve, without complex mathematical formulas or time delay on EMG generation, compared with the previously method which relays on the inverse model. Besides that, one neural network model can address several muscle activation models. However, this model needs to collect large amounts of data, and its effectiveness is only applicable within the range of motion training samples. Further, the model cannot explain the mechanics of body movement system, since it is not based on the biomechanics.

2. Provide input to the controller by human movement, dynamic parameter estimation

This method identifies limb movement intentions by extracting EMG signals feature and using the musculoskeletal physiology model, so its key technologies are the muscle physiology model and musculoskeletal physiological system model. This method is simple, real-time, and combined with the biomechanical properties of the human body. Since surface EMG (sEMG) signal, with the advantages of non-invasive and easy to be collected, is easier for the users or patients to accept. However, the sEMG signal of deep muscle is hard to measure. This method is the main content of this thesis.

1.1.2 Challenges of the EMG-based Neuromusculoskeletal Interface

At present, the challenges of EMG-based neuromusculoskeletal interface are mainly at following five aspects:

1. The quality of signal processing

EMG has non-stationary nature in physiological characteristics. How to effectively process the EMG signals, extract the appropriate feature and eliminate as much noise as possible, all greatly impacts the properties of human-robot interface.

2. Contradictions between running time and the number of muscles

The contributions to the potential joint torque from muscles wrapped the entire joint are different. Since the joint actions depend on the coordination between different muscles, the more calculated muscles means a higher bionic precision and a higher accuracy of movement prediction. However, too many muscles also increases the complexity of interface computing. Thus, how to balance the contradictions between the number of muscles and interface running time, becomes another conditionality for existing interface researches.

3. The accuracy of models

The accuracy of models is one of the most important indicators of whether the model is feasible. According to current interface researches, the root mean square error (RMSE) of EMG based models are about 10^{-34} in single elbow flexion or extension movements [2-6], and the error was even bigger in continues and random movement. The problem of low accuracy of the interface is mainly related to the accuracy of the model, interface feedback and parameters tuning.

4. Parameters tuning and individual differences of the model

In order to make the interface adapt to different individuals, and to improve the accuracy, the model parameters need to be tuned. Till now, there is not a proper and comprehensive parameter analysis method especially for the physiological interfaces. And the most common interface tuning method are still Genetic algorithms (GA), Simulate Anneal Arithmetic (SAA), non-linear least square optimization, many calibration trials (manually) and Nelder-Mead simplex method. Most of them cannot achieve real-time tuning for the interface.

5. The influences of fatigue

Practice has proved that, the EMG signal is significantly affected by fatigue [7]. The temperature and muscle fatigue lead the EMG to a reducing frequency and increasing amplitude [8]. How to reduce its effect and improve the adaptability of the interface comes to be another challenge.

A review of the current researches on these issues is in Section 2.4. This thesis will try to solve some of these problems for improving this kind of human-robot interface.

1.2 Electromyography (EMG)

1.2.1 Advances of EMG

In 1781, Galvani confirmed the close relationship between muscle contraction and electrical signals, which opened a new era of electrophysiology [9]. Rowbottom found that the electrical activity could be recorded during the active muscle contraction, and he proposed the concept of "action potentials" [9]. In 1890, Marey recorded the first "electrical activity", which was what we call EMG (electromyogram) today. Thereafter, human biological signals were used in various application fields.

Currently, the main research areas of EMG are as follows:

1. Used in human-robot interface

EMG is used for the human-robot interface since it contains the information of muscle activation. An interface can extract the feature quantity in the EMG signal as input, calculate with physiological models or mathematic algorithms, and predict the users' movement intention as output (such as Figure 1.1).

2. Used in the study of control mechanism of neuromuscular system

As shown in Figure 1.2, the control mechanism researches of EMG-based neuromuscular system aim at extracting the recruitment, distribution information of neuromuscular motor units and the MUAP waveform information from the EMG, then studying the control mechanism of neuromuscular system, in the end, providing the diagnosis basis for the neuromuscular diseases.

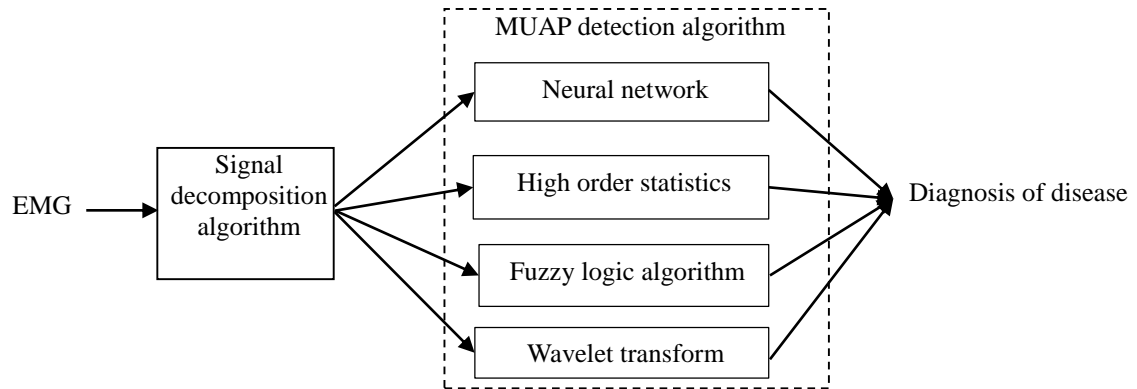


Figure 1.2: EMG-based control mechanism of neuromuscular system

Currently, the MUAP detection algorithms include neural networks, high order statistics, frequency-based blind source separation algorithm, fuzzy logic algorithms, scalogram analysis of continuous wavelet transform, and so on.

1.2.2 Characteristics of EMG-based Human-robot Interface

For the design of human-robot interface, there are three main performance requirements: the accuracy of action recognition, real-time performance of the system, and consistency with human instinct. The EMG as information source can meet these requirements, because of the following reasons:

1. During operation of the intelligent action assistance system, the movement of assistant devices needs to co-operate with human limbs motion based on the human's subjective intention. EMG can most accurately reflect the nervous-muscular motion and be used to quantitatively analyze human motion intent, such as the size of the muscle force, muscle fatigue, muscle contraction, stretching and relaxation.
2. The feature space of EMG signals must contain the appropriate motion commands from the cerebral cortex motor area. By analyzing the muscular EMG signals, the human movement can be 'prophesied' even before the real action took place (due to the electro- mechanical delay

which can be 20- 80 ms). If the "prophecy" information of motor neurons can be clearly identified, the control of intelligent assistance systems is equivalent to the control directly by human brain.

3. Compared to conventional sensors, the weak EMG signal is easier to be detected. For the case when actual action did not occur due to muscle weakness or physical over load, the body intent to complete this action target can still be detected by using EMG signals.

4. EMG measurements are less affected by the sensor itself.

5. In order to drive human limb movement, the mechanical structure of intelligent assistance system needs to directly connect with the assisted human limb. Therefore, it is more convenient to use EMG as an information source.

6. Based on human physiology to control assist devices, the system is more intuitive, natural, easy learning and can achieve autonomous control at the same time. Also, surface EMG has the advantages of non-invasive measurements and easy extraction process.

However, due to the randomness and low voltage of EMG, the noise in signals is difficult to be removed. The noise mainly comes from: a) electromagnetic noise signal from electronic equipment and environment, b) artifacts signal from electrode movement, c) the electrocardiogram inside body or heart activity, d) EMG interaction from adjacent muscles.

The electromagnetic interference from Electronic equipment and environment can only be reduced through the use of high-quality electronic components. The artifacts from the relative motion between electrodes and skin are low-frequency signals and can be filtered by a high-frequency filter. The effect of ECG also needs to be filtered by signal filtering techniques. The impact of EMG interaction from adjacent muscles can be reduced by carefully arranging the electrodes.

1.3 Upper Limb Exoskeleton

Since the world population is rapidly ageing, and with the increased number of diseases such as arthritis, stroke and paralysis, traditional artificial rehabilitation training can no longer meet the current medical needs. Exoskeleton technologies provide new solutions for rehabilitation and support for disabled people. An exoskeleton is the external skeleton that supports and protects the human's body, in contrast to the internal skeleton. Since the development of the first real exoskeleton in the 1960s, it plays a more and more important roles in rehabilitation, military, prosthetic, auxiliary areas over the last fifty years.

1.3.1 Advances of Upper Limb Exoskeleton

Upper limb is the main sport body in human life. Exclude the finger joints, upper limb totally contains 9 degrees of freedom from the shoulder to the wrist [10]. The 9 DOF support the upper limb exceptionally high operability and allow hands to reach a wide workspace. Since upper limb is able to complete the most complex movements, the quality of its motion function directly determines the people's ability of independently living.

The early upper limb rehabilitation robots were evolved from the end-effectors. They ingeniously adjusted human hands and forearms through the physical interaction. Figure 1.3 is an example of an end-effector. However, the motion range of the end-effector robot is limited. With the progress of the study, upper limb rehabilitation robot comes more diversification in resettlement ways and training patterns, so it can provide a more appropriate rehabilitation programs for patients. At present, the mainstream structure of rehabilitation robot is exoskeleton robot. Exoskeleton can be "worn" on the operator, closely contact with the body and move with the operator's movement. The exoskeleton has also been applied in reality.

Figure 1.4 is the robot, named ARMin, developed by Tobias Nef from the University of Zurich, Switzerland [11]. It was an exoskeleton robot with six degrees of freedom, four motors, some displacement sensors and force / torque sensors for position, speed and physical strength measurements. This system had a gravity compensation mechanism, to assist patients to complete the elbow and shoulder rehabilitation.

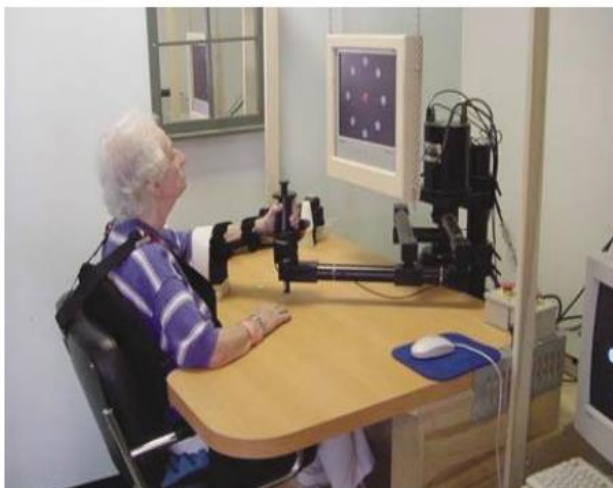


Figure 1.3: The MIT-MANUS end-effector rehabilitation robot [12]



Figure 1.4: ARMin rehabilitation device [11]

Joel Perry from University of Washington designed the exoskeleton robot named CADEN-7, which contained seven degrees of freedom, as shown in Figure 1.5 [13]. It was designed based on the kinematic and dynamic characteristics of normal human activities in free space. It could assist the patient to complete shoulder, elbow and wrist rehabilitation training, also it could be used for the virtual reality simulation of normal people's experimental research

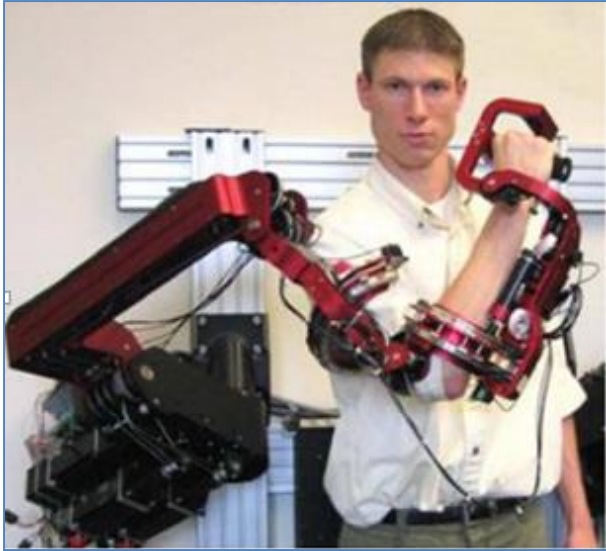


Figure 1.5: CADEN-7 rehabilitation robot [13]

Figure 1.6: Armeo Spring rehabilitation robot [14]

Hocoma Company in Switzerland developed a robot named Armeo Spring, as shown in Figure 1.6. It can assist the patient to complete the multi-articulation motions of upper limb [14]. This system did not provide power, only depending on the patient's voluntary movement to complete rehabilitation training, through the games provided by the system. In addition, the system also had a gravity compensation mechanism to ensure the patient in a smooth motion processes.

1.3.2 Current Limitations

Although the exoskeleton design and power realization have made a great progress, there are still many limitations in applications.

1. The existing exoskeletons are mostly already set with a sports program, which means, they cannot be real-time interaction with the patient or cannot change sport strategy.
2. The existing exoskeleton shapes are not beautiful. So it cannot inspire the patient to actively

complete the rehabilitation training.

3. The power supply is not long-lasting enough, and very expensive. The durability of the actuator is poor and its life is short.

4. The matches between the exoskeleton physical interface and users have some drawbacks.

Herr believed, the limitations of information exchange between a user's nervous system and an exoskeleton device were the ultimate issue of relevant requirements, which means, when the user moves his arm, how exoskeleton device can identify the movement trends and do the right response. EMG-based neuromuscular interface has been regarded as one of the most effective ways to achieve this goal.

1.4 Research Objectives

The overall objective of this thesis is to develop a new EMG-based neuromuscular interface, and try to overcome the current problems in this area. This case study of the thesis is the human elbow flexion/extension and forearm pronation/supination system. Reports on the elbow interface have been very common, but the accuracy of their established models is not high. The forearm rotation is a kind of very complicated movement. This is the first time to build an interface model based on the forearm biomechanical system with a real-time tuning. To this end, a new controller has been developed to control a 5 DOF upper limb exoskeleton. It is an example to verify the feasibility of the human-robot interface in this thesis. The overall objective can be broken down into the following five objectives:

1. Establishment of an EMG-driven elbow physiological model

Establish an EMG-driven elbow physiological model to explore the methods for improving model accuracy, especially to solve the problem of a sharp decline in model prediction accuracy during multi-cycle motions, and verify the applicability and stability of this interface through experiments. The accuracy of EMG-driven interface is closely related to the accuracy of each sub-model: signal processing, activation kinetics, muscle contraction dynamics, musculoskeletal geometry and kinematic model. Among these, the accuracy of musculoskeletal geometry model affects most to the interface. This thesis attempts to simplify the muscles path in new ways, to improve the model accuracy with ensuring the operation speed as a premise.

2. Development of a new method for parameters sensitivity analysis

Grade and classify all the adjustable parameters of the model. Try to assess the parameters sensitivity in a new way, which means to analyze them from offline, online, different actions and different individuals. And develop an online tuning algorithm for the EMG-driven model.

The purpose of parameter tuning is to make the model can precisely match each subject. However, the complexity of the model and parameters determining make it hard and time-consuming to obtain the optimal parameters. A multi-angle analysis of model parameters, helps to build online tuning algorithm. Genetic Algorithm (GA) and Differential evolution (DE) are programmed and separately used for offline and online interface tuning.

3. Establishment of an EMG-driven forearm rotation physiological model

Create an EMG-driven forearm rotation physiological model and experimentally verify the validity of this model. Compared with elbow flexion/extension, the movement amplitudes of forearm muscles are relatively small, no matter from the human physiological structure and exercise or daily life. Therefore, the EMG signals of forearm rotation muscles are weak, the motion are short-time, and the muscle length changes are small. Thus, the interface of forearm rotation has its particularity. This thesis discusses the method of establishing a biomechanical model of this kind of joints.

4. Establishment of a 2-DOF human-robot interface

Establish a 2-DOF human-robot interface for human upper limb movement based on EMG and physiological musculoskeletal model. This interface will provide three kinds of assisting operations of elbow flexion / extension, forearm pronation / supination and the forearm complex motion. For the forearm complex motion, the choice of muscle signal channels, muscle model, musculoskeletal geometry, especially parameter tuning problem are all discussed. The parameters of complex motion can be divided into two kinds: parameters those only affect one of this complex movement, and parameters those affect both flexion/extension and pronation/supination.

5. Design of a controller for the upper limb exoskeleton

In order to verify this EMG-based neuromuscular interface, a 5-DOF wearable exoskeleton is designed. And a controller based on EMG and force information is developed, to achieve the purpose of controlling the exoskeleton robot based on the human subjects' intention. This

exoskeleton design considers the mechanical interference, matching with different users' arm lengths, security, and other features. The result of the interaction between the user and the exoskeleton is the robot or the user to control arm movement. The controller can achieve the interactions of these two types, and also can combine these two types of action to obtain qualifying compound actions. The controller will be applied to the exoskeleton prototypes to validate their performance. And finally the demonstration of the EMG-based neuromusculoskeletal interface are completed.

1.5 Thesis Outline and Contributions

The research of this thesis has been described in Section 1.1. There are total eight chapters of this thesis, including this introduction chapter.

Chapter 2 introduces the latest input technologies of the human-robot interface, and reviews the EMG application fields. It refers the development status of the EMG-based neuromuscular interfaces, and discusses the current challenges facing this area: including the quality of EMG, the number of EMG channels, interface accuracy and model parameters tuning.

Chapter 3 introduces a new method of modeling: a simplified method of the musculoskeletal model, and uses it in the EMG-based elbow neuromuscular interface. Also, the parameters of the physiological model have been comprehensive analyzed and the methods for obtaining physiological parameters have been explored.

Chapter 4 introduces a new thinking to assess the parameters sensitivity. It can evaluate the parameters' hierarchy, individual difference and action difference from multiple angles. A group of multi-subjects and multi-movements experiments are also designed to verify the physiological model of elbow joint and signal processing method.

Chapter 5 details the physiological structure of the forearm bones, forearm rotation axis and forearm rotation muscles related to the forearm neuromuscular interfaces. The assumption for human forearm rotation modeling is given and the forearm rotation musculoskeletal geometry model is established. This is the first time to reverse the real-time forearm rotation biomechanical model as the research object and the accuracy of the model is verified by experiments.

Chapter 6 establishes a 2-DOF human-robot interface for upper limb movement. This interface provides three kinds of operation mode to assist human elbow flexion / extension, forearm pronation / supination, and the complex movement. This chapter also analyzes the muscle signal

selection, muscle model, musculoskeletal geometry treatment during complex movement. It also programs Genetic Algorithm (GA) and Differential Evolution (DE) Algorithm in Matlab, and discusses the test performances of GA and DE as two methods of evolutionary for model parameters tuning. The result shows that DE algorithm can be used in quick online tuning.

Chapter 7 presents a 5-DOF upper limb exoskeleton and a Graphical User Interface (GUI) for the demonstration of interface. The exoskeleton considers the exoskeleton mechanical interference, the match of different users' arm length, and the security features. Based on the two-DOF human-robot interface, the GUI connects users to the exoskeleton, simplifies the operation, and makes the control process and the results are visualized.

Chapter 8 presents a control strategy for the 5-DOF exoskeleton based on the human subjects' intention. It contains two kinds of controller: the EMG based controller uses the integration information of EMG signals as an input and the human-robot interface as control method; the force based controller takes the wrist force sensor signals as an input and the impedance control as control method. Some control experiments for elbow movement are also carried out to assess the effectiveness of EMG-based neuromusculoskeletal interface.

Finally, Chapter 9 summarizes all the research work of this thesis, as well as the contribution and suggestion for future work.

1.6 Chapter Summary

This chapter describes the meaning of EMG- based interactive technology in military, medical, sports, family and other applications. It shows the current two main research directions of this human-robot interaction technology. It illustrates the challenges of EMG-based neuromusculoskeletal human-robot interface. Also it recalls the progress of upper limb exoskeleton research and the limitations of existing upper exoskeleton.

This chapter lists the five main objectives of thesis and briefly overviews its implementation. The first thrust is to create a highly accurate EMG driven model for elbow joint. The second one is to grade, classify and assess the parameters sensitivity and develops an online tuning algorithm. The third is to create an EMG-driven model of forearm rotation. And the fourth is to develop a 2-DOF human-robot interface based on EMG and human physiological musculoskeletal model. The last is to present a 5-DOF exoskeleton and design an EMG and force based information fusion controller to demonstrate the interface.

Chapter 2 Literature Review

In order to enhance the acting ability of limb-damaged patients, restore their normal social life and improve their mental and physical state, the assisted rehabilitation robots have been paid more and more attention to. In addition, the development of human-robot interaction technology in the military, medicine, sports, family, and other fields also needs an intelligent interface. The intelligent human-robot interface system requires the ability to qualitatively and quantitatively analyze the people's request, to accurately and quickly sense the operator input, and to quickly make the appropriate response in accordance with the operators' different movements and intentions.

This chapter summarizes the input technology of human-robot interface and the applications of EMG. It also reviews the researches of EMG-based neuromuscular interface, and discusses the challenges.

2.1 Input of Interface

In the development of the human-computer intelligent system, researchers have been looking for a different control source to control the interface for a long time. Currently, the main types of control sources include human mechanical movement, voice, electroencephalogram (EEG), electromyography (EMG), and so on.

2.1.1 Mechanical Movement of the Human Body

This method is mainly using movement function of the human body, and achieves the mechanical control through the transmission device to trigger the corresponding switch. The rotation of the wrist, elbow flexion, and even the movement of head can all be used as the information input sources of device drivers. There are two methods to obtain the body's mechanical movement: using computer vision and using generic sensor.

1. Use computer vision to acquire the body's movement information

The body's movement is mainly reflected by the joint motion. The human motion analysis based on computer vision collects moving images in sequences by means of three-dimensional video or high-speed camera, then, processes the image sequence or video to analyze joint motion parameters and trajectory [15]. It uses three-dimensional reconstruction method to obtain the spatial coordinates of the photographed object, and use the time series of coordinate values to calculate the corresponding kinematic parameters such as velocity or acceleration [16, 17].

This method is easy to use. Since it uses non-contact way to record, it does not need to impose any constraints to the human body. Thus it can reflect the actual human movement. It can be applied in the motion analysis of sport players, clinical diagnosis assistant, medical gait analysis, computer animation and game production, and the establishment of large-scale of multimedia databases. However, during human joint movement, the computer vision is easily affected by changes of ambient light, interference of background chaos, shadow and occlusion of the moving target and so on. These may increase the difficulty of motion recognition. Meanwhile, the sequence of images requires a large storage space, and the analysis algorithms of images are complexity which makes it difficult to real-time processing. And Due to the space constraints, complexity of device and the high cost, it is hard to meet the needs of applications of intelligent assistance system.

2. Use generic sensors to acquire the body's movement information

This method installs some generic information sensors (such as position sensors, angle sensors, acceleration sensors, force sensors and inertial sensors) between user and interface to obtain the real-time dynamic data of the human body (or parts), and then use appropriate mathematical models to obtain the motion information of the human body [18-21]. Such as Bouten used the acceleration sensor in the tracking identification of daily movement [22]. Zhou estimated the human upper limb movement by inertial sensors [23].

The human motion is impacted by the force of contact interface in environment. Therefore, many scholars did a lot of researches about the human's mechanical behavior in the course of the campaign to discover a deterministic relationship between the force and human movement state. Sazonov used the changes of plantar pressure and heel movement acceleration as variable parameters, and classified different movement patterns by a neural network algorithm[24]. Monika Kohle did the gait analysis through ground reaction force. He used a neural network for abnormal gait identification, and applied it in the clinical gait auxiliary diagnostic and treatment [25]. Chao was also cited plantar pressure information in the gait research and obtained some certain results [26].

With the development of Micro Electro Mechanical Systems, MEMS, the volume of inertial sensors (such as accelerometers, gyroscopes, magnetometers, etc) are becoming smaller and smaller, the sensitivity and the ratio of signal to noise are getting higher and higher, also the power consumption and cost are greatly decreased. Combined with wireless data communication technology, it can be made to wireless wearable device and form a body sensor network which has the perception of motion information and may monitor human movement for a long time. The obtained motion data can be applied in clinical application, 3D animation, virtual reality, and ubiquitous computing. Keith MW in Metro Health centre implanted MEMS force sensors and optical sensors in the disabled patients, to measure the force and torque information of limb joints and muscles. At the same time, Keith used the Hall Effect sensor to provide angle information for the rehabilitation research. Through more than 2 years study, he gained many useful results [27-29]. However, due to the human body's biological reject testability and individual differences, the signal interference is quite large. Also it is not possible to rely on implanting too many kinds of sensors to complete the task of acquiring human motion information.

2.1.2 Voice of the Human Body

Researchers treat the sound information of the patient through a digital processing technology (DSP) and then convert it to the corresponding control instruction. The voice-activated prosthetic has a great advantage in helping paraplegic patients to restore motor function. At present, the voice control method becomes popular in the market, such as the 'simple language prosthetic control system' designed by Udayashankara [30]. Its downside is that the patients' normal communication with others may also lead to prosthetic malfunction. It is also has a problem about how to improve the ability of voice prosthesis to anti the noise from environment.

2.1.3 Electroencephalogram (EEG)

The subjective will of human motion usually comes from cerebral cortex, and the EEG signal from cerebral cortex does not need to relay on residual limb muscles to convey the excitement characteristics. Thus, the information acquisition based on EEG is theoretically the best method to help disabled people communicate with others. Roberts put the detected EEG signals through an 8-order AR model and Bayesian logic classifier to classify the data in order to control the up and down movement of the mouse. The overall performance researched 82% [31]. One of the important

functions of brain-computer interface (BCI) is to be used for the recovery of stroke or paralyzed patients. Using BCI in rehabilitation training may help to improve the quality of the patients' life. By this recovery methods, the cortex area of the patient after treatment has an indications of recombinant [32].

Brain as the center of human nervous system contains complex electrical signals. And the working mechanism of brain still has many unsolved part. Therefore EEG-based action identifying and control are limited to simple body movements. For diverse and complex actions, there still needs in-depth researches.

2.1.4 Electromyography (EMG)

EMG signal is a kind of bioelectricity released by neuromuscular excitability of the human's voluntary movement. The EMG information reflects the functional state of muscles, so it can be used for sensing the body's state of motion and predicting future actions. Cavanagh et al [33] researched on human electromyography phenomenon and experimental proved that: the human's movements, in all forms, are mainly achieved by muscle contraction, and these mechanical contraction movements always occur 20-80ms after the action potential appears. Therefore, it can be trusted that EMG is the root of the electrical signal which generated muscle force. EMG can be used to recognize the human movement patterns, especially in the joint motion identification of the upper and lower limb. The recognition results have already been widely used in the control strategy of humanoid mechanical and artificial prosthesis. Meanwhile, as a nerve stimulation signal, it can also contribute to further applications in human rehabilitation therapy. The surface EMG (sEMG) as a control source is relatively mature. By using the human physiological way to control, it is easy to learn and able to achieve self-control, so it has been regard as an ideal information source for the current research.

Some examples of real input technology for interface are shown in Figure 2.1, and includes the cyber glove system and cybergrasp from CyberGlove Systems LLC in USA [34], sample of haptic interface [35], force sensor gloves, EMG and EEG capture system and sensors [36].

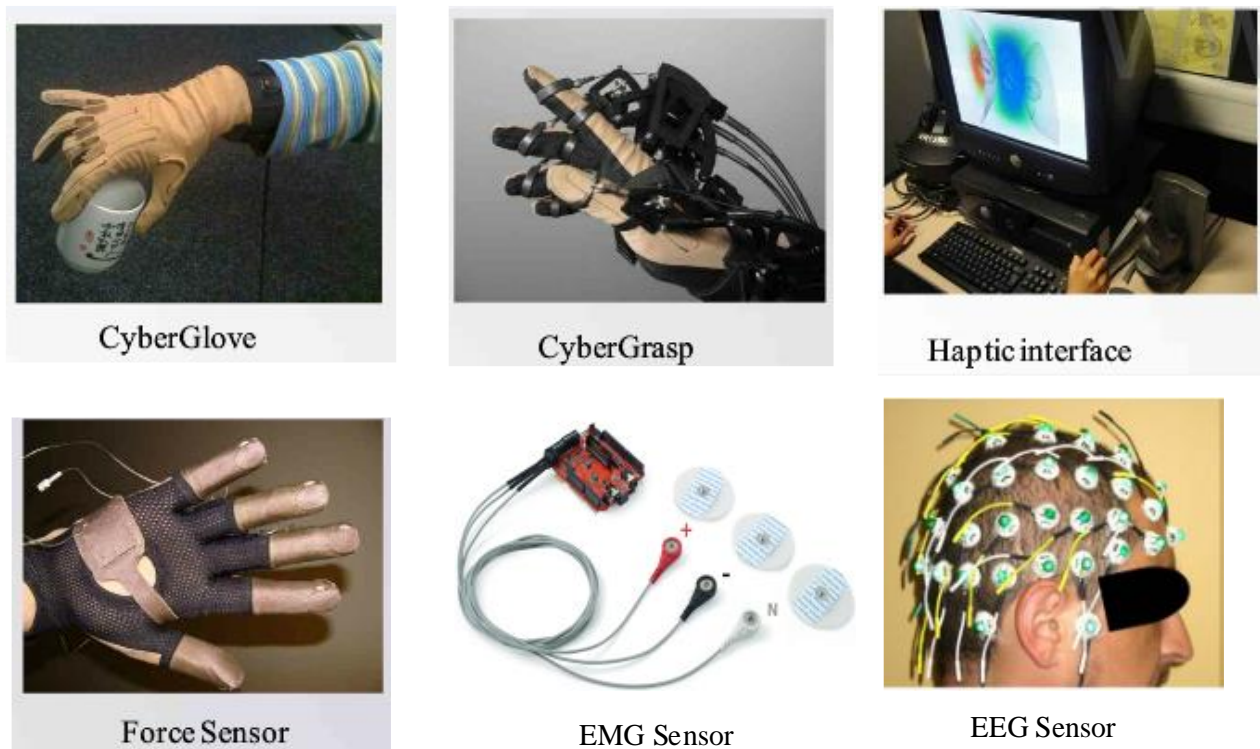


Figure 2.1: Photos of real input technology for interface [34-36]

2.2 Current Applications of EMG

Under well-controlled conditions, changes in EMG signal can quantitatively reflect the muscle activity and the variation rule of the central control features, such as the level of muscle strength, muscle activation patterns, conduction velocity of excited motor unit, local fatigue of muscle activity and the coordination between different muscles. The EMG is closely associated with the active and functional status of muscles. Since it can reflect neuromuscular activity, EMG has some great theoretical significance and practical value in the following aspects.

1. EMG used in sport research

Sport analysis refers to apply the person's physical activity to sports, dance and other training activities. Currently, in many sports, by testing the athletes' physical characteristics, their degree of physical exertion and operation standards can be detected. By referring to the monitoring results, athletes can design proper training programs to improve their acting performance.

For example, EMG can be used to determinate the electro-mechanical delay in human activities, as well as the training of biological recover and psychological state adjustment. By studying the

EMG, the sequence of muscle activation and muscle force can be assessed. The result can be used to analyze and evaluate the athletes' movement. Also, EMG is used to assess the training level of athletes' muscle.

2. EMG used in medical research

Based on the electrophysiological properties of the nerve and muscle, and by using the electrical stimulation of nerves, researchers kept track of the patient's action and reaction wave of feeling, to help the diagnosis of neuromuscular diseases. Till now, this method has a great achievement in treating chronic nonspecific back pain, scoliosis, stroke and Parkinson.

In 2004, Cheung tested on 30 adolescent idiopathic scoliosis patients and concluded that: Simultaneously determining the growth rate of spine and sEMG ratio has a certain value to assess the progress type of adolescent idiopathic scoliosis [37]. Wen Wu took 37 patients who were suffering with lumbar disc herniation as a test. He compared the differences of sEMG from vertical spine muscle and multifidus before and after treatment [38]. The results showed that sEMG can be used as one of the objective indicators of clinical efficacy evaluation of lumbar disc herniation and has a good clinical value. Randy Neblett [39] collected sEMG and ROM (range of motion) to measure and evaluate the lumbar flexion relaxation phenomenon. And he found that all normal subjects had flexion relaxation phenomenon which means that the EMG in extensor state is similar with the one in resting state when lumbar is in maximum flexion. In 1980s, Kralj and Bajd put hand control device into the paralyzed patients walk system and achieved the fusion of walking devices and FES neural prosthetic [40]. Later, ParaCare team in Zurich University invented a hand function recovery system based on the EMG signal FES neural prosthesis, through acquisition of the deltoid EMG signals of the upper limb [41]. Since FES can help patients to complete the task of explicit action, it is regarded the most promising technology in the reconstruction of limb function. And it has successfully helped paraplegics to stand and walk from the wheel chair.

3. EMG used in rehabilitation research

In the design and control system of external skeletal, artificial limbs, wheel chairs and other intellectual products, EMG signals are always used as the control source to drive the intelligent assistance systems working through the way as human intention prefers.

In the exoskeleton system, Sankai, in the University of Tsukuba, successfully developed the HALL (Hybrid Assistive Limb, HAL) system [42](shown in Figure 2.2) which was used to assist in the daily walking and rehabilitation, based on the method of using sEMG and ground reaction

force to predict user's intention [42]. Aiming at clinical rehabilitation, The University of Michigan used EMG signals from calf soleus for control source and established a linear relationship between EMG signal and muscle force, to control the leg movement auxiliary systems [43], shown in Figure 2.3. German Ottobock Company developed an automatic induction hand (SUVA) (shown in Figure 2.4), which can easily and naturally control the prosthetic hand open, close and crawl depending on the strength of EMG signals [44, 45]. It is the mainstream prosthetic hand of the market products.

4. EMG used in gesture recognition and human-computer interaction

Gesture recognition is a method that obtains information related with the gesture by the sensor and use pattern recognition to discriminate the type of the gesture. An EMG-based control system collects different EMG signals from corresponding muscles and identifies different hand gestures to control peripheral devices with the recognition results. The recognition result not only reflects the flexion state and flexion strength of joint, but also reflects the completion process such as shape, position, orientation of the hand gesture in real time. Therefore, EMG is used for a variety of computer interface control, including the electrical device control, automatic sign language translation, assisted Living for people with disabilities, interactive gaming entertainment, battle command, and so on.

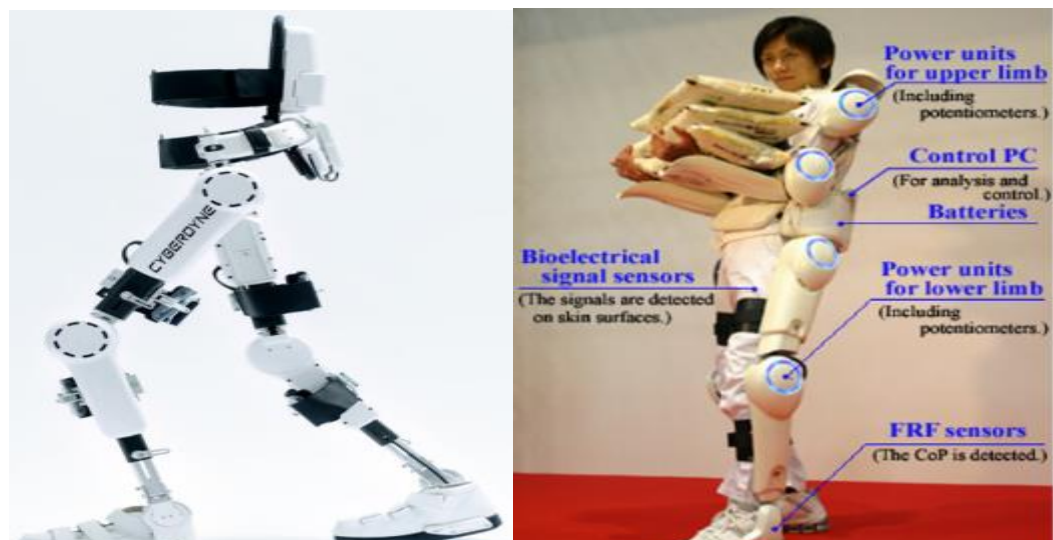


Figure 2.2: HALL(Hybrid Assistive Limb, HAL) system [42]

The EMG-based gesture recognition is not easily impact by the environmental, and its advantages such as lightweight, convenient and inexpensive suit for the application of family living environment. For example, Jong-Sung, Kim et al classified and identified 6 kinds of wrist action to achieve a real-time system to control a computer mouse through sEMG signals from

gestures [46]. Enrico successfully controlled a phone by analyzing different EMG signals [47]. Shinichi used sEMG recognition results of hand and neck movements to control an electric car [48]. Kevin developed a set of virtual joystick based on the sEMG gesture recognition, to control the gaming aircraft flight [49, 50]. He also improved the number of classified gesture category to nine kinds of wrist and finger movements, as shown in Figure 2.5.

Using EMG to identify specific actions can be in advance of the actual action, therefore, the process which extracts EMG signals from human surface and operates by computer can simplify the transfer and treatment process of brain movement instruction. It improves the speed of human-devices interface. This method are widely used in modern military and racing sports, because these applications need a higher flexibility and faster control. The one who manipulates executing agency through EMG gains a quicker interface speed then the opponent, and gets a head start in the battle or the game.

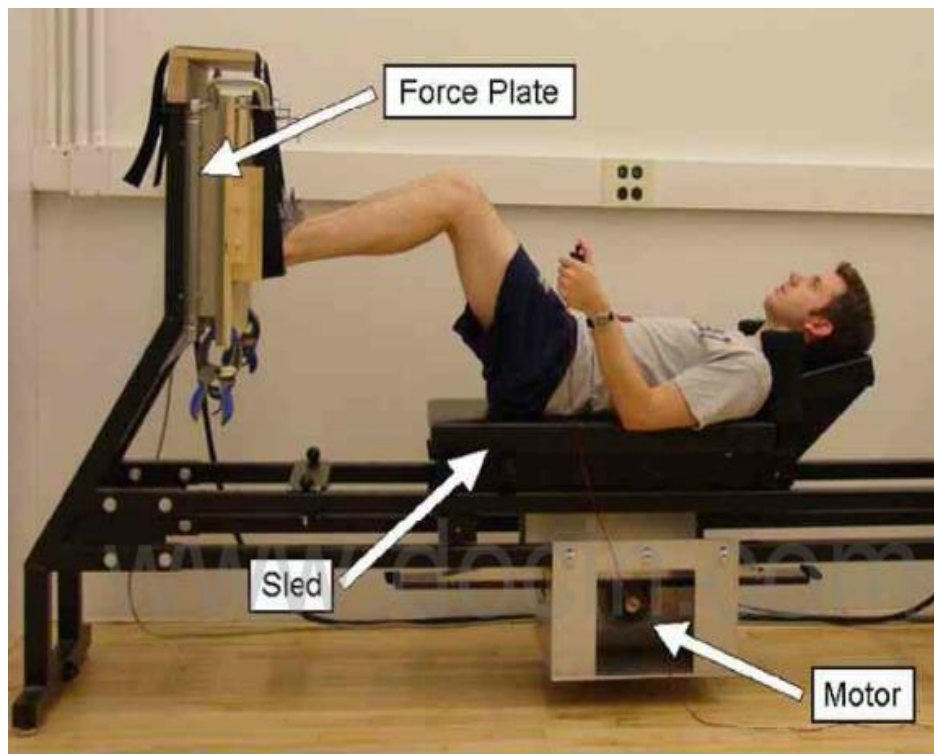


Figure 2.3: The University of Michigan rehabilitation robot [43]



Figure 2.4: Prosthetic hand from Otto bock Company [44, 45]



Figure 2.5: Virtual joystick based on sEMG gesture recognition [49, 50]

5. EMG is used in emotion recognition

In the research of physiological signals-based emotion recognition, the physiological signals are always electromyography (EMG), galvanic skin response (GSR), blood volume pulse (BVP) photoplethysmogram (PPG), skin temperature (SKT), respiration (RSP), Electroencephalogram (EEG), electrocardiogram (ECG) and heart rate signal (Hate Rate). Firstly, extract a certain amount of statistical features based on the characteristics of the different physiological signals. And then, select features by SBS, SFS, SFFS / Fisher, ANOVA or other feature selection methods. Finally, classify through Fisher or KNN classifier and achieve the purpose of emotional identification.

Prendinger et al, from Tokyo University, used EMG and SC for emotional identification [51]. Kim and Bang from Korea gathered the physiological signals of 50 participants in their natural emotion, and identified three and four kinds of emotional states by Support Vector Machine [52].

There are two examples of emotional identification: the smart, portable personal body care and monitoring systems can measure the wearer's breathing, heart rate, blood pressure, sweating, body temperature, muscle reaction and galvanic skin signature to determine the emotional state of the wearer, and physically record the wearer's condition. After a certain time, it may automatically publish a health alarm and propose some care advice or adjustment method to the wearer. Another example is the safe driving intelligent monitoring system: this system uses a non-contact signal acquisition device which can obtain the behavior signature of the driver at any time, examine the driver's "active or passive reactive" particular emotional state and evaluate the driver's attention and physical condition. This system ensures that the driver is in

good condition and reduces the incidence of traffic accidents.

2.3 EMG-based Neuromuscular Interface

Using EMG as input to the musculoskeletal model has been used by researchers at different anatomical locations in isometric or dynamic tasks, such as elbow [53-55], shoulder [56], knee [57-61], ankle [62], jaw, lower back [63, 64] and wrist [65]. The theoretical basis is that: if the EMG signals can be measured precisely and processed adequately to reflect the activation of each muscle crossing the joint and if the activation can be modulated properly by models, it is possible to accurately estimate individual muscle forces over a wide range of tasks and contraction modes.

Buchanan, in [66], used a mixing method of forward and inverse dynamics to cross-validate the forward model. From more than 200 knee flexion/extension torque tests, he found that the calibrated EMG-driven model had a very good forecast, on average $R^2 = 0.91 \pm 0.04$. In addition, if maintaining muscle - tendon parameters unchanged, and only allowing the EMG activation parameters' adjustment, the model can predict the joint angle in the test for two weeks without prediction losses. However, this model has some problems of offline tuning, large computation, time-consuming, and cannot guarantee real-time.

Koo et al [2], noted that before EMG-driven model were used as a reliable tool to estimate muscle force, a supplementary verification test of different tasks and configurations must be completed. Koo firstly determine particular individual parameters for the musculotendon model (based on a series of nine elbow maximum isometric flexion locations: 0-120 °, in a step of 15 °). Then after the calibration, he used the same set of parameters and EMG signals as inputs to the model. By comparing the accuracy and consistency of the model, he predicted the effectiveness and versatility of the model during different dynamic sports activities.

Koo in [2], proposed to test the model's performance by two indexes: the match of joint track and root mean square (RMS), and to show the model forecast accuracy is mission-dependent by univariate variance analysis. With the voluntary loading agreement of elbow flexion (Task 1), he used the linear envelope method to get a result with $RMS = 13.71^\circ \pm 5.89^\circ$. And with the voluntary unloading agreement of elbow extension (Task 2), the $RMS = 34.64^\circ \pm 7.79^\circ$. With the voluntary unloading agreement of elbow flexion (Task 1), the $RMS = 18.67^\circ \pm 8.49^\circ$.

Cavallaro [67] established an EMG driven interface to control a 7 DOF upper limb exoskeleton. He proposed four performance indexes (maximum error, root mean square error, correlation coefficient,

the percentage of time of the absolute error below a specific threshold value) to assess the model predictive capabilities. He also established a functional relationship between the model task execution time (TET) and the number of modeling muscles.

Shao [68] improved the model based on article [66]. He added the viscous resistance to the muscle contraction kinetics ($F_{VE} = F_{Max} \times b_m \times v \times \cos \varphi$), and used the Parallel Simulate Anneal Arithmetic (SAA) as a tuning method.

Sartori and Lloyd [69] presented two methods to achieve real-time modeling. One was the high stiffness tendon treatment, which reduced the computation time. The second one is the design of a new (data processing) method to reduce memory requirements. By using a two-dimensional cubic spline interpolation, instead of 4-dimensional musculotendon estimated value interpolation method, they relaxed the memory requirements. They run the model in real time by placing all the EMG-driven computing models under a common framework - SIMM.

Lloyd in [57], found that the model has the ability to accurately predict the single cycle movement (average RMSE = 6.53 %). However, when there is more than one cycle of movement, a sharp decline appeared in the accuracy of the model (average RMSE = 22 %). This is because the EMG signal has a low reproducibility; the same movement can be generated by a different mode of EMG signals. This means a same tuning model may not work to suit all EMG input mode.

Currently, some research results are summarized in Appendix I. It summaries six group of EMG-based interface systems, including their mechanical structure, number of muscles, signal filter, modeling details and tuning methods.

2.4 Challenges

From the relevant literatures, a great improvement can be seen in the interface development in recent years. However, there are still some gaps between the experimental environment and practical applications. Currently, the challenges of this area are mainly shown in the five following parts:

2.4.1 Quality of Signal Processing

EMG has non-stationary nature in physiological characteristics. How to effectively process EMG signals, extract the appropriate feature and eliminate as much noise as possible, all greatly impacts the properties of human-robot interface. Currently, the filtering techniques includes time-domain

(such as mean value, root mean square value RMSE), frequency domain (such as median frequency), and time-frequency domain (such as wavelet transform).

The advantage of the time-domain method is computationally simple. The disadvantage is the poor stability of identification, since its character changes greatly when the muscle contraction changes. However, it has been widely used, because of its simple character. Currently, the mature prosthetic hand is controlled by the time domain features. The time domain features include: the integral of absolute value (IVA), zero crossing (ZC), variance (VAR), histogram of EMG (HEMG), integrated EMG value (iEMG), and root mean square error (RMSE).

The advantage of the frequency domain method is that, the description of EMG in the frequency domain is relatively stable which conducive to the subsequent EMG pattern recognition. The disadvantage is that the traditional Fourier transform can only characterize the overall frequency characteristics of the signal, but there is no time-resolved feature. So it can only be applied to the stationary signal analysis. The commonly used frequency domain characteristics are: mean power frequency (MPF), media frequency (MF), power spectrum, and so on.

The method of time-frequency domain can provide the information of both time domain and frequency domain. It has been paid more and more attention in the non-stationary signal analysis. Commonly used time-frequency methods include short-time Fourier transform, wavelet transform, Wigner-Ville transform and Choi-Williams transformation.

Since EMG signal is the sole or principal information source of the interface input, an effective signal processing method should be developed to improve the quality of interface input. Apart from optimizing the EMG acquisition process (the selection of electrodes and their positions) to reduce the noise, the signal processing method should also be improved, while ensuring the fast operation time of interface. This is the prerequisites for the performance of existing EMG-based interfaces.

2.4.2 Contradictions between Running Time and Number of Muscles

The contributions to the potential joint torque from muscles wrapped the entire joint are different. Since the joint actions depend on the coordination between different muscles, for the human physiology-based interfaces, the more calculated muscles means a higher bionic precision. However, too many muscles also increase the complexity of interface computing. Thus, how to balance the contradictions between the number of muscles and interface running time, becomes another conditionality for existing interface research. How many muscle signals should be selected as the input of human-robot interface, is a worthy study problem.

Koo in [2], tested all the 7 muscles which wrap the entire elbow joint. The muscles include Biceps Brachii long head, Biceps Brachii short head, Brachioradialis, triceps brachii longus, Triceps Brachii lateralis, Triceps Brachii medialis and Anconeus. He found that: for the flexion without load, the activation of BIC and BRD is quite small, and BRA contributes most to this flexion; for the flexion with load, other elbow flexor start working besides BRA. Koo also found that, the elbow smooth stretch relies on the cooperation of different flexor and extensor. Koo's research did neither fully model the influence range between different muscles, nor accurately simulate in real-time. These may because of the unreliable nature of BRA EMG signal during extension.

In [70], a function of muscle number and task execution time (TET) has been established, shown in Figure 2.6. The black solid line stands for average TET changing with different number of muscles, the dotted line and dash-dotted line represent the maximum and minimum TET. From the picture, the relationship between TET and number of muscles is non-linear. The different complexity results modeled by different muscles also have a non-linear relationship.

There are still problems of choosing a suitable electrode. The size of electrode should be big enough to cover the whole muscle surface, however, that will lead to a crosstalk between adjacent muscles. Meanwhile, some muscles (such as brachialis) will be covered by others, and the surface EMG of these muscles may not able to be measured directly. The standard of maximum endurance of musculoskeletal function has been used to predict BRA's function [31]. This technique can be beyond its current uses and may allow furthering reducing the number of required sEMG electrodes, thereby to achieve a satisfice torque prediction. In the future, a general method to analysis the contributions of related muscles to the joints movement will be established.

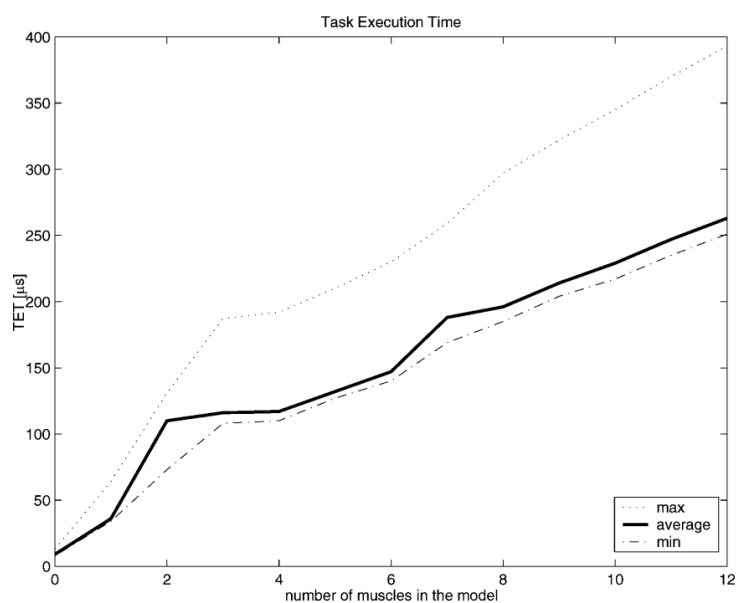


Figure 2.6: The function of number of muscles and TET [70].

2.4.3 Accuracy of Model

At present, the predictive ability of the human-robot interfaces developed so far is limited.

The RMSE of the model from Koo and Mak was $34.64 \pm 7.79^\circ$ in single elbow flexion, and $18.67 \pm 8.49^\circ$ in single extension [2]. Au and Kirsch, had a method to test both shoulder and elbow, but the movement RMSE was about 20° and the elbow RMSE was $19.6 \pm 5.9^\circ$ [3]. Artemiadis and Kyriakopoulos achieved a better result, the RMSE was from 1.76° to 9.0° with the limited of arm movement only in the horizontal planet [4]. The model from Paul [6, 71] had a lower average RMSE (from 4.18° to 10.1°) in single cycle elbow motion, however, for multi-cycle motion (continuous cycle test), his model's accuracy had a sharp decline (RMSE from 15.98° - 36.06°). And there were more variability between different individuals.

The problem of low accuracy of the interface is related to three aspects: a) the accuracy of the model itself, including all parts of EMG-driven model: signal processing, activation kinetics, muscle contraction dynamics, musculoskeletal geometry and kinematics. b) human-robot interface feedback mechanism. c) Online tuning algorithm.

2.4.4 Parameters Tuning and Individual Differences

According to the structure of the model, the calibration parameters can be divided into two kinds: the ones without physiological significance (such as gain or error factor) and the ones with physiological significance (such as muscle parameters, etc.). The accuracy of anatomical data greatly impacts the model's accuracy.

Currently, tuning of the model is mainly divided into two kinds: online and offline. The most popular tuning algorithms are Genetic algorithms (GA), Simulate Anneal Arithmetic (SAA), non-linear least square optimization, many calibration trials (manually) and Nelder-Mead simplex method. Different methods have been used to determine the calibration of parameters.

1. Using a number of calibration tests. During the tests, operate several settled conditions, while maintaining the other conditions are constant, so that the contribution of individual muscles can be isolated [61, 72].
2. Using a group of calibration tests at the same time to determine a plurality of calibration parameters. During tests, use a nonlinear least squares optimization system to change parameters, until the difference between the measured and predicted net joint torque is minimum [59, 73-75].

3. Use electrical stimulation to selectively activate specific muscles, in order to determine the parameters of this specific muscle [75, 76]

Several of documents have highlighted the importance of parameters tuning, and the limitations of existing methods also increases the difficulty to achieve the goals. Offline tuning is large computation and time-consuming. It cannot guarantee real-time operation. In addition, one tuning model cannot work for all EMG input models. Similarly, the RMS has a huge difference with different tests of one subject, or with different subjects [6, 71]. When the tuning process successfully identifies a global (or close to its local) minimum value, during different input period, the result is a compromise in accuracy, in order to obtain the best overall error.

2.4.5 Impact of Fatigue

Practice has proved that, the EMG signal is significantly affected by fatigue [7]. The amplitude and spectral energy of EMG signals are closely related to the muscle fatigue. Petrofsky [8] studied the relationship between EMG and muscle temperature, muscle fatigue and muscle blood flow under conditions of muscle isovolumetric contraction. The results showed that blood flow has little effect on the EMG amplitude and frequency, and temperature and muscle fatigue lead the EMG to a reducing frequency and increasing amplitude.

The main methods to assess fatigue are: The root mean square value (RMS), median frequency (MF) and mean power frequency (MPF). Moritani et al. [77] found that, under normal circumstances, the Fourier spectrum curve of EMG may occur in varying degrees to the left, caused by muscle fatigue. It leded the MPF and MF (which reflect the spectral curves) to a corresponding decline. Park and Meek have tried to consider the issue of fatigue [78]. This process will mainly focus on a certain type of interface parameters in online tuning. It needs a feedback.

2.5 Chapter Summary

This chapter reviewed the input technology of human-robot interface, summarized the applications of EMG. It also recalled the previous studies of EMG-driven neuromuscular interfaces, including the ones used in different anatomical parts: for elbow, shoulder, knee, ankle, jaw, lower back and wrist. From the related literatures, EMG-based interface methods have been developed in recent years. But for now, this area is still facing a number of issues: the low quality of EMG, which used to determine the level of muscle activation; the low accuracy of model, especially the

musculoskeletal model is too simple; the unreasonable feedback mechanism, which lacks of a fast on-line tuning algorithm; too many model parameters, which lacks of comprehensive parameter sensitivity analysis and cannot solve the individual difference problem. These limits provide a basis for this thesis study. The in depth and detailed reviews are shown in the following chapters.

Chapter 3 A Neuromusculoskeletal

Model for the Elbow Joint

This chapter develops an EMG-driven elbow physiological model, it describes the elbow flexion / extension movement in the sagittal plane. Upper limb is considered as two rigid body components (upper arm, forearm and hand). Elbow flexion / extension motion is modeled as a friction hinge joint while ulna rotates around the humerus. The axis of rotation is through the center of small head and pulley sulcus [79]. The elbow physiological model is combined of musculotendon dynamic model and musculoskeletal geometry model. The interface gains each muscle's muscle force by musculotendon model, the joint torque by musculoskeletal geometry model, and the joint angle and the angular velocity by kinematics model. This chapter also analyzes the 23 parameters of EMG-driven model, gives their ranges, to prepare for parameters sensitivity analysis of the model and parameter tuning.

3.1 Background

Human-robot interface, as a precise interaction platform between human and machine, should be able to quickly and accurately response, calculate, predict and feedback to the human actual movement. Human action is actually a process from a muscle making the appropriate contraction with nerve stimulation, to the promote bone and join making the corresponding movement. An effective interface model can be used to mimic this process. EMG signal, as a kind of electromyography generated during muscle contraction after nerve stimulation, can cover all of the information of muscle contraction. It can provides a reliable information source to the interface [80].

Song and Ge [81, 82] established an assumed function model by using statistical theory to reflect neuromuscular activity and obtain human motion parameters. Song and Ge used the Cosine tuning function based on periodic regression theory to describe the neuromuscular activation. In order to

estimate the elbow angle, an upper limb model was developed to clarify the relationship between the surface EMG (sEMG) readings and the direction of movement of the elbow in the horizontal plane. A genetic algorithm was used not only to tune the model parameters, but also to verify whether the triple cosine tuning function was sufficiently accurate to describe the muscle activity. Song and Ge also proposed the usage of fractal theory in analyzing sEMG signals. They analyzed system characteristics from the different levels of signal fractals, extracted the speed signal of limb movement and provided information for real-time control. Since EMG comes from a group of muscles, it is random and easily gets chaotic, so the accuracy of the elbow angle estimated by this model remains to be further improved. Also, the placement of electrodes and human skin conditions limit this model's adaptability for different patients.

In recent years, researchers attempted to use neural network methods to analyze human musculoskeletal function. Neural network-based models were used to build up a relationship between EMG signals and the correspondent kinematic data of human movement [83-86]. Compared with the original method of solving the inverse model, neural network-based models are much simpler, because they do not have complicated mathematical formula or time delays which are generated and associated by EMG. One neural network model can address multiple muscle activation models. For example, Heller established a single hidden layer neural network and reconstructed the EMG signals of semitendinosus and vastus medialis from the kinematic data [87]. Sepulveda developed an EMG model with joint features of two single hidden layer neural networks. The input of the model is the data for 16 muscles through normalized EMG values, and the output is the angle and torque of the hip, knee and ankle [84, 86]. The system was later improved for neuro-fuzzy control [85] and emotion-based interaction [88]. Another representative neural network model is Prentice's model. It used a two-step rate frequency sinusoidal signal as input and the EMG of eight lower limb muscles as output. Later, the author upgraded the model's input with 21 kinematic parameters to describe the muscle activation [83, 89]. The common issue for neural network based models is that they need to collect a large amount of experimental data. Also, the effectiveness normally depends on the training process and is only applicable within the range of motion of the training samples.

Since the structure of neuromusculoskeletal based model [90] is closer to the human physiology, this model is easier and more accurate in reflecting the human body's movement characteristics, which can achieve the intelligent control of interface.

This chapter established an EMG-based nerve musculoskeletal model of human elbow joint for the upper limb, based on the actual physical structure of human body. This model is consisted by

several sub-modules: EMG signal processing, muscle activation calculation, musculotendon model, musculoskeletal model and kinematics model, shown in Figure 3.1. The EMG signals collected from human muscle firstly go to the signal processing model and activation kinetics model to gain the muscle activation, then, from musculotendon model, to gain the muscle force of each muscle, and to obtain the joint torque from musculoskeletal geometry model, finally to calculate the joint angle, angular velocity by kinematics model. Among these, the signal processing techniques, musculotendon model and kinematics model are very mature: The signal processing is mainly completed by linear envelope or nonlinear dynamics. The musculotendon model is mainly based on Hill model (which uses elastoplastic elements to simulate human muscle, tendon and joints, and uses the relationship of muscle length- force and speed-force to gain muscle force). The kinematic model is based on joint torque to seek motion acceleration and then gets the angular displacement by integration.

Therefore, in the research of Neuromusculoskeletal Interface (NI), the musculoskeletal model is a major factor which restricted the accuracy and stability of the human-robot NI.

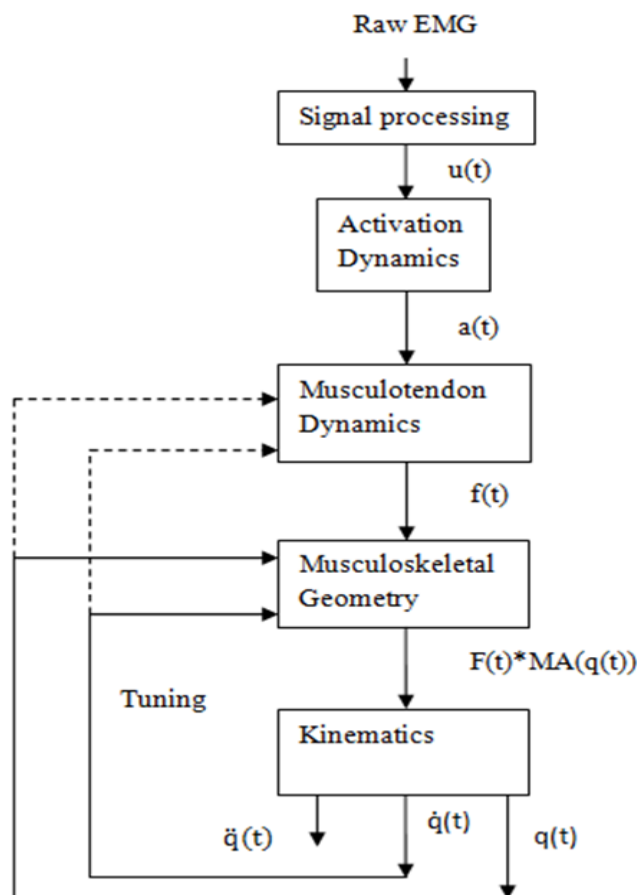


Figure 3.1: Flowchart of EMG-based neuromuscular interface

3.2 Musculoskeletal Geometry Model

In the current studies, there are two main methods to establish the musculoskeletal geometry model.

The first method is to create a large '3D human musculoskeletal platform' by using the computed tomography (CT), magnetic resonance images (MRI) or cadaver colour cryosection (CCC) data, such as SIMM (MusculoGraphics, Inc.), Visual3-D (C-Motion, Inc.), and AnyBody (AnyBody Technology). These platforms modeled the surface of bone in accordance with the actual physical structure of human body, and lined the muscle origin and insertion point by a series of line segments as the muscle path. For example, Koo and Mak analyzed the human elbow flexion and extension movements by OpenSim, and successfully predicted the elbow trajectory with moderate loads [2]. Lloyd et al. used a 3D lower limb musculoskeletal model which was established by Delp and was extended by Buchanan [58, 91], to estimate and predict the ankle joint torque and muscle force [57]. Erdemir et al. analyzed prediction outcomes of three lower limb joints based on musculoskeletal platform [92]. Tang et al analyzed the walking motion based on a systemic 3D musculoskeletal model, and predicted the related muscle force [93]. The advantage of this kind of large-scale data platform model is in line with human physiological structure and to have high precision. However, since they have a large amount of calculation, they are poor in real-time as the human-robot interface.

The other method is to represent the human joint by a single degree of freedom mechanical revolute, and bones and muscles by straight line segments. This kind of model is called 'simplified musculoskeletal model', such as the simplified elbow model in [5, 94-96] and lower limb knee model in [97]. Figure 3.2 was the simplified elbow musculoskeletal model and simplified BRD, BRA path by Murray [98]. JC was the hinge center. The muscular start point and the insertion point formed a straight line. ma was the moment arm. The advantages of this approach are fast calculation and real-time processing. However, the accuracy of the model is not good enough, since it is not close to the human actual physical structure. Also, this kind of model cannot calculate when the line of muscle force crosses the joint center.

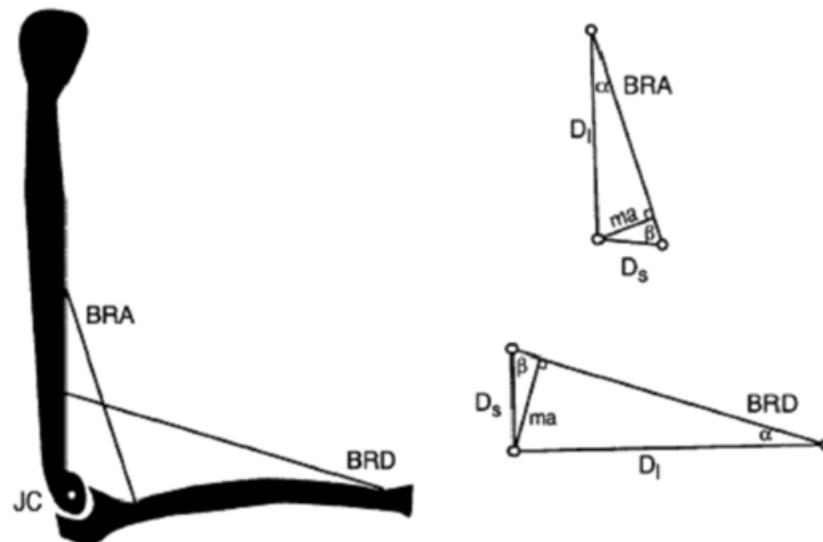


Figure 3.2: Simplified elbow model by Murray [98]

For this reason, this chapter designed a new musculoskeletal model for the human-robot interface, to solve the problems of the existing models. This design took the complexity of the human muscle path into consideration, to make it not only close to the human physiology structure, but also ensure the simple processing requirements of this real-time interface.

This chapter uses the human elbow motion as an example, and the human physiology and anatomy as the theoretical basis, establishes a musculoskeletal model by simplifying the biceps, triceps, humerus, radius and ulna. For the elbow flexion and extension movement, the elbow can be approximated as a single degree of freedom hinge joint. Since the wrist is stationary to the forearm for this movement, the palm and forearm can be simplified as a whole part. To ensure the uniqueness of elbow motion, the shoulder is set immobility, and the upper arm is held naturally saggy. The initial state of the model is: the arms drooping naturally and the palm facing the body side. At the initial state, the angle between the forearm and the extension cord of upper arm is the resting angle.

According to the initial state, the coordinate system of elbow joint model is as follows: Set the sagittal plane as coordinate plane, the elbow center as the origin of coordinates, upper arm as the Y-axis, the angle between forearm and the extension cord of upper arm as joint angle d , and the elbow flexion corresponding to a positive displacement, shown in Figure 3.3.

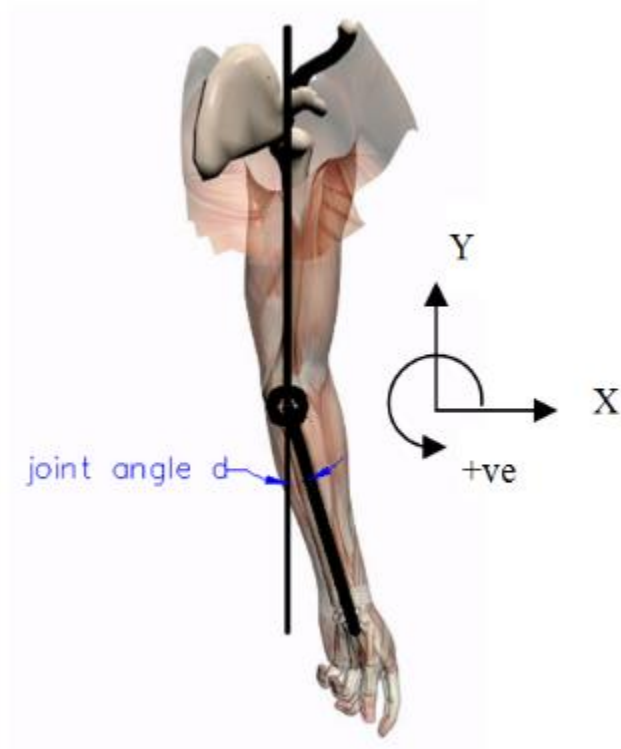


Figure 3.3: Coordinate system of elbow joint model

The musculoskeletal model is established in this coordinate system, shown in Figure 3.4, where A is the shoulder, E is the elbow, the straight line AE is the simplified humerus with defined length as Hum , EF is the simplified forearm (including the radius and ulna) and hand with a defined total length as L_{Arm} . For the elbow flexion and extension movements, biceps and triceps muscles contribute most, so this research only take these two muscle groups as research subjects. Based on the anatomical data, the muscle starting points of biceps and triceps are simplified to point A (shoulder), the attachment points on forearm are respectively B3 and T3, the distances between the attachment points and the elbow joint are respectively defined as U_{bi} and U_{tr} . The insertion points on muscle path are respectively set as B2 and T2, which means the bicep is simplified into segment AB_2 and B_2B_3 , the triceps is simplified as segment AT_2 and T_2T_3 .

The proportion constant of the two segments length of biceps muscle is defined as K_{pbi} , which means $K_{pbi} = \frac{\overline{AB_2}}{\overline{B_2B_3}}$. Also, the proportion constant of triceps path is defined as K_{ptr} , so the $K_{ptr} = \frac{\overline{AT_2}}{\overline{T_2T_3}}$.

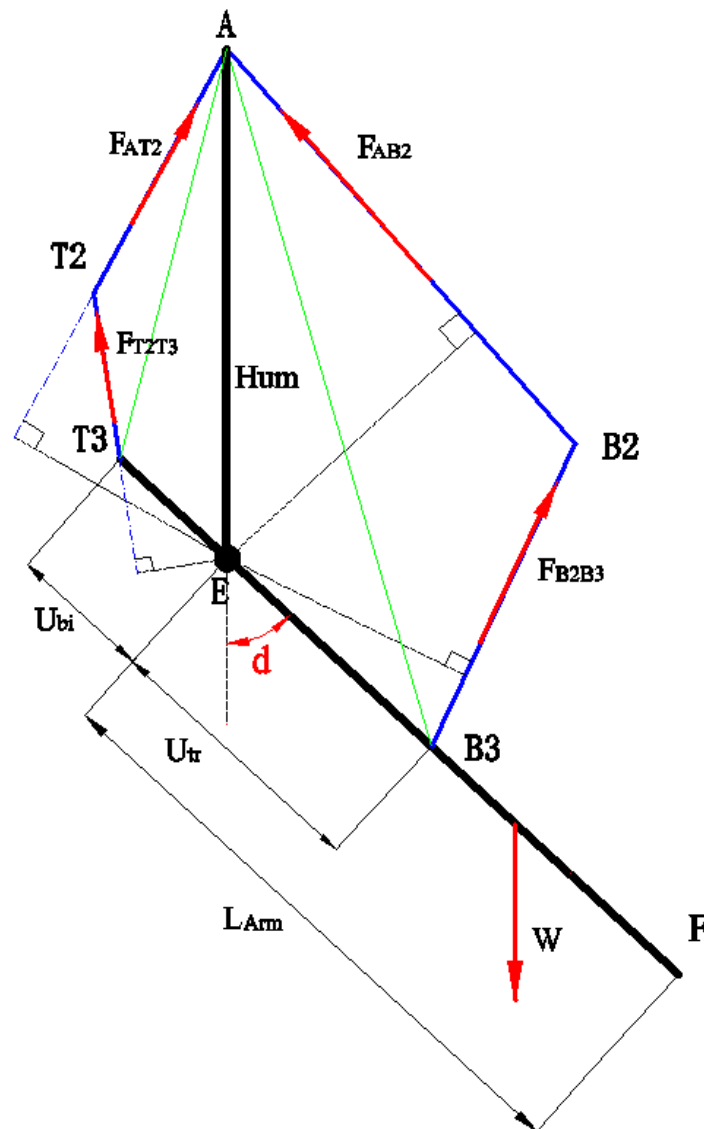


Figure 3.4: Musculoskeletal model of elbow joint. The blue lines are the muscle path, black lines are the skeleton, and dashed line is the moment arm of segmented muscles

Based on the physiological properties of muscle, the assumptions of geometry model are as follows:

1. Suppose point A (connecting humerus with muscle groups) is fixed, point B3 and T3 (connecting the radius and ulna with muscle groups) are changing with individual differences. So the U_{bi} and U_{tr} are individual differences tuning parameters.
2. Suppose during muscles stretching process, the unit length of the muscle changes uniformly, which means the K_{pbi} and K_{ptr} remain intact with the same test subject, and the changes in muscle force and muscle length are proportionally distributed by K_{pbi} and K_{ptr} .
3. Suppose the relative position of muscle path is remains unchanged (α and α_1 are unchanged), shown in Figure 3.5, which means the muscle path only contract during movement,

not bent.

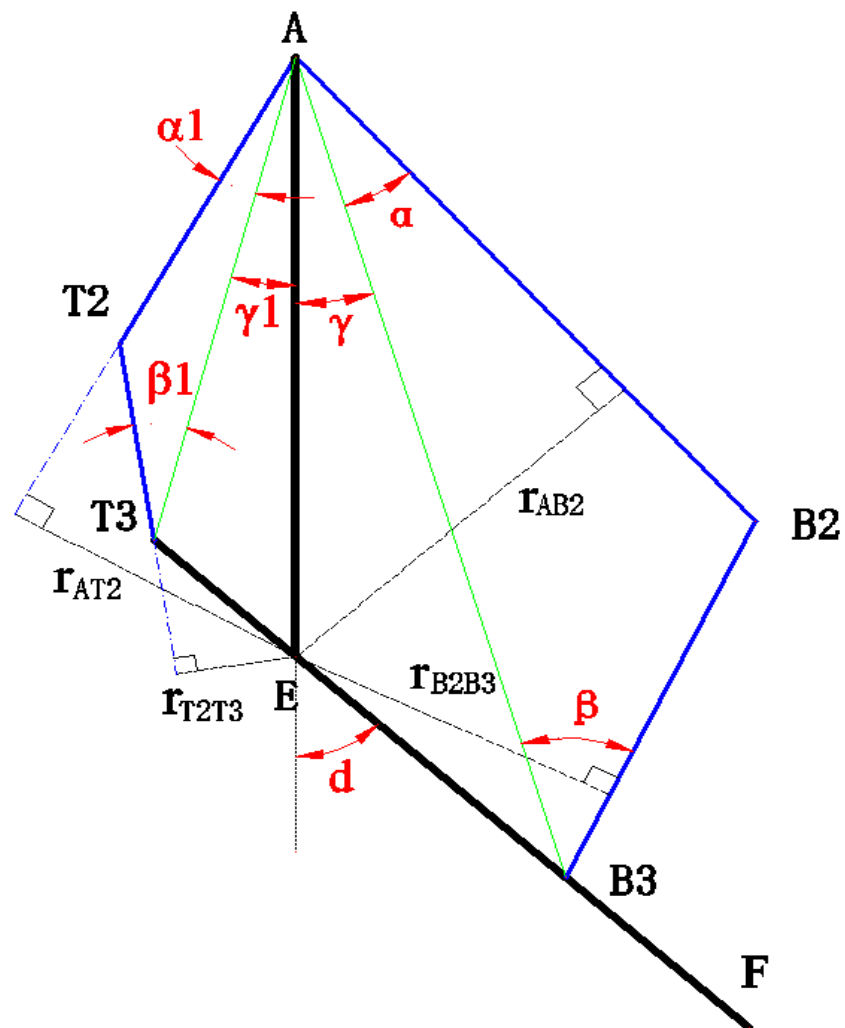


Figure 3.5: Geometry of the musculoskeletal model

The detailed calculation is as follows:

Bicep is simplified into segment AB_2 and B_2B_3 , so the Biceps muscle length (Bilength Length) is calculated as:

$$\text{Bilength} = \overline{AB_2} + \overline{B_2B_3} \quad (3.1)$$

where:

$$\overline{AB_3} = \sqrt{\text{Hum}^2 + U_{bi}^2 - 2 \cdot \text{Hum} \cdot U_{bi} \cdot \cos(\pi - d)} \quad (3.2)$$

$$\sin \beta = \sin \alpha \cdot K_{pbi} \quad (3.3)$$

$$\overline{B_2B_3} = \frac{\overline{AB_3} \cdot \sin \alpha}{\sin(\pi - \alpha - \beta)} \quad (3.4)$$

$$\overline{AB_2} = K_{pbi} \cdot \overline{B_2B_3} \quad (3.5)$$

The moment arms of biceps muscle (r_{AB_2} and $r_{B_2B_3}$):

$$\gamma = \sin^{-1}\left(\sin(\pi - d) \cdot \frac{U_{bi}}{\overline{AB_3}}\right) \quad (3.6)$$

$$r_{AB_2} = \sin(\gamma + \alpha) \cdot \text{Hum} \quad (3.7)$$

$$r_{B_2B_3} = \sin(d - \gamma + \beta) \cdot U_{bi} \quad (3.8)$$

Therefore, the total moment of biceps (M_{bi}) can be summed by the moment of each separate sections:

$$M_{bi} = M_{AB_2} + M_{B_2B_3} = F_{bi} \cdot \frac{1}{K_{pbi} + 1} \cdot (K_{pbi} \cdot r_{AB_2} + r_{B_2B_3}) \quad (3.9)$$

Similarly, for the triceps muscle length ($Trlength$):

$$Trlength = \overline{AT_2} + \overline{T_2T_3} \quad (3.10)$$

where:

$$\overline{AT_3} = \sqrt{\text{Hum}^2 + U_{tr}^2 - 2 \cdot \text{Hum} \cdot U_{tr} \cdot \cos d} \quad (3.11)$$

$$\sin \beta_1 = \sin \alpha_1 \cdot K_{ptr} \quad (3.12)$$

$$\overline{T_2T_3} = \frac{\overline{AT_3} \cdot \sin \alpha_1}{\sin(\pi - \alpha_1 - \beta_1)} \quad (3.13)$$

$$\overline{AT_2} = K_{ptr} \cdot \overline{T_2T_3} \quad (3.14)$$

The moment arms of triceps muscle (r_{AT_2} and $r_{T_2T_3}$):

$$\gamma_1 = \sin^{-1}(\sin d \cdot \frac{U_{tr}}{AT_3}) \quad (3.15)$$

$$r_{AT_2} = \sin(\gamma_1 + \alpha_1) \cdot Hum \quad (3.16)$$

$$r_{T_2T_3} = \sin(d + \gamma_1 - \beta_1) \cdot U_{tr} \quad (3.17)$$

Therefore, the total moment of triceps (M_{tr}) is as follow:

$$M_{tr} = F_{tr} \cdot \frac{1}{K_{ptr} + 1} \cdot (K_{ptr} \cdot r_{AT_2} + r_{T_2T_3}) \quad (3.18)$$

Discussions of this model:

The establishment of this new musculoskeletal model provides a new idea for the muscles path simplification of real-time neuromuscular interface. One or several insertion points can be selected in the muscle path to form the polyline segments muscle path instead of the traditional straight line path. While ensuring the geometry relationship of the same muscle but different segments unchanged, (e.g. the geometry of triangle AB_2B_3 is unchanged), and ensuring the stretching proportion the same (e.g. K_{pbi}), the model can calculate the sub-force, sub-moment arm and sub-moment of each muscle segment to thereby obtain the total joint moment.

Compared with the traditional single muscle line model, this multi-segment model has the following advantages: With the ensuring of operation speed, multi-segment model is closer to the actual human physical structure. When the joint angle $d=0^\circ$, the muscle path of single line model crosses the joint center, which leads the joint torque equal to 0. This multi-segment model can easily solve the 'passing body' issues and expand the calculation of joint angle range to $[-5 \sim 130^\circ]$, which is more consistent with the human actual joint angle range. Also, this simplification has a more accurate result (shown in Section 4.2.4).

3.3 Musculotendon Model

Since muscles, tendons and joints combine into a mechanical redundancy system, muscle force cannot be uniquely determined. In order to forecast or measure the muscle force during motion, a physiological musculotendon model needs to be developed. In recent years, the most representative of musculotendon models are based on the traditional Hill model, Huxley model and rheological

model.

In 1938, Hill first proposed the three-element muscle model: a non-linear contractile element arranged in series with a linear elastic elements, then paralleled an elastic element. It assumes that the contractile elements are truly linear elastic when muscle is stationary and use the length changes to describe the change of muscle force and distribution between elastic and contractile elements[99]. Even though many improvements have been made to adapt to newly discovered muscle structures, the Hill model still contains the limitation that its accuracy is based on a series of assumptions. Without these assumptions, it cannot correctly distribute the muscle force. Also, these models do not consider the factors of neural regulation which means the models cannot be directly used in dynamic situations.

The Hill model contains muscle physical and mechanical properties. However, it still has some limitations. First the transformation from muscle activation to muscle force is not completely understood. Secondly, it is hard to determine muscle–tendon moment arms and the lines of action. There are lots of difficulties with measuring in cadavers, and even harder in a living person accurately. Finally, it is difficult to estimate joint moments, because it is prone to error to accurately obtain the estimates of force from each muscle, and there are seldom standards to verify whether the forces predicted are correct [91].

In 1957, Based on the anatomical structure and physiological contraction of muscles, Huxley proposed a cross-bridge kinetics model, also named as Huxley model, which was combined by cross-bridge and actin-binding [100]. This model expressed the constitutive model of muscle contraction and gave the relationship between tension and speed in microcosmic point. However, the Huxley model is a one-dimensional model and does not take the impact of neural networks into consideration.

The muscle rheological model is a further development of the Huxley model. Different from the Huxley model, it considers the inherent flexibility of each muscle microfilament and uses nonlinear contraction (CE) instead of the cross-bridge. Also, the one-dimensional rheological model is similar to the Hill model, but it only describes the muscle movements within the scope of continuum mechanics and regards the whole muscle as a combination of a series of such rheological models.

Through the way of contraction dynamics, the musculotendon model associates the muscle activation to the musculotendon force as a result. This block simulates muscle as an active tissue, models the interaction between the muscle fibers and the tendon, and considers the mechanical properties of the tendon tissue [101]. This chapter take the musculotendon model similar to the one's of Q. Shao [68],

shown in Figure 3.6. The muscle unit consists of a contractile force element (FCE), passive elastic force (FPE) and viscous force (FVE).

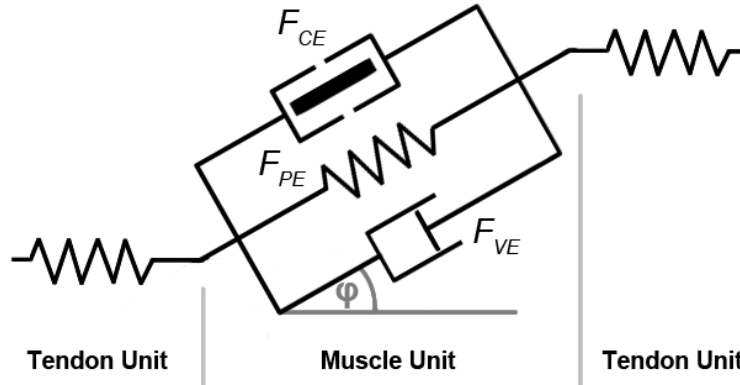


Figure 3.6: Musculotendon model [68]

Since the elbow tendon stiffness is quite high and the length is very short comparing to the muscles, the parameters of tendon can be settled as limited values or simplified as a spring [2, 66, 68, 70]. The total muscle force is the summary of muscle active contractile force (F_{CE}), muscle passive force (F_{PE}) and muscle Viscous force (F_{VE}).

$$F = F_{CE} + F_{PE} + F_{VE} \quad (3.19)$$

Based on other researches, the active contractile force F_{CE} relates to muscular activation $a(t)$, muscle force-length relationship f_l , muscle force-velocity relationship f_v and the maximum muscle force F_{max} [66, 68, 70].

$$F_{CE} = R * a(t) * f_l * f_v * F_{max} * \cos \varphi \quad (3.20)$$

where R is a subject-specific parameter, that is related to muscle size and strength, and φ is the pennation angle of the muscle.

The muscle force-length relationship f_l and muscle force-velocity relationship f_v [6] can be calculated as follow:

$$f_l = 1 - \left(\frac{l_n - 1}{0.5} \right)^2 \quad (3.21)$$

where

$$l_n = \frac{l}{l_{opt}} \quad (3.22)$$

$$f_v = \frac{0.1433}{0.1074 + \exp(-1.409 * \sinh(3.2 * v_n + 1.6))} \quad (3.23)$$

where

$$v_n = \frac{v}{0.5 * v_0 * (A + 1)} \quad (3.24)$$

l is the current muscle length, l_{opt} is the optimum muscle length.

The muscle passive force [66]

$$F_{PE} = F_{Max} * \frac{e^{10 * C_{Pass}(l_n - 1)}}{e^5} * \cos \varphi \quad (3.25)$$

where C_{Pass} is a parameter that allows adjustment to suit subject specific passive elastic properties.

The muscle Viscous force F_{VE} is given by [68]:

$$F_{VE} = F_{Max} * B * v_n * \cos \varphi \quad (3.26)$$

where B is the damping coefficient for the viscosity.

3.4 Kinematic Model

Once the force of each muscle group is calculated, these forces are applied to determine the entire joint torques. If there are some external loads or intersegment dynamics or gravitational forces contributed to the moments, all of these must be summed to calculate the total joint moment [66]. The movement caused by joint moments can be computed by basic dynamics (i.e., Lagrangean or Eulerian dynamics). Also, the equations depend on the number of joints and the number of degrees of freedom at each joint [66].

This method is widely accredited nowadays; however it still has some limitations. Once the joint movement is beyond a simple single-joint one, the equations can become very complex. Also, in order to solve these equations, inertial parameters must be estimated for each of the moving body segments [66].

The damping moment of elbow motion can be calculated as follow:

$$M_p = -\beta\omega \quad (3.27)$$

where β is the damping coefficient of elbow. ω is the angular velocity of the forearm.

The moment caused by forearm and hand gravity can be calculated as follow:

$$M_w = -m \cdot g \cdot \frac{1}{2} L_{\text{Arm}} \cdot \sin d \quad (3.28)$$

where m is the mass of the forearm and hand, g is the gravitational constant, L_{Arm} is the forearm length from elbow joint centre to the ending point.

The total moment of elbow joint is:

$$M_{\text{Tot}} = K_{\text{Bi}} * M_{\text{bi}} - K_{\text{Tr}} * M_{\text{tr}} + M_{\text{P}} - M_{\text{W}} + M_{\text{L}} + O \quad (3.29)$$

where the subscript Bi and Tr stands for biceps and triceps, K_{Bi} and K_{Tr} are the constant representing the error in musculoskeletal model, O is the moment compensation constant. M_{L} is the external load moment. $M_{\text{L}} = 0$, when there is no external load.

For each time step, the angular displacement and angular velocity can be obtained using the following equations:

$$d(t + \Delta t) = d(t) + \omega(t) \cdot \Delta t + \frac{M_{\text{Tot}}}{2I} \cdot \Delta t^2 \quad (3.30)$$

$$\omega(t + \Delta t) = \omega(t) + \frac{M_{\text{Tot}}}{I} \cdot \Delta t \quad (3.31)$$

where $d(t)$ is the angular displacement, $\omega(t)$ is the angular velocity, I is the inertia moment of the forearm and hand, Δt is the sampling period.

3.5 Preliminary Verification of the Neuromuscular Elbow Interface

In order to verify the elbow physiological model developed in this chapter, a simple elbow neuromuscular interface has been used in this section to drive an 1-DOF elbow robot [102]. This 1-DOF interface hardware was developed by Pau and Chen [102] and this thesis connect it to the neuromuscular model in this chapter for the elbow model verification. This verification can also help to evaluate the feasibility of neuromuscular interface and the ability of elbow physiological

model.

3.5.1 A Prototype of Elbow Neuromuscular Interface

The interface was consisted by a printed circuit board (PCB) (includes EMG leads for signal acquisition, amplification and analogue filtering), a STM32F4 Discovery development board (for EMG signal processing, forearm displacement calculation and motor control), and a single DOF joint (with attached motor and rotary encoder for position feedback).

1. Analogue Signal Filtering

The signal acquisition and filter circuits were settled on a PCB by using a standard operational amplifier. Two identical circuits with the same ground were used for the biceps and triceps muscles. The raw EMG signal acquisition and filtering occurs in five stages (Figure 3.7), which are the signal amplifier, high pass filter, precision rectifier, low pass filter and the final amplifier. This PCB board contains all the components to perform the five steps.

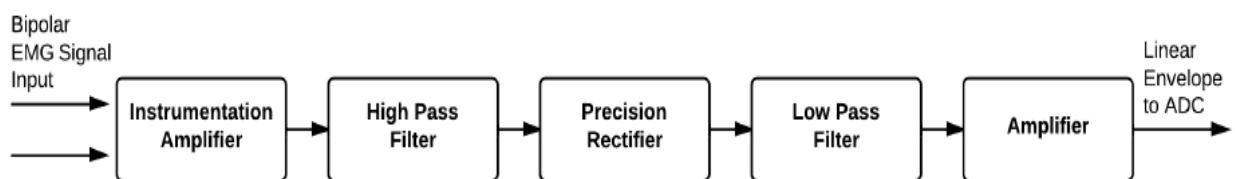


Figure 3.7: Stages in hardware to create a linear envelope from raw EMG signals [102].

2. Microcontroller Implementation

After the EMG signal was filtered at 1200Hz, an STM32F4 Discovery board (STMicroelectronics, Switzerland) was used to acquire and process the signal, in order to calculate the forearm movement angle. The hardware system is shown in Figure 3.8. The elbow physiological model was converted from the Simulink into embedded C to implement on the microcontroller board. The output is an analogue voltage signal of the predicted displacement from the physiological model. A LCD and several push buttons allow the users to easily view and adjust the model parameters.

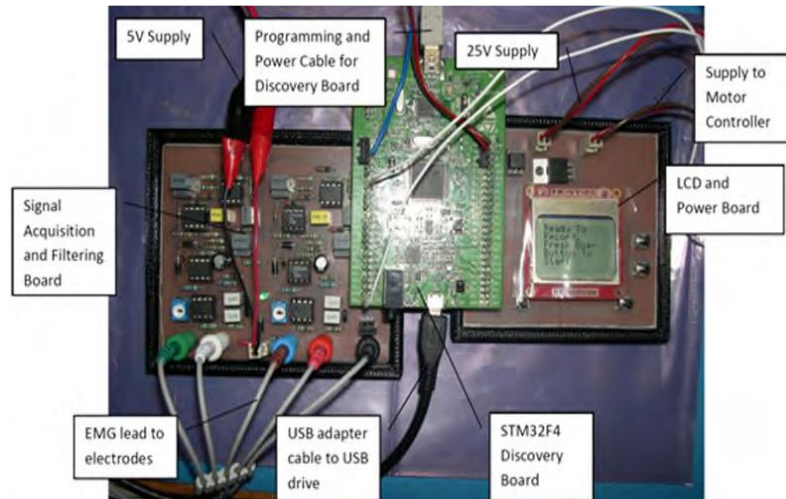


Figure 3.8: The neuromuscular interface hardware system [102].

3. A SDOF Elbow Joint

A simple single degree of freedom (SDOF) was used to represent the elbow joint and rapidly prototyped using a 3D printer, shown in Figure 3.9. Its joint is actuated by a 25V DC motor (driven by a LSC30/2 motor driver from Maxon, Switzerland). The forearm component rotates while the upper arm was fixed as a base. A rotary potentiometer with a closed loop control system was used to keep tracking the rotation joint. The joint can move over a -20° to 150° . A proportional controller was put in the prototypes to manage the feedback data from the potentiometer, and to adjust the input of motor driver based on the reference signal from neuromuscular model. The flowchart is shown in Figure 3.10. EMG signal was firstly detected and filtered as the input of the neuromuscular interface. With the calculation of musculotendon model, musculoskeletal model and kinematic model, the interface predicted the joint angle. Then the angle was compared with the measured position from rotary potentiometer. Finally, the compared result was used to control the SDOF through a motor controller.

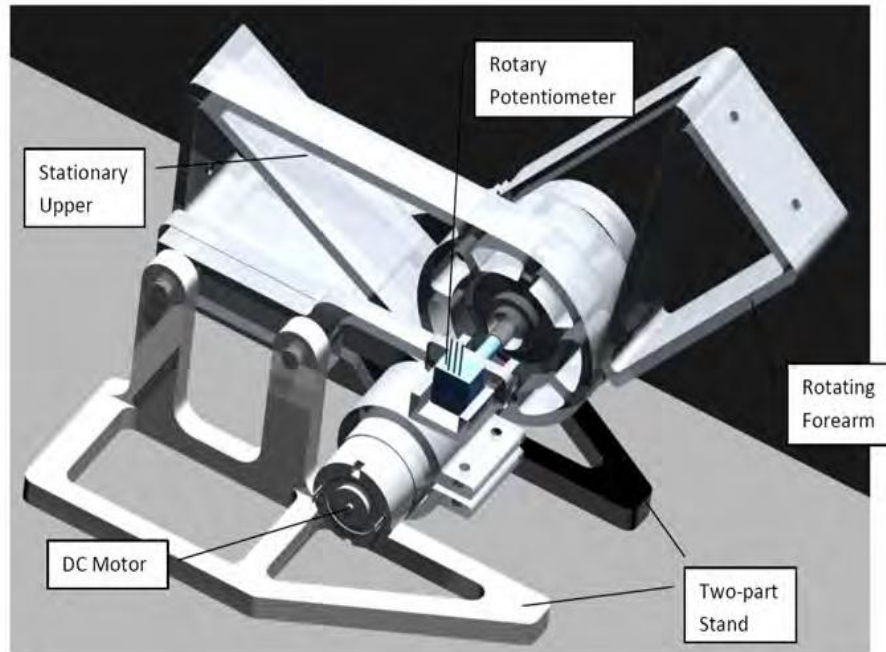


Figure 3.9: Single degree of freedom representation of the elbow joint [102].

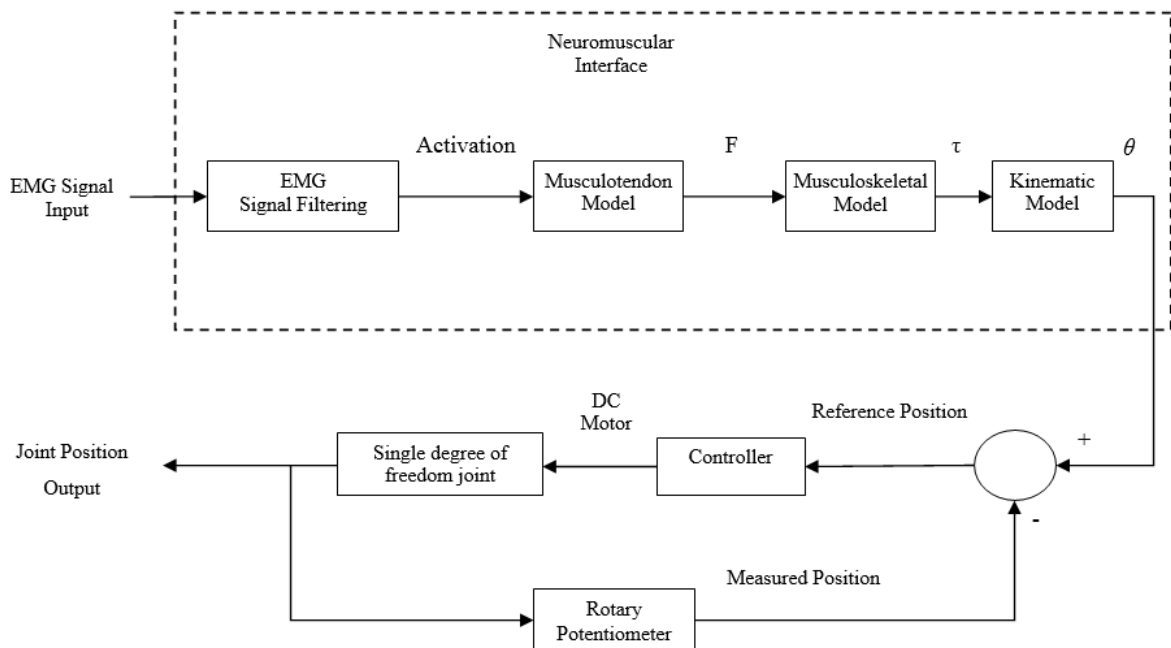


Figure 3.10: Neuromuscular interface and single degree of freedom joint in a closed loop system.

3.5.2 Preliminary Verification of Elbow Neuromuscular Interface

Raw sEMG data from one subject was tested as the input for the preliminary verification. The sEMG signal was recorded with the g.USBamp, and the elbow joint position output from SDOF were compared with the measured angles from the Polaris system (In details in Section 4.2.1). Three types of movements for elbow flexion and extension were tested: a) A single cycle full range flexion-extension movement from nature position, b) continues multi cycles and full range movement from nature position, c) random movement from any position.

The SDOF output results (which was also the interface predicted movement results) and the measured actual angle results are compared in Figure 3.11-3.13 (a). Also the absolute value of errors between them is shown in Figure 3.11-3.13 (b). Figure 3.11 is one of the results in single cycle elbow flexion and extension movement. It shows the changes of measured angle (red line) and predicted angle (blue line) during 7 second moving time. The root mean square error (RMSE) is 13.3768. During a simple flexion and extension, the model is accurate in the beginning and end, but has a larger error in the wave peak (the elbow angle close to 135°). Figure 3.12 shows the result of continues cycle test, and its RMSE is 17.7737. During continues movement, the problems in model accuracy starts to appear. The main error still occur at the limit position (wave peaks). And in Figure 3.13, the elbow is in random motion. The trend of predicted movement can still follow the measured angle, however the accuracy is hard to be guaranteed. Its RMSE is 18.3193.

By comparing all the results, it is clear that the model prediction is broadly in line with the movement trends. It means elbow interface and SDOF control system can approximately predict the subject's movement. However, the accuracy of prediction is not good, especially in random movement. The main reasons for this deviation are because that the model parameters cannot perfectly match the collected sEMG and cannot catch up with the individual differences from different experiment subjects. In order to improve the model's accuracy, the parameters need to be further analyzed and tuned to better fit the individual differences.

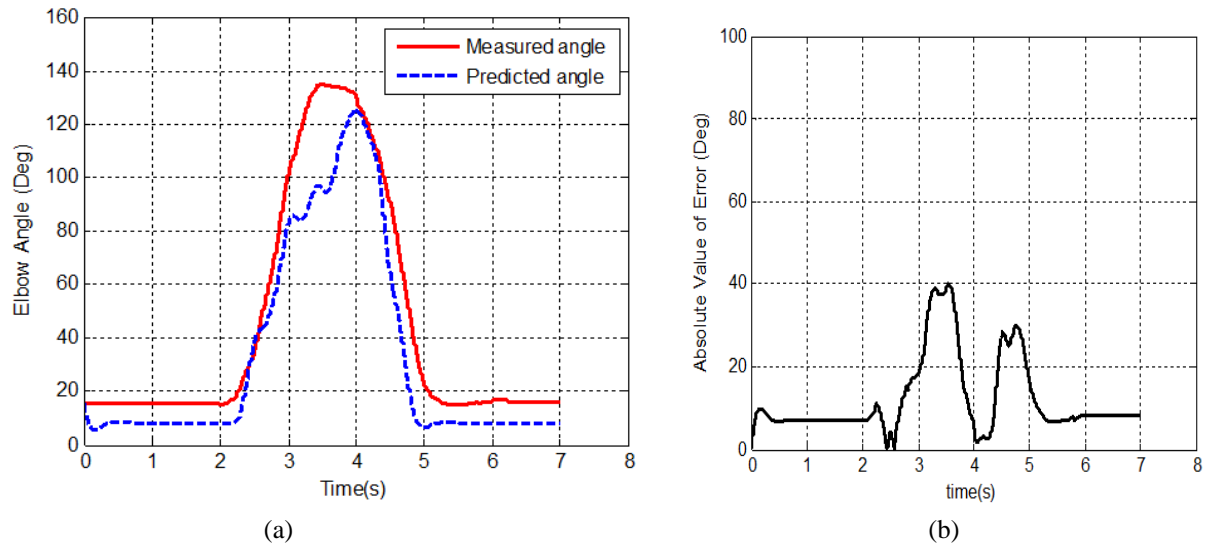


Figure 3.11: Preliminary result of elbow single cycle flexion and extension (a) predicted angle and measured angle of elbow joint (b) the absolute errors between them

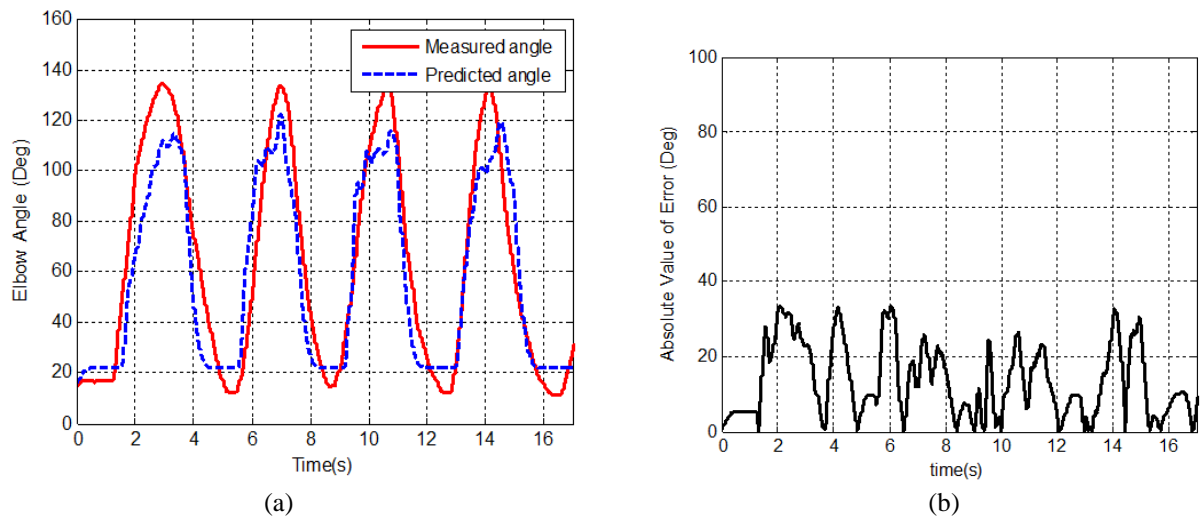


Figure 3.12: Preliminary result of elbow continues cycle flexion and extension (a) predicted angle and measured angle of elbow joint (b) the absolute errors between them

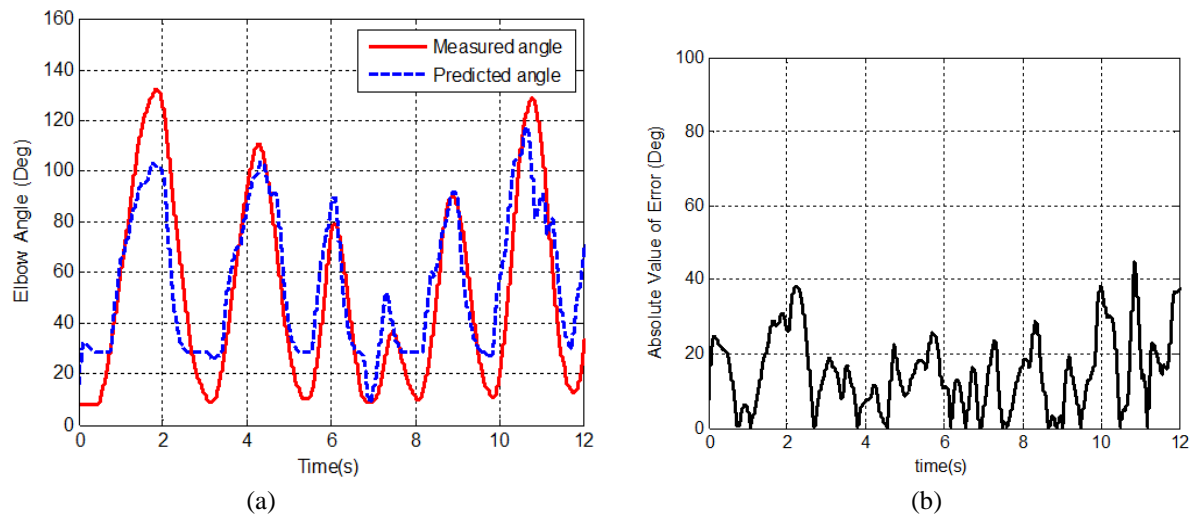


Figure 3.13: Preliminary result of elbow random movement (a) predicted angle and measured angle of elbow joint (b) the absolute errors between them

3.6 Model Parameters

The previous sections of this chapter have described the musculotendon model, musculoskeletal model, kinematic model of elbow joint and the periodical result. The models include a number of personalization parameters. They provide the deformability and adaptability of model to better fit the individual characteristics. Based on the structure of the model, the parameters can be divided into two kinds: the ones without physical significance (such as gain, error coefficient, etc.), and the ones with physiological significance (such as muscle parameters, etc.). The accuracy of anatomical data greatly impacts the accuracy of model.

The EMG-driven model has 23 feature parameters. Table 3.1 lists the symbols, belonging models, their definitions and physiological ranges of these 23 parameters. The physiological ranges are either from direct anthropometry, or anatomy and physiology literatures. The most important model parameters include: optimum muscle length (l_{opt}), tendon slack length (L_{Ts}), pennation angle (θ), maximum muscle force (F_{max}) and the musculoskeletal parameters related to moment arm (MA). The accuracy of movement prediction is particularly sensitive to these parameters.

The parameters about muscle force in Holzbaaur's model [103] were obtained from test. The optimal fiber length was renormalized to an optimal sarcomere length of 2.2–2.8 μm . The optimal sarcomere length was consistency. F_{max} is the product of physiological cross-sectional area (PCSA) and a particular stress. The PCSA of each muscle is the muscle mass divided by the generalized optimal fiber length. In Holzbaaur's model, the specific tension 45N/cm² was used on forearm and

hand muscles, 140 N/cm^2 was on elbow and shoulder muscles. The tendon slack length cannot be measured directly, its choice needs to match the operation length of the muscle, and the individual measurements of active and passive muscle moment. The selection of tendon slack length is related to the muscle tendon length from the estimates of cadavre research. Garner and Pandy [104] chose another method of determining the muscle parameters. They use optimization algorithms to select muscle parameters from the predefined physiological limit parameters. Although this approach may be effective, but it is also possible to lead unknown error into the all parameters of the system. Optimal fiber length, tendon slack length, and pennation angle can be measured from cadaver studies [91]. Among these three, the tendon slack length is the most difficult one to measure, but it can be unlimited approximated using a numerical method [105].

There are some inertial parameters of human body, such as the quality, centroid position and the rotation inertia of each body segment. They are the basic parameters of musculoskeletal biomechanics research. These parameters can be derived from statistical formulas. And the variables in these formulas are actually the physiological parameters, including age, gender, height and weight.

Furthermore, the age-related model parameters includes: isometric strength, force-velocity relation, active force-length relation, passive force-length relation, activation dynamics, tendon stiffness and so on [106].

These parameters in the model need to be tuned to accommodate individual variations so that the interface can be used by different patients. The tuning process requires a defined objective function and a search algorithm to minimize the error. By using nonlinear optimization, Buchanan reduced the chances of converging to a local minimum [91]. Also, some researches, such as [97], provided experimental values and scope of muscle length and joint angles. Though, the more parameters have been used, the better adaptation between estimated and measured joint moments has been achieved. But too many parameters may not be good [66]. For example, some parameters have limited predictive abilities. By choosing too many this kind of parameters, the model will be ‘overfit’ [107].

The Section 4.1 discusses the model parameter sensitivity analysis, which lays the foundation for parameter tuning. Section 7.2 describes the parameter tuning algorithm.

Table 3.1 The summary of all the tunable parameters in neuromusculoskeletal model.

Belonging model	Parameter	Definition	Physiological limitation	Physiological range [68, 108-110]	Unit
Musculotendon Dynamics Model	R_{bi}, R_{tr}	User-specific coefficient for muscle size	Yes	Specific by users	—
	$L_{opt_{bi}}, L_{opt_{tr}}$	Optimal fiber length	Yes	0.15-0.35	m
	L_{Ts}	Tendon slack length	Yes	0.15-0.3	m
	ϕ_{bi}, ϕ_{tr}	Pennation angle	Yes	$\phi_{bi} = 0^\circ$ $\phi_{tr} = 9 - 12^\circ$	$^\circ$
	$F_{max_{bi}}, F_{max_{tr}}$	Maximum muscle force	Yes	0.5-1.5	kN
	B_{bi}, B_{tr}	User-specific coefficient for viscosity	Yes	0.05-0.15	Ns/m
	$C_{pass_{bi}}, C_{pass_{tr}}$	User-specific coefficient for elasticity	Yes	1~6	—
Musculoskeletal Geometry Model	Hum	Length of humerus	Yes	From anthropometry	m
	U_{bi}, U_{tr}	Muscle attachment distance to joint center	Yes	From anthropometry	m
Kinematics model	K_{bi}, K_{tr}	User-specific skeletal error coefficient	None	Specific by users	—
	β	Overall damping coefficient	Yes	$\beta = 0.1 - 0.5$	Nms/rad
	O	Moment compensation constant	None	0-1	Nm
	d_r	Resting angle	Yes	$5-15^\circ$	$^\circ$
	L_{Arm}	Length of forearm	Yes	From anthropometry	m
	m	Mass of forearm and hand	Yes	From anthropometry	kg

Parameters in Table 3.1 are sorted by the model it owns. Wherein the subscript bi represents biceps, tr represents triceps.

3.7 Chapter Summary

This chapter has developed an EMG-driven physiological model of elbow joint, which includes the

Hill-type musculotendon model, a musculoskeletal geometry and a kinematics model to predict the elbow movement. In the previous simplified musculoskeletal geometry model of elbow, the muscle is simplified as a line from starting point to the attaching point. This leads to the following problems: First, the model's accuracy is poor, especially when the forearm moves randomly. Second, this model is not based on human actual physical structure, it cannot calculate the situation when muscle force lines cross the joint. This chapter designs a new musculoskeletal model, based on the anatomical data. It simplifies the biceps and triceps muscles to two-segments-polyline from muscle starting point, through insertion point, to the attachment point, and reasonable assumptions are built based on the physiological properties of muscle. This design solves the above problems of the prior models and still keep the advantage of real-time.

EMG-driven model includes many personalized parameters. They provide a better deformability and adaptability of model to the individual characteristics. From a preliminary verification, based on the comparison results between a SDOF elbow joint output and measured actual joint angle, the feasibility of the model has been proved, but also, the gaps in model accuracy has shown as well. In order to improve the elbow model, the parameters need to be further analyzed and tuned. This chapter basically analyzes some of the main parameters and their determining methods, and details the ranges of 23 elbow physiological parameters. This lays the foundation to the sensitivity analysis of model parameters and the parameters tuning.

Chapter 4 Feasibility Analysis and

Validation of the Elbow Model

Based on the preliminary test of the elbow neuromusculoskeletal model in Chapter 3, there are some urgent requirements for tuning the model parameters to improve the model accuracy and to adapt to individuals. Before that, a sensitivity analysis must be completed in order to reduce the number of parameters used in the tuning. This chapter establishes a new sensitivity analysis method of model parameters. Based on the analysis results, all the parameters have been grouped for further treatment. This chapter also describes the method of EMG signal processing, which is to extract the muscle activation by linear envelope and nonlinear dynamics. By designing multi subjects and multi movement's experiments for elbow joint, the elbow neuromusculoskeletal model and proposed signal processing methods are further and fully validated.

4.1 Parameter Sensitivity

4.1.1 Background

Chapter 3 has introduced an EMG-based physiological musculoskeletal model for elbow joint. In this model, there are lots of parameters whose values are mainly from anatomical experiments or literatures. These parameters are listed in Table 3.1. Since the impact of these parameters to the model is not clear and their values directly affect the accuracy of prediction result, therefore, a parameter tuning model needs to be established to ensure the reliability of the model and adaptability to specific individuals. In order to reduce the number of online tuning parameters and ensure the real-time property of the system, a sensitivity experiment is set up in this section to evaluate the parameters sensitivity to the model.

In the current publications, parameter sensitivity studies to neuromuscular model were limited, especially for the number of analyzed parameters was quite few. The existing literatures were mainly

focusing on the impact of general musculotendon parameters sensitivity [111-114] to model, but lack of the impact of muscle-skeleton parameters. Secondly, most of the existing researches were based on human lower limb model and its parameters [111-113]. For example, Scovil and Ronsky analyzed the muscle force in human running and walking and motion simulation [111]. Groote et al. assessed five main parameters sensitivity to Hill model in gait dynamic simulations [112]. Redl et al. only studied three muscle parameters sensitivity: optimal muscle-fiber length, muscle physiological cross-sectional area (PCSA), and tendon rest length [113]. Garner and Pandy also estimated three muscle parameters of upper limb: peak isometric force, optimal muscle-fiber length, and tendon slack length [114].

For the assessment methods, an earlier and standardized sensitivity analysis method has been employed [115-117]. It defined that the sensitivity was the normalized output change divided by normalized parameter change. However, the method could only be used in evaluating individual output, not in multi-outputs (such as running and walking) [111]. Another method was to calculate the partial derivative of the muscle equations with respect to each model parameter [115, 118]. This method could provide a continuous state over time and parameter change, but it required the calculation formula to be simple and well known, so it could not suit the complex human physiological model or a large number of numerical solution [111]. To date, some new sensitivity assessment methods are gradually applied, such as static optimization [113], summed cross-sensitivity [113], local and global assessment method [119], and so on. However, these methods were not commonly used in bio-complex structure, and did not meet the individual adaptive needs of interface model. Therefore using one single assessment method may easily cause the one-sidedness of parameter analysis and incomplete understand of parameter properties.

Disagreements also existed between the sensitivity results of different studies. Such as the compliance parameter sensitivity to Hill model in the series elastic unit and the maximum muscle force sensitivity to simulation result had arguments in literatures [111, 120-122]. Such sensitivity variation may be due to the usage of different models, or different movement [111], or the subjects' individual characteristics (like age or muscle active level) [113]. In this case, besides the sensitivity level (high or low) analysis, parameter properties (individual difference or action difference) are also need to be classified, to achieve a comprehensive understanding of the model parameters

Based on the limitations of current researches and the variability in reported sensitivity results, This thesis improved the standard sensitivity assessment method by Lehman and Stark [115], and built a new three-step layered approach to assess 19 parameters sensitivity to the neuromusculoskeletal model in elbow flexion and extension simulation.

4.1.2 Experimental Setup for Sensitivity Analysis

Six subjects (3 male and 3 female) were chosen to join this experiment. They were asked to achieve three kinds of elbow joint motion. Each motion needed to be repeated five times. Then the EMG signals of biceps and triceps and the joint actual movement angles were recorded. The detailed trial is explained as follow:

- Single cycle fully flexion and extension: The subjects were asked to fully flex and extend his arm with a natural speed from a relaxing position.
- Continuous cycle fully flexion and extension: The continuous cycle test required the subjects to keep fully flexing and extending with a natural speed for 20 seconds.
- Variable motion: The variable motion test required the subjects to flex and extend continuously in different ranges and speed. The movement continued about 20 seconds.

4.1.3 Sensitivity Analysis Method

The sensitivity analysis has two main purposes: First, to determine which parameters affect the accuracy of model prediction; the second is to analyze whether these parameters sensitivities are affected by different individuals or different actions. To achieve these two objectives, we designed a three-step layered approach. The first step is to determine the sensitivity level of each parameter to the model by offline and none signal quantification calculation. The second step is to use the same subject but different motions to compare the differences in model's prediction result. This step can analyze the action difference of parameters. The third step is to change the subjects (with different age, gender and muscle activity) to compare the individual difference of parameters.

1.Non-Signal Quantization Layer (NSQL)

This is a preliminary layer for model parameters. The model runs without human EMG data and the normalized muscle activation is fixed as a constant value (0.05) to compare the differences in prediction results (Figure 4.1 (A)). The sensitivity rate is calculated in Equation (4.1):

$$S_{nonP} = \frac{(D_{P_{n+1}} - D_{P_n})/D_{P_n}}{(P_{n+1} - P_n)/P_n} \quad (4.1)$$

Where P_n is the n-th (from small to big) value of parameter P in its biological range. D_{P_n} is the predicted angle output of the model when parameter P gets to P_n . S_{nonP} is the sensitivity rate

when parameter P changes, and it is the proportional change in normalized output divided by normalized parameter and it represents the effect of this parameter sensitivity to the model.

2. Action Difference Analysis (ADA)

On the basis of NSQL, 19 tunable parameters are analyzed through action prediction test (Figure 4.1 (B)). By inputting a subject's EMG signal from three experiments to the model, the RMSE (root-mean-square error) between predicted joint angle and actual joint angle is recorded with the changes of parameter. Also, the sensitivity rate is used as a quantified comparison of this RMSE change. The calculation is in Equation (4.2) and (4.3):

$$\text{RMS} = \sqrt{\frac{1}{j} \sum_j (D_{\text{pred}} - D_{\text{actu}})^2} \quad (4.2)$$

$$\text{Smov}_P = \frac{(\text{RMS}_{P_{n+1}} - \text{RMS}_{P_n})/\text{RMS}_{P_n}}{(P_{n+1} - P_n)/P_n} \quad (4.3)$$

where D_{pred} and D_{actu} are the predicted and actual measured angle sequence, RMS stands for the root mean square, j is the number of sample angles, and Smov_P is the sensitivity ratio of parameter P.

3. Individual Difference Analysis (IDA)

Some individual parameters have great impact on model's output only when changing the subject, but have lower sensitivity with the same subject doing different movements. These parameters only need to be measured or offline tuned before the test start or replace interface users. This can not only guarantee the model suitability for individuals, but also reduce the number of real-time tuning parameters. In order to separate the individual parameters, a sensitivity test is done as follow: input the EMG signals of 'continuous cycle movements' from subjects A, B and C; then change the value of adjustable parameters (within the physiology range) and calculate the differences in RMS (by the same flowchart in Figure.4.1 (B).); finally, count the sensitivity rate of parameters by Equation (4.4).

$$\text{Sind}_{AP} = \frac{(\text{RMS}_{AP_{n+1}} - \text{RMS}_{AP_n})/\text{RMS}_{AP_n}}{(P_{An+1} - P_{An})/P_{An}} \quad (4.4)$$

where the subscript A represent the individual subject A.

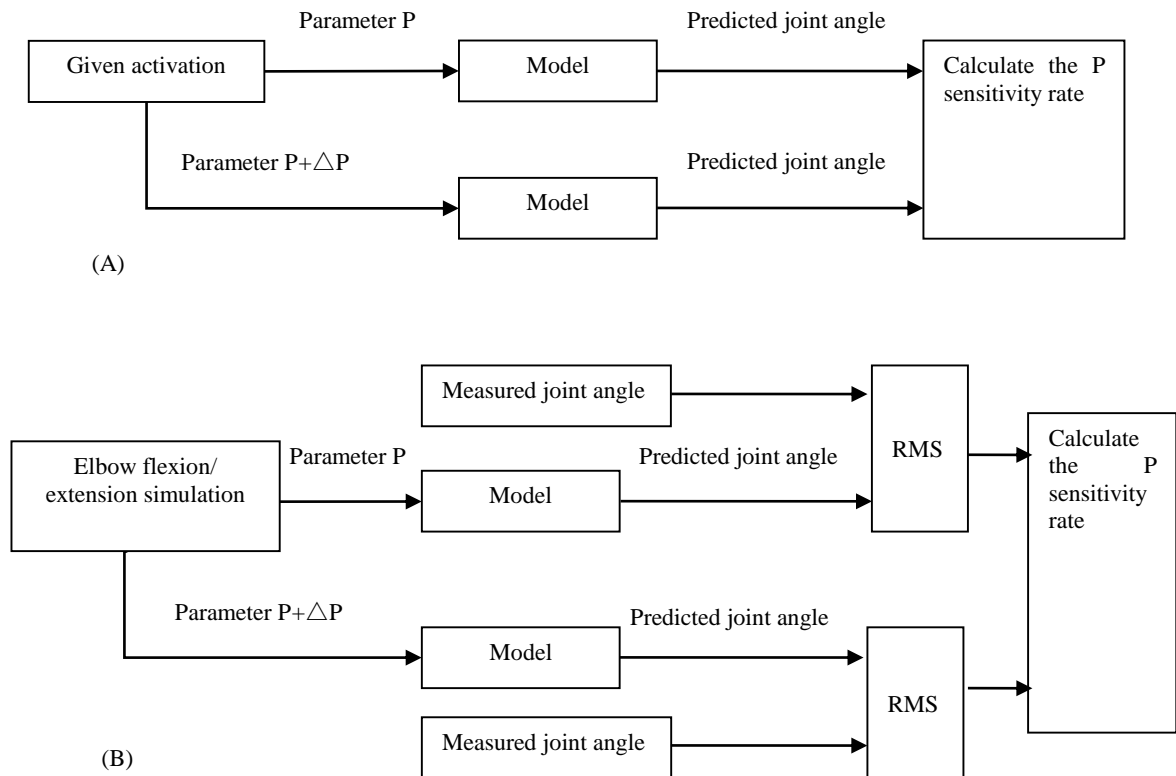


Figure 4.1: Model sensitivity evaluation methods. (A) With settled muscle activation (NSQL). (B) Movement simulation which include ADA and IDA

4.1.4 Sensitivity Analysis Results

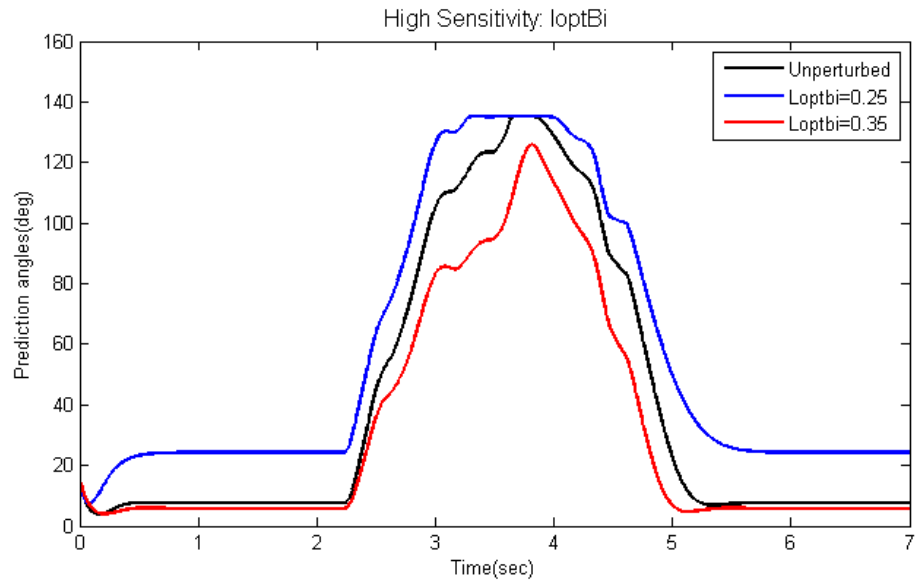
The elbow physiological model has been programmed by Simulink (Matlab), to obtain predicted joint angle. In the sensitivity analysis, the output value of the original model should be firstly determined. Then, the specified parameter is adjusted. The model runs two time steps to get the result with new parameter after change. Based on the method in Section 4.1.3, 19 tunable parameters (listed in Table 4.1), which are the most impact ones to the model, are analyzed. The results are as follows:

The first step of sensitivity analysis (with given activation) excludes the impact of activation degree to the predicted results, so as to make the change of model parameters as the only factor in results changing. Parameters, according to their sensitivity rates, have been divided into high level ($S_{non_p} > 1$), low level ($1 > S_{non_p} > 0.1$), and extremely low level ($S_{non_p} < 0.1$). The sensitivity rates of the 19 tunable parameters are shown in Table 4.1. From the result, we could see the $Lopt_{bi}$, Hum , K_{bi} , $Lopt_{tr}$, and so on are the most sensitive parameters, and C_{passtr} , and B_{tr} are the least sensitive ones.

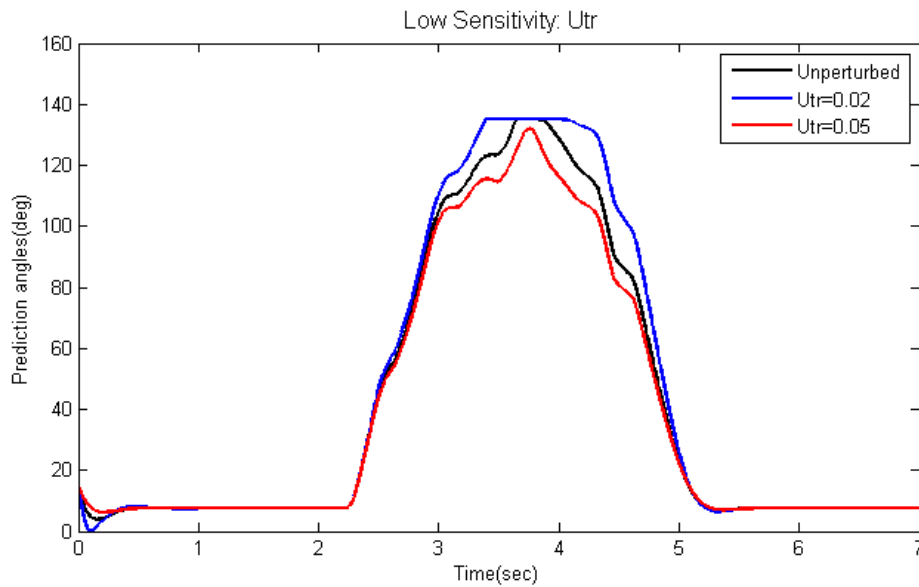
Table 4.1 Sensitivity rates and layer of 19 tunable parameters

Parameters	Range in trials	Sensitivity rates	Sensitivity layer
$Lopt_{bi}$	0.15-0.35	16.0453	High (8)
Hum	0.2-0.28	6.1995	
K_{bi}	0.1-1.9	4.3958	
$Lopt_{tr}$	0.25-0.35	3.4768	
C_{passbi}	1-3	2.9388	
U_{bi}	0.03-0.08	1.9900	
R_{bi}	1-3	1.2270	
F_{maxbi}	1000-1500	1.1348	
m	1-3	0.8839	Low (9)
R_{tr}	1-3	0.7369	
K_{tr}	0.1-1.9	0.7182	
L_{Arm}	0.3-0.5	0.6315	
U_{tr}	0.02-0.06	0.4050	
β	0.1-0.5	0.3157	
O	0-1	0.2174	
F_{maxtr}	1000-1500	0.1699	
B_{bi}	0.05-0.15	0.1403	
C_{passtr}	1-3	0.0795	Extremely low (2)
B_{tr}	0.05-0.15	0.0440	

The parameters listing order in Table 4.1-4.4 is based on the descending order of their off-line sensitivity rates. Changes in the model prediction result caused by parameters from different sensitivity layer are shown in Figure 4.2. Figure 4.2 (A) is the changes of predicted angle during a single cycle elbow flexion and extension movement. With different value of $Lopt_{bi}$, the angle wave change is obvious, which means the $Lopt_{bi}$ is a high sensitivity parameter. Figure 4.2 (B) is the angle change with different value of U_{tr} . As U_{tr} is a low sensitive parameter, the angle wave does not change much. From the Figure we could visually see the different effect of different parameters on model properties.



(A)



(B)

Figure 4.2: Single cycle flexion and extension movement angle with different parameter value. (A) The predict result with high sensitive parameter $Lopt_{tr}$. (B) The result with low sensitive parameter U_{tr}

Table 4.2 shows the results of Action Difference Analysis (ADA). For comparison purposes, all the values of sensitivity rate are normalized between 0-1. The sensitivity rates of $Lopt_{tr}$, R_{bi} , B_{bi} , C_{passtr} and B_{tr} change a lot in all kinds of movements, which shows that they are significant Action Difference Parameters. The sensitivity rates of some other parameters, such as F_{maxbi} , L_{Arm} , U_{tr} , β , F_{maxtr} have a mutation only for some special movement, so they do not belong to Action Difference Parameters, they still need to be taken more care of during tuning.

Table 4.2 Sensitivity rates of 19 tunable parameters in different actions

Parameters	Settled activation	Single cycle fully flexion and extension	Continuous cycle fully flexion and extension	Variable motion
$Lopt_{bi}$	0.8023	0.8226	0.8957	0.8213
Hum	0.3100	0.7994	0.7734	0.7147
K_{bi}	0.2198	0.1467	0.0864	0.0682
$Lopt_{tr}^*$	0.1738	0.9028	0.0256	0.0026
C_{passbi}	0.1469	0.1620	0.1862	0.2320
U_{bi}	0.0995	0.3068	0.2080	0.1780
R_{bi}^*	0.0614	0.1274	0.0084	0.0013
F_{maxbi}	0.0567	0.1527	0.0867	0.0676
m	0.0442	0.1420	0.0906	0.0788
R_{tr}	0.0368	0.0140	0.0444	0.0333
K_{tr}	0.0359	0.0250	0.0490	0.0321
L_{Arm}	0.0316	0.1465	0.0906	0.0780
U_{tr}	0.0203	0.1060	0.0077	0.0041
β	0.0158	0.0202	0.0160	0.0043
O	0.0109	0.0304	0.0346	0.0359
F_{maxtr}	0.0085	0.0271	0.0075	0.0043
B_{bi}^*	0.0070	0.0201	0.0009	0.0005
C_{passtr}^*	0.0040	0.0701	0.0003	0.0004
B_{tr}^*	0.0022	0.0001	0.0014	0.0005

The parameters with * in the table are the ones with large variation in different actions.

Through the third step (IDA), the sensitivity rates of each parameter to different subjects are listed in Table 4.3. In general, Hum, $Lopt_{tr}$, C_{passbi} , F_{maxbi} , U_{tr} , F_{maxtr} and C_{passtr} are the Individual Difference Parameters.

Table 4.3 Sensitivity rates of 19 tunable parameters in different subjects

Parameters	Subject A	Subject B	Subject C
$Lopt_{bi}$	0.8710	0.8438	0.8518
Hum *	0.8464	0.7057	0.6882
K_{bi}	0.1553	0.1411	0.2202
$Lopt_{tr}$ *	0.9559	0.4970	0.4970
C_{passbi} *	0.1715	0.1179	0.0990
U_{bi}	0.3249	0.2239	0.2211
R_{bi}	0.1349	0.0931	0.1461
F_{maxbi} *	0.1616	0.1410	0.2127
m	0.1503	0.1418	0.1956
R_{tr}	0.0149	0.0183	0.0645
K_{tr}	0.0265	0.0175	0.0626
L_{Arm}	0.1551	0.1428	0.1890
U_{tr} *	0.1122	0.0363	0.0181
β	0.0213	0.0395	0.0277
O	0.0322	0.0239	0.0503
F_{maxtr} *	0.0287	0.0051	0.0160
B_{bi}	0.0213	0.0380	0.0072
C_{passtr} *	0.0743	0.0163	0.0013
B_{tr}	0.0001	0.0003	0.0003

The parameters with * are the ones with large variation in different subjects.

4.1.5 Discussion

Based on the results of above three steps of analysis, the parameters can be analyzed as follows:

Optimal fiber length $Lopt_{bi}$ and $Lopt_{tr}$

These two parameters have shown high sensitivity in all the above tests. It is the similar result with the conclusion by [111, 122, 123]. The sensitivity rate of $Lopt_{bi}$ was the highest one in offline test and two action tests. Also, it stayed in high level during a wide range of $Lopt_{bi}$. in Figure 4.3 (a-c).

The sensitivity of $Lopt_{tr}$ showed a large variations (0.1738, 0.9028, 0.0256, 0.0026) in ADA, which

certifies $Lopt_{tr}$ as an Action Difference Parameter. At the same time, in IDA test, it still showed a large change of sensitivity (0.9559, 0.4970, 0.4970), which means $Lopt_{tr}$ is also an Individual Difference Parameter. Based on Figure 4.4 (a-c), it only had a larger mutations in the start, but the sensitivity had gradually leveled off followed by the progress of action.

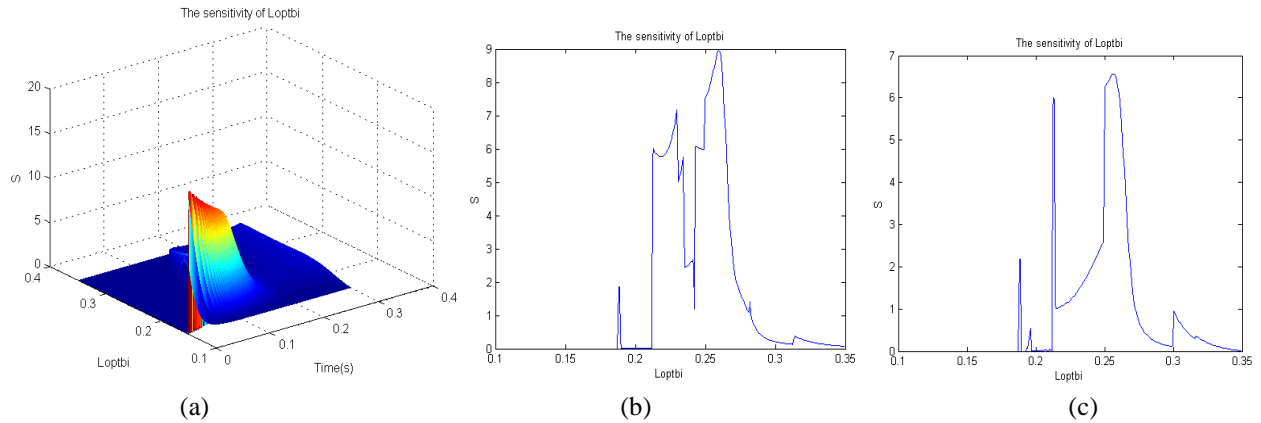


Figure 4.3: The sensitivity of $Lopt_{bi}$

(a) The sensitivity of $Lopt_{bi}$ during NSQL test, it changed over time (corresponding joint Angle) and the physiological range of parameter. (b) The sensitivity of $Lopt_{bi}$ during 'Continuous cycle' movement test over the change of parameter. The peak was 8.9568 (without normalization)/ 0.8957 (with normalization). (c) The sensitivity of $Lopt_{bi}$ during 'Variable motion' test. The peak was 6.5702 (without normalization)/ 0.8213 (with normalization).

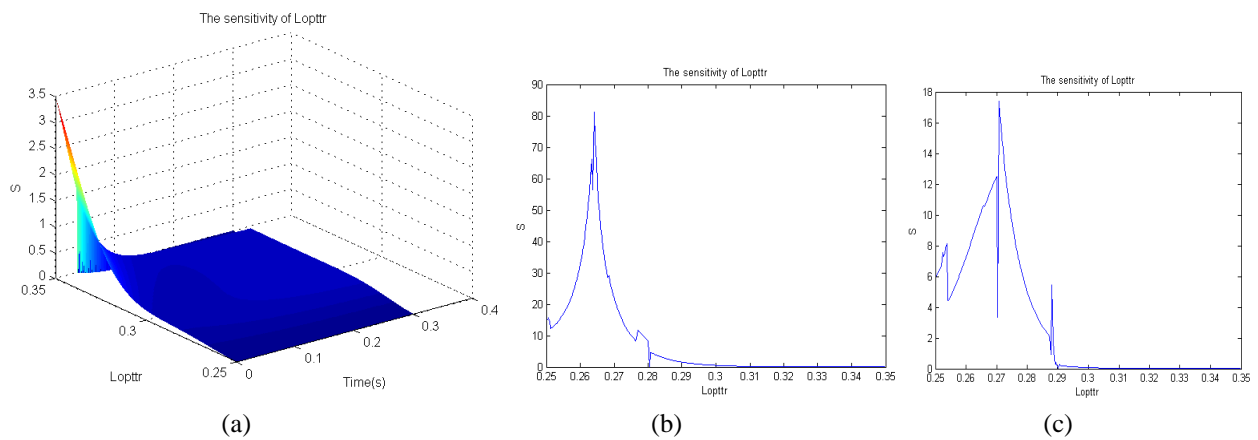


Figure 4.4: The sensitivity of $Lopt_{tr}$

(a) The sensitivity of $Lopt_{tr}$ with settled activation in NSQL test (b) The sensitivity of $Lopt_{tr}$ from subject A. The peak was 81.2507 (without normalization)/ 0.9559 (with normalization). (c) The sensitivity of $Lopt_{tr}$ from subject C. The peak was 17.3938 (without normalization)/ 0.4970 (with normalization).

Length of humerus Hum

In the NSQL test, it belonged to high sensitivity parameter (Figure 4.5 (a)), and showed a large differences (0.8464, 0.7057, 0.6882) in IDA test (Figure 4.5 (b) and (c)), whereas in the case of different action from the same subject, sensitivity changed was small. Based on this, we conclude that Hum is an Individual Difference Parameter. This result is consistent with the physiological

significance. Although this parameter cannot be directly actually measured, but it can be estimated from the length of subject's upper arm by anthropometry method.

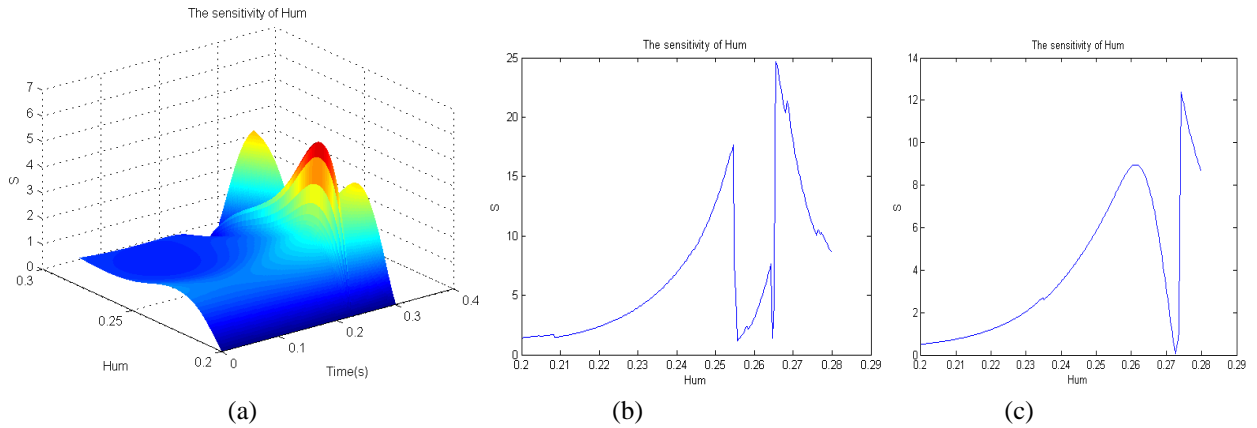


Figure 4.5: The sensitivity of Hum

(a) The sensitivity of Hum in NSQL test. (b) The sensitivity of Hum from subject C. The peak was 24.6985 (without normalization)/ 0.7057 (with normalization). (c) The sensitivity of Hum from subject B. The peak was 12.3869 (without normalization)/ 0.6882 (with normalization).

User-specific elasticity coefficient C_{passbi} and C_{passtr}

C_{passbi} had a high sensitivity in NSQL test, and a large difference in IDA test (Figure 4.6 (a-c)). It shows that C_{passbi} , as an Individual Difference Parameter, is easily influenced by different subjects. For C_{passtr} , even though it had both of the Action Difference (0.0040, 0.0701, 0.0003, 0.0004) and Individual Difference (0.0743, 0.0163, 0.0013), but since its sensitivity rates in all cases were quite low (less than 0.1), which means the effect on model result was small. This parameter does not need any tuning process.

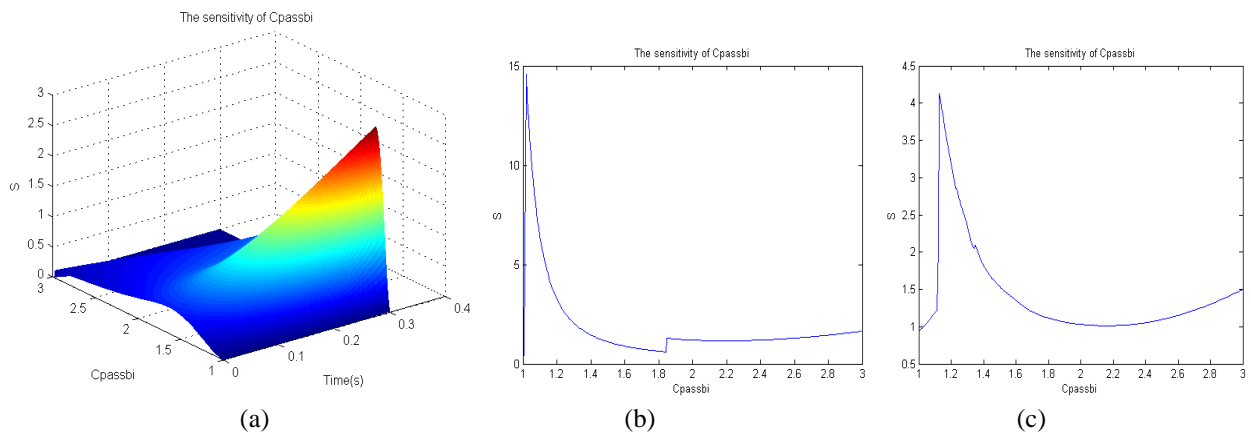


Figure 4.6: The sensitivity of C_{passbi}

(a) The sensitivity of C_{passbi} in NSQL test. (b) The sensitivity of C_{passbi} from subject A. The peak was 14.5767 (without normalization)/ 0.1715 (with normalization). (c) The sensitivity of C_{passbi} from subject C. The peak was 4.1259 (without normalization)/ 0.1179 (with normalization).

Muscle attachment distance to joint center U_{bi} , and U_{tr}

These two parameters cannot be directly measured inside human body, and the so called muscle group is just an assumed theory and non-existence in actual physiology. The sensitivity of U_{bi} showed the differences in ADA or IDA test, but because of its high value in the whole process (Figure 4.7) and all tests, U_{bi} needs to be regarded as an online tuning parameter.

In IDA test, U_{tr} had a special performance. To some subjects, such as subject A, it produced a higher sensitivity effect. But to the other subject, its sensitivity was quite low (Figure 4.8). Therefore, sensitivity of these parameters needs to be re-tested when the subject changes.

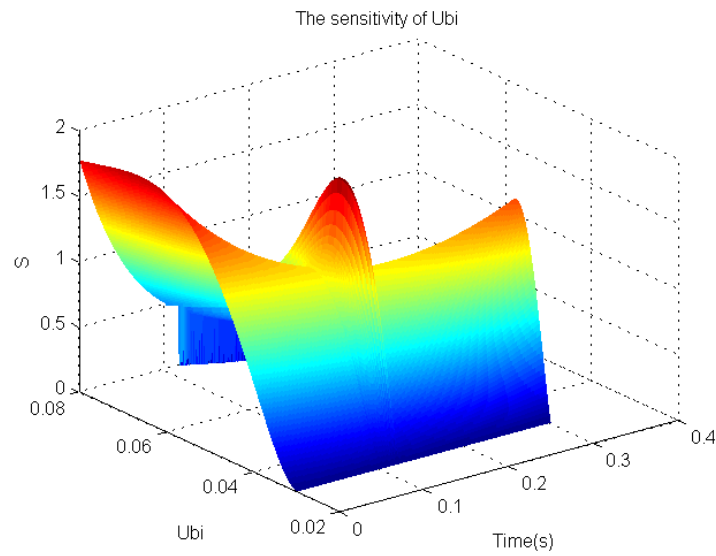


Figure 4.7: The changes of sensitivity of U_{bi} during NSQL test over time and parameter.

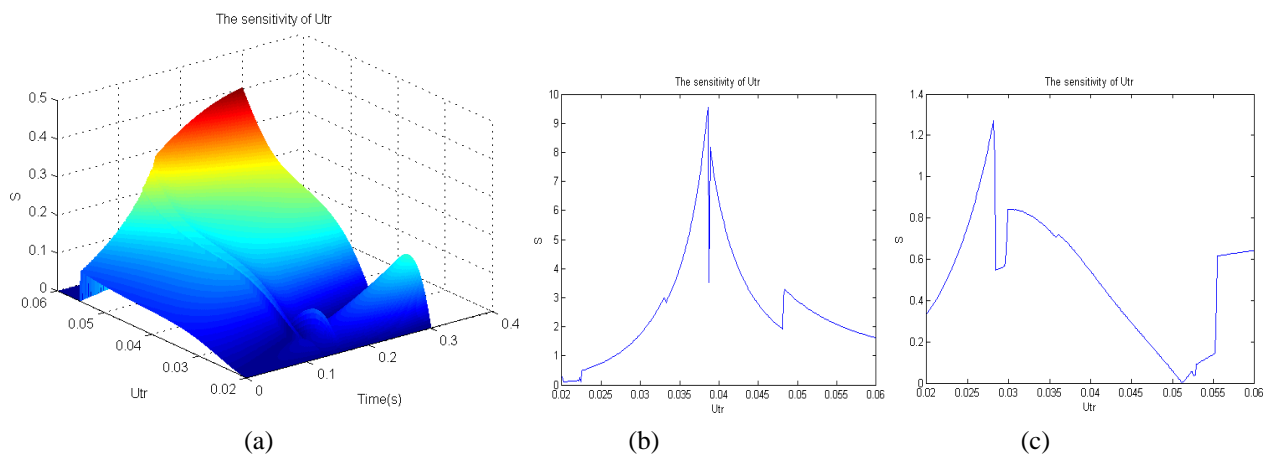


Figure 4.8: The sensitivity of U_{tr} (a) The sensitivity of U_{tr} in NSQL test. (b) The sensitivity of U_{tr} from subject A. The peak was 9.5386 (without normalization)/ 0.1122 (with normalization). (c) The sensitivity of U_{tr} from subject C. The peak was 1.2699 (without normalization)/ 0.0363 (with normalization).

User-specific coefficient of bicep muscle size R_{bi}

Its sensitivity rate showed no difference in IDA test, but a significant one in ADA test (0.0614, 0.1274, 0.0084, and 0.0013). So it belongs to an Action Difference Parameter (in Figure 4.9 (a-c)). In other people's studies, this parameter was directly ignored in the muscle force process, in [2, 68]. Although Sartori et al. [69] proposed to consider the individual differences in muscle size and strength, but they did not analyze the value and performance of this parameter in their research.

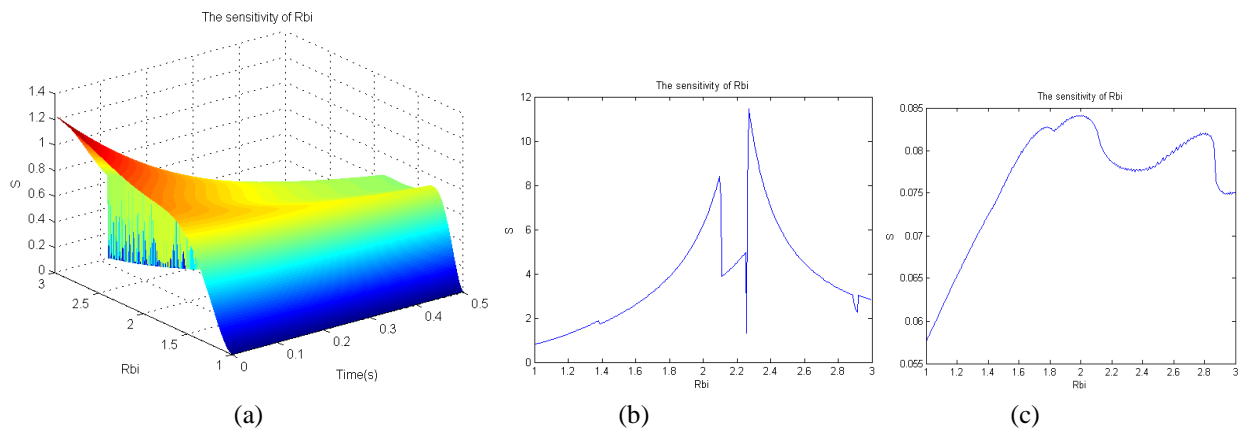


Figure 4.9: The sensitivity of R_{bi} (a) The sensitivity of R_{bi} in NSQL test. (b) The curve of R_{bi} during 'Single cycle' movement test. The peak was 11.4645 (without normalization)/ 0.1274 (with normalization). (c) The curve of R_{bi} during 'Continuous cycle' movement test. The peak was 0.0841 (without normalization)/ 0.0084 (with normalization).

Maximum muscle force of biceps F_{maxbi}

Maximum muscle force of biceps (F_{maxbi}) is important, because it affects the muscles active and passive contraction strength. With the same subject but different actions, the changes of sensitivity were not obvious, but in IDA test, the sensitivity rate showed big differences (0.1616, 0.1410, 0.2127), so it belongs to the Individual Difference Parameter. As can be seen from Figure 4.10, during the entire simulation process, the sensitivity ratio kept in a high degree, indicating that it impacted a lot on the model's sensitivity. So the F_{maxbi} requires an online real-time tuning.

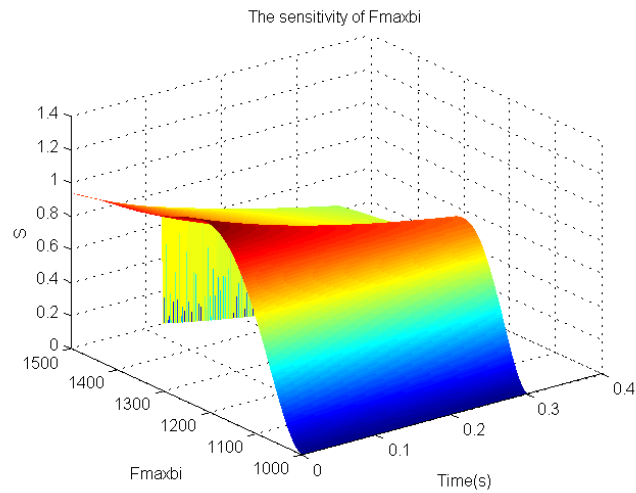


Figure 4.10: The sensitivity of $F_{\max bi}$ in NSQL test.

The other parameters

The two parameters including the mass of forearm and hand (m) and the length of forearm (L_{Arm}), belong to human physiological parameters. The parameter m will affect the two physical variables: the torque generated by the gravity of forearm and hand, and the inertia of forearm. Since these two parameters did not show high sensitivity in the offline NSQL test (Figure 4.11), they only need to be measured by human biology method according to different individuals, before the model runs. For parameter B_{tr} and C_{passtr} , although they respectively belong to Action Difference and Individual Difference Parameters, but because of its low sensitivity in all tests, they do not require tuning. The remaining parameters are in low sensitivity and have little effect on the model, so they do not need to be considered tuning.

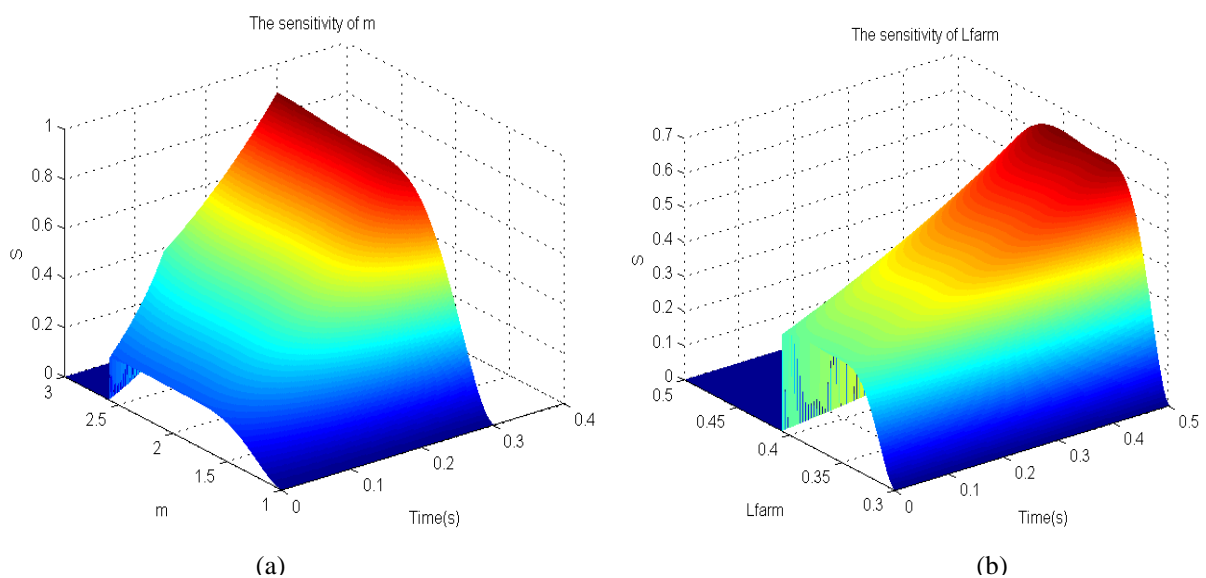


Figure 4.11: (a) The sensitivity of m in NSQL test. (b) The sensitivity of L_{Arm} in NSQL test.

Since the musculotendon model in this thesis is an upper limb model, which means the tendon length in upper limb muscle groups is much shorter than the muscle length, so the tendon can be simplified as a rigid body. Meanwhile, due to the pennation angle of upper limb muscle is quite small, this thesis has not taken the pennation angle \emptyset into consideration. However, when the research comes to lower limb, especially about the muscles connected to knee joint, the impacts of tendon parameters cannot be ignored. For example, articles [111-113] all have analyzed the importance of tendon slack length.

Based on the results above, the 19 tunable parameters' property, sensitivity layer and processing methods in tuning or optimization can be summed up in Table 4.4.

Table 4.4 Property, layer and processing method of 19 tunable parameters

Parameters	Property	Sensitivity layer	Processing method
$L_{opt_{bi}}$	General parameter	High	Online tuning
Hum	Individual difference	High	Measurement and offline tuning
K_{bi}	General parameters	High	Online tuning
$L_{opt_{tr}}$	Individual difference and action specificity	High	Measurement and offline tuning
$C_{pass_{bi}}$	Individual difference	High	Measurement and offline tuning
U_{bi}	General parameters	High	Online tuning
R_{bi}	Action specificity	High	Online tuning
$F_{max_{bi}}$	Individual difference	High	Measurement and offline tuning
m	Individual difference	High	Measurement
R_{tr}	General parameters	Low	Constant
K_{tr}	General parameters	Low	Constant
L_{Arm}	Individual difference	High	Measurement
U_{tr}	Individual difference	Low	New sensitivity test with subject change
β	General parameters	Low	Constant
O	General parameters	Low	Constant
$F_{max_{tr}}$	Individual difference	Low	Offline tuning
B_{bi}	Action specificity	Low	Constant
$C_{pas_{str}}$	Individual difference and action specificity	Low	Constant
B_{tr}	Action specificity	Low	Constant

During the tests, the changing ranges of parameters in this thesis were their actual human

physiological ranges, rather than the perturbing range in the vicinity of the standard value in literature [111-113]. Such settings can fully exhibit the impacts on model parameters sensitivity of all the possibilities.

4.2 The Elbow Physiological Model Validation

This section describes the experimental setup for elbow movement, EMG signal processing and test results, to verify the elbow physiological model developed in Chapter 3. This test sets up multiple subjects, their movements including simple elbow flexion/extension to complex random motion. The performance of the new model is validated, with multiple individual data. Also, linear envelope and muscle activation dynamics are used to extract the muscle activation. The data in this section is based on the parameters sensitivity analysis in Section 4.1, and the GA offline parameters tuning. Section 7.2 in this thesis introduces two kinds of parameter tuning algorithm and designed an online tuning method.

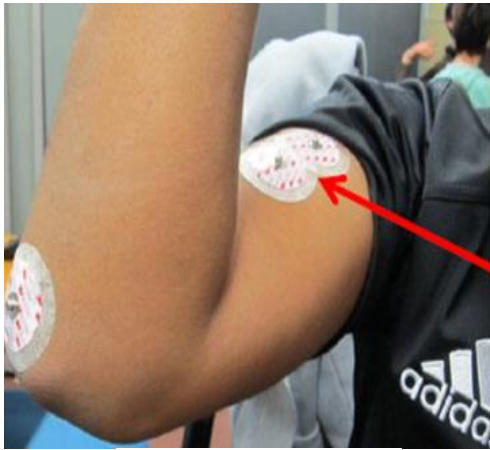
4.2.1 Experimental Setup for Model Validation

4.2.1.1 Subjects

6 subjects (3 males and 3 females, age 25 ± 5) volunteered as subjects for this study. None of the subjects were experiencing upper limb disease. The males' height was 175 ± 5 cm, weight was 80 ± 10 kg. The females' height and weight were 160 ± 5 cm and 55 ± 5 kg. The study was approved by the University of Auckland Human Participants Ethics Committee (UAHPEC) and all participants provided informed consent.

4.2.1.2 Apparatus

The flowchart of experiment apparatus setup is shown in Figure 4.12. During subject's movement, the surface EMG (sEMG) signals are collected from subject's skin by electrodes, then the raw sEMG signals are transferred to the amplifier for the preliminary processing. At the same time, the Spherical arm rig moves with the subject's arm, and the Polaris Spectra motion capture can record the rig's moving angle in order to record the actual elbow joint motion. After the signals from amplifier are transferred into the models in computer, the model will calculate and predict the joint angle. Finally, the predicted movement can be compared with the actual movement in Matlab software.



a) Electrodes



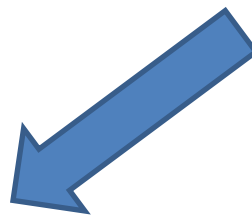
c) Spherical Arm Rig for arm position



b) g.USBamp signal amplifier



d) Polaris Spectra for motion capture



e) Model in Matlab

Signal Acquisition System

The muscle sEMG was recorded by disposable Red Dot Monitoring electrodes (3M, USA), and they

were placed with a inter electrode distance of 20 mm around the recommended sensor locations with the orientation parallel to the muscle fibres. The electrode placement was noted from literature to be over the middle to lower bicep group and in the center of the triceps group (Figure 4.12 (a)). The ground however was chosen to be positioned over the olecranon which is located just lower of the elbow joint. This location is chosen as there is very little muscle located near this area causing less chance for disturbance such as cross over noise from other muscle groups or unknown artifacts.

A g.USBamp bio signal amplifier (Guger Technologies, Austria) (16 channels)(Figure 4.12 (b)) was used for the raw signal filtering. The bipolar EMG channels were sampled at 1200Hz and hardware filtered with a 50Hz notch filter.

Motion Capture System

The arm movement was recorded by the Polaris Spectra (Northern Digital Incorporated, USA) (Figure 4.12 (d)). It is a motion tracking system that can track passive markers with high accuracy (up to 0.3 mm RMS) at up to 60Hz. It has been used to track the subject arm position and orientation in 3D space. The setup has to be very precise, or it won't register the users' movements on the NDI motion capture system. Figure 4.12 (c) displays how the rig is to be placed over the arm.

4.2.1.3 Experimental design

The subjects were asked to have meal 2 hours before experiment and to not physically exercise in the previous 24 hours. Participant arm hair was shaved if needed and the skin was cleaned with alcohol. The conductive paste and electrodes were placed on the skin after the alcohol vaporization. A stand still position was required during the experiment. This natural position is neutral as all joints are relaxed and the hands are facing the front.

This trail design consisted of a $3 \times 5 \times 5 \times 5 \times 5$ repeated measures design where the MVC test was repeated three times, the single or circle movements were five times. The groups of movement were as follow:

- (1) MVC test was the first step to measure the maximum isometric contractions of each muscle group. The subject was asked to pull up and push down against a stationary desk by his maximum force and keep each movement up to 10 seconds. This test was recorded three times and averaged.

A minimum 1 minutes rest should be placed after this step.

- (2) Single cycle test required the subject to fully flexed his arm with a natural speed from a whole

arm relaxing position, (and stopped for 5 second), then fully extended, again with a natural speed.

(3) Continuous cycle full range test required the subject to keep fully flexing and extending with a natural speed for 20 seconds.

(4) Continuous cycle half range test required the subject to flex and extend from the range about 180° to 90° of elbow joint.

(5) Continuous cycle increasing range test started with small amplitude that gradually increases till fully flexing and extending.

(6) Random movement test required the subject to flex and extend in continues and any range of flexion and extension in different speed, to estimate the effect of non-linear dynamics.

4.2.2 EMG Signal Processing and Muscle Activation

Since the EMG signal has a character of weakness, low-frequency and high-resistance, it is unavoidable to introduce different kinds of noise. The main sources of noise include 50Hz frequency interference, background noise, high-frequency interference and artificial motion. To cancel the noise, a linear envelope method (LE) [5, 6] has been used for effectively gathering the muscle activations from the EMG signal. Specific steps are as follows:

High-pass filter:

High pass filter removes the DC offsets and low-frequency noise generated by the motion of electrodes. Based on the type of filter and electrode, the cut-off frequency is generally from 10 to 30Hz. A good filter should have a zero phase delay, so it will not shift the EMG signal in time. For this research, a 2nd order Butterworth high-pass filter has been used with a 20Hz cut-off frequency.

Full-wave rectification:

Full-wave rectification is used to invert the negative components of EMG signal, in order to reflect all signal activity in positive domain.

Low pass filter:

The general cut-off frequency ranges about 3-10Hz. In this study, a 2nd low-pass Butterworth filter with 3Hz cut-off frequency has been chosen to produce the linear envelope.

Normalization:

EMG signal values are normalized by dividing the peak during maximum voluntary contraction

(MVC), to conform the values to be between 0-1.

The rationality of linear envelope processing is that, during a single Motor Unit Action Potential (MUAP) activation, the muscle will produce a contraction response. The full-wave rectifier is considered as a summation of all action potential waves from a variety of amplitudes of motor unit action. Muscle tension can be seen as the sum of muscle contraction caused by all active power units [2]. According to the literature, the different muscles time delay (or electromechanical delay) is about 10-100ms [124]. This means that if a 2nd order low-pass Butterworth filter with a cutoff frequency of 3Hz is used, the delay equals to 50 milliseconds of motor delay. So, the substance of the linear envelope is to simulate the tension waveform during isometric muscle contractions.

Muscle activation

The result from this linear envelope can be directly regarded as neural activation $u(t)$. It is mainly about the nonlinear problem between neural activation $u(t)$ and muscle activation $a(t)$. Muscle activation may be the most important uncertainty source within the EMG-driven model, so the accuracy of this block will affect the accuracy of the whole interface a lot.

Then the muscle activation can be calculated from:

$$a(t) = \frac{e^{Au(t)} - 1}{e^A - 1} \quad (4.5)$$

Where A determines the degree of nonlinearity[70]

For the neural activation $u(t)$, the transition point(i.e., approximately 30% value) from nonlinear to linear is not a constant. The parameter A is used to describe the curvature. Also, it relates to the nonlinear quantity between EMG and activation. The actual value of A is decided by calibration or commissioning process, normally $-3 < A < 0$.

Thresholding:

A threshold is given below which the $a(t)$ is floored to zero. This is to account for uncertain or environmental activities in the EMG signal, even when there are no active contractions present.

4.2.3 Model Validation

4.2.3.1 Model Setup

For the elbow physiological model in Chapter 3, according to the anatomy and physiology, the length proportionality constant of two biceps muscle path segments K_{pbi} and of two triceps muscle path segments K_{ptr} are set to constant values, which means $K_{pbi} = \frac{\overline{AB_2}}{B_2B_3} = 1.081$, and $K_{ptr} = \frac{\overline{AT_2}}{T_2T_3} = 4.053$. The relative positional angles of muscle path are set to constant values as well, namely $\alpha = 6.28^\circ$ and $\alpha_1 = 9.26^\circ$.

Based on the Table 4.1, 14 parameters are chosen for the tuning, includes all the high sensitive parameters ($Lopt_{bi}$, Hum, K_{bi} , $Lopt_{tr}$, C_{passbi} , U_{bi} , R_{bi} , F_{maxbi}), part of the low sensitive parameters (m , L_{Arm} , U_{tr} , F_{maxtr}), and two signal processing parameters (A , ThreTr). Table 4.5 lists the tuning parameters and their ranges. Wherein, A is the degree of nonlinearity, ThreTr is triceps threshold. The values of other remaining parameters are fixed from measuring or literatures [125].

Table 4.5 Tuning parameters

Test Port	parameters	range in experiments
1	$Lopt_{bi}$	0.25-0.35
2	$Lopt_{tr}$	0.25-0.35
3	F_{maxbi}	1000-1500
4	F_{maxtr}	1000-1500
5	C_{passbi}	1-3
6	R_{bi}	1-3
7	K_{bi}	0.8-1.9
8	Hum	0.2-0.35
9	U_{bi}	0.01-0.06
10	U_{tr}	0.02-0.06
11	A	-1-+1
12	m	1.3-1.6
13	L_{Arm}	0.2-0.45
14	ThreTr	0.02-0.05

This thesis designed two kinds of parameter tuning algorithm (GA and DE) in MATLAB software,

GA is used for offline tuning, and DE for online tuning. The detailed information is shown in Section 7.2. The data in this section are offline tuned by GA. For each individual experiment, the optimization process was repeated at least four times, to minimize the probabilities of GA returned local minima.

4.2.3.2 Experimental Results

By modeled and simulated in Matlab and Simulink, the prediction angle and actual angle of elbow motion in a variety of subjects are obtained. The root mean square error (RMSE) between them can be calculated as follow:

$$\text{RMSE} = \sqrt{\frac{1}{n} \sum_{i=1}^n (D_{\text{pred}} - D_{\text{actu}})^2} \quad (4.6)$$

where, n is the number of samples, D_{pred} is the predicted joint angles, D_{actu} is the actually measured joint angles.

Single cycle test

For the single-cycle full flexion and extension movements of six subjects, the predicted results are very accuracy, which means the test is quite reproducible. The RMSEs of all subjects were $4.51^\circ \pm 2.25^\circ$. Figure 4.13 shows the comparison of the predicted and actual angle of subject E. As can be seen from the figure, the model is accurate during the elbow flexion and extension movements and in the maximum flexion angle, but has a bigger error during relaxing in the natural state before and after the operation began. The main cause of this error is due to the difference of resting angle for different subjects. The predictive ability of this model in single-cycle movement is similar compared with Pau's result [5] (Table 4.6).

Continuous cycle full range test

For continuous movement, the advantage of this model is more significant. The RMSEs of all subjects were $12.64^\circ \pm 4.11^\circ$. One representative result is shown in Figure 4.14. From the figure, during the entire 22 seconds of the test, the prediction results of the model are well matched with the actual results for the flexion and extension movements. It has some errors only when the elbow reaches the maximum flexion due to the fast speed in changes. The result of this subject has also shown that, the model can still accurately predict the joint movement when the elbow is fully extended (the joint angle reaches 0°). Thus, it is verified that this model can solve the forecasting

problems when the muscular force line through the joint center.

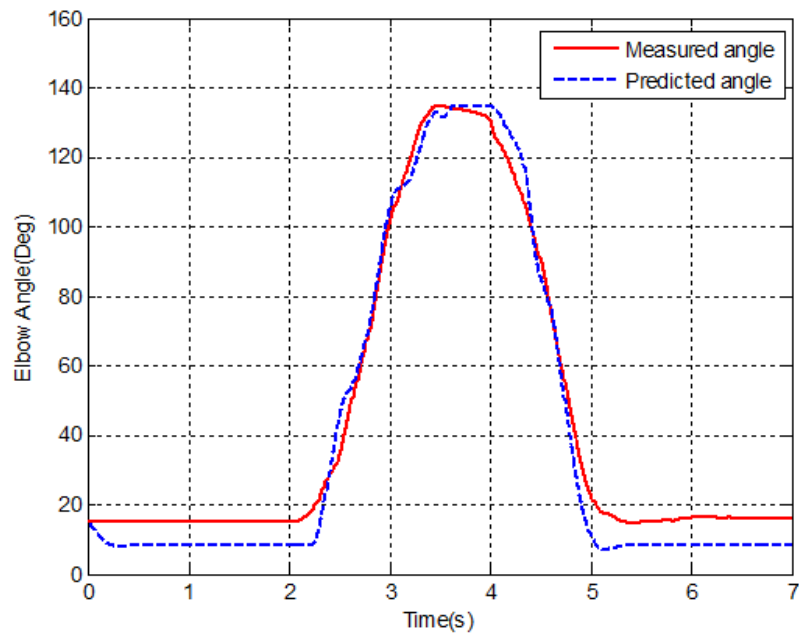


Figure 4.12: Result of a single cycle test with RMSE of 4.42° .

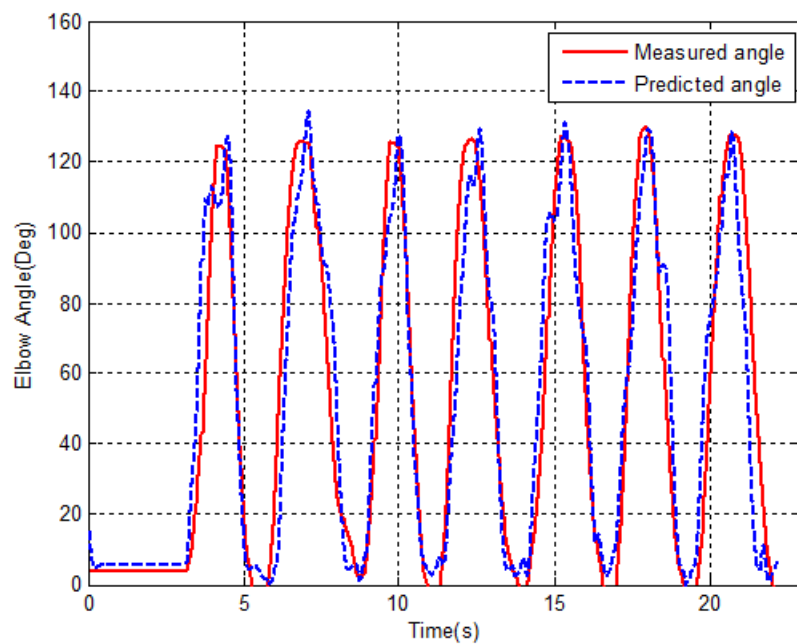


Figure 4.13: Result of a Continuous cycle full range test with RMSE of 12.97° .

Continuous cycle half range test

For the continuous cycle half range test, the results validate the predictive ability of model to the smaller amplitude vibration. The RMSEs of all subjects were $12.5^\circ \pm 3.25^\circ$. During the experiments, occasionally the prediction point was generated in advance of the actual movement

occurrence, such as the first two and the last two waveforms in Figure 4.15. The cause of this phenomenon is due that the EMG signal is directly from the muscle electrical stimulation signal, which means it is produced before the beginning of the real muscle contraction. Also, because of the real-time property of the model, there is almost no time delay in the calculation speed. Therefore, the model prediction can be synchronous or slightly ahead of the actual human movement.

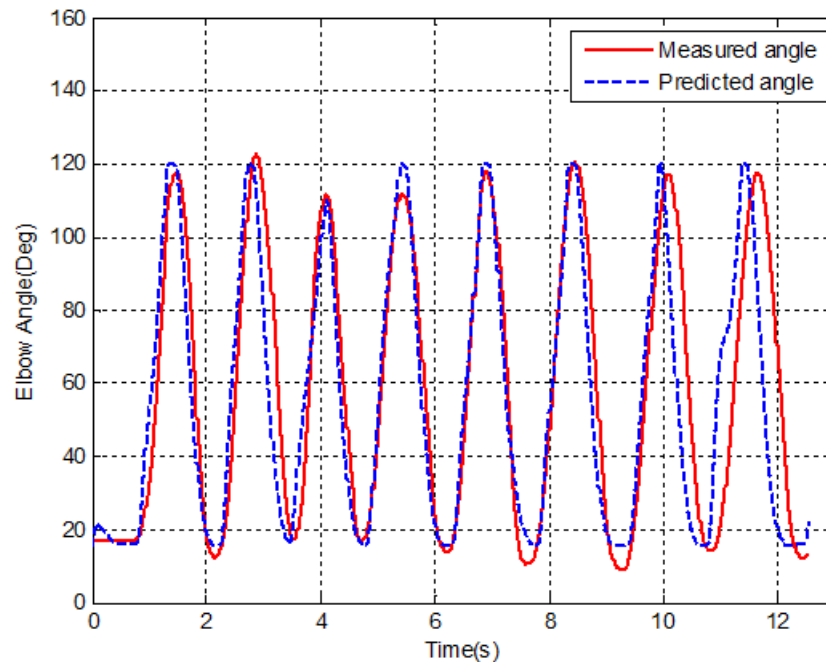


Figure 4.14: Result of a Continuous cycle half range test with RMSE of 12.71°

Continuous cycle increasing range test

For the Continuous cycle increasing range test, the results show the predictive ability of the model to the changing magnitude movements. The RMSEs of all subjects were $10.98^{\circ} \pm 3.57^{\circ}$. For example, the result of Subject F is shown in Figure 4.16. The predicted angle was perfectly matched with measured angles in the first few waves.

Random movement test

Finally, the random movement test for elbow motion is the ultimate test of the predictive ability of the model. This test is closer to the body movement in real life situation, compared to the previous movements. Thus it is more able to assess the actual practical value of the model. For this variable magnitude, variable speed and completely random movement form, this model still shows its good stability: The RMSEs of all subjects were $13.7^{\circ} \pm 2.13^{\circ}$. For example, Figure 4.17 shows that the predicted angle curve can perfectly follow the actual angle curve. Even at the position with the largest angle differences (the fourth curve peaks), the prediction angle curve can still completely fit

the changing trend of the actual movement.

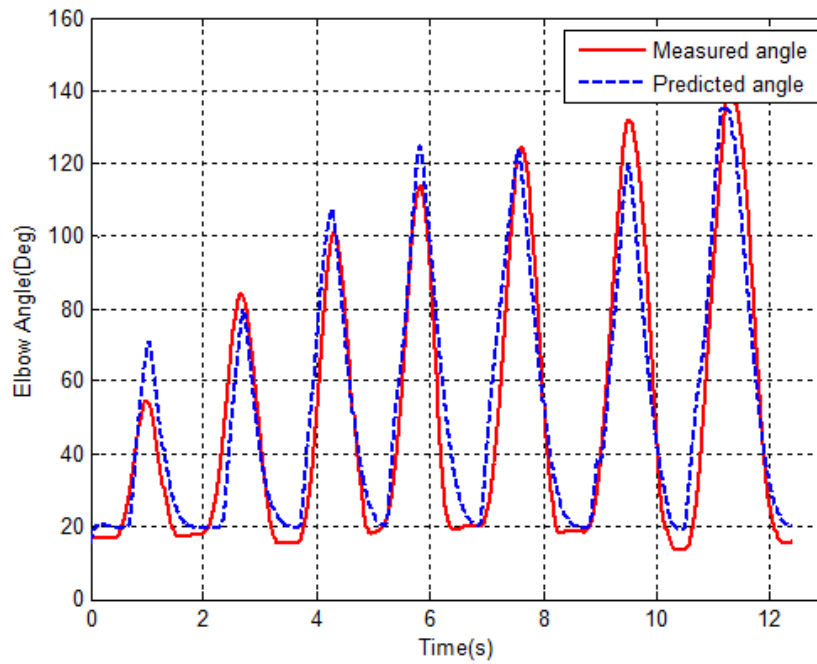


Figure 4.15: Result of a Continuous cycle increasing range test with RMSE of 9.86° .

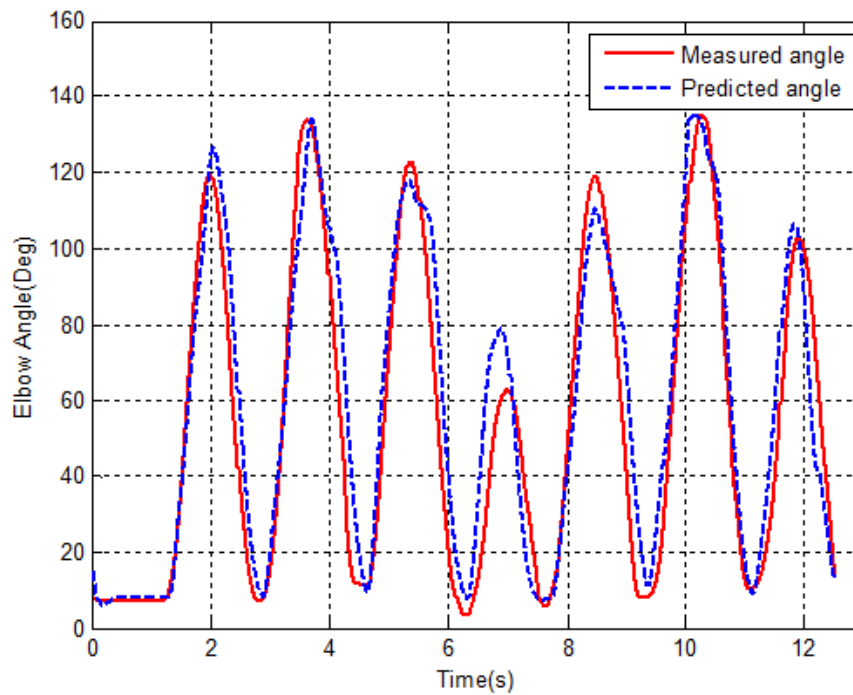


Figure 4.16: Result of a Random movement test with RMSE of 11.57° .

4.2.3.3 Discussion

In this chapter, six subjects and five kinds of elbow flexion/extension movements were used in the experiments to evaluate the overall performance of the physiological model. The results prove that the interface not only has a good predictive ability in simple movements, but also can make a good match in the predictions and actual results for the complex amplitude or random motion. This is superior to other studies. For all subjects, each action was repeated five times. The RMSE ranges of all results were within 50% of its average. This indicates that the designed experiments are repeatable, and the interface has a high stability and individual adaptability to external disturbances.

Table 4.6 shows the comparison of RMSEs from the model of Pau [71] and the model in this thesis under the same experimental conditions. For simple movement such as single cycle motion, the predictive abilities of these two models are similar. However, when the movement complexity increases, such as the random variation of magnitude and trajectory, the accuracy of Pau's model is sharp declined, while, the model of this thesis is not only able to identify different new track and motion magnitude, but also still maintaining a high accuracy.

This good performance is due to the new musculoskeletal model in this thesis. It took the elasticity segments combination to simulate the muscle paths, which is closer to the actual physical structure of the elbow joint, in order to improve the accuracy of the predicted results. Furthermore, this design solves the problem that the single linear model cannot calculate the joint torque when the joint angle is close to 0° . This extended the range of model prediction to $[-5-135^\circ]$, which matches the normal human range of motion.

In addition, the results of this study are comparable to the results of other research teams. For the model of Koo et al [2], the RMSE of the single cycle elbow flexion was $34.64 \pm 7.79^\circ$, and the RMSE of the single cycle elbow extension was $18.67 \pm 8.49^\circ$. For the model designed by Artemiadis and Kyriakopoulos [126], the RMSE was from 1.76° to 9.0° , since their experiment limited the arm to move only in the horizontal plane. The model from Smith and Brown [127] could predict the elbow motion in the sagittal plane, the RMSE of the model changes from 6.5° to 34.3° .

The rest angle errors may be caused by the parameters without tuning. This Chapter only tuned the 14 main parameters and got the quite accurate results. More parameters joined in the tuning may lead to a better result, but will surely reduce the performance of real-time.

Table 4.6 Accuracy comparison of the models of James Pau and this thesis

Test	RMSE in Pau's model	RMSE in this thesis
Single cycle test	6.53 °±3.2 °	4.51 °±2.25 °
Continuous cycle full range test	22.00 °±6.6 °	12.64 °±4.11 °
Continuous cycle half range test	18.6 °±6.5 °	12.5 °±3.25 °
Continuous cycle increasing range test	19.5 °±5.3 °	10.98 °±3.57 °
Random movement test	22.4 °±5.0 °	13.7 °±2.13 °

The data are the RMSE from all subjects.

4.3 Chapter Summary

In this chapter, all 23 parameters of the EMG-driven model proposed in the previous chapter were analyzed, and among them, 19 parameters with the greater impact to the model were chose. These 19 adjustable parameters were graded on sensitivity and classified on characteristics from three points of view. The hierarchy of importance of these parameters, action difference and individual difference were assessed. . The parameters sensitivity analysis to the model resulted in a relatively small subset used for tuning. Finally, 14 parameters were used in the model tuning. The other parameters were from literatures.

The EMG signals were processed by linear envelope and nonlinear dynamics method. A group of experiments with several subjects and several kinds of movement were designed in this chapter, for the verification of the elbow physiological model and signal processing methods. The results showed that the model designed in chapter 3 can accurately identify new tracks and different range of motions, such as the average RMSE of random movement test was 13.7 °. Compared with the results in Section 3.5, the result in this Chapter is much more improve. It shows the performance and importance of parameter sensitivity analysis and tuning. Also, the accurate results indicates that the method based on physiological model can easily identify new movements.

Chapter 5 A Neuromusculoskeletal Model for the Forearm Pronation and Supination

This Chapter established a neuromusculoskeletal model as an implementation of the human-robot interface for forearm pronation/supination movement. The flowchart of human-robot interface is shown in Figure 3.1, Chapter 3. Wherein, the EMG signal processing, nonlinear muscle activation dynamics, musculotendon dynamics and the kinematic model are similar to the corresponding models of elbow flexion / extension in Chapter 3. Only the musculoskeletal geometric model for forearm rotation is different.

Based on a large number of studies, there are some researches about forearm physiological simplification [128-132], however, the neuromusculoskeletal model of forearm rotation as the implementation of human-robot interface has seldom been reported. A neuromusculoskeletal interface model must comply with human physiological structure, simple, practical, and easy for online tuning. In this respect, this chapter will firstly study the related human physiology structures to forearm pronation/supination, then establish the musculoskeletal geometry model of forearm motion, and analyze the related model parameters. Finally, experiments are used to verify the effectiveness of the model.

5.1 Physiological Structure of the Forearm Rotation

The human body is a complex living structure. From the anatomical point of view, the human body is consisted of bones, joints and muscle. The bones and joints are the overall framework of the human body, and the muscles are the power source of human movement. The human physiological

processes are all dominated by the nervous system. From the origin of life to the development so far, the body's nervous system is the most complex and most comprehensive control system.

5.1.1 Physiological Skeleton Structure of the Forearm

The forearm of human body is the part between the elbow and wrist joints. Forearm includes the radius and ulna, as shown in Figure 5.1. The ulna locates to the close side of human body, and the radius locates to the far side of human body. The radius and ulna are connected by the interosseous membrane, and they forms the proximal radioulnar joint near the elbow, and forms the distal radioulnar joint near the wrist. The proximal and distal radioulnar joints are the combined joint. These constitute the anatomical basis of forearm rotation.

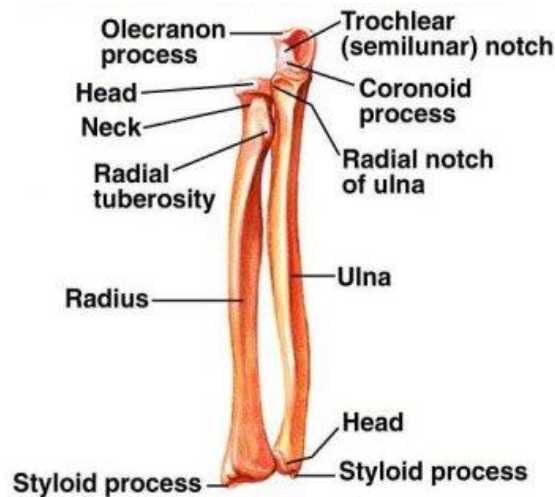


Figure 5.1: The forearm skeleton

Forearm skeletal system is simple, but the forearm rotation is a very complicated movement. The proximal radioulnar joint is rounded by an annulus from the radial head cylindrical lip and radial notch in ulna. The annular ligament accounts about 3/4 of the fibers annulus. So it can adapt to rotation of the elliptical radial head.

During forearm rotation, the ulna is generally considered fixed, the rotation axis is from the center of the radial head to the bottom of the ulnar styloid process. Along this axis, radius has the upper and lower two lordosis which are the pronation bow and supination bow. The radial curve locates on the connection of radial neck and radial body, which is the radial tuberosity projecting to the ulnar, about 11.3° . It is the ending point of biceps. The lower and outer side are the ending point of supinator. The radial tuberosity locates 1/3 of the radial outer side projecting to the radial side,

about 9.3° . The pronator teres contacts and stops here, called 'supination bow' and 'pronation bow'. Radius rotates along the rotation axis of two bow. In the proximal radioulnar joint, radius does the 'rotation' movement along the radial notch of ulna. In the distal radioulnar joint, radius does the 'revolution' movement along ulna head.

There is a fibrous tissue between the forearm bones, known as the interosseous membrane, as shown in Figure 5.2. The interosseous membrane connects almost the entire length of the ulna. The tightness of the interosseous membrane is changed with the rotation of the forearm. When the forearm is in neutral position, the two bones are nearly parallel, the gap between the backbones are the largest, the tightness in the upper and lower interosseous membrane are the same, which leads the radius and ulna in a stabilizing position. When the forearm is pronation or supination, the gap between backbones is more narrow, and the tightness of upper and lower membrane are different, so the stability between bones is disappeared.

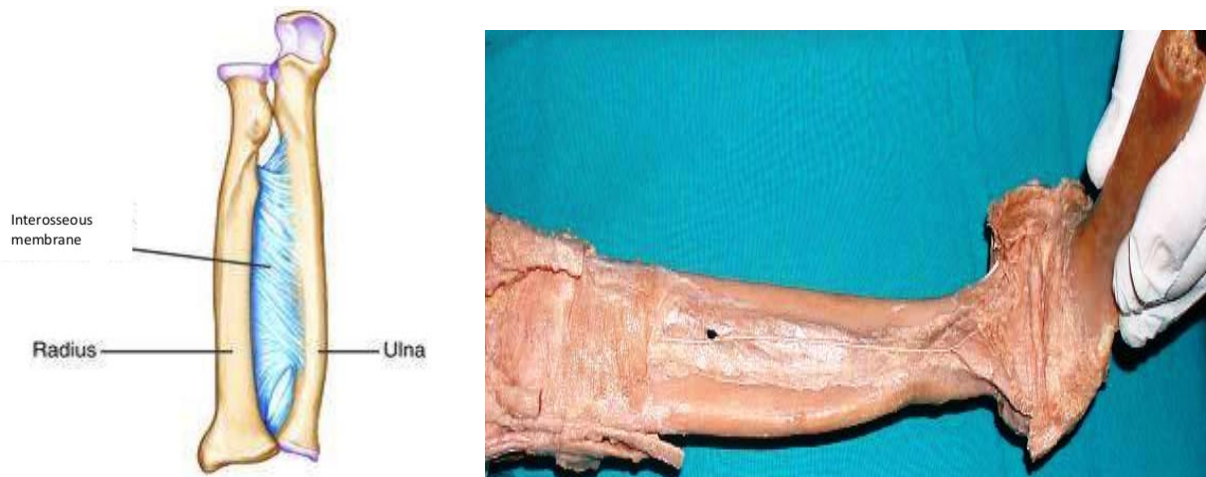


Figure 5.2: The forearm interosseous membrane

The oblique cord and interosseous membrane limit a maximum range for the forearm pronation/supination movement. When the forearm pronation 15° - 20° , the oblique cord begins to tense. When till the 70° , the oblique cord and upper interosseous membrane are totally tensed, which limits the rotation of the forearm. During supination at 20° to the neutral position, the interosseous membrane is in the substantially isotonic state and the gaps between ulnar and radial is the largest. By proceeding pronation or supination, the upper and lower interosseous membrane are no longer in isotonic state. The oblique cord and upper interosseous membrane are tense during pronation, and the lower interosseous membrane are tense during supination, which limits excessive forearm supination. So the maximum angle of pronation movement is 80° - 90° , and the maximum angle of supination movement is 90° - 100° .

5.1.2 Forearm Rotation Axis and Rotation Center of the Distal Radioulnar Joint

With the continuous study of the distal radioulnar joint movement, people have a more in-depth understanding of the forearm rotation axis and the rotation center of ulnar head [133]. Generally believed that the axis of the forearm rotation through the proximal radial head and the cross-section center of the distal ulnar head, shown in Figure 5.3. When the distal radioulnar joint in level, the rotation axis is slightly to the back side in pronation, and slightly to the palm side in supination. Since the curvature of ulnar head is greater than the curvature of the radial sigmoid notch [134], the ulna head will have a sliding and rolling movement on the sigmoid notch during the forearm rotation. The sliding direction of ulna head is to the back side in pronation and to the palm side in supination.

In 2010, Matsuki [135] measured the maximum rotation angle of radius was 157° (80° for pronation and 77° for supination), through a study of dynamic rotation activities of normal people with X-ray and CT scan. When the ulnar head moved to the 30° position of forearm supination from the extreme starting position, the rotation center of the spin ulnar head moved about 1.3mm to the palm side. Also, in the extreme position of pronation, the center moved 2.6mm to the backside. Therefore, during the forearm rotated from the extreme position of supination to the extreme position of pronation, the ulnar head moved totally 3.9mm from the palm side to the back side. At the position of supination 30° , neutral position, pronation 30° and pronation 60° of forearm movements, there is a significant change of the rotation center of ulnar head (Figure 5.3(b)).

In 2008 and 2010, Tay et al. [136, 137] used the vivo CT scan to test the forearm rotation axis, and found that the rotation axis of forearm located from the palm side radial head to the back side radial head, and the axis was changing during forearm rotation. With forearm pronation, the rotation center of ulnar head mildly shifted to the back side. With the forearm supination, the center moved towards to the palm side. The proximal rotation center of forearm was close to the center of joint surface of the radial head, and the distal end of the rotation center was at the back side of the dorsal ulnar head. The center changed with the forearm movement. The rotation center of the distal radioulnar joint was 1.9mm back side of the ulnar head and 0.5mm palm side of the ulnar head [135].

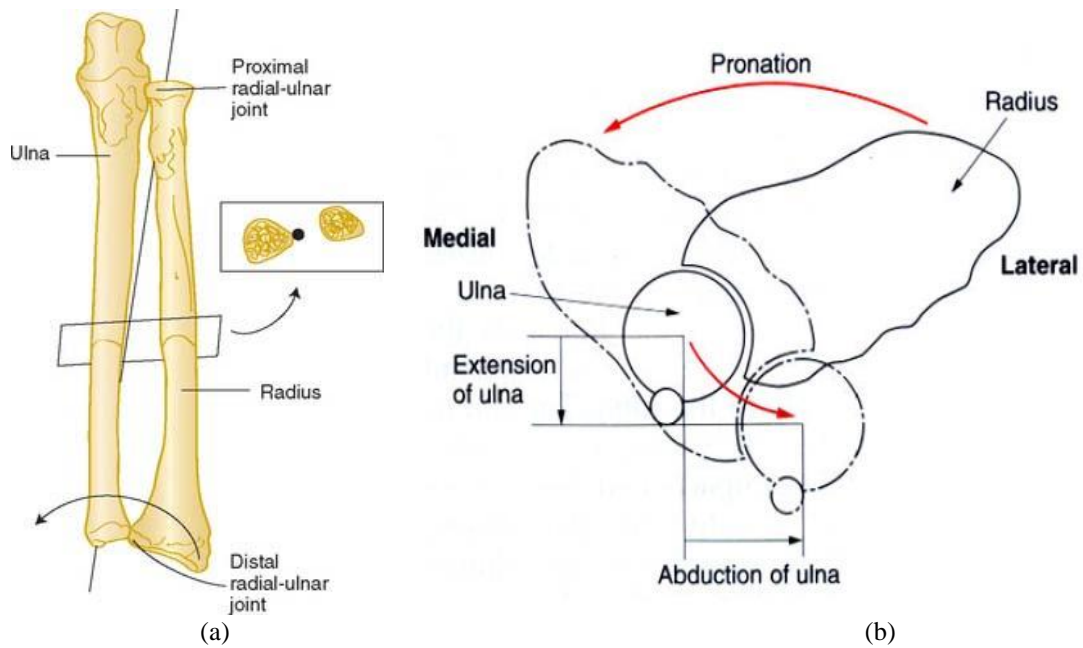


Figure 5.3: The axis of the forearm rotation [135-137]

In 2012, Kataoka [138] rebuilt the radius and ulna based on the CT scans of 28 volunteers forearms, to study the relationship between the distance of forearm rotation center to the anatomic distal ulna center and ulna variance. When the negative variation of ulnar was obvious, the distance between rotation axis centers and anatomical distal ulna center was larger, and the rotation center was more close to the base of the ulnar styloid.

In short, although the axis of forearm rotation is changing during the forearm moves, the basic axis proximally through the radial head, and distally through the center of ulnar head cross-section. In the horizontal plate of distal radioulnar joint, the rotation axis is slightly close to the back side in pronation, and close to the palm side in supination.

5.1.3 Forearm Muscles

Muscles can transfer the body's internal chemical energy into mechanical energy, so it is the power source of human motion. According to the form and distribution of muscle cells, muscles can be divided into skeletal muscle, smooth muscle and cardiac muscles three categories. Among them, the skeletal muscles are controlled by the nervous system, and cardiac muscles and smooth muscles are not controlled by the nervous system. Skeletal muscles are the basis of human motion and take part in all kinds of human physical movement. The skeletal muscles mainly place in the human limbs and trunk, and take up 2/5 of body weight. Usually one muscle crosses one or two joints, the muscle across one joint is called single-joint muscle, and the one across two joint is called two joint muscle.

The main muscles involved in forearm rotating includes pronator teres, pronator quadratus, brachioradialis, biceps, supinator muscle, etc. Researches have shown that the pronator teres and pronator quadratus play a major role in pronation movement, and the supinator is the major muscle in supination movement. Biceps can also help with the supination. In addition, the so call "forearm rotation regulator"- brachioradialis helps the pronator in pronation and supinator in supination.

Based on the structural characteristics, the pronation and supination muscles are divided into two groups: a) the pronator quadratus and supinator, their ending points are away from the rotating bow. One of this two muscles is contraction while the other is relaxation during forearm rotation. b) pronator teres and biceps, their ending points are at the rotation bow, and they are longus. Pronator teres, pronator quadratus and supinator all have shallow muscle parts, which are easier for the collection of EMG signal. The muscles position are shown in Figure 5.4. Generally, the connection point which is in the front of human or near the limbs is called the starting point, and the one away from the limbs is called ending point.

Pronator teres has two starting points. They are respectively from the humeral medial epicondyle and ulna tuberosity. The ending point of pronator teres is the outer edge of the middle radial (pronator tuberosity) on the lower bow part of radius. According to the fiber directions and different starting and ending points, pronator quadratus is divided into the superficial and deep layers. The main role of the superficial muscular is to help forearm pronation. It starts from the 1/4 of front distal ulna, and ends 1/4 of distal radius. The fibers of deep muscle limit the ulna and radius for the stability of the distal radioulnar joint. Supinator starts from the epicondyle of the humerus and bypass the radial to end at 1/3 of outside of the radial tuberosity. It is a small piece of muscle at the rear side of axis, and divided into superficial muscle and deep muscle.

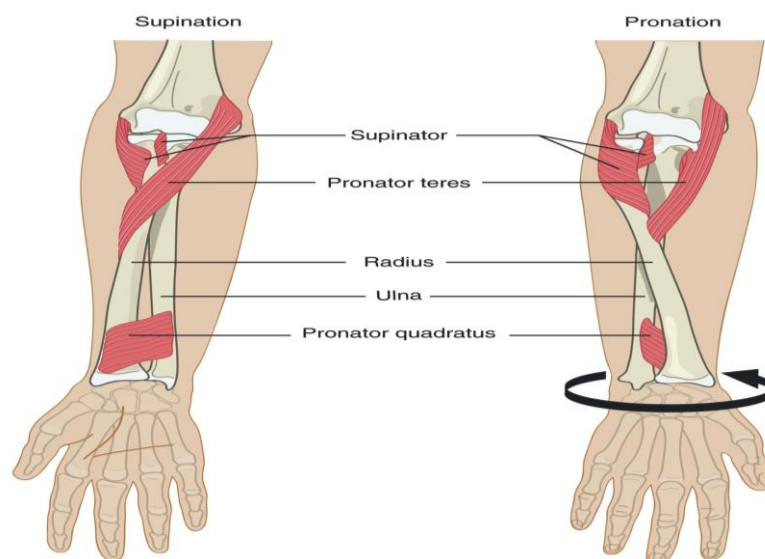


Figure 5.4: Muscles for forearm pronation and supination

5.2 Development of the Forearm Musculoskeletal Model

From a number of literatures, the researches about forearm movement are mainly about the muscles contribution or biological structure analysis [129, 139-141], joint force and moment calculation [131], forearm signal analysis [128, 130, 142], and some large 3D model kinematic analysis [135, 137, 143]. There is no neuromusculoskeletal model as the implementation of human-robot interface with real-time tuning for forearm pronation and supination. Currently, the studies involving the musculoskeletal system functional model, are mainly some simulation software platforms of musculoskeletal modeling, such as SIMM (MAC MusculoGraphics company), AnyBody (AnybodyTechnology), Adams (MSC Software), Visual3-D (C-Motion company), or one point joint simplification.

SIMM is a computational model of biological systems which can be used for models establishment, animation and three-dimensional musculoskeletal system analysis. It can accurately simulate the movements of human and animal. Now the human musculoskeletal models of SIMM were created by hundreds of biomechanics to simulate the motions such as stepping, running, cycling and stair climbing. It allows the researchers to develop a model which can faithfully reproduce the known neuromuscular skeletal system function. SIMM is an interactive software package which allows users to develop, evaluate and modify almost all musculoskeletal structures [134, 144]. SIMM allows users to build model for an accurate reflection of the muscle force generation, skeleton geometry, joint kinematics and dynamics.

However the establishment of SIMM model requires the SIMM file loader to create a data structure representing the musculoskeletal model by reading a set of bone, a joint document and a muscle file. It has a large database of skeletons with complex geometry and muscles with complex muscle path. Therefore, it cannot achieve real-time tuning, and not suitable for this kind of human-robot interface.

This thesis is going to establish a kind of human-robot interface for forearm pronation and supination. The musculoskeletal model of this interface must meet the human body physiological structure as reference, simple and practical, and easy for online tuning.

5.2.1 Assumptions of the Forearm Modeling

In order to build a model suitable for human-robot interface, necessary simplification is the first thing to consider. Because of the complexity of human physiological structure, it is difficult for a

model to full compliance with human physiological characteristics. Also, a real physiological structure model cannot quickly respond to the changes of users or actions because of the lots of tuning time. So a simplified model for the uses of real-time interface need to be established based on human anatomy, and the assumptions of this model are shown as follow:

1. Definition of forearm rotation

The neutral position of forearm refers to the shoulder close to the body side, elbow in 90° flexion, palm straight and inward side and thumbs up side. The movement with palm downward is the pronation, and the movement with palm upward is supination. Figure 5.5 shows the relative position of the radius and ulna in forearm pronation, supination and neutral position.

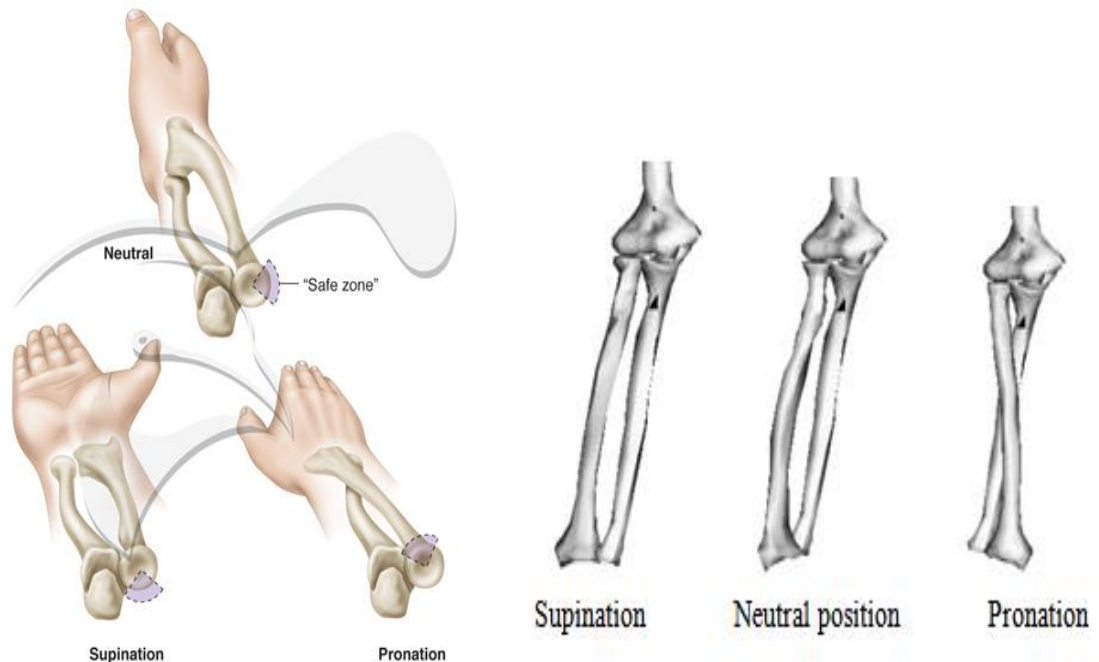


Figure 5.5: Definition of forearm rotation and the relative position of the radius and ulna

2. Motion range of forearm rotation

The maximum angle of normal pronation and supination are 180°-190°, wherein pronation 80°-90°, supination 90°-100°.

3. Rotation axis

During rotation, the ulna is regarded as fixed, and the axis is through the center of the radial head at proximal side, and through the center of cross-section of ulnar head at distal side. The

offset of rotation axis is ignored during forearm supination/pronation [135].

4. Forearm modeling

In order to make the musculoskeletal geometry of the forearm movement more close to the human physiological characteristics, the ulna size and radius size of a cadaveric forearm in hospital have been measured as a reference to the model. The measurement position of bone and corresponding size data are in Figure 5.6 and Table 5.1.

5. Muscle modeling

Three muscles, pronator teres, pronator quadratus and supinator, are selected to establish the physiological model of forearm rotation.

Table 5.1 The size of ulna and radius of a cadaveric forearm

Position	Radial diameter (mm)	Ulna diameter (mm)	Space between Radial and Ulna (mm)
Cross-section A (maximum diameter of the top)	14.17	21.95	-
Cross-section B (constriction below the maximum diameter)	11.10	16.87	-
Cross-section C (1/4 from the top)	11.97	12.0	-
Cross-section D (1/2 from the top)	14.90	10.21	4.3
Cross-section E (1/4 from the bottom)	13.99	9.97	11.05
Cross-section F (maximum diameter of the bottom)	22.63	13.72	11.79

Radial length: 201mm. Ulna length: 217mm;

6. Muscle path

The muscle path directly affects the calculation of muscle length and muscle force, also affects the accuracy of the musculoskeletal model. The method of modeling muscle path must be both to meet the physiological characteristics of the muscle and to achieve the purpose of rapid calculation. According to the characteristics of pronator teres, pronator quadratus and supinator, the pronator teres and pronator quadratus are simplified to the straight lines connected to the muscle starting and ending point. The supinator is simplified to a straight line segment and an arc.

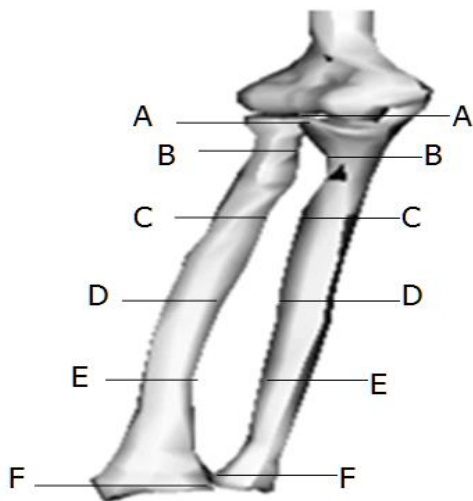


Figure 5.6: Measured skeleton

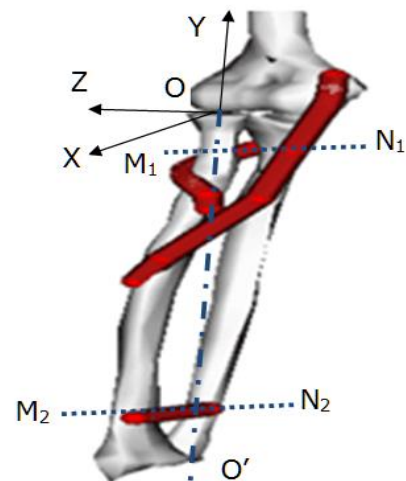


Figure 5.7: Coordinate system of forearm rotation model

5.2.2 Musculoskeletal Model of Forearm Rotation

Based on the above assumptions, the muscles were simplified by straight lines and arcs, and the skeletons are simplified by circles. This simplification aims at most simplifying the complex biological structures into the more clearly geometric structures which are easier for calculation. The coordinate system of forearm musculoskeletal model is shown in Figure 5.7. During the forearm rotation, ulna is fixed and radial rotates around the central axis OO' . The coordinate origin passed the center of radial head, Y axis is along the center axis OO' to the above direction, X axis is to the front direction, Z axis direction is determined with the right-hand rule.

The musculoskeletal model involves three computations: muscle length, twisting moment and moment arm. The twisting moment and moment arm are calculated in profile M_1N_1 and M_2N_2 . M_1N_1 is a profile through the starting point of supinator and perpendicular to the central axis OO' . The twisting moment and moment arm of supinator are calculated in profile M_1N_1 , so does the ones of pronator teres. This is because, the length change of pronator teres above M_1N_1 is small and can be ignored. The profile M_2N_2 is through the starting point of pronator quadratus and perpendicular to the central axis OO' . The twisting moment and moment arm of pronator quadratus are calculated in profile M_2N_2 .

The musculoskeletal models of these three muscles are as follows:

1. Supinator (SUP)

Figure 5.8 shows the musculoskeletal model of the projection of supinator in profile M_1N_1 . The M_1N_1 is on the XZ plane with $Y = -22$. A_1 is the fixed point of muscle (the projection of supinator starting point in M_1N_1). B_1 is the moving point of muscle (the projection of supinator ending point in M_1N_1). The circle O is the radial, and circle O_1 is the ulnar. O is the rotation axis (in profile M_1N_1 , the rotation axis is approximately coincident with the radius center).

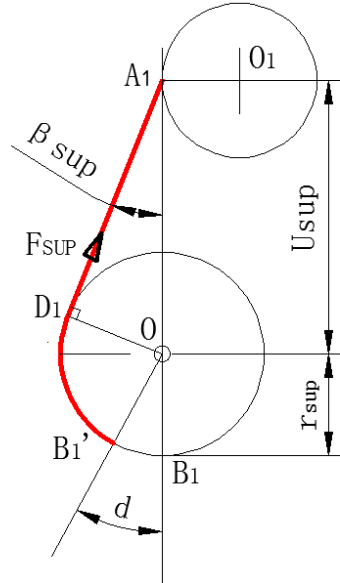


Figure 5.8: The musculoskeletal model of supinator

In YOZ plane, the angle between supinator and profile M_1N_1 is α_{sup} .

Suppose the coefficient:

$$K_{sup} = \frac{1}{\cos(\alpha_{sup})} \quad (5.1)$$

$$OA_1 = U_{sup} \quad (5.2)$$

Radius of rotation:

$$r_{sup} = OB_1 = OD_1 \quad (5.3)$$

where B_1 is the ending point of supinator on neutral position.

For any angle d , it is delimited that supination is positive and pronation is negative. Thus:

$$\beta_{\text{sup}} = \angle OA_1D_1 = \sin^{-1} \frac{r_{\text{sup}}}{U_{\text{sup}}} \quad (5.4)$$

The projection length of supinator on profile M_1N_1 :

$$l_{\text{sup}1} = \overline{A_1D_1} + \widehat{D_1B_1'} = U_{\text{sup}} \cos(\beta_{\text{sup}}) + r_{\text{sup}} (90 + \beta_{\text{sup}} - d) * \frac{\pi}{180} \quad (5.5)$$

The actual length of supinator is:

$$l_{\text{sup}} = l_{\text{sup}1} K_{\text{sup}} \quad (5.6)$$

The moment arm and twisting moment of supinator are as follow:

$$MA_{\text{sup}} = r_{\text{sup}} \quad (5.7)$$

$$M_{\text{sup}} = MA_{\text{sup}} F_{\text{sup}} / K_{\text{sup}} \quad (5.8)$$

where F_{sup} is the muscle force of supinator.

2. Pronator Teres (PT)

Figure 5.9 shows the musculoskeletal model of the projection of pronator teres in profile M_1N_1 . A_3 is the fixed point of muscle (the projection of pronator teres starting point in M_1N_1). B_3 is the moving point of muscle (the projection of pronator teres ending point in M_1N_1). O is the rotation axis (in profile M_1N_1 , the rotation axis is approximately coincident with the radius center).

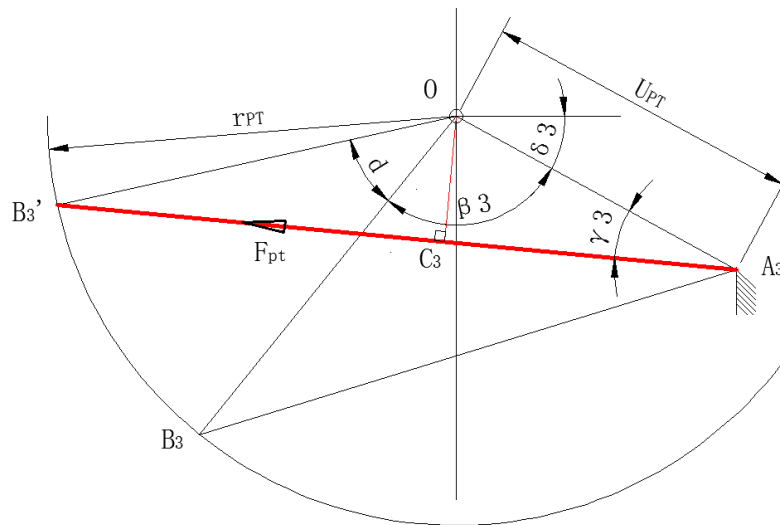


Figure 5.9: The musculoskeletal model of pronator teres

In YOZ plane, the angle between pronator teres and profile M_1N_1 is α_{PT} .

Suppose the coefficient:

$$K_{PT} = \frac{1}{\cos(\alpha_{PT})} \quad (5.9)$$

$$OA_3 = U_{PT} \quad (5.10)$$

Radius of rotation:

$$r_{PT} = OB_3 \quad (5.11)$$

Based on the physiological structure, the angle between OA_3 and Z axis is $\delta_3 = 28^\circ$. B_3 is the ending point of pronator teres on neutral position. The length of pronator teres on neutral position $l_{PT0} = A_3B_3 = 44\text{mm}$. Thus:

$$\beta_3 = \angle A_3OB_3 = \cos^{-1} \frac{OA_3^2 + OB_3^2 - A_3B_3^2}{2 \cdot OA_3 \cdot OB_3} = 100.05^\circ \quad (5.12)$$

For any angle d , the projection length of pronator teres on profile M_1N_1 :

$$l_{PT1} = A_3B_3' = \sqrt{r_{PT}^2 + U_{PT}^2 - 2r_{PT}U_{PT}\cos(\beta_3 + d)} \quad (5.13)$$

The actual length of pronator teres is:

$$l_{PT} = l_{PT1}K_{PT} \quad (5.14)$$

From the law of sine:

$$\gamma_3 = \angle OA_3B_3' = \sin^{-1} \frac{r_{PT} \sin(\beta_3 + d)}{l_{PT1}} \quad (5.15)$$

The moment arm and twisting moment of pronator teres are as follow:

$$MA_{PT} = OC_3 = U_{PT} \sin \gamma_3 \quad (5.16)$$

$$M_{PT} = MA_{PT}F_{PT}/K_{PT} \quad (5.17)$$

where F_{sup} is the muscle force of pronator teres.

3. Pronator Quadratus (PQ)

Figure 5.10 shows the musculoskeletal model of the projection of pronator quadratus in profile M_2N_2 . The M_2N_2 is on the XZ plane with $Y = -200$. A_2 is the fixed point of muscle (the projection of pronator quadratus starting point in M_2N_2), B_2 is the moving point of muscle (the projection of pronator quadratus ending point in M_2N_2). O is the rotation axis (in profile M_2N_2 , the rotation axis is approximately coincident with the ulna center).

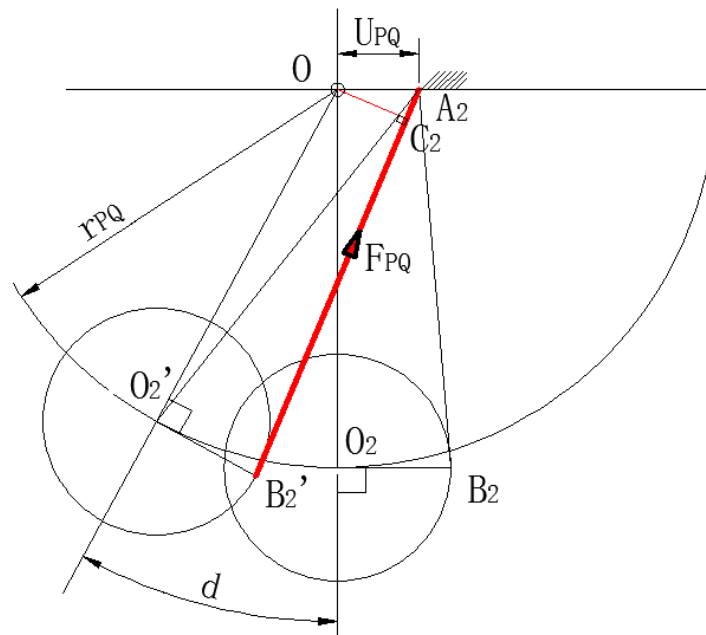


Figure 5.10: The musculoskeletal model of pronator quadratus

Circle O_2 is radius, the radius of radius circle is as follow:

$$O_2B_2 = O_2'B_2' = 9\text{mm} \quad (5.18)$$

The radius of radius rotation around the rotational center O is:

$$r_{PQ} = OO_2 \quad (5.19)$$

In YOZ plane, the angle between pronator quadratus and profile M_2N_2 is $\alpha_{PQ} = 0^\circ$.

Suppose:

$$OA_2 = U_{PQ} \quad (5.20)$$

B_2 is the ending point of pronator quadratus on neutral position. For any angle d :

$$A_2O_2' = \sqrt{r_{PQ}^2 + U_{PQ}^2 - 2r_{PQ}U_{PQ}\cos(90^\circ + d)} \quad (5.21)$$

$$\angle OO_2'A_2 = \sin^{-1} \frac{U_{PQ} \sin(90^\circ + d)}{A_2O_2'} \quad (5.22)$$

The actual length of pronator quadratus is:

$$l_{PQ} = A_2B_2' = \sqrt{O_2B_2'^2 + A_2O_2'^2 - 2 \cdot O_2B_2' \cdot A_2O_2' \cdot \cos(90^\circ - \angle OO_2'A_2)} \quad (5.23)$$

The moment arm of pronator quadratus is:

$$\angle OA_2O_2' = 90^\circ - d - \angle OO_2'A_2 \quad (5.24)$$

$$\angle B_2'A_2O_2' = \sin^{-1} \frac{O_2B_2' \sin(90^\circ - \angle OO_2'A_2)}{l_{PQ}} \quad (5.25)$$

$$MA_{PQ} = OC_2 = U_{PQ} \sin(\angle OA_2O_2' + \angle B_2'A_2O_2') \quad (5.26)$$

The twisting moment of pronator quadratus is as follow:

$$M_{PQ} = MA_{PQ}F_{PQ} \quad (5.27)$$

where F_{PQ} is the muscle force of pronator quadratus.

The total joint twisting moment is as follow:

$$M_{Tot} = \frac{MA_{PT}F_{PT}}{K_{PT}} + MA_{PQ}F_{PQ} - MA_{sup}F_{sup}/K_{sup} + M_p + O \quad (5.28)$$

where

$$M_p = -\beta\omega \quad (5.29)$$

M_p is the dynamic torque between joints, β is the damping coefficient of forearm motion, ω is the forearm angular velocity (rad/s), O is a compensation amount.

Finally, coincide the profile M_1N_1 and M_2N_2 , with the projections of muscle SUP, PT and PQ, along Y axis, to obtain a geometry model of three muscles and skeletons in neutral position, as shown in Figure 5.11. This is a beautifully and simple geometry. It also proves such a truth while the structure of the human body is perfect and complex, but also coincidence with the simple geometry. Figure 5.12 is the geometry model of three muscles in any position.

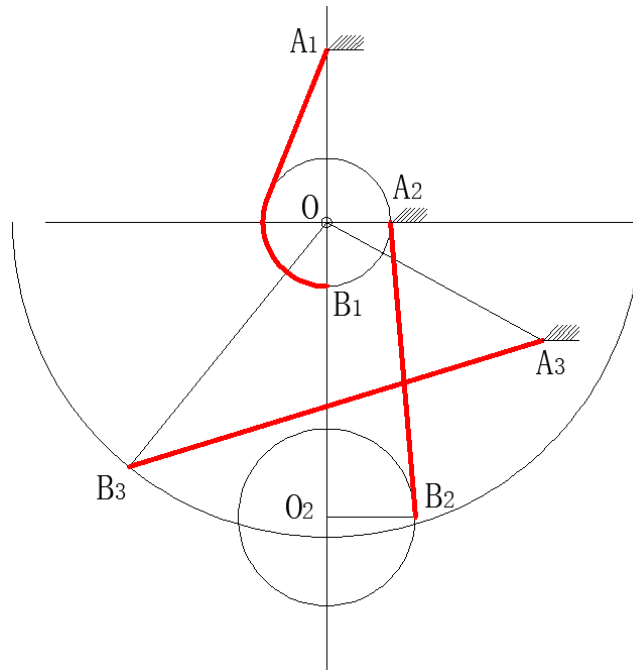


Figure 5.11: Musculoskeletal geometry model of three muscles in neutral position

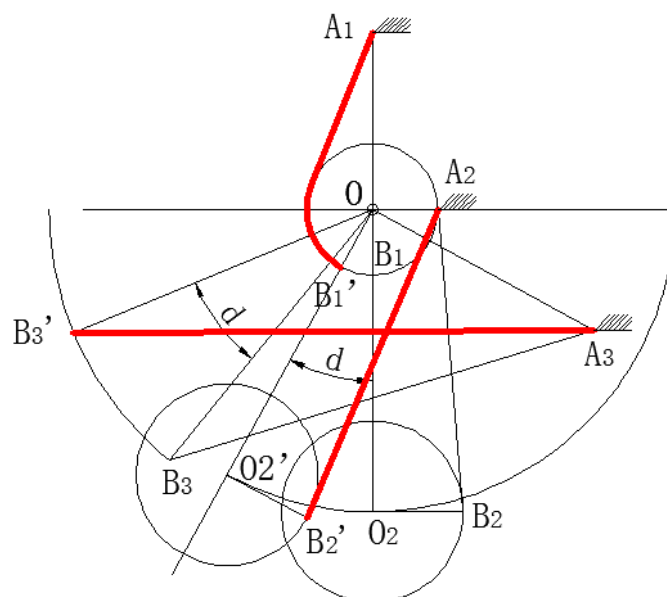


Figure 5.12: Musculoskeletal geometry model of three muscles in any position

5.3 Model Validation

5.3.1 Test procedures

The experimental data was acquired from four healthy subjects (two male and two female), between 25 and 28 years old. The experimental procedure for this study was approved by the Ethics Committee of the University of Auckland, and also with the subjects well informed and consent to participate in. Each subject was instructed to perform five different actions. The neutral position is the standing position, shoulder close to the body in inner side, elbow 90° flexion, palm straight and inward side, and the thumb upside. The rotation with palm downward is pronation, and the one with palm upward is supination. There are five groups of movement for the subjects' forearm, as follows:

- The first set of motion involves a basic movement, the forearm rotates from the palm downward extreme position to the palm upward extreme position (Sup-Pro), at a moderate speed.
- The second set of movement is also a basic movement, the forearm rotates from the palm upward extreme position to the palm downward extreme position (Pro-Sup), at a moderate speed.
- The third set of motion is an extended consecutive movement, the forearm rotates continuously from fully pronation to supination and backwards to pronation with full rotation range (Forearm Continuous Cycles Test).
- The fourth set of motion is an example of daily life activities, the forearm rotates continuously with random amplitudes and different speeds (Random movement test).
- The fifth set is a supplement experimental group, the forearm rotates from the palm downward extreme position to the palm upward extreme position (Sup-Pro) at a moderate speed, but holds a weight of 0.5kg.

Each movement trial lasted 2 to 8 seconds and five trials were performed for each type of movement set. To prevent fatigue, there were several 60-second rests between the trials.

5.3.2 Results

The flowchart is shown in Figure 5.13, where MATLAB / Simulink module has been used to program the signal processing, muscle force, joint torque and kinematic calculation models, to

simulate the forearm rotation.

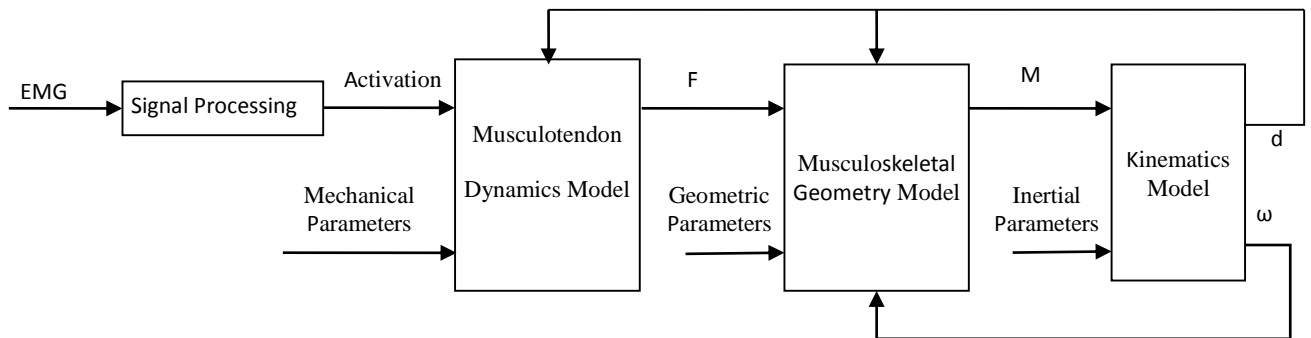


Figure 5.13: Flowchart of model simulation for forearm rotation

The model parameters were divided into two groups, one is the fixed value (with little effect to the model while the value changing), another group can be measured from an individual or be tuned. Based on the sensitivity study similar to the elbow model sensitivity analysis in Chapter 4, 14 parameters were eventually selected for the tuning parameters (Table 5.2), and 10 less sensitive parameters were fixed as in Table 5.3. The genetic algorithms (GA) and differential evolution (DE) were used respectively to optimize these parameters. The tuning objective function is the minimum of the root mean square error (RMSE) between predicted and measured forearm rotation angle. For each of the subjects and their actions, GA and DE tuning algorithms were respectively run for four times.

Table 5.2 Tuning parameters in forearm pronation and supination model

Parameters	Description	Unit	Tuning Range
R_{SUP}	Individual coefficient of SUP	-	1-3
R_{PT}	Individual coefficient of PT	-	1-3
$C_{passSUP}$	User-specific coefficient for elasticity of SUP	-	1-3
C_{passPT}	User-specific coefficient for elasticity of PT	-	1-3
F_{Maxsup}	Maximum muscle force of SUP	N	300-600
F_{MaxPT}	Maximum muscle force of PT	N	200-400
F_{MaxPQ}	Maximum muscle force of PQ	N	50-200
l_{optsup}	Optimization muscle length of SUP	m	0.01-0.04
l_{optPT}	Optimization muscle length of PT	m	0.02-0.05

l_{optPQ}	Optimization muscle length of PQ	m	0.01-0.03
U_{sup}	Distance from SUP starting point to the Radius rotation center	mm	15-20
U_{PT}	Distance from PT starting point to the Radius rotation center	mm	22-27
r_{sup}	Distance from SUP ending point to the Radius rotation center	mm	6-10
r_{PT}	Distance from PT ending point to the Radius rotation center	mm	30-34

The PT represents pronator teres, PQ represents pronator quadratus, and SUP represents supinator.

The information of muscle force and muscle length is from OpenSim, and the other remaining parameters information is from the anatomy test or calculation.

Table 5.3 Fixed parameters in forearm pronation and supination model

Parameters	Description	Unit	Value
R_{PQ}	Individual coefficient of PQ	-	1
C_{passPQ}	User-specific coefficient for elasticity of PQ	-	1
B_{PQ}	User-specific coefficient for viscosity of PQ	Ns/m	0.1
B_{PT}	User-specific coefficient for viscosity of PT	Ns/m	0.1
B_{SUP}	User-specific coefficient for viscosity of SUP	Ns/m	0.1
β	Damping coefficient of forearm motion	Nms/rad	0.2
U_{PQ}	Distance from PQ starting point to the Radius rotation center	mm	6
r_{PQ}	Distance from PQ ending point to the Radius rotation center	mm	30.5
K_{sup}	In YOZ plane, coefficient of the angle between SUP and profile M_1N_1	-	3.16
K_{PT}	In YOZ plane, coefficient of the angle between PT and profile M_1N_1	-	1.62
O	Moment compensation constant	Nm	0.2
I	Moment of inertia of forearm and hand	kgm ²	0.0055

The PT represents pronator teres, PQ represents pronator quadratus, and SUP represents supinator.

The information of muscle force and muscle length is from OpenSim, and the other remaining parameters information is from the anatomy test or calculation.

5.3.2.1 Characteristics of Forearm Musculoskeletal Model

Compared with elbow flexion/extension, the amplitude of forearm muscles usage is much smaller, in terms of human physiological structure, or circumstances of daily life and exercise. In addition, the rotation joint range of forearm motion is relatively small. Thus, the musculoskeletal model of

forearm rotation has its particularity, and mainly represented in the following aspects:

1. The weakness of muscle signals

In a complete forearm Pro- Sup process, Figure 5.14 is the sEMG signal and activation of the pronator teres (PT). Figure 5.15 is the signal and activation of PT with a 0.5kg weight. In contrast, the sEMG signals was significantly enhanced when the hand held weights. This is because, the muscle strength and motion stability are enhanced with external weights.

Figure 5.16 shows the sEMG signal and activation of biceps (Bi) during a complete elbow flexion/extension process. Compared with Figure 5.14, the sEMG signal of Bi is much larger than the one of PT. This is due to the different physiological structure and different frequency of muscle usage in people's daily lives, which leads the muscles for flexion/extension stronger than the muscles for pronation/ supination.

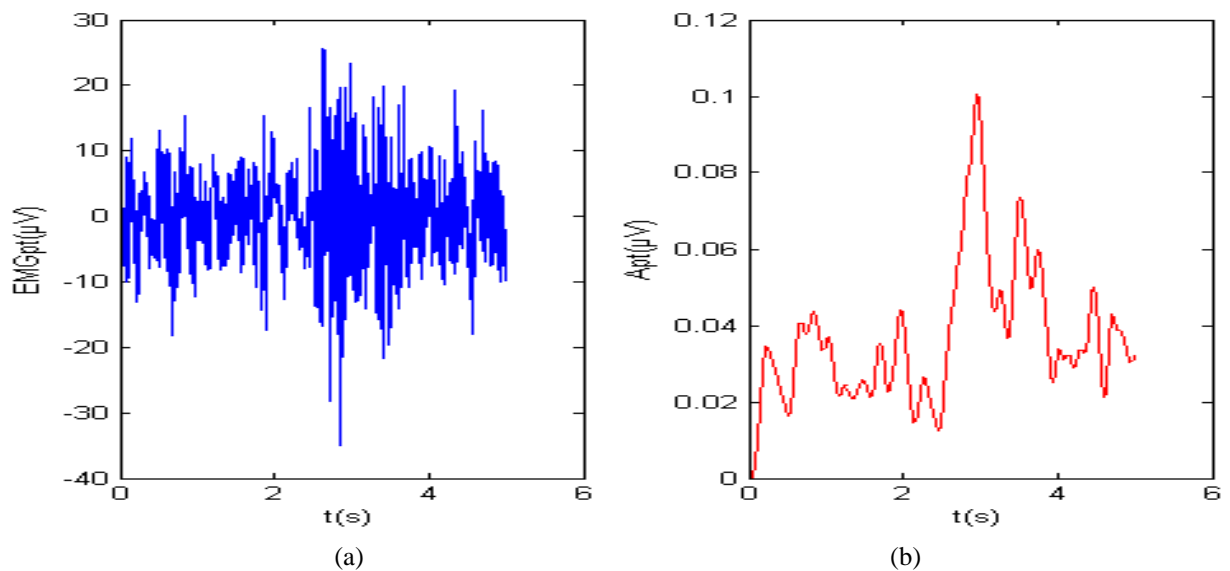


Figure 5.14: The sEMG signal and activation of pronator teres (PT) in Sup-Pro

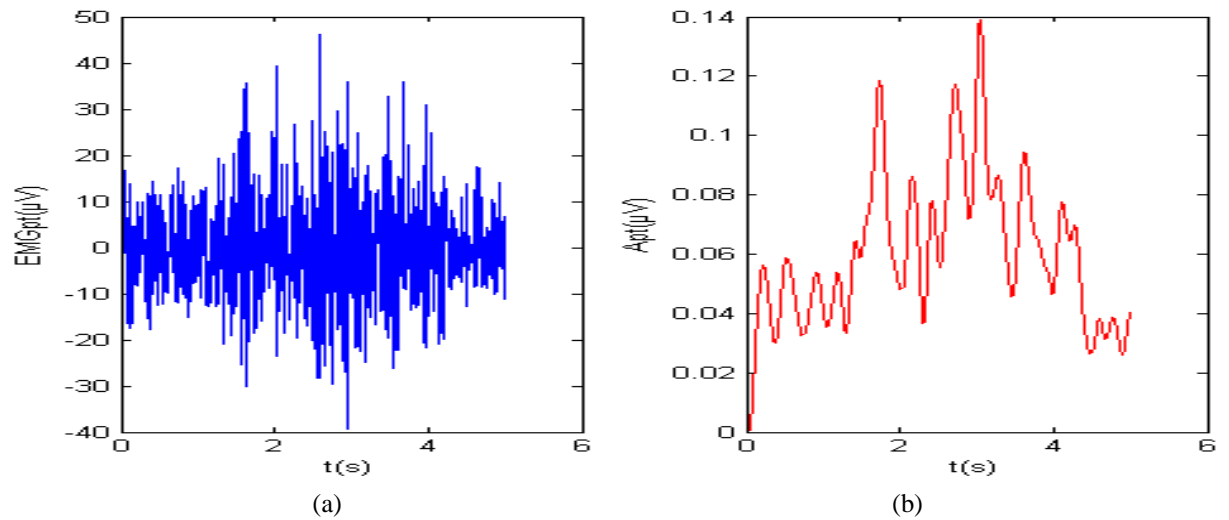


Figure 5.15: The sEMG signal and activation of PT with a 0.5kg weight in Sup-Pro

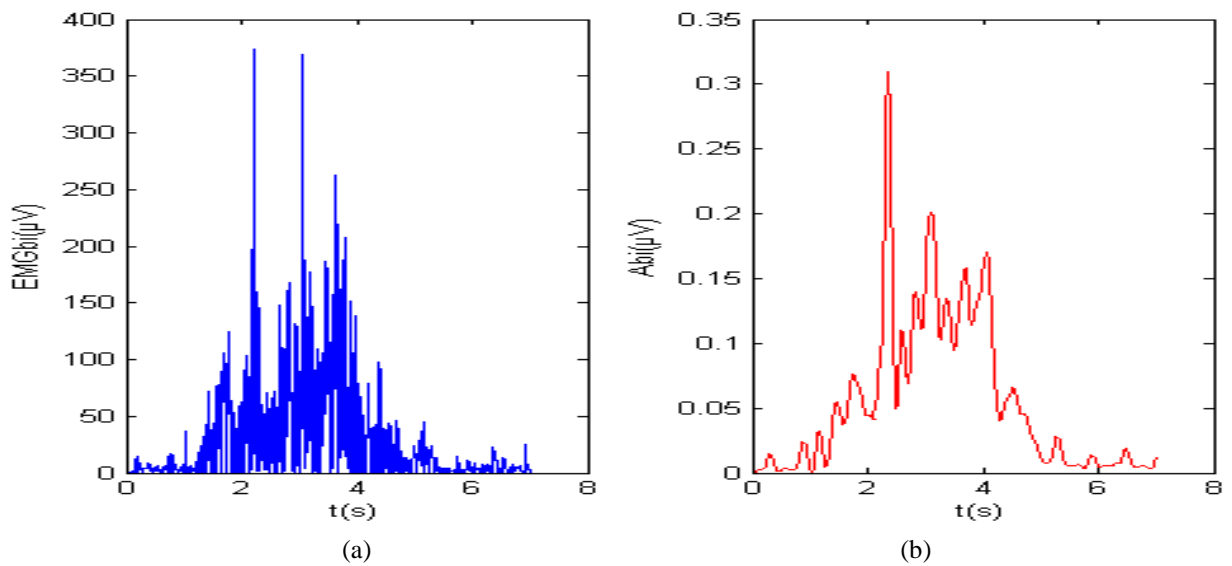


Figure 5.16: The sEMG signal and activation of biceps (Bi) in flexion-extension

2. The small changes in muscle length and moment arm

Figure 5.17 shows the length changes of PT, PQ and SUP during Sup-Pro process. Especially the muscle length changes of PQ and SUP were only 0.0103m and 0.0159m ($L_{pt1} = 0.0465\text{m}$). These results are similar to the muscle length changes in OpenSim models. Also, from Figure 5.17 (b), the changes in moment arm of PT, PQ SUP were small as well. This is due to the physical structure of the forearm and the three muscles. Thus, the total joint moment and moment changes, which is

generated by muscle length, muscle force and moment arm, are correspondingly small. The trend of moment is similar to the result of Hale's [139].

Overall, the sEMG signals of forearm rotation muscles are weak, the movement time is short, and the signals are more susceptible to be interfered. The muscle length changes of PQ is small. Also, since PT, PQ and SUP all have both deep and shallow portions, the signal capture is more difficult.

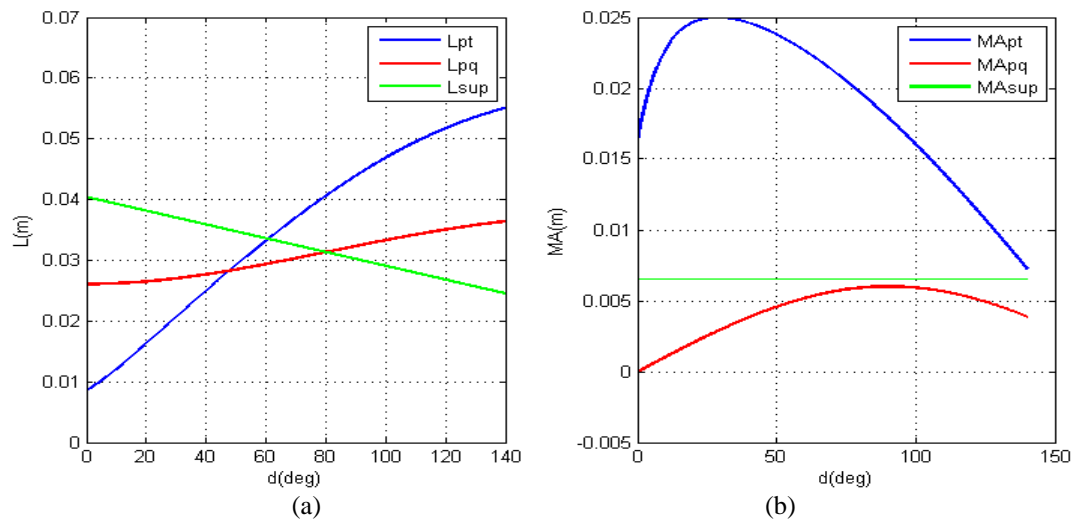


Figure 5.17: (a) The changes of muscle length of PT, PQ and SUP (in Sup-Pro) . (b) The changes of moment arm of PT,PQ and SUP (in Sup-Pro)

5.3.2.2 Prediction Results of Forearm Rotation

The sample RMSE results and joint angle curves of Sup-Pro, Pro- Sup, Forearm Continuous Cycles and Random movement Test are shown in Figure 5.18-5.21.

For a basic pronation or supination movement (such as in Figure 5.18 and Figure 5.19), the tuned predicted joint angles were accurately matched the measured joint angle. The RMSEs in all Sup-Pro tests with different subjects and different times were within 3.15° – 8.47° . The RMSEs in Pro- Sup Tests were within 4.71° – 9.69° .

For a complex forearm movement (such as in Figure 5.20 and Figure 5.21), the RMSEs of all Continuous Cycles Tests were within 12.75° – 18.25° , and the RMSEs of Random Movement Tests were within 10.5° – 16.36° . Compared with basic movement test, although there were some prediction errors in the curve peak or valleys, where related to the extreme positions of pronation or supination, but the movement trends were still consistent. The reason is that, when the forearm just starts to a opposite direction, such as from max Sup to Pro, the main effective muscle - pronator starts to contract and generates muscle force, however, the supinator has not fully relaxed yet. In

this case, the EMG-based model will calculate both pronation moment and supination moment at the angle-curve peak, and may leads to a error. When the forearm is smoothly into a basic movement process (Pro- Sup or Sup-Pro), the EMG signals are more clear and easier to be detected, so the predicted joint angle is more accurate. This forearm prediction problem does not occur during elbow flexion/extension movement tests, because of the specific characteristics of forearm musculoskeletal model discussed in Section 5.3.2.1.

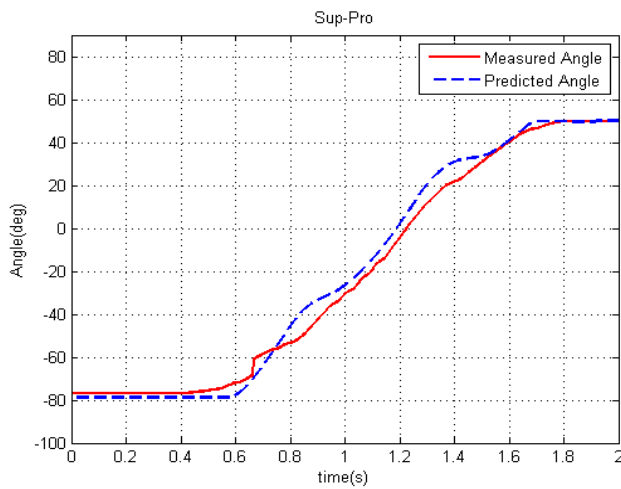


Figure 5.18: A result of the basic Sup-Pro Test. (RMSE=5.10 °)

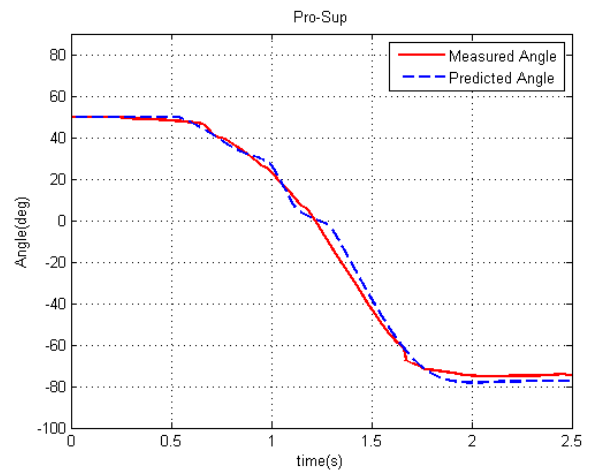


Figure 5.19: A result of the basic Sup-Pro Test (RMSE=3.71 °)

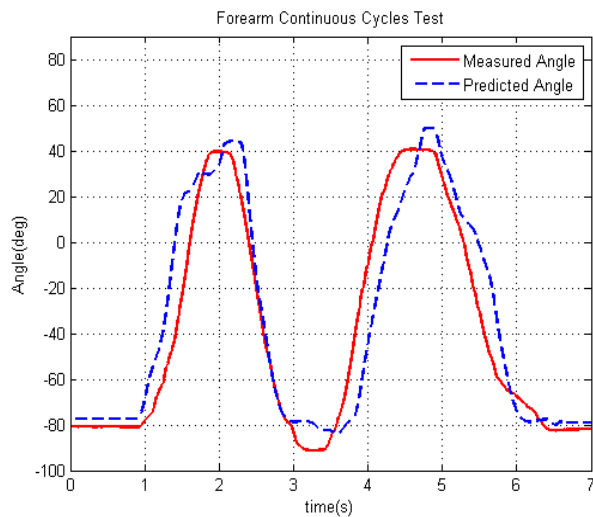


Figure 5.20: Result of the Forearm Continuous Cycles Test.

RMSE=16.80 °

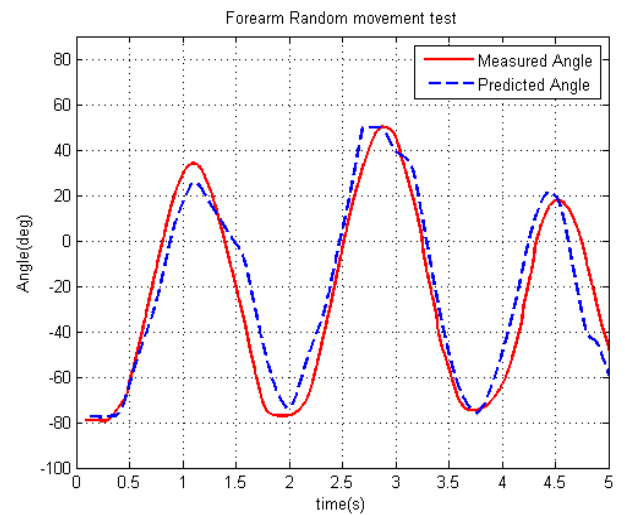


Figure 5.21 A result of the Random movement test.

RMSE=12.86 °

Table 5.4 shows the summary of RMSEs for 4 subjects and 5 set of tests. The overall average is the average of all subjects RMSEs in one set of movement, which were 5.88 °, 5.94 °, 15.31 °, 13.35 ° and 5.58 °. These results indicate that the musculoskeletal model of forearm has a certain accuracy and stability in pronation and supination movement prediction.

Table 5.4 Summary of forearm experimental results (RMSE in Degrees)

Subject	Sup-Pro	Pro- Sup	Continuous Cycles	Random Movement	Sup-Pro (With 0.5 kg weight)
A	3.15 °±2.83 °	4.71 °±3.25 °	12.75 °±6.83 °	10.5 °±5.85 °	3.22 °±3.25 °
B	6.45 °±3.22 °	4.78 °±4.65 °	15.43 °±3.43 °	14.41 °±4.76 °	6.28 °±4.34 °
C	5.45 °±4.25 °	6.56 °±3.88 °	14.82 °±7.81 °	12.12 °±4.75 °	5.33 °±3.29 °
D	8.47 °±3.68 °	9.69 °±2.67 °	18.25 °±8.46 °	16.36 °±6.78 °	7.48 °±3.79 °
Total Average	5.88 °	6.44 °	15.31 °	13.35 °	5.58 °

5.3.3 Discussion

The results in Table 5.3 shows the variability of this EMG-based forearm model. For the above 5 sets of movement, there is a large difference in the RMSE value of the same subject in different tests. The difference in RMSE of different subjects in a similar movement is small.

In test Group 1 (Sup-Pro), Group 2 (Pro- Sup) and Group 5 (Sup-Pro, Holding a weight of 0.5 kg), the average RMSEs of all one-way movements are low (from 5.58 ° to 6.44 °). This means the model can accurately predict all the one-way movement.

For the complex movement in Group 3 (Continuous Cycles), the accuracy of the model is reduced, and there is more variability between different individuals. For the Group 4 of random motion, the total average RMSE is smaller compared with continuous cycles movement. The elbow flexion/extension tests in Chapter 4 also had a similar result. This may be the reason that the freedom of random motion makes the subjects easier to relax.

The above results show that the forearm pronation/supination model in this chapter can accurately identify and predict the movement coming from different subjects, so it is able to meet the different individual variability.

The next step is the extension on the number of subject and the diversity of the movement, in order to complete a more in-depth statistical analysis and the more certainty observations. Meanwhile, fatigue should be considered in the experiment, since EMG signals are significantly influenced by fatigue. Online parameters tuning is considered to solve the fatigue issues.

5.4 Chapter Summary

This chapter has established a neuromusculoskeletal model for forearm rotation.

In view of the forearm rotation is a very complicated movement, this chapter firstly analyzed the physiological structure of the forearm skeletal system, and determined the forearm rotation center that is proximally through the radial head and distally through the center of ulnar head cross-section. Also, the forearm major muscles and their positions have been analyzed.

The sizes of a hospital cadaver ulna and radius were measured in this chapter, as a reference to the model establishment. According to relevant physiological data, a musculoskeletal model, including three muscles (PT, PQ, SUP) and two skeletons (ulna, radius), has been established. By the comprehensive usage of the actual measurement data and the theoretical formulas, the model parameters have been initially determined. With MATLAB / Simulink for programming, the biomechanical model of forearm rotation has been successfully simulated.

Five groups of experiments of forearm rotation have been designed. According to the results, the particularity of this forearm musculoskeletal model has been pointed out. 14 selected model parameters are respectively tuned by Genetic Algorithms (GA) and Differential Evolution (DE). The cost function is the root mean square error (RMSE) between the predicted and measured forearm rotation angle. By analyzing the experimental RMSEs of five groups test, the accuracy and feasibility of this forearm biomechanical model has been confirmed. During the vilification, the forearm model can mostly achieve real-time when the tuning takes only the key parameters and with a not large tuning range. And the limitation of running time is all because of the tuning method, not the model itself. Further information about real-time tuning is informed in Chapter 6.

Chapter 6 A Neuromuscular Interface

for Motion Prediction of the Upper Limb

In previous chapters, this thesis has discussed EMG signal processing and established the muscle model, musculoskeletal geometry model and kinematics model of elbow joint flexion / extension. Also, based on the physiological structure of forearm pronation / supination, a new musculoskeletal geometry model of forearm rotation has been developed. Since the movement of human upper limb is a combination of elbow joint movement and forearm movement, so this chapter presents a two degree of freedom (2-DOF) neuromuscular interface (NI) for the human upper limb movements by integrating the elbow and forearm models. So till now, the interface can predict three kinds of upper limb movements: elbow flexion / extension, forearm pronation / supination and complex movement. Also, in order to improve the performance of this 2-DOF NI, two kinds of tuning methods are developed and compared in this chapter.

6.1 Interface Design

The elbow flexion / extension and forearm pronation / supination can be regarded as two independent movements or combined into a composite motion (shown in Figure 6.1). They are independent from each other in the muscle signal selection: the elbow flexion / extension relies on biceps and triceps, the forearm pronation / supination depends on supinator, pronator teres and pronator quadratus. When the human arm acting as complex motion, ten channels are used to separately measure the five muscles EMG. The results for all muscles from signal envelope and muscle activation dynamics processing are put in one data file.

The muscle models of elbow flexion / extension and forearm pronation / supination are the same. They are formed based on the Hill model and full consideration of active force, passive force and

viscous force. However, some muscle model parameters of these two movement, such as the maximum muscle force (F_{Max}) or the optimal muscle fiber length (l_{opt}), are different.

The musculoskeletal geometry models of elbow flexion / extension and forearm pronation / supination are totally different. Most parameters of these two models vary widely. Thus, in the composite movement, the two musculoskeletal models are operated as two completely independent modules. The kinematic models of the elbow and forearm rotation are the same, and some parameters such as the forearm length (l_{Arm}) and the quality of forearm (m) are also the same.

Therefore, when the elbow flexion / extension and forearm pronation / supination models are combined, the operation of each model is independent unit and not interfere with each other. However, in parameters tuning, some new considerations should be taken: Some parameters belong to the independent movement, which means they only affect flexion / extension or pronation / supination movement, such as the maximum muscle force (F_{Max}), the optimal muscle fiber length (l_{opt}), the distance from the muscles SUP start point to the radius rotation center (U_{sup}), the distance from muscles SUP end point to the radius rotation center (r_{sup}) and so on. And some other parameters belong to both of the movements, which means they affect the flexion / extension and pronation / supination movements at the same time, such as the forearm length (l_{Arm}), the quality of forearm (m). Thus, these common parameters are important to be considered in the composite movement.

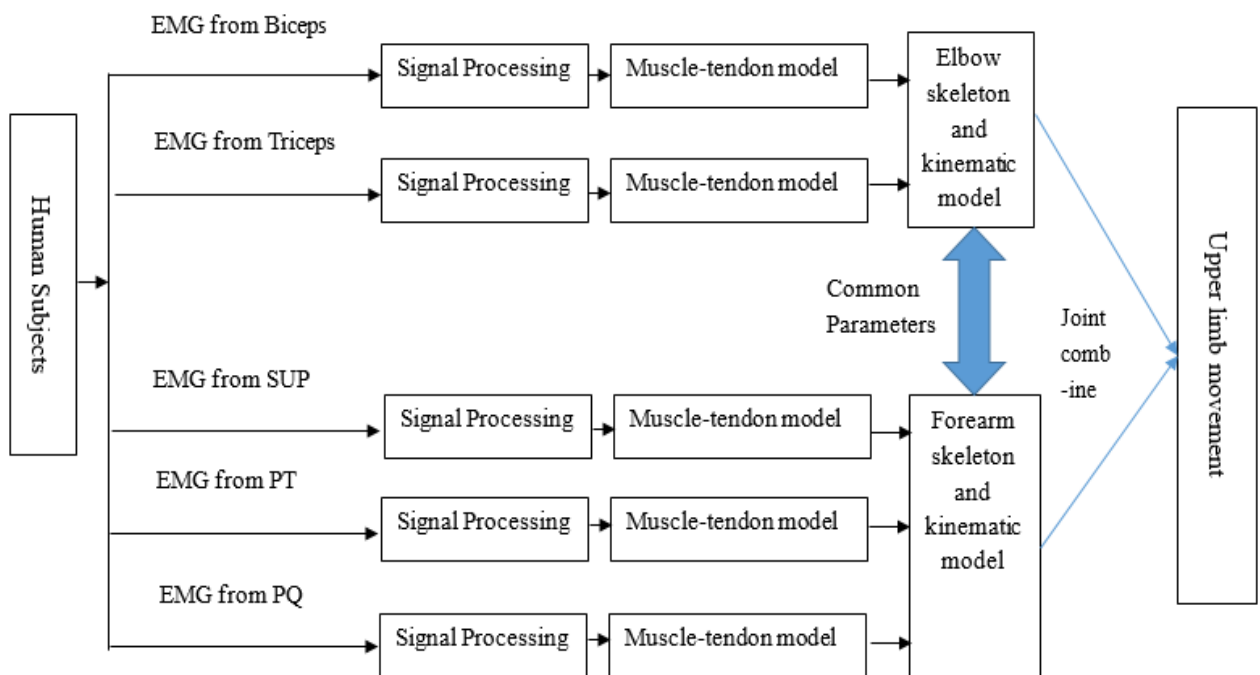


Figure 6.1 2-DOF interface of the elbow flexion/extension and forearm pronation/supination

6.2 Tuning Methods to Model Parameters

The purpose of parameter tuning is to make the model precisely match each subject. The objective function of tuning is minimizing the RMS (root mean square) between the model predicted joint angle and the actual joint angle. Since each tuning parameter has its certain range, mainly the physiological limitations of human body. Thus, the model tuning belongs to the optimization problem to obtain the combinatorial variables for minimizing the objective function under the given constraints. In nearly 30 years, in order to meet the needs of solving different optimization problems, the evolutionary algorithms get more and more attention, and are widely used in various fields, based on its high parallelism, self-organizing, self-adaptive and self-learning characters.

Evolutionary algorithms are a class of algorithm referencing the biological law of evolution[145]. They simulate the biological reproduction, mutation, recombination and selection. For an optimization problem, they randomly select a certain number of candidate solutions from the solution space to form an initial population, and use an encoding method for encoding the initial population. The initial population forms a new generation by the heredity, variation and hybridization. Then the algorithms determine the merits of this new population by its fitness function, to simulate the natural survival through this process. After several generations' survival, the fittest optimum population is gained, namely the optimal solution. The evolutionary algorithms have the following advantages: 1. By using the genetic code of optimization variables as calculating and searching objects, the algorithms can not only work for numerical optimization problems, but also for non-numerical optimization problems. 2. By only using the "fitness" message as the optimization information, and without other supporting information, the evolutionary algorithms can be applied to various optimization problems. 3. With the group search strategy, the algorithms can achieve the parallel searching and is more particularly suitable for multi-objective optimization strategy. 4. With random searching mechanism, the robustness of the algorithm is enhanced. Overall, the evolution algorithm, as a global search method, has the advantages of universality, parallelism, robustness and simplicity.

In the 2-DOF human-robot interface for upper limb movement, two kinds of evolutionary algorithm have been used for the model parameters tuning: Genetic Algorithm (GA) and Differential Evolution (DE)

6.2.1 Genetic Algorithm (GA)

GA was firstly proposed by professor Holland J at the University of Michigan (United States) in 1975. The basic flowchart of GA is shown in Figure 6.2. GA includes two processes: initialization and evolution, and the process of evolution includes three genetic manipulation: selection, crossover and mutation.

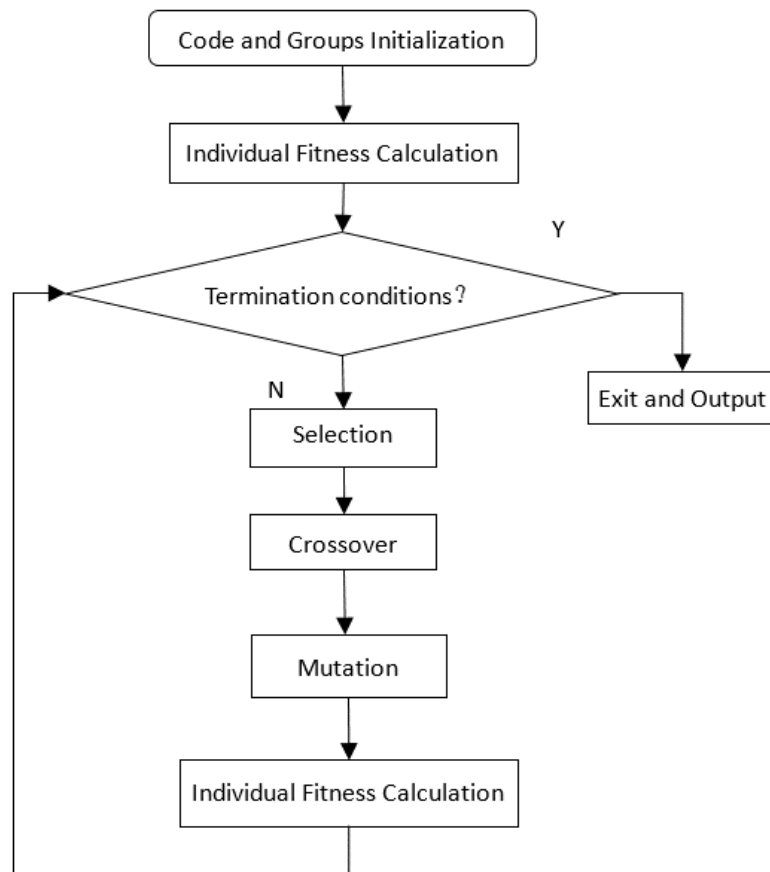


Figure 6.2: The Flowchart of Genetic Algorithm

When programming in MATLAB, the GA option in the Global Optimization Toolbox can be used for the tuning work. However, the time of tuning processing is too long.

In this chapter, GA was programmed in MATLAB for tuning calculation. The running speed was much faster than using the toolbox. The RMS between the predicted joint angle and the actual measured joint angle was set as the objective function of GA. The equation of objective function is shown in Equation (6.1)

$$\min f = \sqrt{\frac{1}{n} \sum_{i=1}^n (D_{\text{pred}} - D_{\text{actu}})^2} \quad (6.1)$$

where f is the fitness function, n is the number of samples, D_{pred} is the predicted joint angle, D_{actu} is the actual measured angle.

For example, for the elbow flexion and extension model, a total of 14 parameters (the physical meanings of these parameters is shown in Chapter 3) were tuned, which comprising:

$$X(1) = \text{params. } L_{\text{opt}_{\text{bi}}}$$

$$X(2) = \text{params. } L_{\text{opt}_{\text{tr}}}$$

$$X(3) = \text{params. } F_{\text{max}_{\text{bi}}}$$

$$X(4) = \text{params. } F_{\text{max}_{\text{tr}}}$$

$$X(5) = \text{params. } C_{\text{pass}_{\text{bi}}}$$

$$X(6) = \text{params. } R_{\text{bi}}$$

$$X(7) = \text{params. } K_{\text{bi}}$$

$$X(8) = \text{params. } \text{Hum}$$

$$X(9) = \text{params. } U_{\text{bi}}$$

$$X(10) = \text{params. } U_{\text{tr}}$$

$$X(11) = \text{params. } A$$

$$X(12) = \text{params. } m$$

$$X(13) = \text{params. } L_{\text{Arm}}$$

$$X(14) = \text{params. } \text{ThreTr}$$

The X , which could make the objective function reach minimum, is the optimal solution.

The algorithm parameters of GA were defined as follows:

number of population members: NIND=50;

maximum number of iterations: MAXGEN=100;

number of variables: NVAR=14;

precision of variables: PRECI=20;

crossover probability: GGAP=0.8;

By the usage of Global Optimization Toolbox in MATLAB, the tuning time was about 1 hour. By the usage of self-programmed GA, the time was around 40 minutes.

One of the tuning results of single cycle test for elbow flexion/extension is shown as follow: The tuned RMSE=3.3056 ° The optimal solution of the 14 tunable parameters is shown in Table 6.1. The pictorial representation of these 14 parameters in optimal solution is in Figure 6.3. Where the abscissa represents the 14 parameters in Table 6.1 and the ordinate represents the optimal solution for these 14 parameters. Figure 6.4 represents the change in RMSE and the population mean, over the course of the 100 iterations. At the beginning (RMSE error is large), the convergence speed is faster. As the number of iterations increases, the convergence speed decreases as the solution becomes closer to the optimal solution.

Table 6.1 The optimal solution of 14 tunable parameters

Test Port	Parameter	Optimal solution
1	Lopt _{bi}	0.331506520754357
2	Lopt _{tr}	0.347649476670720
3	F _{maxbi}	1360.14076246334
4	F _{maxtr}	1248.36983525260
5	C _{passbi}	1.39150389814749
6	R _{bi}	2.00340519276161
7	K _{bi}	1.21064959588012
8	Hum	0.313466990916243
9	U _{bi}	0.0301293469708890
10	U _{tr}	0.0460200271797439
11	A	-0.00617270581503469
12	m	1.57408196838567
13	L _{Arm}	0.377477147557399
14	ThreTr	0.0496197124669194

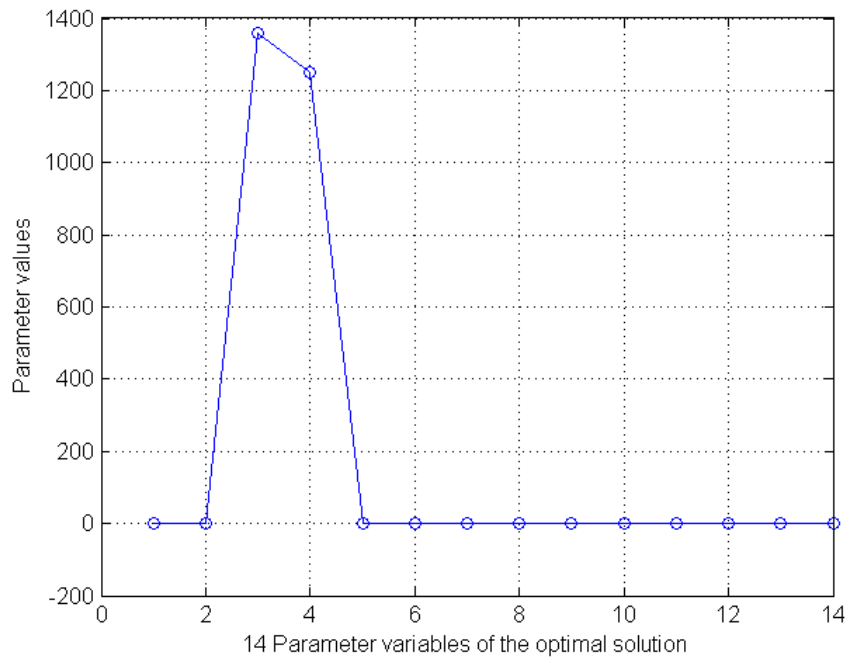


Figure 6.3: The optimal solution of 14 tunable parameters

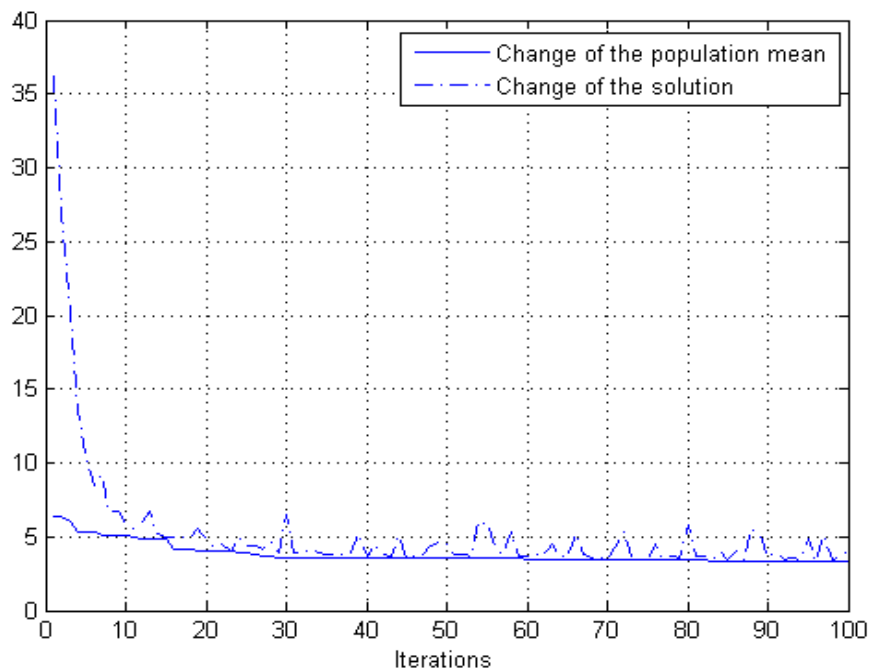


Figure 6.4: The change of the optimal solution and the change of population mean

Since GA was proposed, it was widely used for project design, machine learning, pattern recognition, image processing, etc. Nevertheless, there are still many limitations in GA theory and

application methods, such as premature convergence, slow speed for convergence and low efficiency. In this thesis, each of experimental tests in chapter 4 and 5 has been tuned by GA for four times. As shown in Table 4.6, Chapter 4, all the RMSEs of this study are significantly smaller than James Pau's study. This indicates that the accuracy of GA is still relatively high.

6.2.2 Differential Evolution (DE)

DE was first proposed by Storn and Price in 1995. It is a new simple and efficient global optimization algorithm. The main steps are consistent with other evolutionary algorithms, including mutation, crossover and selection. The most important operator of DE is the differential mutation. Two individual vectors randomly selected from the population are firstly differenced. After the difference vector is weighted, it is summed with the third individual vector according to certain rules to get individual mutant vector. Then, the mutant vector is crossed with the parent individuals to get trial vector. Lastly, by comparing the fitness of trial vector and parent vector, the better one is saved in the next generation population. Thus, the populations of DE are continuously iterative calculated by differential mutation, crossover and selection, until the termination condition is reached. Since DE algorithm is used in one-to-one selection operation, the elitism will not be lost in the process of evolution. At the same time, DE can better maintain the diversity of the population compared to the sort or tournament selection [146]. The basic processes of DE is shown in Figure 6.5.

DE algorithm has been widely studied and successfully applied within 20 years. It has the following advantages:

1. Simple structure and easy to use: The mainly genetic manipulation of DE is the differential mutation. Since this mutation is only related to the addition and subtraction of vectors, it is easy to implement.
2. Superior performance: DE algorithm is reliable, efficient and robust in features, so its performance is better than many other evolutionary algorithms.
3. Adaptability: The differential mutation of DE has self-adaptive capacity in evolution step and searching direction. It can automatically adjust depending on the objective function scene.
4. Low complexity in time: The time complexity of basic DE algorithm is zero [147]. It allows the algorithm to solve large-scale and expensive computational problems.

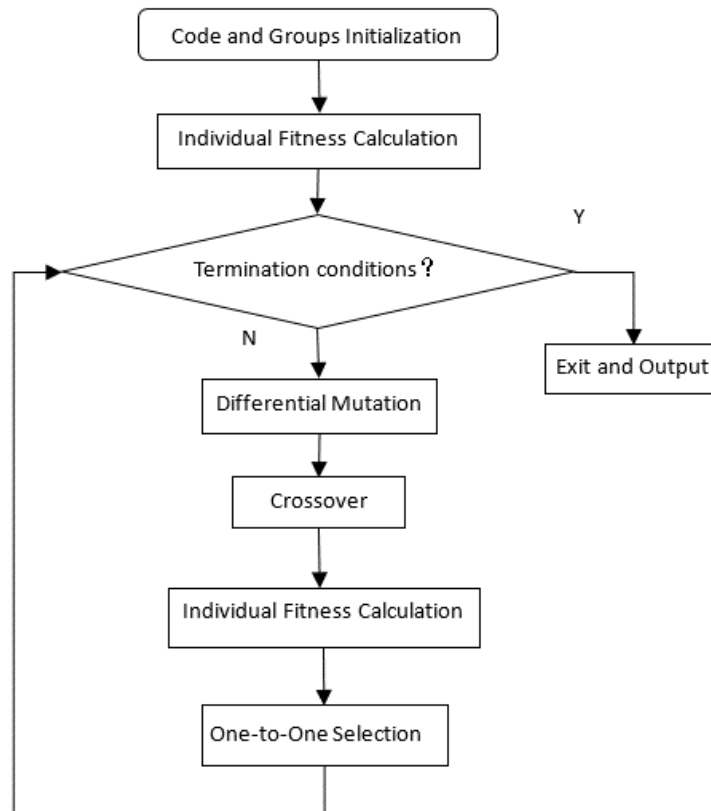


Figure 6.5: The flowchart of basic differential evolution algorithm

This thesis used the Function 'differential evolution' from DE algorithm by Kenneth Price and Rainer Storn, and compiled the DE calculation program. The running time of DE was significantly shorter than GA. The RMS between the predicted joint angle and the actual measured joint angle was set as the objective function of DE. The equation of objective function is shown in Equation (6.1). The algorithm parameters of DE were defined as follows:

number of population members: $N_p=140$;

maximum number of iterations: $Maxiter=300$;

number of variables: $NVAR=14$;

DE-stepsize: $F=0.7$;

crossover probability: $CR=0.9$;

One of the tuning results of single cycle test for elbow flexion/extension is shown as follow: The tuned $RMS=5.8799^\circ$. The optimal process only took 8 minutes. The pictorial representation of the 14 parameters in optimal solution is shown in Figure 6.6. The change of the optimal solution during optimization is in Figure 6.7. As can be seen from Figure 6.7, compared with GA, the cost function

value of DE is jumping during iteration, but the cost function value of GA is gradually changing from large to small (shown in Figure 6.3).

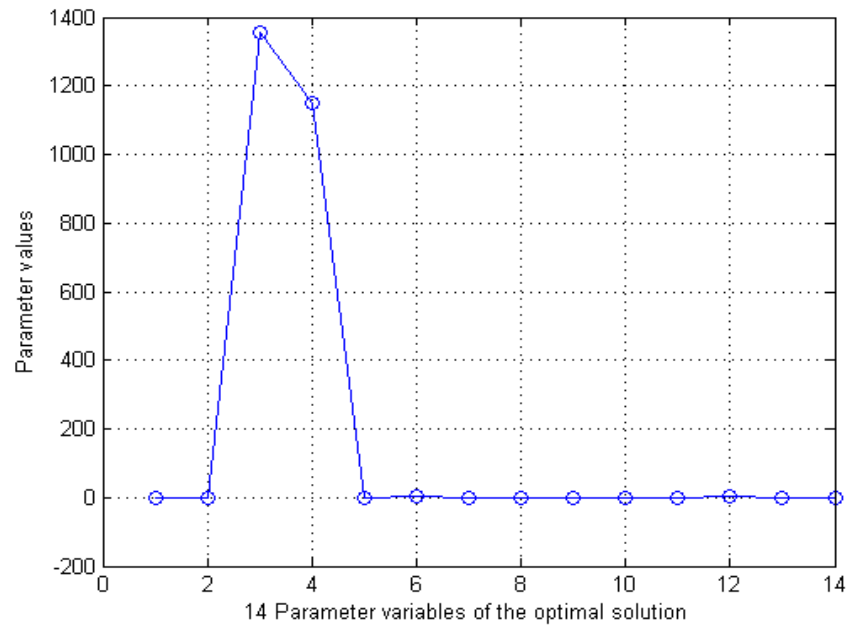


Figure 6.6: The optimal solution of 14 tunable parameters

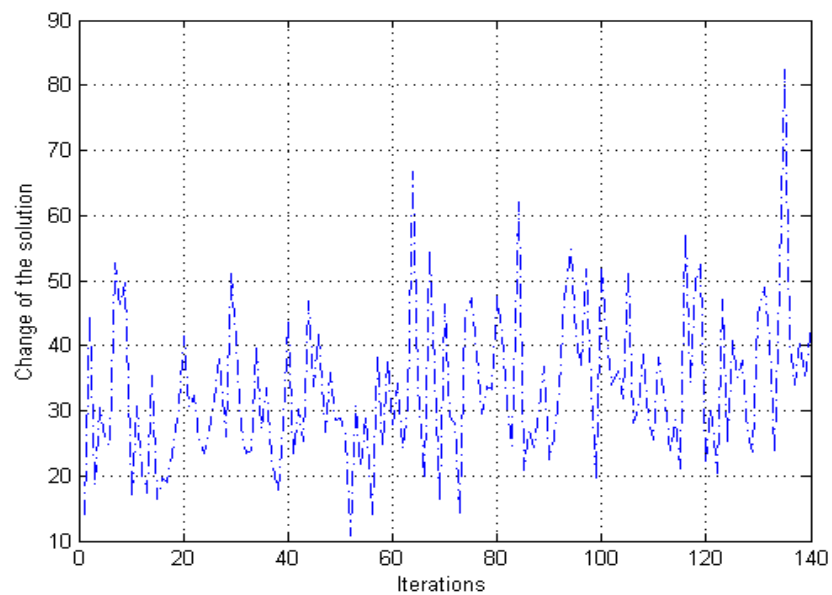


Figure 6.7: The changes of the optimal solution

The performances of DE and GA algorithm were compared by a group of experiments at the following three aspects: the quality of the final solution, the speed of convergence and the success rate. Under the same set conditions in parameters, the quality of the final solution of GA algorithm was slightly higher than that of DE algorithm. For example, in a single cycle test of elbow joint,

during a total of 10 times optimization, the RMS of DE algorithm could quickly converge to 3.59° - 10.78° , and the RMS of GA could converge to 2.45° - 5.32° . However, the convergence speed of GA was significantly lower than that of DE. For all the elbow single cycle test, every optimization in DE could be finished within 8 minutes, while the optimization of GA needed about 40 minutes. And the success rates of GA algorithm and DE algorithm were comparable.

Therefore, in view of the high accuracy and fast convergence of DE algorithm, it can be used for fast online tuning. The GA algorithm can only be used for offline tuning.

6.3 Chapter Summary

This chapter established a 2-DOF human-robot interface for upper limb movement. This is a new neuromuscular interface based on human EMG and physiology musculoskeletal model. This interface provides the operations to predict human elbow flexion / extension, forearm pronation / supination, and the complex movements. The treatment methods of signal selection, muscle model and musculoskeletal geometry model were given during the composite movement formed by elbow flexion / extension and forearm pronation / supination.

This chapter focused on GA and DE the two kinds of evolutionary algorithms as the model parameter tuning method. GA and DE calculations were programmed in MATLAB. The performances of DE and GA algorithm were compared by experiments in three aspects (the quality of final solution, the speed of convergence, the success rate), and the results showed that: Under the same set conditions of parameters, the quality of the final solution of GA algorithm was slightly higher than that of DE algorithm. The convergence rate of GA was significantly lower than that of DE algorithm. The success rates of GA algorithm and DE algorithm were comparable. Thus, DE algorithm can be used for fast online tuning, and GA algorithm can only be used for offline tuning.

Chapter 7 A GUI Design to Facilitate the NI Validation

In order to validate the Neuromuscular Interface (NI) of upper limb, a 5 Degree of Freedom (DOF) upper limb exoskeleton has been designed by our research group [148]. This chapter will show the basic information about the hardware of this exoskeleton. By aiming at connecting the exoskeleton to the designed NI (in Chapter 6) and for the purpose of easier usage, a Graphical User Interface (GUI) is designed. This GUI also acts as a bridge between the lab research and the commercial or public applications.

7.1 Introduction of a 5-DOF Upper Limb Exoskeleton

In another study of our research group, a 5-DOF left upper limb exoskeleton has been developed [148]. Among the 5-DOF, 4-DOF were used to drive the spherical 3-DOF movement of human shoulder, and completed the shoulder adduction and abduction, internal and external rotation, flexion and extension. And the rest 1-DOF was used to drive the elbow flexion and extension movement. Figure 7.1 shows the CAD model of this exoskeleton, and Figure 7.2 is an application of this exoskeleton. The Joint 1-3 represent the 3-DOF of human shoulder joint. The Joint 4 is connected to the human upper arm to compensate the position changes of upper arm during shoulder moves. The Joint 5 is the elbow joint, with a handle on the top for users to hold. The whole exoskeleton has been hold by a metal frame, so its weight will not be attached to the users.

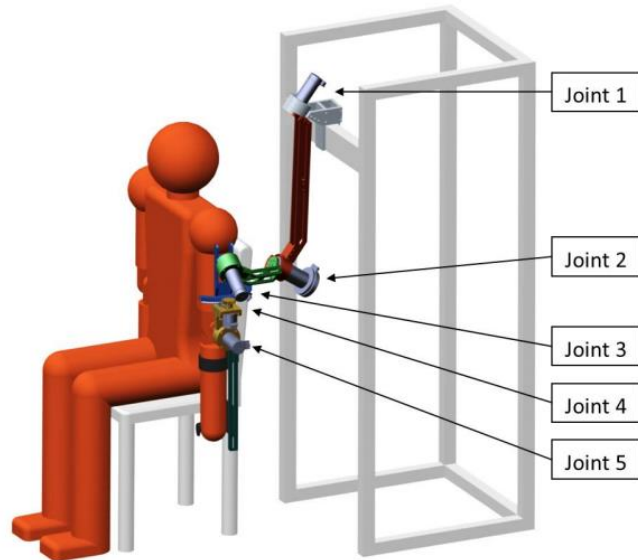


Figure 7.1: CAD model of the 5-DOF upper limb exoskeleton [148].

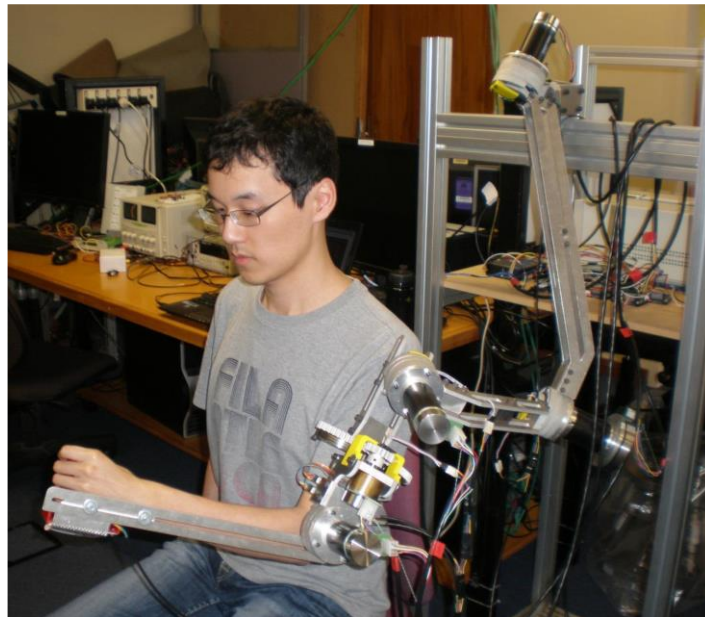


Figure 7.2: The 5-DOF exoskeleton used by a healthy person [148].

There are many important design considerations in the prototype of exoskeleton, to ensure that the exoskeleton can complete its operational requirements, and are friendly to the user. The considerations include the range of exoskeleton joint motion, joint alignment, actuators and sensors, and safety features. These are going to be introduced as follows.

7.1.1 Range of Exoskeleton Joint Motion

In the workspace of human upper limb, the exoskeleton should not have interferences with the users or between the different parts of the exoskeleton. The limitation of each joint displacement is based on the warranty of no interferences. The limited angular range of each exoskeleton joints are listed in Table 7.1

Table 7.1 Range of motion of exoskeleton joints

Exoskeleton Joint	Clockwise Limit /°	Counter-Clockwise Limit /°	Total Range of Motion/°
1	14	-89	103
2	120	-25	145
3	-57	-132	75
4	18	-78	96
5	180	55	125

7.1.2 Joint Alignment

Within the entire workspace, the five joints of exoskeleton are aligned with the corresponding human joints. Joint 1,2,3,4 are aligned with the shoulder joints and the Instantaneous Center of Rotation (ICOR) of shoulder. Joint 5 is always aligned with the user's elbow joint. To accommodate users with different upper limb lengths, the link lengths of the exoskeleton corresponding to human upper arm and forearm portion were adjustable, so the joints could be aligned. When the users take a sitting position, the height of the exoskeleton can also be adjusted by changing the support frame, to ensure the shoulder alignment. Table 7.2 shows the size of the typical human body segments and the corresponding adjustable range of exoskeleton segments. The upper limb length of adult are obtained from the average value in literature [149].

Table 7.2 Dimensions of upper limb and exoskeleton segments

Segment	Average Adult Dimensions (mm)	Exoskeleton Dimensions (mm)	
		Lower Limit	Upper Limit
Shoulder ICOR to Elbow	278	255	335
Elbow to Palm	349	125	365
Shoulder to Ground	1000	800	1200

7.1.3 Actuators and Sensors

Compared with ordinary robots, although the load of the rehabilitation robot is small, there are more high requirements to the response speed and accuracy of the drive system. Therefore, the DC motor and gear box are chosen as the exoskeleton driver. The Maxon 24V brushless DC motor and the gearbox (MAXON motor, Switzerland) [150] are chosen for driving the five exoskeleton joints. The controllers of Maxon ESCON are used to drive each motor. The parameters of each gearbox and the combination joint output are shown in Table 7.3.

Sensors are installed on the exoskeleton in order to measure the five joints rotation angle of exoskeleton and the force between users upper limb and exoskeleton. The angular displacement is used to determine the posture and control of the exoskeleton upper limb for real-time. The measurement of interaction force is applied for the interactive control. The AMS magnetic encoders (AMS, Austria) [151] are installed on the outer side of skeleton joints to directly measure the angular displacement of the joint. The measurement of force is achieved by the customized force sensor [148].

Table 7.3 Specifications of the motor-gearbox units

Joint	Motor-Gearbox Combination		Nominal Gearbox Output	
	Maxon Motor	Gearbox (r :1)	Speed (rpm)	Torque (Nm)
1	EC 45 Flat 50W 24V	156:1 Planetary	33.7	9.3
2	EC 90 Flat 90W 24V	91:1 Planetary	28.8	29.0
3	EC 45 Flat 50W 24V	319:1 Planetary	16.5	16.9
4	EC 45 Flat 50W 24	47:1 Spur	111.7 (18.6*)	3.0 (18.0*)
5	EC 45 Flat 50W 24V	156:1 Planetary	33.7	9.3

*Values after a further reduction of 6:1 by the Joint 4 rail mechanism.

7.1.4 Safety Features

Exoskeleton is directly connected with the body of the user, so the accident or failure would easily cause serious damage to the user. In the exoskeleton robot system, many features have already been considered to ensure users safe and comfortable operation. The mechanical stops are used for each joint, to prevent the joint movement of exoskeleton beyond the standard operating range. The magnetic encoder sensors were used to monitor the position of each joint, and to prevent the joint beyond the limitation. When there was a problem, the exoskeleton users or external users can effectively stop the exoskeleton robot via an emergency stop button.

7.2 System Architecture and Graphical User Interface

Graphical User Interface (GUI) is the interface for information exchange between the human and robot. The users of exoskeleton are normally patients, they need to move following the exoskeleton. The whole movement process is in high degree of automation, and with little human intervention operation. Therefore, it is indispensable to provide an application interface which can be easily understood by all users.

7.2.1 The Operating Procedures of the Interface

The flowchart of Operating Procedures for the interface is shown in Figure 7.3 Firstly, the system initialization is used to detect whether all hardware connection. Then, the state of exoskeleton is judged whether it is normal. If abnormal, the abnormality alarm displays and the system returns to the start. If normal, the exoskeleton starts to formal work. In Signal Acquisition and Processing Module, the EMG signal acquired by the system is pretreated to get the muscle activation. Then, the Joint Angle Prediction module is used to get the RMS error between the measured and predicted joint angles. If the RMS error is too large, it indicates that the parameters of physiological model are inappropriate. The Tuning Model is used. After tuning, the exoskeleton controller is chosen depending on the size of the muscle activation, The Expected Joint Torques is converted to Control Commands, driving the exoskeleton robot movement.

7.2.2 Graphical User Interface (GUI)

A GUI was developed in Matlab for operating the 2-DOF interface and the 5-DOF exoskeleton. It includes two main parts: motion selection and module selection. Figure 7.4 shows the main interface of the GUI. The first step is to select a motion type. There are three types can be chosen: elbow flexion and extension, forearm pronation and supination, and cooperative movement. After selecting a motion, the interface can start predicting joint movement with its original settings by pressing the start button. If the users want to change the settings of each module or check the phased results, the four module buttons will work. The main modules of software system include: Signal Acquisition and Processing System Module, Joint Angle Prediction System Module, Physiological Parameters Tuning Module, EMG Based Controller Module (EBC), Force Sensors Based Controller Module (FBC)

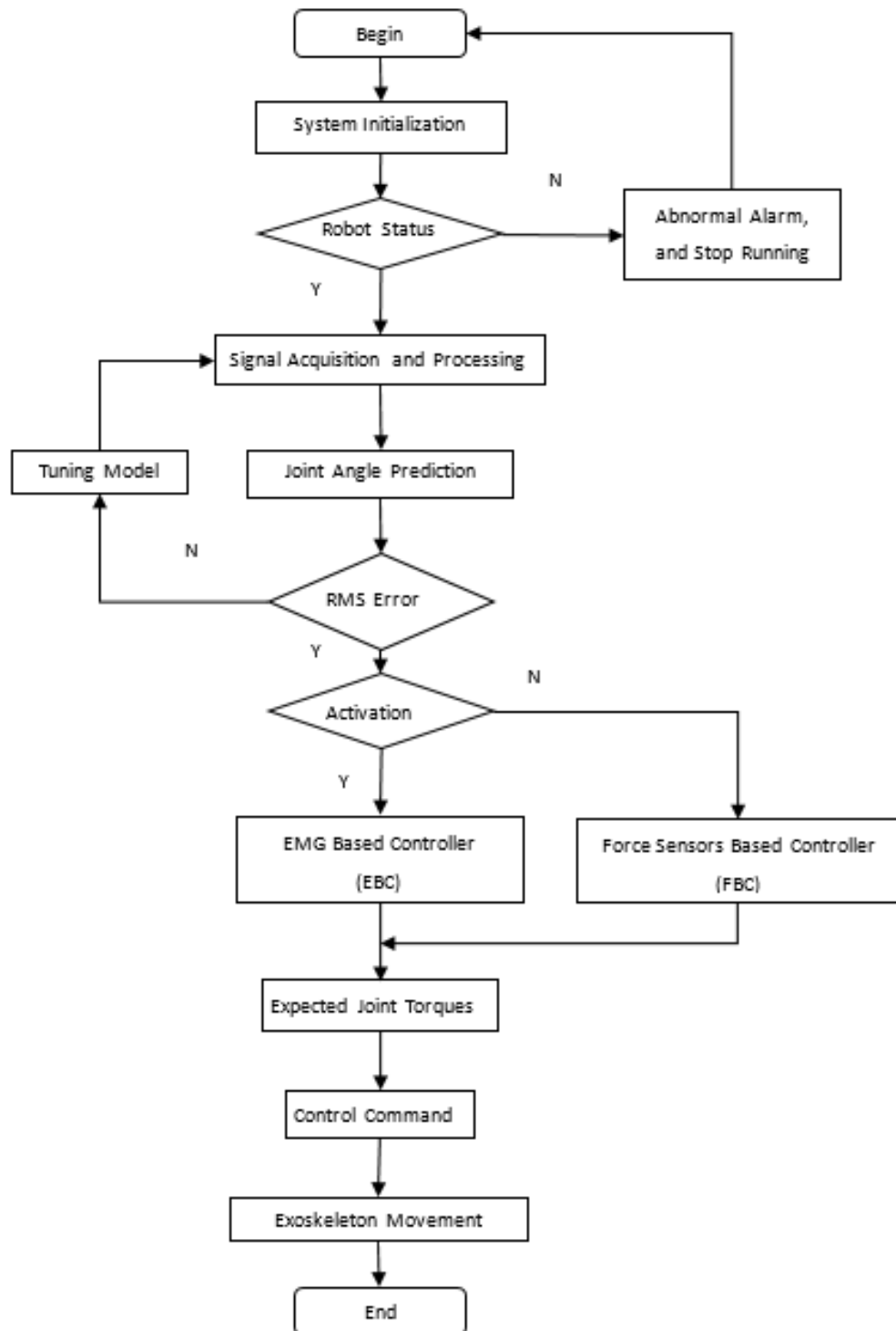


Figure 7.3: The human-robot interface operating procedures

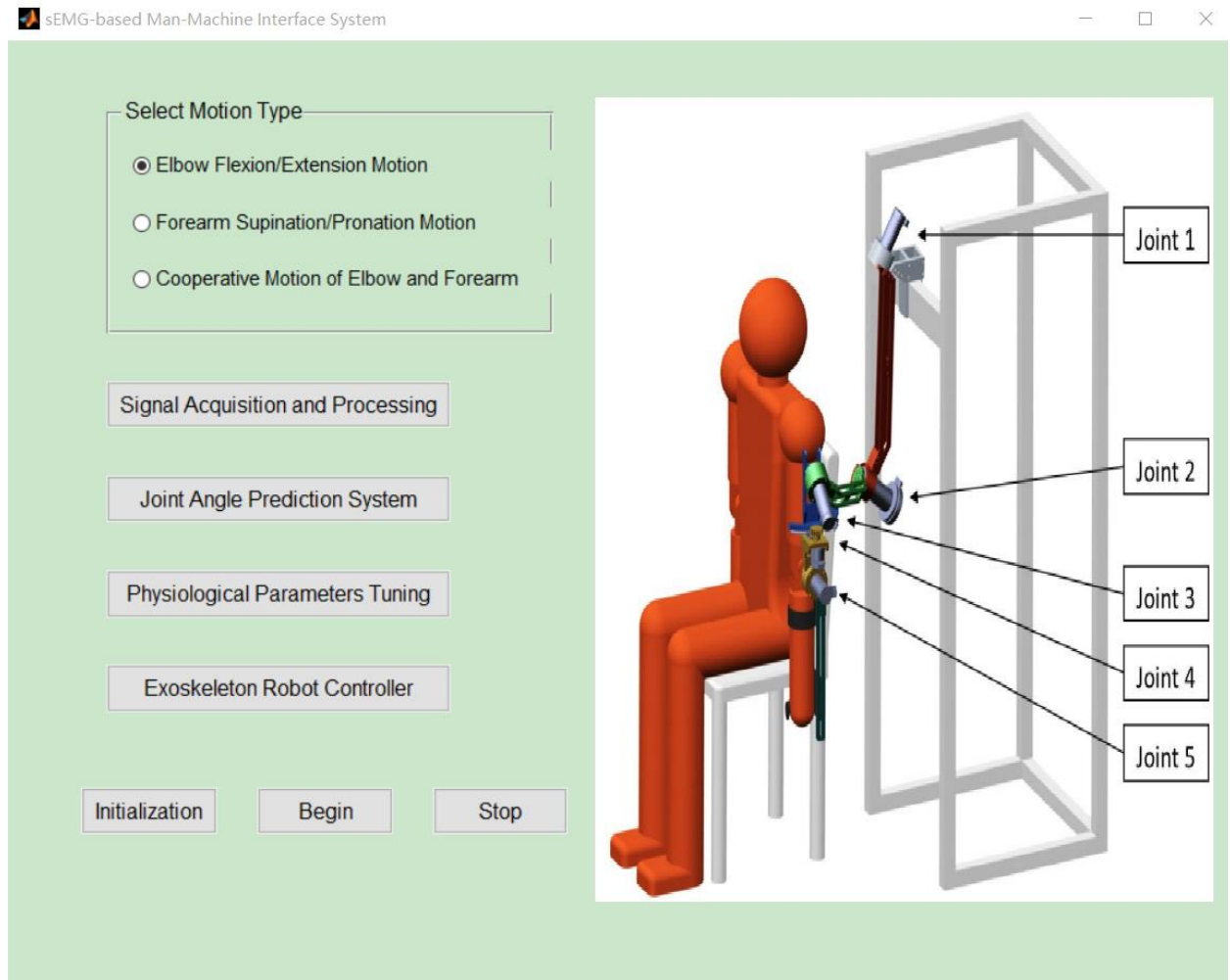


Figure 7.4: The main interface of this GUI

Module 1. Signal Acquisition and Processing System Module

It is used for setting the acquisition parameters of EMG signal (Sample Rate Per Chan, Samples Per Chan, Num Chan), and for obtaining the EMG signals. Envelope method has been used for data processing of the human muscle surface signal (details in Chapter 4) to obtain the degree of muscle activation. The interface of this module is shown in Figure 7.5. The module includes three parts: the signal collection part is used to show the raw EMG signals from biceps or triceps; the parameter setting part is used for changing the collection parameters; and the signal processing part shows the result of signals after linear envelop processing.

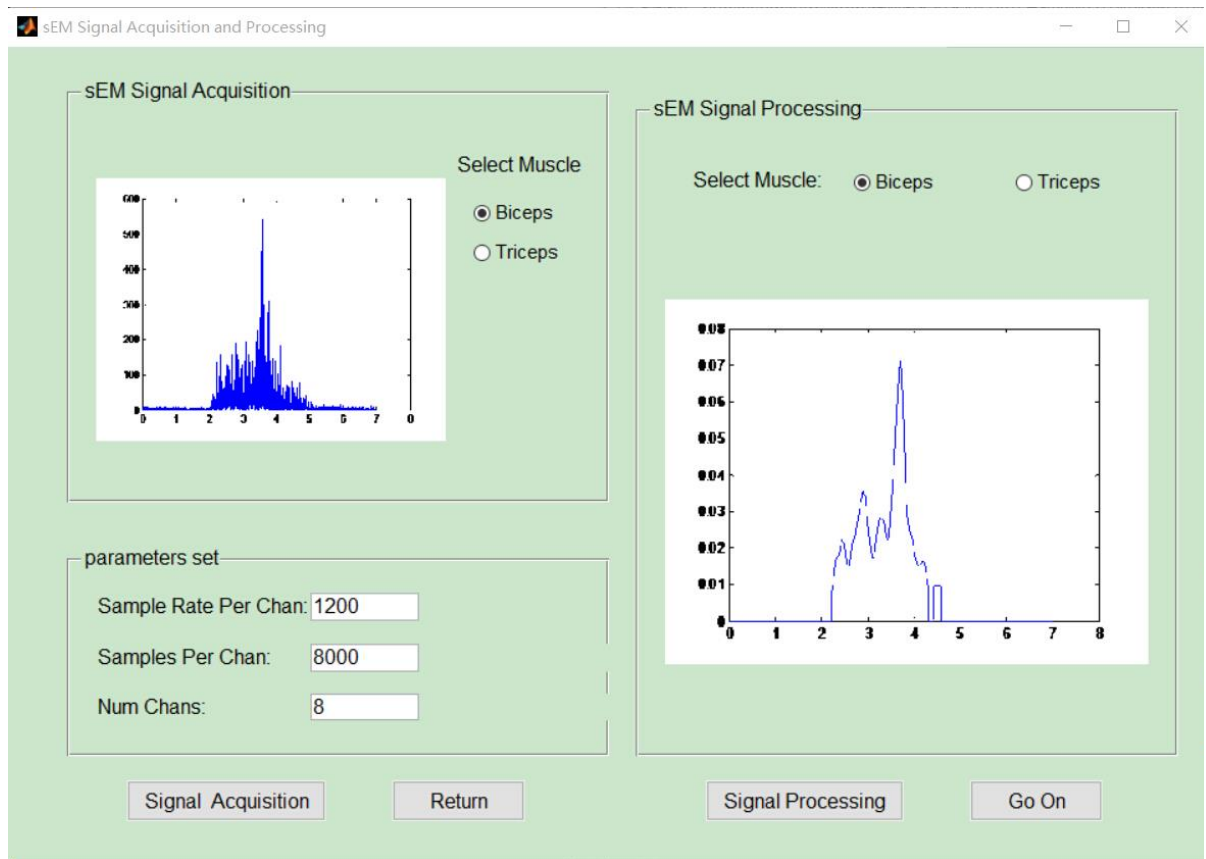


Figure 7.5: Signal Acquisition and Processing System interface

Module 2. Joint Angle Prediction System Module

This module is the main module of the software system. It includes the configurations of musculotendon model, musculoskeletal model and kinematics model, programming by Matlab Simulink software. The program of Joint Angle Prediction System is shown in Figure 7.6, and its interface is shown in Figure 7.7. This module is the main calculation of the neuromuscular interface. It contains the models developed in Chapter 3, 4 and 5. It takes the processed EMG signals from last module and predict the joint angle. In the module interface (Figure 7.7), the changes of predicted angle (blue line) and measured angle (green line) are shown, as well as RMSE between them.

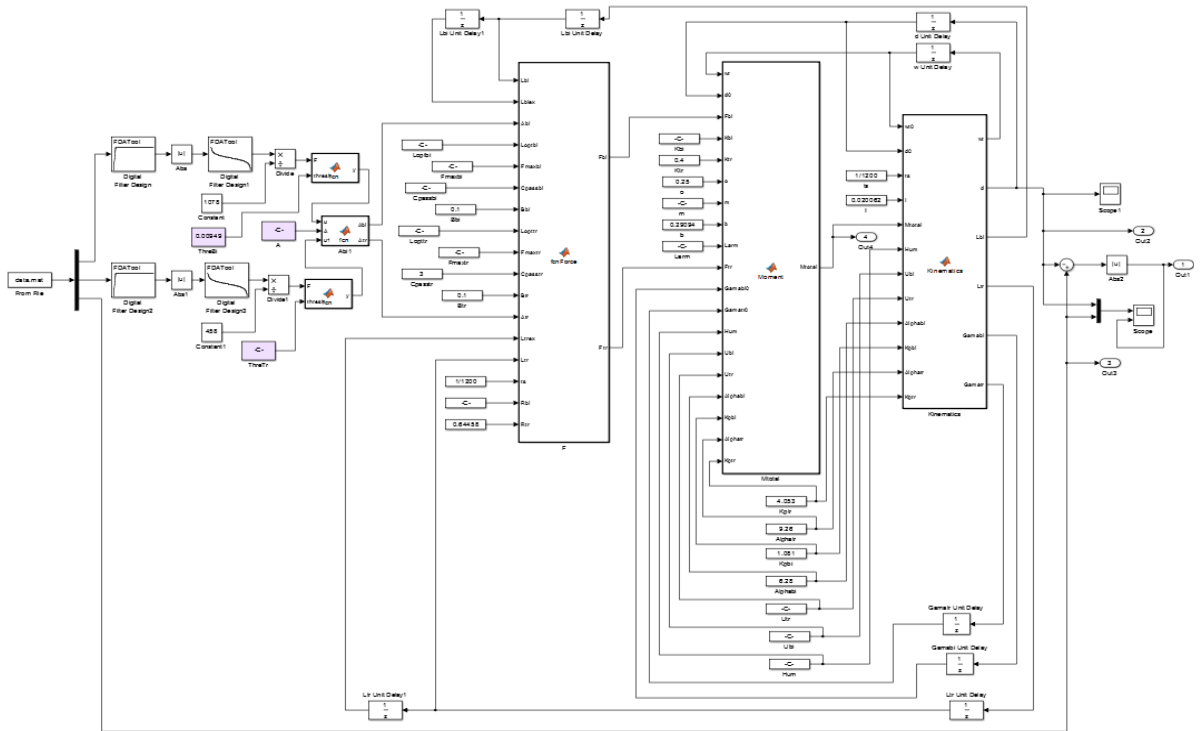


Figure 7.6: Joint Angle Prediction System program



Figure 7.7: Joint Angle Prediction System interface

Module 3. Physiological Parameters Tuning Module

If the RMS error between the measured and predicted joint angle exceeds the threshold, it means the parameters of physiological model is inappropriate and the data enter the Tuning Model. The acceptable tuning methods include: Genetic Algorithm (GA), Differential Evolution (DE), Simulated Annealing (SA), and Partial Derivative Algorithm. The interface (shown in Figure 7.8) displays a tuning result and all the parameter values during the optimal solution.

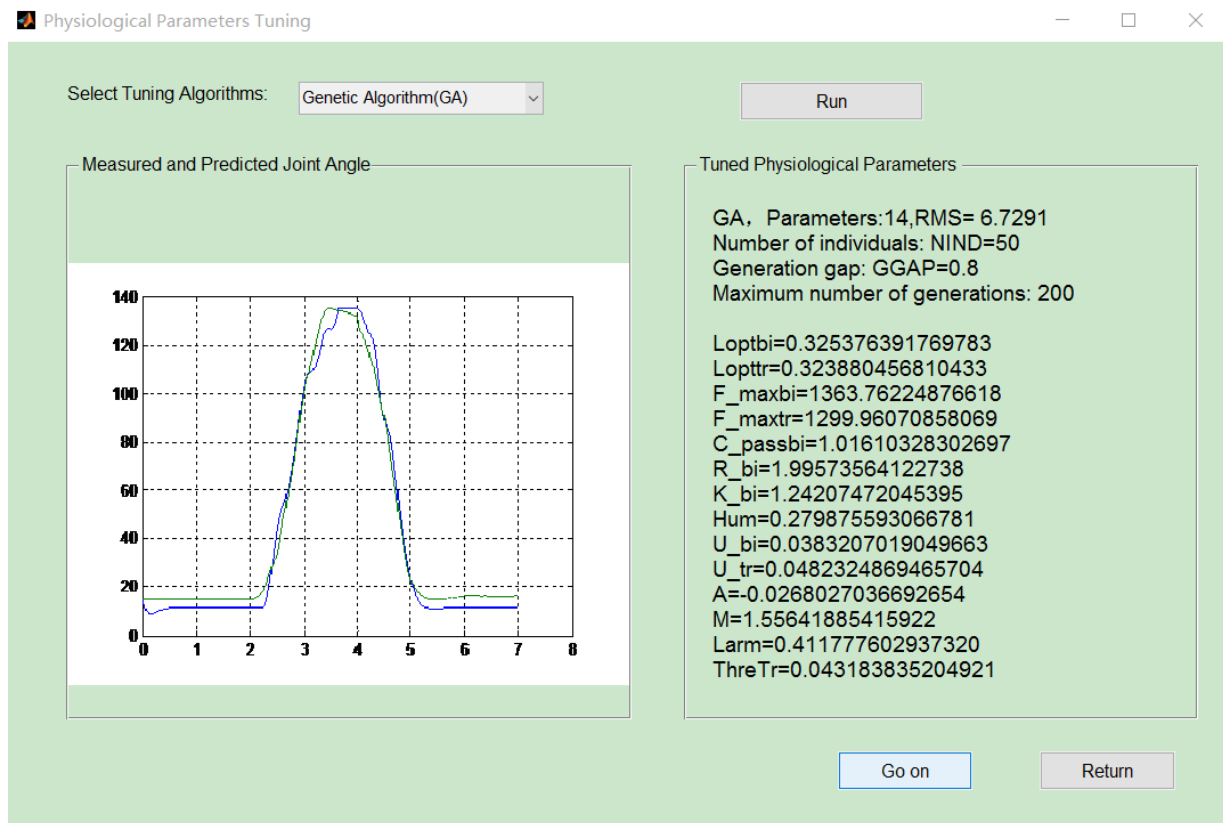


Figure 7.8: Physiological Parameters Tuning interface

After the operations of the first three modules, the motion prediction for individual users has been completed. If the exoskeleton is needed for the rehabilitation patients' assessment, then the control strategies are ready to be selected in the following modules. The controller of exoskeleton is chosen depending on the level of the muscle activation. It includes the EMG Based Controller (EBC) Module and Force Sensors Based Controller (FBC) Module, the details are in Chapter 8.

Module 4. Force Sensors Based Controller Module (FBC)

This controller has been completed by another research in this research group [148].

Module 5. EMG Based Controller Module (EBC)

This controller is used to convert the expected joint torques calculated by musculoskeletal model to control commands for driving the exoskeleton. The interface of this EMG Based Controller (EBC) Module is in Figure 7.9. It shows the real-time control result (joint angle) and the motor torque changing with running time. This design helps the users to check the running conditions of the exoskeleton.

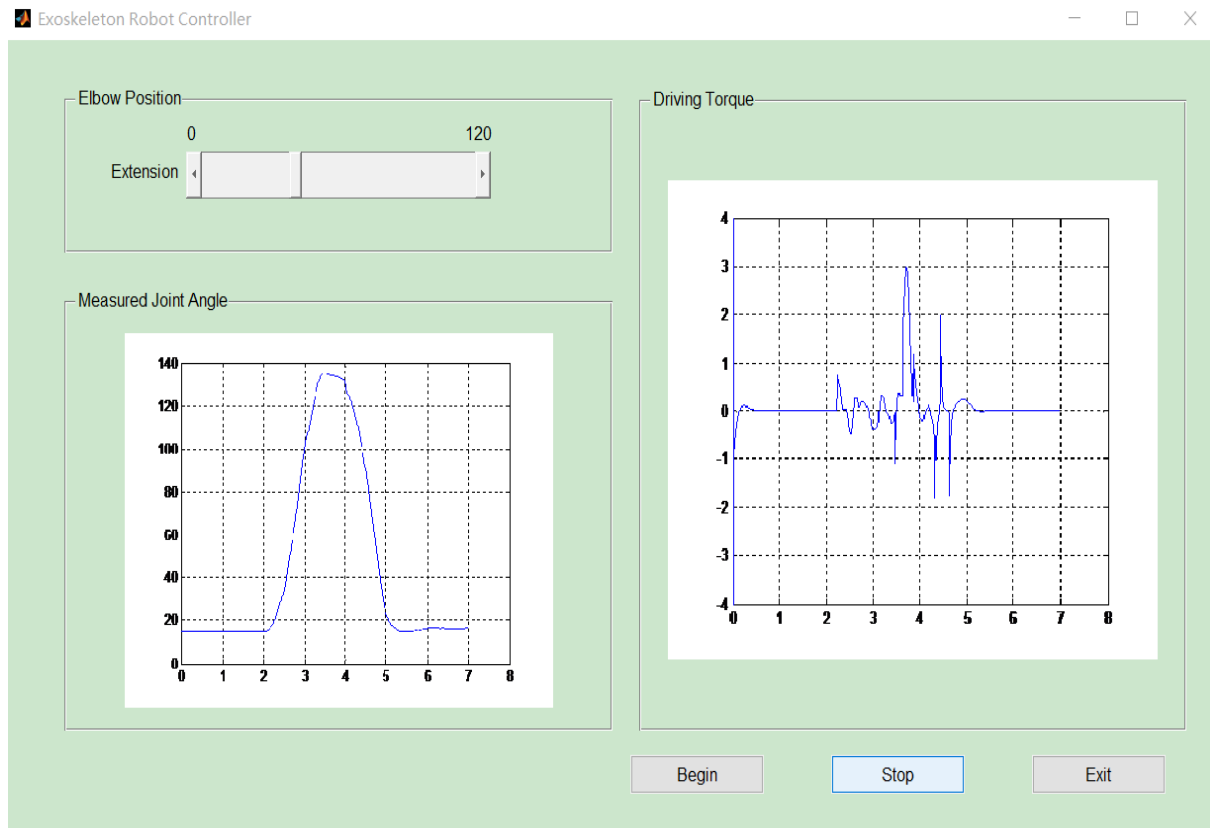


Figure 7.9: EMG Based Controller Module (EBC) interface

7.3 Chapter Summary

In order to verify the 2-DOF neuromuscular interface of upper limb, a 5-DOF exoskeleton has been used in this chapter. The EMG-based controller of this exoskeleton will be developed in detail in Chapter 8. For the convenience of users, a graphical user interface (GUI) has also been designed in Matlab for operating the 2-DOF interface and the 5-DOF exoskeleton. This chapter introduced the main module of the software system and showed the usage of this GUI.

Chapter 8 NI Validation through Exoskeleton Control

A 5 Degree of Freedom (DOF) upper limb exoskeleton has been introduced in Chapter 7. It was used to be controlled by the impedance control [148]. At present, the common control strategies used for exoskeletons are mainly position control and impedance control [152-156]. Rahman et al tracked the exoskeleton by non-linear torque calculation control [157]. Some other researchers used the EMG signal to control the exoskeleton [70, 158, 159]. Also, some commercial exoskeleton device, such as Hand Mentor and Robot Suit HAL-5, can all be controlled by EMG. For the human-robot interaction of exoskeleton, EMG signals are used in many of the upper limb exoskeletons [70, 158, 159]. Baklouti et al proposed to use face and mouth posture as exoskeleton control command [160].

There are many ways for the upper limb exoskeleton to obtain the human movement intention, such as force / torque signal, neuromuscular electrical signal, EEG signal and so on. In this thesis, the upper limb exoskeleton combined the EMG signals and wrist force signal to analyze the human movement intent. Two types of human-robot interaction approaches were used, one was the EMG-based interface controller, and the other was the impedance-based interface controller.

For the EMG-based control (EBC), the EMG from disabled arm or healthy side upper limb of the patient is used to "understand" the user's subjective moving intents. This control method can achieve the information interaction between the upper limb exoskeleton and the patient, to complete the autonomy rehabilitation process. For the impedance control, the exoskeleton applies a force to the user through its structure motion, which means the mobile exoskeleton moves the human upper limb, and the exoskeleton has a current position, but when the user exerts force to it, the system will deviate from this position. This makes the interaction between the user and exoskeleton can achieve flexible position control.

This chapter develops an EBC controller, and with the combination of FBC controller, it achieves

the verification propose of the EMG-based Neuromuscular Interface.

8.1 Control Strategies of the 5-DOF Exoskeleton

8.1.1 Overall Design of the Control System

The exoskeleton robot developed in this thesis is used to assist the movement of body weaken person (such as the elderly, the disabled, and the injured people). If the exoskeleton can offer power assist to them in daily activities and rehabilitation, according to the user's movement intention, this will be a very bright future. The EMG signal from human muscle directly reflects human movement intent. The feature space of EMG signal contains many motion commands from the corresponding cortex region. By analyzing muscle EMG signals, it possible to "Prophecy" the action before the real action took place (due to the electro-mechanical delay which can be 20-80 ms). If the "prophecy" information of motor neurons can be clearly identified, it is equivalent to control the exoskeleton directly by the brain. In that way, a new intelligent human-robot interface can be achieved.

In this thesis, the patient's muscle EMG is the main input of the exoskeleton control. However, there are two problems of the EMG signal based controller. First, different users for the same action will not create the same EMG signals (individual differences). Second, the muscle EMG signals are susceptible to fatigue, electrode position changes, EMG training and other factors, which may led to a low muscle activation. The solution of the first problem is adding a tuning model in the EMG signal based controller (EBC), to help the controller adapt to different users. The method of solving the second problem is changing to use a Force sensor-based controller (FBC) when the levels of muscle activation are low. The FBC takes an impedance control, and enables a flexible position control between the upper limb of users and exoskeleton.

The overall structure of the exoskeleton controller is shown in Figure 8.1. In Figure 8.1, the information data from human subject is calculated through two close loops: One is the EBC which takes the EMG signal as input, calculates each muscles' force by musculotendon model, computes the joint torque by musculoskeletal model and results the joint torque to the controller selection. Also, a real-time tuning based on the comparison of measured and predicted joint angle is included in the EBC controller. The other is the FBC which takes the wrist force and elbow angle as input, and uses the exoskeleton joint feedback to optimize the output torque. By making the wrist force to 0, through the PD control, impedance control and admittance control, the FBC achieve the desired

auxiliary results. The choice of these two controller for expected assisting force is depended on the amount of input, which mainly means the activation of muscles. When the activation is high, the EBC is chosen. When the activation is low, the FBC starts to work. When the activation is moderate, both EBC and FBC start to control. By the fusion of EBC and FBC as the input information for control system, the purposes to control exoskeleton based on human intention can be achieved. The first phase of the exoskeleton controller work is to select the input control signal. The second stage is to complete the exoskeleton control work according to the type of input signals.

8.1.2 EMG Based Controller (EBC)

The control principle of EBC is as follow: With the layout of EMG electrodes on user's upper limb, the users move the upper limb according to their own wishes. After the weak upper limb EMG signals are captured by electrodes, filtering, amplification and A/ D conversion processing are used to analyze the signal information, then the signal information is send to the host computer via a USB port. The regular monitoring thread within the host computer constantly monitors whether there are any action EMG generated. When the judgment operation starts, a message is send to start the EMG acquisition thread. The EMG acquisition thread collects the EMG signal of motion in 1200HZ frequency, and a linear envelope method is used to extract muscle activation. Then the muscle force is gained through musculotendon model, and the joint torque is obtained by musculoskeletal model. Finally, the joint torque is converted into the torque command to drive motors of the upper limb exoskeleton, in accordance with the user's motion intention.

In order to adapt the EBC controller to different users, the individual parameters of the user need to be tuned before the exoskeleton robot formal work. This tuning is introduced in Chapter 4.

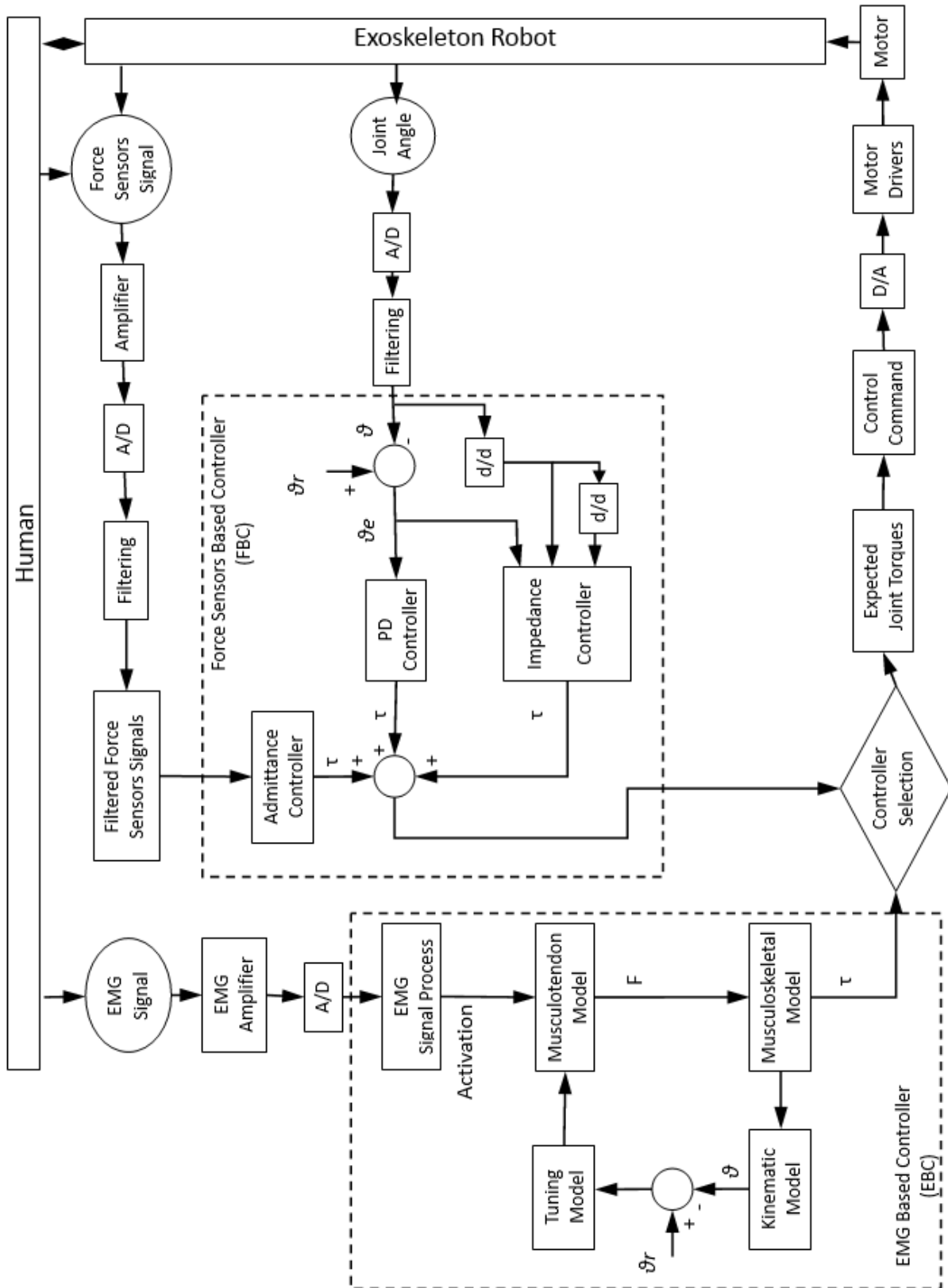


Figure 8.1: Schematic diagram of the controller.

8.1.3 Force Based Controller (FBC)

Wrist force (which is the force caused by difference motions between exoskeleton wrist and the patient wrist) is also used as a kind of input information for the controller. The FBC is based on the principle of impedance control, to lead the wrist force caused by the differences of joint motion to zero. This part is shown in another study [148] of our research group.

The equation of impedance control is written as:

$$\tau = M (\ddot{\theta}_r - \ddot{\theta}) + B(\dot{\theta}_r - \dot{\theta}) + K(\theta_r - \theta) \quad (8.1)$$

where τ is the desired joint torque, θ_r is the desired joint angle of the exoskeleton, θ is the measured joint angle of the exoskeleton. K , B , M are the spring coefficient, viscous coefficient, moment of inertia.

Finally, the joint torque is converted to the torque command to drive motors and the exoskeleton robot.

8.1.4 Motor Driver Settings

In the control flowchart, after controller selection, the desired joint torque is obtained as the motor driver input. Then the desired joint torque is converted to the driving commands of the motor to drive the exoskeleton.

This thesis selected the EC45 servo motor and ESCON36 / 3EC motion controller produced by Maxon. The servo motor comes with a Hall sensor. ESCON controllers can be connected to a PC via USB cable, and be set by ESCON Studio application configuration. ESCON36 / 3EC is the efficient four-quadrant PWM controller. And ESCON36 / 3EC has both digital and analog input and output functions. J1 is the power connector. J2 and J2A are the link connectors of motor and the Hall sensor. J5 is the digital input and output connector. J6 is the analog input and output connector. J7 is the USB connector.

ESCON controller can be set by three following aspects:

1. Set the motor parameters

Based on the specifications of the motor (in Maxon's manual), the motor speed constant, the thermal time constant of the winding, and the pole pair number of the motor are settled.

2. Select the control mode

ESCON controller has speed control, speed adjustment and electric current control, three modes. The electric current control has been chosen for this thesis. It is a comparison between the actual motor current (actual motor torque) and the set current value (desired joint torque). If there is a deviation, the motor current is adjusted. Since the large current represents to the high torque, during the servo motor operation, the torque control can be completed by the current control. The current control loop is within the motion controller, it has the characteristics of small calculation and fast response.

In EBC controller, the desired joint torque can be obtained through the EMG signal processing, musculotendon model and musculoskeletal model calculation. One group of results are shown in Figure 8.2-8.6. They are the total desired joint torque (including both biceps and triceps) for elbow flexion / extension from different experiments. Figure 8.2 is the joint torque for elbow single cycle movement during seven seconds. Figure 8.3 is the result of elbow continuous movement with the increasing amplitude, in 12 seconds. Figure 8.4 is the result of elbow random movement in 13 seconds. Figure 8.5 is the elbow joint torque in continuous full range movement during 24 seconds. And Figure 8.6 is the joint torque of elbow continuous half range movement.

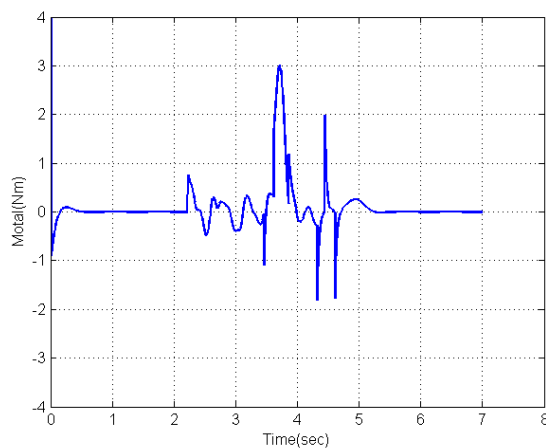


Figure 8.2: Desired torque for Single cycle test.

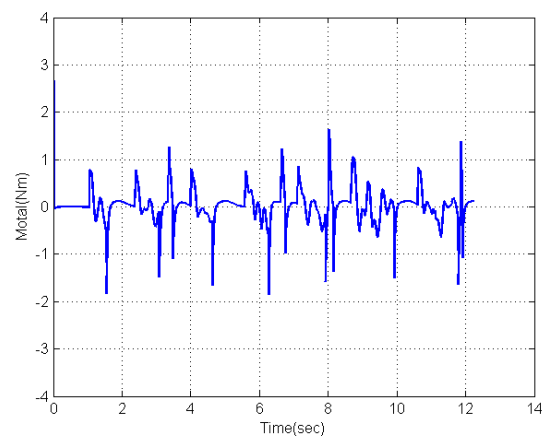


Figure 8.3 Desired torque for Continuous cycles starting with a small amplitude that gradually increases test

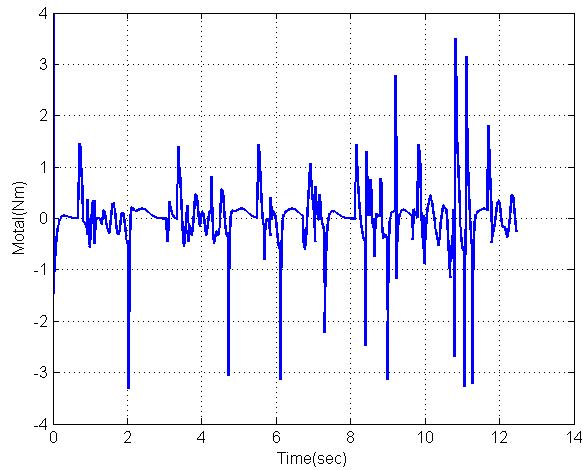


Figure 8.4: Desired torque for Random movement test.

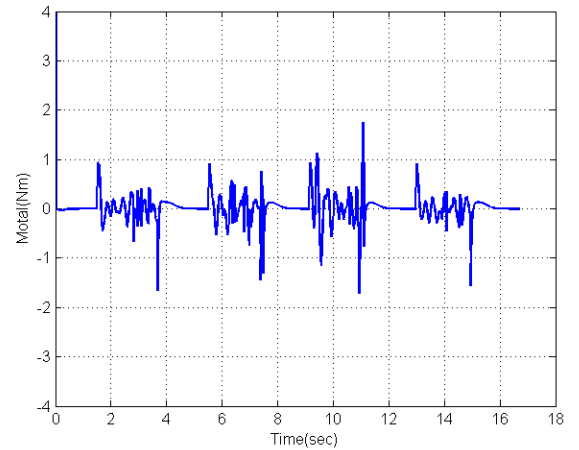


Figure 8.5 Desired torque for Continuous cycles test.

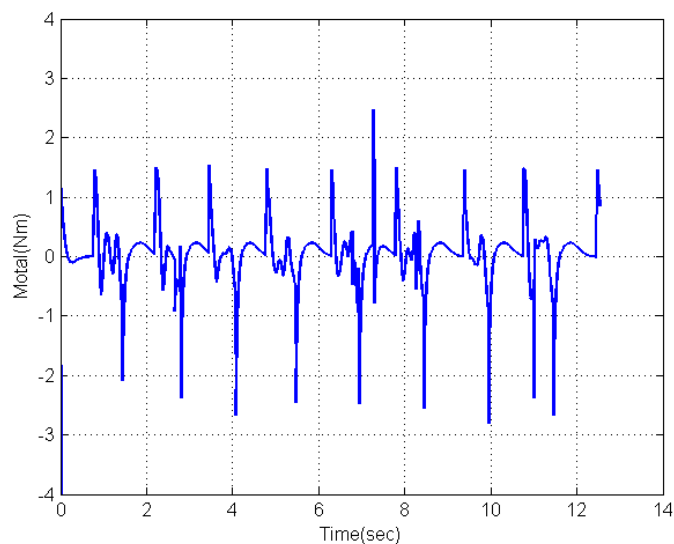


Figure 8.6: Desired torque for elbow flexion motion for Continuous cycles at half the range of capable motion

3. Set the digital input configuration

Three enter lines are used to set the ESCON: One is used to enable the motor, one is used to select the direction of actuator, and the last one is used for the PWM to set the output level. (Note: the PWM sent to ESCON controller must have 10% -90 % duty cycle).

The flowchart of motor control calculation is shown in Figure 8.7. The motor control takes the desired joint torque as input, calculate the motor current, convert to PWM and then control the motor movement.

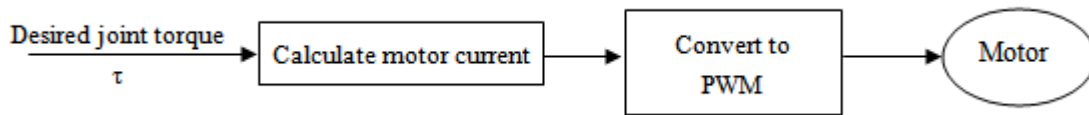


Figure 8.7: The flowchart of motor control calculation

For a given desired torque τ , the desired motor current i can be calculated as follow:

$$i = \frac{\tau}{k_t \times k_r \times \eta} \quad (8.2)$$

where k_t is the motor torque constant, k_r is the gearbox reduction constant, η is the total efficiency of the gearbox and motor.

For the conversion from desired output current i to PWM, firstly, a suitable maximum output level is set as 90% of duty cycle of the PWM. Then the output of the duty cycle is calculated by Simulink model.

8.2 Validation of the Elbow Neuromuscular Interface

The EBC purposed in this chapter and the 5-DOF upper limb exoskeleton were tested to verify the EMG-based neuromusculoskeletal interface.

8.2.1 Experimental Setup

In order to assess the effectiveness of the proposed method, a group of control experiments of elbow movement have been conducted. The experimental subjects are three healthy male (coded as A, B, C). In this experiment, each subject was asked to complete the elbow flexion/extension in five different kinds of movement. These movements occurred in the sagittal plane, standing posture. The forearms and hands were relaxed during all the actions, to prevent the interference from wrist and finger movements. Each experiment lasted approximately 10 to 20 seconds, and every movement is instanced five trials. To prevent the fatigue effect, there were several 60 seconds rests within the test interval. The five kinds of movements were as follow:

1. Single cycle of full flexion and full extension from a neutral, relaxed position at a moderate speed.

2. Random movement performed at the discretion of the user, with different amplitudes and at varying speeds.
3. Continuous cycles of full flexion and full extension.
4. Continuous cycles at half the range of capable motion (about 90° elbow angle).
5. Continuous cycles starting with a small amplitude that gradually increases over the course of the trial.

In order to clearly verify the results of EBC, each experiment respectively has a comparison of the test with exoskeleton robot assisting and without assisting.

The elbow flexion / extension motion is a collaborative effort of different muscles. The muscles for flexion are biceps brachii, brachioradialis and brachialis, and the muscles for extension are the triceps brachii, and anconeus. In this study, two major muscles are chosen to place the electrodes. The EMG signal of biceps (Channel 1) and triceps (Channel 2) are obtained to control the elbow flexion / extension motion.

8.2.2 Experimental Results and Analysis

Firstly, a single cycle elbow flexion/extension test (Group 1) was conducted. Figure 8.8 showed the experimental results of subject A, while the results without the assistance of exoskeleton are shown in part (a), and the results with assistance are in (b). During elbow flexion/ extension, biceps contribute most, therefore, the experimental results only showed the surface EMG (sEMG) signal from biceps (Channel 1). The results (Figure 8.8) shows that the muscle activation in Channel 1 was lower with exoskeleton assistance, for the same movement. In this set of experiments, compared with the no exoskeleton assistance movement, the sEMG signals of A has a 81.5% decrease. This proved the obvious effect of the EBC controlled exoskeleton assistance.

Figure 8.9 and 8.10 showed the test results of random motion (Group 2) of subject A and B. As described above, the results without exoskeleton assistance are shown in (a), and the results with assistance are in (b). The results only shows the sEMG signals of biceps muscle (Channel 1). The results show that: the muscle activation with assistance was significantly lower. And in these cooperation tests, the muscle activation levels of A and B were respectively decreased 65.9% and 58.3%, with the exoskeleton assistance.

In addition, with the same test settings, the activation decrease of subject A and B are different. This indicates that the EBC is able to well adapt to the physiological condition of different individuals.

This is because all the individual physiological parameters (In Chapter 4) of each subject were tuned by genetic algorithm to fit the models before the experiment. Thus, the EMG-based neuromusculoskeletal interface can adapt to any physiological condition of the test subjects.

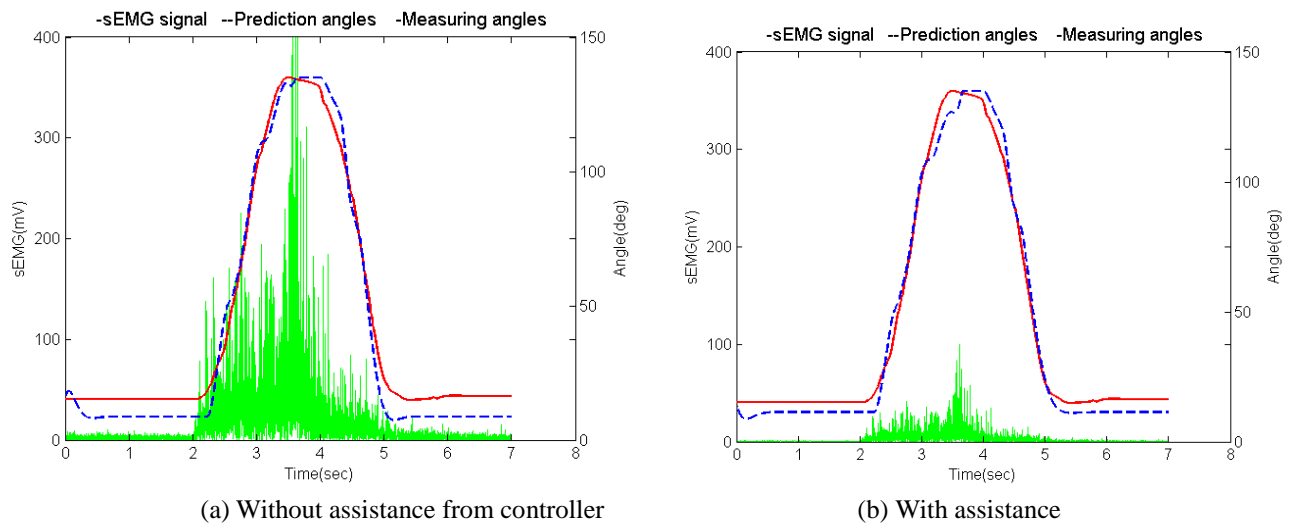


Figure 8.8: Single cycle test results (Channel 1) for elbow flexion motion with Subject A

Blue line: predicted angle, Red line: measured angle, Green line: EMG signal

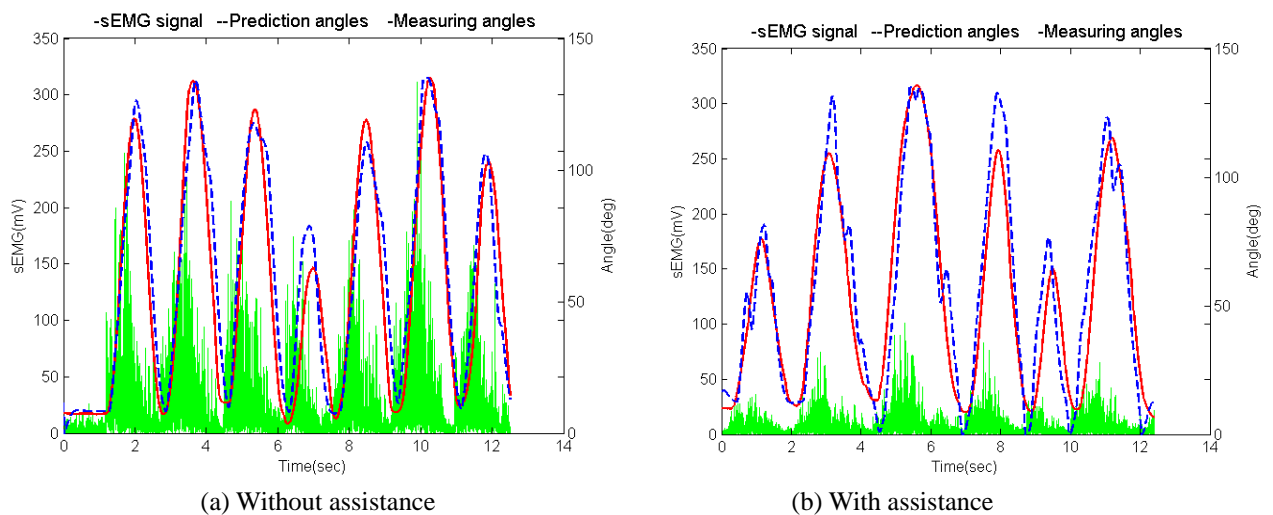


Figure 8.9: Random movement test results (Channel 1) for elbow flexion motion with Subject A

Blue line: predicted angle, Red line: measured angle, Green line: EMG signal

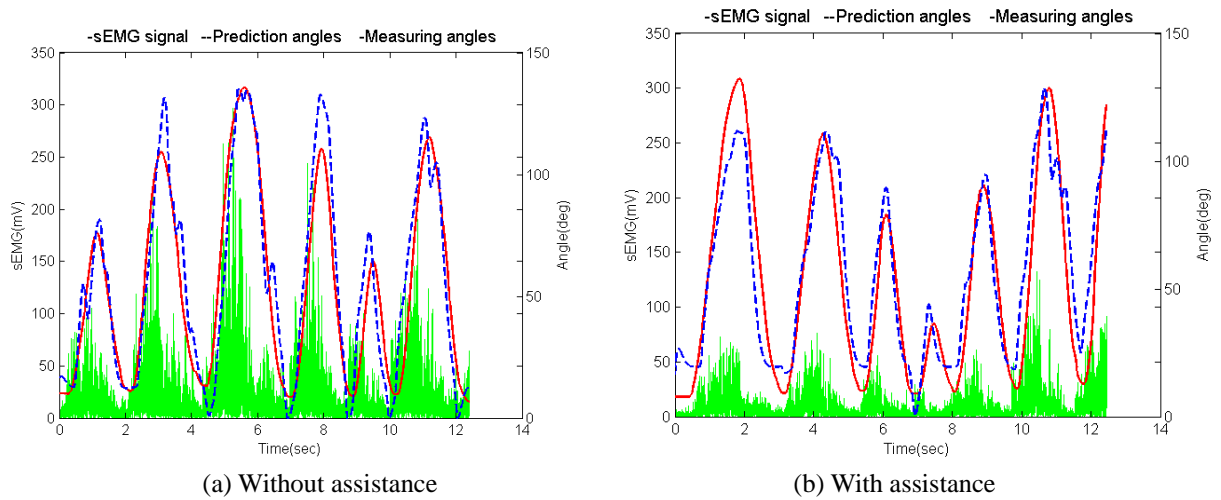


Figure 8.10: Random movement test results (Channel 1) for elbow flexion motion with Subject B

Blue line: predicted angle, Red line: measured angle, Green line: EMG signal

Figure 8.11 shows the results of subject A with the full-size continuous motion (Group 3). The set of test is the same with above tests. The results show that, the muscle activation levels decreased 72.7% with the exoskeleton's assistance.

Figure 8.12 shows the results of half range continuous motion test (Group 4) by the subjects A. Similarly, the activation decrease is 69.2%.

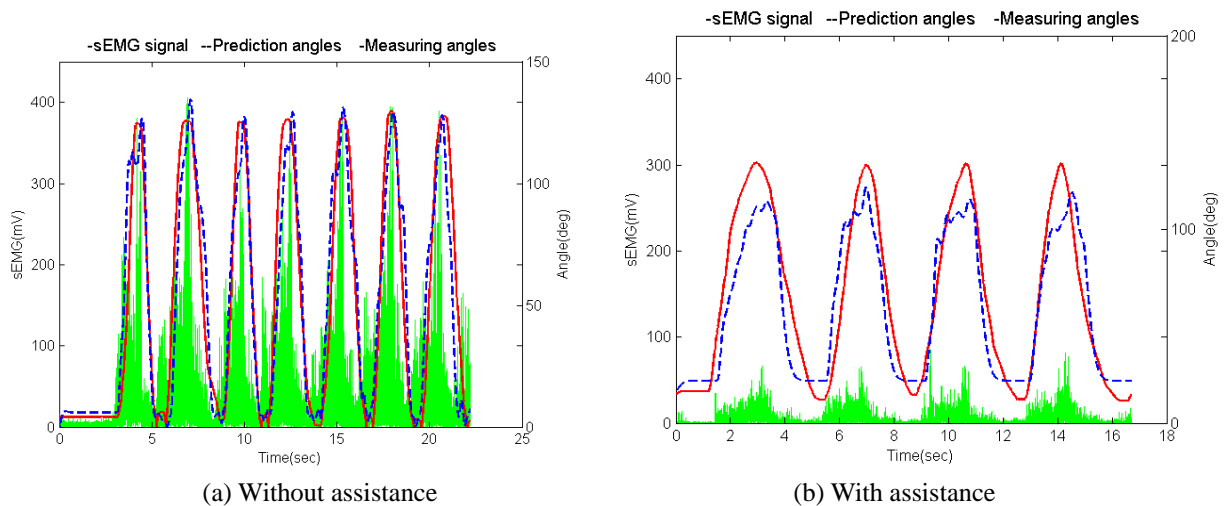


Figure 8.11: Continuous cycles test results (Channel 1) for elbow flexion motion with Subject A

Blue line: predicted angle, Red line: measured angle, Green line: EMG signal

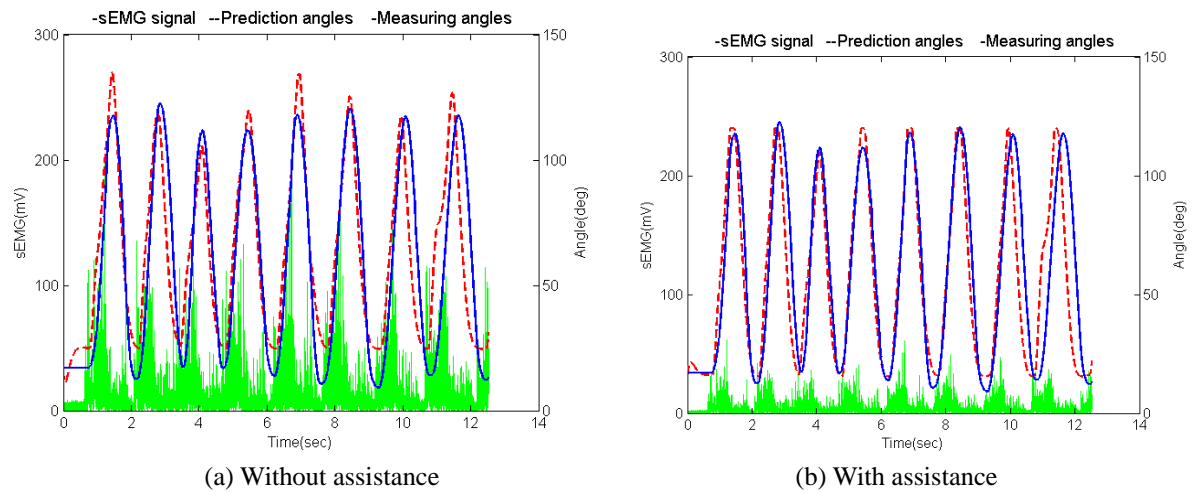


Figure 8.12: Continuous cycles at half the range of capable motion test results (Channel 1) for elbow flexion motion with Subject A

Blue line: predicted angle, Red line: measured angle, Green line: EMG signal

Figure 8.13 and 8.14 shows the results of Continuous cycles at increasing range movement test (Group 5) with subject A and B. Respectively, the decreases of muscle activation are 52.7% and 62.1%. The differences in decrease rate also show the online adaptability of the EMG-based neuromusculoskeletal interface.

From all the results in different kinds of movement test, the decreases of muscle activation were all over 52% when the assistance worked. It showed that the assistance effect offered by exoskeleton robot is obvious. At the same time, it proved the good control performance of the EBC. Therefore, the exoskeleton systems can effectively support the usage of any elbows movements and with any subjects.

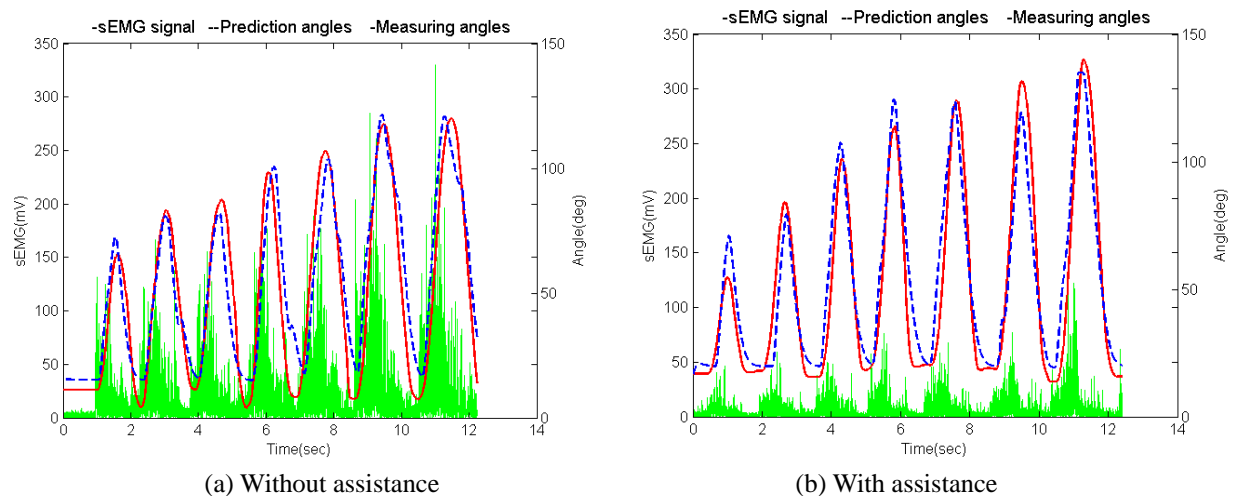


Figure 8.13: Continuous cycles starting with a small amplitude that gradually increases test results (Channel 1) for elbow flexion motion with Subject A

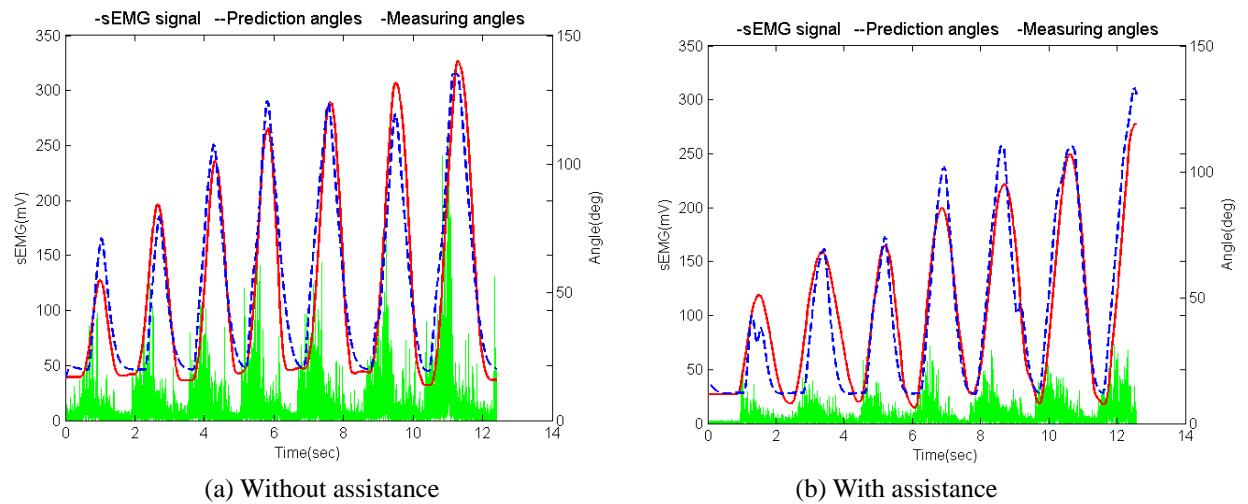


Figure 8.14: Continuous cycles starting with a small amplitude that gradually increases test results (Channel 1) for elbow flexion motion with Subject B

Blue line: predicted angle, Red line: measured angle, Green line: EMG signal

8.3 Chapter Summary

This chapter proposed a new controller, which uses the fusion information of EMG signal and wrist force signal as the controller input, to control the 5-DOF exoskeleton. The purposes of controlling exoskeleton based on the human intention have been achieved. In this chapter, EMG has been used as the main input information of the exoskeleton. In EBC, the neuromusculoskeletal model is the main part of the control system. In order to solve the individual difference properties of the EMG signals, the tuning model has been added in the EBC, so that the controller can adapt to different users. Since the EMG signal is easily susceptible to muscle fatigue, electrode position changes and other factors, the wrist force sensor-based controller (FBC) has taken in charge when the muscle activation is too low.

This chapter also gave the setup of the motor driver. The current controller was chosen for the elbow joint control. The flowchart and calculation formula of motor control were given, and the three digital inputs of ESCON drives were set, as well, in this chapter.

In order to evaluate the EMG-based Neuromuscular Interface proposed in this thesis, the 5-DOF exoskeleton prototype and its EBC controller were tested in a group of elbow movement experiments. Each experiment respectively has a comparison between the control with exoskeleton assessment and without assessment. All the results have proved the obvious effect of proposed

exoskeleton on assessment. To verify the individual adaptability of the EBC, the experimental results with same motion but different subjects have been obtained. The results indicate the adaptability of EBC to all kinds of physiological conditions of different individuals. They also show the online adaptability of the EMG-based Neuromuscular Interface

Chapter 9 Conclusions

Currently, the requirements of individual assisting systems for elderly and disabled people are daily increasing, as well as the function expansion of prosthetic control, military, residential and commercial robots. However, due to the limitations of traditional human-robot interface (HRI), they cannot be controlled according to the user's intention. EMG-based HRI is one of the promising approaches to solve these problems, so it becomes a popular research area in recent years.

The existing EMG-based HRIs have the problems of low accuracy in model, no online tuning for model parameters, large individual differences and so on. This thesis has achieved its main goal - to develop a new method of neuromuscular interface which could be applied to any human joint. This thesis took the elbow flexion/extension and forearm pronation/supination as case studies, and showed the process of establishing EMG-based models for real time human robot interaction. Firstly, the elbow and forearm physiological models were established to predict the elbow and forearm rotation movement. Experiments were used to verify the practicability and stability of the interfaces. Secondly, the parameter sensitivities of the models were analyzed in multi-angles. An online tuning algorithm for the EMG-driven models was developed and validated. Finally, a 2 degree of freedom (DOF) upper limb exoskeleton was designed with an EMG and force information fusion controller. It achieved the purpose of controlling an exoskeleton robot based on the human subjects' intention. This chapter summarizes the whole work, and indicates the potential areas for future research.

9.1 Main Achievements and Contributions

The main achievement of this thesis was to develop a new EMG-based neuromuscular interface. Through a comprehensive review of literatures the main research gaps in the past EMG-based HRIs were identified. Several new ideas to solve some of these problems were proposed including the following key areas: a) Improve the accuracy of the model by changing the muscle path; b) Assess the parameters sensitivity by a new idea, and classify all the adjustable parameters of the model in details. This is conducive to establish an online tuning algorithm. c) Based on a 5-DOF wearable exoskeleton robot, design a controller based on the fusion of EMG and force information to verify

the feasibility of the above EMG neuromuscular interface. It helps to achieve the purposes of controlling the exoskeleton robot with subjects' intention.

These new ideas proposed in the thesis are entirely feasible. **Firstly**, a new elbow physiological model was developed. By evaluating the RMSE indicators, the accuracy of this model has significantly improved compared to the accuracy of models in literatures. Also, an EMG-driven forearm pronation/supination model was developed. This is the first time such a model is proposed to reveal the forearm biomechanical structure for predicting movements based on EMG measurements. **Secondly**, based on the three-step layered approach proposed in this thesis, 19 adjustable parameters were graded and their characteristics were classified. The Action Difference Parameters and Individual Difference Parameters were identified as well. This method of parameter estimation provides foundation for tuning parameters to accommodate the differences between users and has universal significance. **Thirdly**, an online differential evolution algorithm was designed for parameters tuning. The evaluation and tuning of model parameters can not only improve the performance of the interface, but also partly solve the problems of individual differences. **Finally**, an upper limb assisting system was developed. It included a 2-DOF (one was for the elbow flexion/extension, the other was for the forearm pronation/supination) neuromuscular interface (NI), a 5-DOF exoskeleton, and a fusion exoskeleton control. This exoskeleton was user-friendly by a designed GUI. Also, the controller based on the fusion of the EMG and force information was designed to verify that the EMG controller could control the exoskeleton robot based on human subjects' intention. Further details of the above research results are set forth below.

An EMG-driven physiological model of the elbow joint

In the prior studies, there are two mainly modeling methods of simulating human physiology. The first method is to create a large '3D human musculoskeletal platform' by using the computed tomography (CT), magnetic resonance images (MRI) or cadaver colour cryosection (CCC) data, such as SIMM (MusculoGraphics, Inc.). Koo and Mak analyzed the human elbow flexion and extension movements by OpenSim, and successfully predicted the elbow trajectory with moderate loads [2]. Erdemir et al. analyzed prediction outcomes of three lower limb joints based on a musculoskeletal platform [92]. Tang et al analyzed the walking motion based on a systemic 3D musculoskeletal model, and predicted the related muscle force [93]. This kind of model is accurate, but hard to achieve real-time because of its large amount of calculations required. The other method is to represent the human joint by a single degree of freedom mechanical revolute, and bones and muscles by straight line segments. This 'simplified musculoskeletal models', such as the elbow model in [5, 94-96] and lower limb knee model in [97], are fast in calculation and can achieve

real-time processing. However they are poor in accuracy during complex random movement of the forearm, and cannot calculate when the line of muscle force crosses the joint center.

This thesis designed a new elbow musculoskeletal model based on the anatomical data, simplified the biceps and triceps muscle groups by a two-segments-polyline through muscle starting point, insertion point, and adhesion point, and built some reasonable assumptions based on the physiological properties of muscle. This model solved the above problems of the prior literature models. It included the musculotendon model, musculoskeletal model and kinematics model. By the experiments of multi-subjects and multi-movements, the new model was verified to be able to accurately identify different new track and range of motions. For example, the average RMSE of random motion test was only 13.7° . The performance was greatly enhanced than the previous models (such as the model in [5]). Meanwhile, on the premise of ensuring the operation speed, the new model was closer to actual human physiological structure. It solved the 'passing body' issues (when the joint angle $d=0^\circ$, the muscle path of single line model crosses the rotation center.), and expand the calculation of joint angle range to $[-5 \sim 130^\circ]$, which is more consistent with the human actual joint angle range.

An EMG-driven physiological model of the forearm rotation.

The forearm pronation / supination motion is completed by groups of muscles working together. In terms of human physiological structure or daily life and exercise, the usage of muscles for forearm rotation is relatively few. In addition, the movement range of forearm rotation joint is relatively small. Thus, the human-robot interface for forearm rotation is particularly difficult. The difficulty mainly lies in the weakness of muscle EMG, shortness of movement time, easy interference of the signal, small length changes of muscle. And since, some muscles have both deep and shallow portions contributing to the movement, their signals are more difficult to be captured. In view of this, the studies of small amplitude movement, such as forearm pronation / supination movements, are less. Kiguchi in [161] used the EMG from forearm muscles and nerve fuzzy controller to control the assisting forearm exoskeleton. This neuro-fuzzy control method is complicated, and without physiological significance. Forearm rotation physiological model in this thesis was evolved from the elbow model, and it was the first one of this kind of model. It could only use the EMG activities from the shallow parts of pronator teres (PT), pronator quadratus (PQ), and supinator (SUP) three muscles to predict continuous rotation movements. This model contained three EMG signal processing, three Hill-typed musculotendon models, a physiological musculoskeletal model and a kinematics model. The experiments with four human subjects showed the effectiveness of this method. The RMSE of a basic Sup-Pro Test was 5.88° . The average RMSE of Forearm Continuous

Cycles Test was 15.31 °. And the average RMSE of Random Movement Test was 13.35 °. The establishment of this forearm rotation physiological model has opened up a new way for studying the complex motion prediction system of small amplitude joint movement.

Sensitivity grading and properties classification of model parameters

In the current publications, sensitivity studies of neuromuscular model are limited, especially for the number of analyzed parameters is quite few. The existing literatures were mainly focusing on the impact of general musculotendon parameters sensitivity [111-114] to model, but lack of the impact of individual parameters or muscle-skeleton parameters. Secondly, most of the existing researches were based on human lower limb model and its parameters [111-113]. For example, Groote et al. assessed five main parameters sensitivity to Hill model in gait dynamic simulations [112]. Redl et al. only studied three main parameters sensitivity to muscle model: optimal muscle-fiber length, muscle physiological cross-sectional area (PCSA), and tendon rest length [113]. Though Garner and Pandy estimated the properties of upper limb muscles, they still only optimized three parameters - peak isometric force, optimal muscle-fiber length, and tendon slack length [114]. More comprehensive parametric analysis for upper limb is needed.

This thesis used the EMG-based elbow physiological model as an example, and designed a three-step layered approach for model parameter sensitivity analysis. Firstly, an offline and no test signal calculation was used to determine the optimization level of each parameter. Then, the action difference and individual difference of each parameter are analyzed in step two and three. The three steps cooperate with each other to comprehensively show the parameters characters and the impacts on the model. Sensitivity analysis of the model parameters resulted in a relatively small subset of the parameters used for parameter tuning. It laid a good foundation for parameter tuning. Also, this three-step layered approach provided a new way for the analysis of other model parameters.

An online tuning method for EMG driven models

The purpose of parameter tuning is to enable the model to match a subject based on the EMG measurements and predicted outputs. Many researchers were looking for a quick and easy method of tuning operation. At present, genetic algorithm (GA) is one of the most widely tuning algorithms used EMG-driven models [66, 162, 163]. The nonlinear least squares optimization is also been used to tune the parameters until the minimum difference between the measured and predicted joint torques [59, 74, 75, 164]. The tuning algorithm in [66] was Parallel Simulate Anneal Arithmetic (SAA). Genetic algorithms can achieve high accuracy, but it is time-consuming and it does not always get the global minimum. Thus, GA cannot be used for online tuning. For the single elbow

flexion/extension test, of tuning 14 parameters, the minimum RMSE was low to 3.3056° . The tuning time by MATLAB Global Optimization Toolbox was about one hour, and was about 40 minutes by self-programmed GA. Differential Evolution (DE) algorithm is a new simple and efficient global optimization algorithm. This thesis compiled a DE calculation program, and its calculation was significantly faster than the GA.

This thesis compared the performances of DE and GA in three aspects (quality of the final solution, the convergence speed, the success rate) by experiments. Under the same parameters setting conditions, the quality of the final solution of GA algorithm was slightly better than DE algorithm. For example, for the single cycle elbow flexion/extension, with 10 times optimization, the RMS by DE could quickly converge to 3.59° - 10.78° , and the RMS of GA was 2.45° - 5.32° . However, the convergence speed of GA was significantly lower than the DE algorithm. For example, for the single cycle elbow movement, the tuning with DE could always be completed within 8 minutes (sometimes even quick to below 2 minutes), while the GA needed about 40 minutes. The success rates of GA algorithm and DE algorithm were comparable. Therefore, in view of the high accuracy and fast convergence capability of DE algorithm, it can be used for fast online tuning. The GA algorithm can only be used for off-line tuning.

The human-robot interface of 2-DOF movement

This thesis established an EMG and physiological musculoskeletal model based human-robot interface system. This interface provided different auxiliary operations for single elbow flexion / extension, forearm pronation / supination, and complex movements. It also gave the methods of handling muscle signal channel, muscle model and musculoskeletal geometry model, during the complex motions of forearm. During the combination of elbow model and forearm rotating model, the calculating of each model is independent and without interference. However, in parameters tuning, there were some new considerations. Some parameters belonged to the independent movement, such as F_{MAX} , l_{opt} and U_{sup} . And some other parameters belonged to the complex movement, such as the forearm length and forearm quality. Thus, in the complex movement, these common parameters needed to take more considerations. Finally, a graphical user interface (GUI) was developed in Matlab for operating the 2-DOF interface and a 5-DOF exoskeleton.

A controller based on the fusion of EMG and force information

This thesis proposed a controller based on the fusion of EMG and force information. The EMG signals or wrist force were used as an information input to the control system. It achieved the purposes of controlling the exoskeleton based on the intention of human subjects. In the

EMG-based controller (EBC), the neuromusculoskeletal model was the main body of the control system. In order to solve the individual different properties of the EMG signals, a tuning model was added in the EBC to adapt to different users. Since the EMG signal was easily affected by muscle fatigue and the electrode position change, when the muscle activation was too low, a wrist force sensor based controller (FBC) was directly into usage. The FBC used the impedance control, it could enable the exoskeleton to achieve flexible position control when interacting with the user's limb.

In order to assess the effectiveness of the EMG-based Neuromuscular Interface, the control experiments with different subjects and elbow movements were conducted, on the 5-DOF exoskeleton and the EBC controller. During each experiment, the movement with or without the exoskeleton-assisted system were compared. In 5 sets of experiments, compared to the ones without assisting exoskeleton, the biceps muscle activations of one subject were reduced by 81.5%, 65.9%, 72.7%, 69.2 % and 52.7%, with the help of exoskeleton. These results proved that the power assisting effect of proposed exoskeleton was obvious. The same motion control experiments with different individuals also verified the adaptability of EBC to different individuals. It also showed the online adaptabilities of the EMG-based Neuromuscular Interface.

9.2 Future Work

This thesis has developed a 2-DOF neuromuscular interface. It is hoped that this method can be applied to other joints in human body and military, medical, entertainment and other fields. Throughout the study, the establishment of the physiological model for forearm rotation movement was very difficult, thus the thesis measured the muscle and skeleton sizes of a cadaveric forearm as modeling basis. The advantage of selecting physiological model as human-robot interface was that it did not need training data, and there was a clear physiological significance. But also there were many challenges. Wherein, the minimum number of muscle in the physiological model was hard to choose. The number of muscles affected the accuracy of the model, the complexity and the task execution time of the model system. A set of experiments can be designed to test this: To try to simplify the model and ensure the model without distortion as the principle, in the beginning of the experiment, as much as possible EMG channels are used. Then evaluate the signals by linear envelope, feature selection or correlation analysis to determine the optimal number of channels and EMG sampling location. Finally, establish a set of common methods of analyzing the related muscle's contributions to the joint movement.

The greatest impact to the accuracy of EMG-driven model is the characteristic parameters. According to the model structure, the calibration parameters can be divided into two kinds: the parameters without physiological significance (such as gain), and the parameters with physiological significance (such as muscle parameters). The accuracy of anatomical data greatly impacts model accuracy. This thesis determines the main parameters affecting the musculoskeletal model performance by sensitivity analysis. However, the effect of age (such as the elderly muscle atrophy), disease, physical training and muscle fatigue to musculoskeletal model are not analyzed. Since these factors affect EMG signals, this study also has a very practical significance.

In this thesis, the elbow flexion / extension and forearm pronation / supination could be regarded as single movement or a complex movement. In the muscle signal selection, they were independent: the biceps and triceps were selected for elbow flexion / extension, and the supinator, pronator teres and pronator quadratus were selected for forearm pronation / supination. When the forearm does complex motion, five channels were used to measure the surface EMG of these five muscles, and the results by signal envelope and muscle activation dynamics processing were saved in one data file. However, in the complex movement, the model still needs some improvements, including the muscles choice which affect the two separate motion at the same time, the signal processing of common muscles, the interaction of this 2-DOF, and the analysis of common parameters.

EMG can well express the users' intention and actually be applied to the interface. However, due to the randomness and low voltage resistance of EMG, the noise in the signal is difficult to be removed. And the situations of subjects' physical health, muscles and physiological changes (fatigue) compositely affect the determination of muscle activation. For the patients with very weak EMG (such as stroke patients), it is recommended to measure the EMG from patient's healthy limb. There still needs more detailed study of muscle fatigue. The EMG data used in this thesis were only from healthy subjects, so the usage of this interface for patients with physical disabilities also needs to be verified.

Both of the elbow flexion/extension and forearm pronation/supination models can normally follow movement intention based on human EMG signals. However, since EMG signal is the only information source, in some specific cases, these models still have some limitations. For example, when the subject holds his joint but generates muscle strength, the EMG signal will change according to the muscle contraction, causing the models to calculate the corresponding muscle force and joint moment, and predict the joint motion angle. However, with the fact that the joint of subject is still, there is a difference between the predicted movements and the actual movements. Similarly, this model does not accurately predict the pause of the joint movement in cases when the

muscles of patient is healthy but the joint is damaged (blocked or cannot not fully complete the intended movement). An external motion tracking sensor in real-time should be added, to work with the tuning model, to adjust the predicted joint angle in real time based on the changes of actual angle in this particular case.

The exoskeleton developed in this thesis was used to assist movements of the body weaken people (such as the elderly, the disabled, and the injured people). The EMG signals and wrist force were used as input information to the control system, and EMG-based controller (EBC) and wrist force-based controller (FBC) were also designed. EBC was as the main controller. When the level of muscle activation for weakening human body was low, the impedance control of FBC was in use. In this thesis, the elbow motion experiments were used to assess the effectiveness of the EBC control. However, all of the test data were from healthy subjects. How EBC applicants in weakening human body and how to set the threshold of low level muscle activation are still need to be experimentally determined.

In the future, this kind of interface can not only be applied to the daily lives of people with disabilities, but also can be extended to support the human complex movements, such as interactive games and entertainment, sports competition or military tasks. It can help the pilots control the aircraft to combat the enemy in air, help the F1 racer drive the formula one racing car in complex road conditions, and give the players more interactive gaming experience.

9.3 Chapter Summary

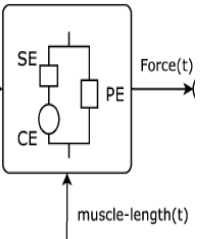
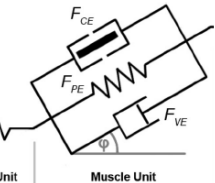
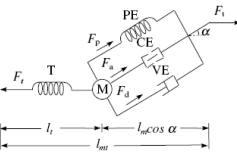
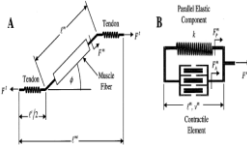
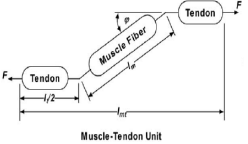
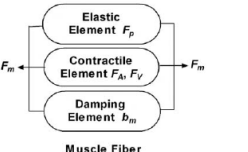
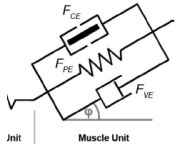
This thesis has presented a method of developing an EMG-based neuromuscular interface for the effective interaction between humans and automatic devices, established EMG-based neuromuscular models for elbow and forearm rotation, completed the sensitivity grading and characteristics classification of model parameters, developed the offline and online tuning methods suitable for EMG-driven models to verify the validity of the model, designed a controller based on the fusion of EMG and force information and verify the adaptability of EMG-based neuromuscular interface, by the elbow joint as case study. The tools developed in this thesis can provide valuable experience for the EMG-based interface researches. The continued development of this approach will ultimately achieve the seamless integration between humans and automatic devices.

Appendix I

The researches summary of EMG-based human-robot interface systems

No./Author	[70](2006) E. E. Cavallaro University of Washington	[5, 6, 165](2012) James W. L. Pau The University of Auckland	[2] (2005) Terry K.K. Koo The Hong Kong Polytechnic University	[66] (2004) Thomas S. Buchanan University of Delaware	[68] (2009) Related to No.9 Qi Shao University of Delaware	[69] (2010) Massimo Sartori University of Padova
Mechanical structure	1 DOF Cybex exercise machine potentiometer Used for: 7 DOF Exoskeleton arm	1 DOF Polaris Spectra (NDI,Canada)	Electrogonio-meter	1 DOF video cameras force plates (in a gait laboratory)	1 DOF (knees) video cameras force plates (in a gait laboratory)	7 DOF (lower limb) dynamometer (Biodex, USA)
Number of muscles	7	2	7	7	4	13
Signal processing (Filter)	4th Butterworth	Butterworth	Butterworth	Butterworth	Butterworth	

Appendix I

<p>Muscle activation Dynamics</p>	<p>Neural activation $u(t)$</p>				$u(t) = \alpha e^{-(t-d)} - \beta_1 u(t-1) - \beta_2 u(t-2)$	$u(t) = \alpha e^{-(t-d)} - \beta u(t-1) - \beta_2 u(t-2)$	
	<p>Muscle activation $a(t)$</p>	$a(t) = \frac{A^{u(t)} - 1}{A - 1}$ <p>None linear processing</p>	<p>Linear envelope</p>	$a(t) = \text{Max} \begin{cases} \text{Max}[E(t-t')] & \forall t', \exists 0 \leq t' < \tau_2 \\ \text{Max}[E(t-t')e^{-\frac{(t-t')}{\tau_1}}] & \forall t', \exists t' \geq \tau_2 \end{cases}$ <p>Linear envelope</p>	$a(t) = \frac{e^{Au(t)} - 1}{e^A - 1}$	$a(t) = \frac{e^{Au(t)} - 1}{e^A - 1}$	$a(t) = \frac{e^{Au(t)} - 1}{e^A - 1}$
<p>Muscle contraction Dynamics</p>	<p>Muscle-tendon model</p> 				 		
	<p>Tendon stiffness processing</p>	∞	∞	<p>Hard Stiffness</p>	<p>Limited value</p>	<p>Limited value</p>	∞
	<p>Active contractile</p>	$F_{CE} = a * f_l * f_v * F_{CE_{max}}$	$F_{CE} = R * f(l) * f(v) * A * F_{Max}$	$F_a = \sigma_m \cdot PCSA \cdot f_l(l_m) \cdot f_v(\dot{l}_m) \cdot a(t)$	$F_{CE} = f_A(l) * f(v) * a(t) * F_{Max} * \cos(\phi)$	$F_{CE} = f_A(l) * f(v) * a(t) * F_{Max} * \cos(\phi)$	$F_{CE} = f_A(l) * f(v) * a(t) * F_{Max} * \delta * \cos(\phi)$

Appendix I

	force						
	F_{CE}						
	Passive force F_{PE}	$F_{PE} = \left[\frac{F_{max}}{e^S - 1} \right] \left[e^{((S/\Delta M_{max})\Delta L)} - 1 \right]$	$F_{PE} = F_{Max} \frac{e^{10 * C_{pass} (l_n - 1)}}{e^5}$		$F_{PE} = f_P(l) * F_{Max} * \cos(\phi)$ $f_P(l) = \frac{e^{10 * (l_n - 1)}}{e^5}$	$F_{PE} = f_P(l) * F_{Max} * \cos(\phi)$ $f_P(l) = \frac{e^{10 * (l_n - 1)}}{e^5}$	$F_{PE} = f_P(l) * F_{Max} * \delta * \cos(\phi)$
	Viscous force F_{VE}	0	$F_{VE} = F_{Max} * B * v_n$		0	$F_{VE} = F_{Max} * b_m * v * \cos(\phi)$	$F_{VE} = F_{Max} * b_n * v * \delta * \cos(\phi)$
Musculoskeletal geometry model	Muscular force lines	Polyline	Line	SIMM	Line		
	Force arm calculation	$b_i = (\vec{r}_i \times F) \bullet k_i$	Triangular relationship	SIMM	$r(\theta) = \frac{\partial \ell^{mi}(\theta)}{\partial \theta}$		
	Musculoskeletal parameter	Other articles	Other articles	Some subjective criteria Other articles SIMM	Other articles cadaver measurement		SIMM Other articles
Tuning model	Tuning model (performance)	$E_{max} = \max_i M(i) - M(i) $	$E_{rms} = \sqrt{\frac{1}{N} \sum_{i=1}^N (\phi(i) - \bar{\phi}(i))^2}$	$E_{rms} = \sqrt{\frac{1}{N} \sum_{i=1}^N (M(i) - M(i))^2}$	$\min \sum_1^n (M^j - M^{measured})^2$	$E_{rms} = \sqrt{\frac{1}{N} \sum_{i=1}^N (\phi(i) - \bar{\phi}(i))^2}$	$\min \sum_1^n (M^j - M^{measured})^2$

Appendix I

	indicators)	$E_{rms} = \sqrt{\frac{1}{N} \sum_{i=1}^N (M(i) - M(i))^2}$ $\rho = \frac{C_{MM}}{\sigma_M \sigma_M}$ $\eta_S = \frac{\sum_{k=1}^N 1}{N} \quad (\forall k \quad M(k) \leq S)$					
	Tuning algorithm	Genetic Algorithms (GA)	Many calibration trials	Nelder–Mead	Non-linear least square optimization	Parallel Simulate Anneal Arithmetic, SAA	Simulate Anneal Arithmetic, SAA
	The number of tuning parameters	11		8		10	

Appendix II

Publications

During the course of the PhD the following were primary authored:

Journal articles:

- R. Tao, S. Xie, Y. Zhang et al., “Review of EMG-based neuromuscular interfaces for rehabilitation: elbow joint as an example,” *International Journal of Biomechatronics and Biomedical Robotics*, vol. 2, no. 2, pp. 184-194, 2013.
- R. Tao., S. Xie., M Zhang., “A New Musculoskeletal Model in Predicting Forearm Pronation and Supination for Use in Human-robot Interaction” *Journal of Biomechanics*. (Under review)

Conference papers:

- Tao, R., Xie S. Q., and Zhang Y. X., “Review of EMG-based Neuromuscular Interface for Upper Limb Control”, 19th International conference on Mechatronics and Machine Vision in Practice, Auckland, New Zealand, November 28-30 2012.
- Tao, R., Xie, S. Q., Zhang Y. X. and Pau, J., “sEMG-based Neural-musculoskeletal Model for Human-robot Interface”, The 9th IEEE Conference on Industrial Electronics and Applications (ICIEA 2014), 2014, Hangzhou, China.
- Ran Tao, Shane (Shengquan) Xie, James W.L. Pau, “A Study of EMG-based Neuromuscular Interface for Elbow Joint”, the 7th International Conference on Intelligent Robotics and Application (ICIRA 2014), 2014, Guangzhou, China

References

- [1] O. Fukuda, T. Tsuji, M. Kaneko, and A. Otsuka, "A human-assisting manipulator teleoperated by EMG signals and arm motions," *IEEE Transactions on Robotics and Automation*, vol. 19, no. 2, pp. 210-222, 2003.
- [2] T. K. Koo, and A. F. Mak, "Feasibility of using EMG driven neuromusculoskeletal model for prediction of dynamic movement of the elbow," *J Electromyogr Kinesiol*, vol. 15, no. 1, pp. 12-26, Feb, 2005.
- [3] A. T. Au, and R. F. Kirsch, "EMG-based prediction of shoulder and elbow kinematics in able-bodied and spinal cord injured individuals," *IEEE Transactions on Rehabilitation Engineering*, vol. 8, no. 4, pp. 471-480, 2000.
- [4] P. K. Artemiadis, and K. J. Kyriakopoulos, "EMG-based control of a robot arm using low-dimensional embeddings," *IEEE Transactions on Robotics*, vol. 26, no. 2, pp. 393-398, 2010.
- [5] J. W. L. Pau, S. S. Q. Xie, and A. J. Pullan, "Neuromuscular Interfacing: Establishing an EMG-Driven Model for the Human Elbow Joint," *Biomedical Engineering, IEEE Transactions on*, vol. 59, no. 9, pp. 2586-2593, 2012.
- [6] J. W. L. Pau, H. Saini, S. S. Q. Xie, A. J. Pullan, and G. Mallinson, "An EMG-driven neuromuscular interface for human elbow joint." pp. 156-161.
- [7] R. M. Enoka, S. Baudry, T. Rudroff, D. Farina, M. Klass, and J. Duchateau, "Unraveling the neurophysiology of muscle fatigue," *Journal of Electromyography and Kinesiology*, vol. 21, no. 2, pp. 208-219, 2011.
- [8] J. S. Petrofsky, and C. A. Phillips, "Interactions between fatigue, muscle temperature, blood flow and the surface EMG," *NAECON 1980*, pp. 520-527, 1980.
- [9] M. Rowbottom, and C. Susskind, *Electricity and medicine: history of their interaction*: Palgrave Macmillan, 1984.
- [10] J. Yang, K. Abdel-Malek, and K. Nebel, *The Reach Envelope of a 9 Degree-of-Freedom Model of the Upper Extremity*, DTIC Document, 2003.
- [11] T. Nef, M. Guidali, V. Klamroth-Marganska, and R. Riener, "ARMin-exoskeleton robot for stroke rehabilitation." pp. 127-130.
- [12] H. I. Krebs, J. J. Palazzolo, L. Dipietro, M. Ferraro, J. Krol, K. Ranekleiv, B. T. Volpe, and N. Hogan, "Rehabilitation robotics: Performance-based progressive robot-assisted therapy," *Autonomous robots*, vol. 15, no. 1, pp. 7-20, 2003.
- [13] J. C. Perry, J. Rosen, and S. Burns, "Upper-limb powered exoskeleton design," *IEEE/ASME transactions on mechatronics*, vol. 12, no. 4, pp. 408, 2007.
- [14] D. Gijbels, I. Lamers, L. Kerkhofs, G. Alders, E. Knippenberg, and P. Feys, "The Armeo Spring as training tool to improve upper limb functionality in multiple sclerosis: a pilot study," *Journal of NeuroEngineering and Rehabilitation*, vol. 8, no. 1, pp. 5, 2011.
- [15] M. Nixon, and A. S. Aguado, *Feature Extraction & Image Processing for Computer Vision*: Academic Press, 2012.
- [16] T. B. Moeslund, and E. Granum, "A survey of computer vision-based human motion capture," *Computer Vision and Image Understanding*, vol. 81, no. 3, pp. 231-268, 2001.
- [17] N. M. Oliver, B. Rosario, and A. P. Pentland, "A Bayesian computer vision system for modeling human interactions," *Pattern Analysis and Machine Intelligence, IEEE Transactions on*, vol. 22, no. 8, pp. 831-843, 2000.

- [18] G. E. Loeb, R. Davoodi, M. Mileusnic, R. Ananth, A. Inmann, and I. E. Brown, "Strategic development of sensorimotor prosthetic technology." pp. 1539-1542 Vol.2.
- [19] B. Brunner, K. Arbter, and G. Hirzinger, "Task directed programming of sensor based robots." pp. 1080-1087 vol.2.
- [20] W. Sansen, A. Claes, D. De Wachter, L. Callewaert, and M. Lambrechts, "A smart sensor for biomedical applications." pp. 1088-1089 vol.4.
- [21] B. J. Hosticka, "Analog circuits for sensors." pp. 97-102.
- [22] W. Bouten, E. W. Baaij, J. Shamoun-Baranes, and K. C. Camphuysen, "A flexible GPS tracking system for studying bird behaviour at multiple scales," *Journal of Ornithology*, vol. 154, no. 2, pp. 571-580, 2013.
- [23] H. Zhou, T. Stone, H. Hu, and N. Harris, "Use of multiple wearable inertial sensors in upper limb motion tracking," *Medical engineering & physics*, vol. 30, no. 1, pp. 123-133, 2008.
- [24] E. S. Sazonov, T. Bumpus, S. Zeigler, and S. Marocco, "Classification of plantar pressure and heel acceleration patterns using neural networks." pp. 3007-3010.
- [25] M. Kohle, D. Merkl, and J. Kastner, "Clinical gait analysis by neural networks: issues and experiences." pp. 138-143.
- [26] I. J. Alexander, E. Y. Chao, and K. A. Johnson, "The assessment of dynamic foot-to-ground contact forces and plantar pressure distribution: a review of the evolution of current techniques and clinical applications," *Foot & Ankle International*, vol. 11, no. 3, pp. 152-167, 1990.
- [27] M. W. Keith, P. H. Peckham, G. B. Thrope, K. C. Stroh, B. Smith, J. R. Buckett, K. L. Kilgore, and J. W. Jatich, "Implantable functional neuromuscular stimulation in the tetraplegic hand," *The Journal of hand surgery*, vol. 14, no. 3, pp. 524-530, 1989.
- [28] B. Smith, P. H. Peckham, M. W. Keith, and D. D. Roscoe, "An externally powered, multichannel, implantable stimulator for versatile control of paralyzed muscle," *Biomedical Engineering, IEEE Transactions on*, no. 7, pp. 499-508, 1987.
- [29] K. L. Kilgore, P. H. Peckham, M. W. Keith, G. B. Thrope, K. S. Wuolle, A. M. Bryden, and R. L. Hart, "An implanted upper-extremity neuroprosthesis. Follow-up of five patients," *The Journal of Bone and Joint Surgery (American)*, vol. 79, no. 4, pp. 533-41, 1997.
- [30] V. Udayashankara, and M. Shivaram, "Sound sensitive artificial hand." pp. 2337-2338.
- [31] P. Sykacek, S. J. Roberts, and M. Stokes, "Adaptive BCI based on variational Bayesian Kalman filtering: an empirical evaluation," *IEEE Transactions on Biomedical Engineering*, vol. 51, no. 5, pp. 719-727, 2004.
- [32] E. Buch, C. Weber, L. G. Cohen, C. Braun, M. A. Dimyan, T. Ard, J. Mellinger, A. Caria, S. Soekadar, and A. Fourkas, "Think to move: a neuromagnetic brain-computer interface (BCI) system for chronic stroke," *Stroke*, vol. 39, no. 3, pp. 910-917, 2008.
- [33] P. R. Cavanagh, and P. V. Komi, "Electromechanical delay in human skeletal muscle under concentric and eccentric contractions," *European journal of applied physiology and occupational physiology*, vol. 42, no. 3, pp. 159-163, 1979.
- [34] CyberGlove. "CyberGlove Systems."
- [35] T. H. Massie, and J. K. Salisbury, "The phantom haptic interface: A device for probing virtual objects." pp. 295-300.
- [36] L. Koessler, L. Maillard, A. Benhadid, J. P. Vignal, J. Felblinger, H. Vespignani, and M. Braun, "Automated cortical projection of EEG sensors: Anatomical correlation via the international 10-10 system," *NeuroImage*, vol. 46, no. 1, pp. 64-72, 5/15/, 2009.
- [37] K. M. Cheung, T. Wang, G. Qiu, and K. D. Luk, "Recent advances in the aetiology of adolescent idiopathic scoliosis," *International orthopaedics*, vol. 32, no. 6, pp. 729-734, 2008.
- [38] W. WU, H. Guozhi, and X. LIU, "Department of Physical Medicine and Rehabilitation, Zhujiang Hospital, The First Military Medical University, Guangzhou 510282, China; Application of surface EMG in evaluation of effectiveness of clinical interventions for

- lumbar intervertebral disc prolapse [J],” *Chinese Journal of Physical Medicine and Rehabilitation*, vol. 9, 2002.
- [39] R. Neblett, R. J. Gatchel, and T. G. Mayer, “A clinical guide to surface-EMG-assisted stretching as an adjunct to chronic musculoskeletal pain rehabilitation,” *Applied psychophysiology and biofeedback*, vol. 28, no. 2, pp. 147-160, 2003.
- [40] A. R. Kralj, and T. Bajd, *Functional electrical stimulation: standing and walking after spinal cord injury*: CRC press, 1989.
- [41] S. Jezernik, G. Colombo, T. Keller, H. Frueh, and M. Morari, “Robotic orthosis lokomat: A rehabilitation and research tool,” *Neuromodulation: Technology at the neural interface*, vol. 6, no. 2, pp. 108-115, 2003.
- [42] Y. Sankai, “HAL: Hybrid assistive limb based on cybernics,” *Robotics Research*, pp. 25-34: Springer, 2010.
- [43] L. J. Huston, and E. M. Wojtys, “Neuromuscular performance characteristics in elite female athletes,” *The American journal of sports medicine*, vol. 24, no. 4, pp. 427-436, 1996.
- [44] R. C.-D. Lovely, “Commercial Hardware for the Implementation of Myoelectric Control,” *Powered Upper Limb Prostheses: Control, Implementation and Clinical Application; 11 Tables*, 2004.
- [45] Z.-X. Huang, X.-D. Zhang, and Y.-N. Li, “Design of a grasp force adaptive control system with tactile and slip perception.” pp. 1101-1105.
- [46] K. Jong-Sung, J. Huyk, and S. Wookho, “A new means of HCI: EMG-MOUSE.” pp. 100-104 vol.1.
- [47] E. Costanza, S. A. Inverso, and R. Allen, “Toward subtle intimate interfaces for mobile devices using an EMG controller.” pp. 481-489.
- [48] S. Aso, A. Sasaki, H. Hashimoto, and C. Ishii, “Driving electric car by using EMG interface.” pp. 1-5.
- [49] K. R. Wheeler, and C. C. Jorgensen, “Gestures as input: Neuroelectric joysticks and keyboards,” *IEEE pervasive computing*, vol. 2, no. 2, pp. 56-61, 2003.
- [50] K. R. Wheeler, “Device control using gestures sensed from EMG.” pp. 21-26.
- [51] H. Prendinger, and M. Ishizuka, “The empathic companion: A character-based interface that addresses users' affective states,” *Applied Artificial Intelligence*, vol. 19, no. 3-4, pp. 267-285, 2005.
- [52] H.-C. Kim, S. Pang, H.-M. Je, D. Kim, and S.-Y. Bang, “Support vector machine ensemble with bagging,” *Pattern recognition with support vector machines*, pp. 397-408: Springer, 2002.
- [53] C. J. Feng, A. F. Mak, and T. K. Koo, “A surface EMG driven musculoskeletal model of the elbow flexion-extension movement in normal subjects and in subjects with spasticity,” *Journal of Musculoskeletal Research*, vol. 3, no. 02, pp. 109-123, 1999.
- [54] T. Buchanan, S. Delp, and J. Solbeck, “Muscular resistance to varus and valgus loads at the elbow,” *Journal of biomechanical engineering*, vol. 120, no. 5, pp. 634, 1998.
- [55] J. Soechting, and M. Flanders, “Evaluating an integrated musculoskeletal model of the human arm,” *Journal of biomechanical engineering*, vol. 119, no. 1, pp. 93, 1997.
- [56] B. Laursen, B. R. Jensen, G. Németh, and G. Sjøgaard, “A model predicting individual shoulder muscle forces based on relationship between electromyographic and 3D external forces in static position,” *Journal of Biomechanics*, vol. 31, no. 8, pp. 731, 1998.
- [57] D. G. Lloyd, and T. F. Besier, “An EMG-driven musculoskeletal model to estimate muscle forces and knee joint moments in vivo,” *Journal of Biomechanics*, vol. 36, no. 6, pp. 765-776, 2003.
- [58] D. Lloyd, and T. Buchanan, “A model of load sharing between muscles and soft tissues at the human knee during static tasks,” *Journal of biomechanical engineering*, vol. 118, no. 3, pp. 367, 1996.
- [59] D. G. Lloyd, and T. S. Buchanan, “Strategies of muscular support of varus and valgus

- isometric loads at the human knee,” *Journal of Biomechanics*, vol. 34, no. 10, pp. 1257-1267, 2001.
- [60] S. J. Olney, and D. A. Winter, “Predictions of knee and ankle moments of force in walking from EMG and kinematic data,” *Journal of Biomechanics*, vol. 18, no. 1, pp. 9-20, 1985.
- [61] S. C. White, and D. A. Winter, “Predicting muscle forces in gait from EMG signals and musculotendon kinematics,” *Journal of Electromyography and Kinesiology*, vol. 2, no. 4, pp. 217-231, 1992.
- [62] D. P. Ferris, K. E. Gordon, G. S. Sawicki, and A. Peethambaran, “An improved powered ankle-foot orthosis using proportional myoelectric control,” *Gait & Posture*, vol. 23, no. 4, pp. 425-428, 2006.
- [63] K. P. Granata, and W. Marras, “An EMG-assisted model of trunk loading during free-dynamic lifting,” *Journal of Biomechanics*, vol. 28, no. 11, pp. 1309-1317, 1995.
- [64] M. A. Nussbaum, and D. B. Chaffin, “Lumbar muscle force estimation using a subject-invariant 5-parameter EMG-based model,” *Journal of Biomechanics*, vol. 31, no. 7, pp. 667-672, 1998.
- [65] T. S. Buchanan, M. J. Moniz, J. P. A. Dewald, and W. Z. Rymer, “Estimation of muscle forces about the wrist joint during isometric tasks using an EMG coefficient method,” *Journal of Biomechanics*, vol. 26, no. 4-5, pp. 547-560, 1993.
- [66] T. S. Buchanan, D. G. Lloyd, K. Manal, and T. F. Besier, “Neuromusculoskeletal Modeling: Estimation of Muscle Forces and Joint Moments and Movements From Measurements of Neural Command,” *JOURNAL OF APPLIED BIOMECHANICS*, vol. 20, no. 4, pp. 367-395, 2004.
- [67] S. Cososchi, R. Strungaru, A. Ungureanu, and M. Ungureanu, "EEG Features Extraction for Motor Imagery." pp. 1142-1145.
- [68] Q. Shao, D. N. Bassett, K. Manal, and T. S. Buchanan, “An EMG-driven model to estimate muscle forces and joint moments in stroke patients,” *Comput Biol Med*, vol. 39, no. 12, pp. 1083-8, Dec, 2009.
- [69] M. Sartori, D. G. Lloyd, M. Reggiani, and E. Pagello, "Fast operation of anatomical and stiff tendon neuromuscular models in EMG-driven modeling." pp. 2228-2234.
- [70] E. E. Cavallaro, J. Rosen, J. C. Perry, and S. Burns, “Real-Time Myoprocessors for a Neural Controlled Powered Exoskeleton Arm,” *Biomedical Engineering, IEEE Transactions on*, vol. 53, no. 11, pp. 2387-2396, 2006.
- [71] J. W. Pau, S. S. Xie, and A. J. Pullan, “Neuromuscular interfacing: establishing an EMG-driven model for the human elbow joint,” *Biomedical Engineering, IEEE Transactions on*, vol. 59, no. 9, pp. 2586-2593, 2012.
- [72] A. Hof, and J. Van den Berg, “EMG to force processing II: Estimation of parameters of the Hill muscle model for the human triceps surae by means of a calfergometer,” *Journal of Biomechanics*, vol. 14, no. 11, pp. 759-770, 1981.
- [73] T. Buchanan, S. Delp, and J. Solbeck, “Muscular resistance to varus and valgus loads at the elbow,” *TRANSACTIONS-AMERICAN SOCIETY OF MECHANICAL ENGINEERS JOURNAL OF BIOMECHANICAL ENGINEERING*, vol. 120, pp. 634-639, 1998.
- [74] Y.-W. Chang, F.-C. Su, H.-W. Wu, and K.-N. An, “Optimum length of muscle contraction,” *Clinical Biomechanics*, vol. 14, no. 8, pp. 537-542, 1999.
- [75] T. K. Koo, A. F. Mak, and L. Hung, “In vivo determination of subject-specific musculotendon parameters: applications to the prime elbow flexors in normal and hemiparetic subjects,” *Clinical Biomechanics*, vol. 17, no. 5, pp. 390-399, 2002.
- [76] K.-k. T. Koo, “Neuromusculoskeletal modeling of the elbow joint in subjects with and without spasticity,” 2002.
- [77] T. Moritani, M. Muro, and A. Nagata, “Intramuscular and surface electromyogram changes during muscle fatigue,” *Journal of Applied Physiology*, vol. 60, no. 4, pp. 1179-1185, 1986.
- [78] E. Park, and S. G. Meek, “Fatigue compensation of the electromyographic signal for

- prosthetic control and force estimation," *IEEE transactions on biomedical engineering*, vol. 40, no. 10, pp. 1019-1023, 1993.
- [79] J. London, "Kinematics of the elbow," *J Bone Joint Surg Am*, vol. 63, no. 4, pp. 529-535, 1981.
- [80] R. Tao, S. Xie, Y. Zhang, and J. W. Pau, "sEMG-based neural-musculoskeletal model for human-robot interface," in *Industrial Electronics and Applications (ICIEA), 2014 IEEE 9th Conference on*, 2014, pp. 1039-1044.
- [81] Q. Song, and Y. Ge, "Extraction of elbow joint intention from surface EMG signals in horizontal plane " in the 7th World Congress on Intelligent Control and Automation, Chongqing, China, 2008, pp. 1931 - 1934
- [82] Q. Song, M. Liu, L. Tong, Y. Yu, and Y. Ge, "Extraction of elbow joint intention from sEMG signals in horizontal plane using cosine tuning functions," in *Robotics and Biomimetics, 2007. ROBIO 2007.*, Sanya, China, 2007, pp. 2206- 2211.
- [83] S. D. Prentice, A. E. Patla, and D. A. Stacey, "Artificial neural network model for the generation of muscle activation patterns for human locomotion," *Journal of electromyography and kinesiology : official journal of the International Society of Electrophysiological Kinesiology*, vol. 11, no. 1, pp. 19-30, 2001.
- [84] F. Sepulveda, D. M. Wells, and C. L. Vaughan, "A neural network representation of electromyography and joint dynamics in human gait," *Journal of Biomechanics*, vol. 26, no. 2, pp. 101-109, 1993.
- [85] S. Micera, W. Jensen, F. Sepulveda, R. R. Riso, and T. Sinkjaer, "Neuro-fuzzy extraction of angular information from muscle afferents for ankle control during standing in paraplegic subjects: an animal model," *IEEE transactions on bio-medical engineering*, vol. 48, no. 7, pp. 787-794, 2001.
- [86] F. Sepulveda, M. H. Granat, and A. Cliquet, "Two artificial neural systems for generation of gait swing by means of neuromuscular electrical stimulation," *Medical engineering & physics*, vol. 19, no. 1, pp. 21-28, 1997.
- [87] B. Heller, P. Veltink, N. Rijkhoff, W. Rutten, and B. Andrews, "Reconstructing muscle activation during normal walking: a comparison of symbolic and connectionist machine learning techniques," *Biological Cybernetics*, vol. 69, no. 4, pp. 327-335, 1993.
- [88] E. Leon, G. Clarke, V. Callaghan, and F. Sepulveda, "Real-time detection of emotional changes for inhabited environments," *Computers & Graphics*, vol. 28, no. 5, pp. 635-642, 2004.
- [89] S. D. Prentice, A. E. Patla, and D. A. Stacey, "Simple artificial neural network models can generate basic muscle activity patterns for human locomotion at different speeds," *Experimental brain research. Experimentelle Hirnforschung. Experimentation cerebrale*, vol. 123, no. 4, pp. 474-480, 1998.
- [90] R. Tao, S. Xie, Y. Zhang, and J. W. Pau, "Review of EMG-based neuromuscular interfaces for rehabilitation: elbow joint as an example," *International Journal of Biomechatronics and Biomedical Robotics*, vol. 2, no. 2, pp. 184-194, 2013.
- [91] T. S. Buchanan, D. G. Lloyd, K. Manal, and T. F. Besier, "Estimation of Muscle Forces and Joint Moments Using a Forward-Inverse Dynamics Model," *Medicine & Science in Sports & Exercise*, vol. 37, no. 11, pp. 1911-1916, 2005.
- [92] A. Erdemir, S. McLean, W. Herzog, and A. J. van den Bogert, "Model-based estimation of muscle forces exerted during movements," *Clinical Biomechanics*, vol. 22, no. 2, pp. 131-154, 2007.
- [93] G. Tang, L.-w. Qian, G.-f. Wei, H.-s. Wang, and C.-t. Wang, "Development of software for human muscle force estimation," *Computer methods in biomechanics and biomedical engineering*, vol. 15, no. 3, pp. 275-283, 2012.
- [94] Q. Ding, X. Zhao, A. Xiong, and J. Han, "A novel motion estimate method of human joint with EMG-driven model." pp. 1-5.

- [95] D. Kistemaker, A. Van Soest, and M. Bobbert, "A model of open-loop control of equilibrium position and stiffness of the human elbow joint," *Biological Cybernetics*, vol. 96, no. 3, pp. 341-350, 2007.
- [96] E. P. Doheny, M. M. Lowery, M. J. O'Malley, and D. P. Fitzpatrick, "The effect of elbow joint centre displacement on force generation and neural excitation," *Med Biol Eng Comput*, vol. 47, no. 6, pp. 589-98, Jun, 2009.
- [97] C. Fleischer, and G. Hommel, "A Human--Exoskeleton Interface Utilizing Electromyography," *Robotics, IEEE Transactions on*, vol. 24, no. 4, pp. 872-882, 2008.
- [98] W. M. Murray, S. L. Delp, and T. S. Buchanan, "Variation of muscle moment arms with elbow and forearm position," *Journal of biomechanics*, vol. 28, no. 5, pp. 513-525, 1995.
- [99] A. V. Hill, "The Heat of Shortening and the Dynamic Constants of Muscle," *Proceedings of the Royal Society of London. Series B, Biological Sciences*, vol. 126, no. 843, pp. 136-195, 1938.
- [100] A. F. Huxley, "Muscle structure and theories of contraction," *Progress in biophysics and biophysical chemistry*, vol. 7, pp. 255-318, 1957.
- [101] G. Pipeleers, B. Demeulenaere, I. Jonkers, P. Spaepen, G. Van der Perre, A. Spaepen, J. Swevers, and J. De Schutter, "Dynamic simulation of human motion: numerically efficient inclusion of muscle physiology by convex optimization," *Optimization and Engineering*, vol. 9, no. 3, pp. 213-238, 2007.
- [102] J. W. Pau, T. S. Chen, S. S. Xie, and A. J. Pullan, "A neuromuscular interface for the elbow joint." pp. 214-219.
- [103] K. S. Holzbaur, W. Murray, and S. Delp, "A Model of the Upper Extremity for Simulating Musculoskeletal Surgery and Analyzing Neuromuscular Control," *Annals of Biomedical Engineering*, vol. 33, no. 6, pp. 829-840, 2005.
- [104] B. A. Garner, and M. G. Pandy, "Musculoskeletal model of the upper limb based on the visible human male dataset," *Computer methods in biomechanics and biomedical engineering*, vol. 4, no. 2, pp. 93-126, 2001.
- [105] L. M. Schutte, M. M. Rodgers, F. E. Zajac, and R. M. Glaser, "Improving the efficacy of electrical stimulation-induced leg cycle ergometry: an analysis based on a dynamic musculoskeletal model," *Rehabilitation Engineering, IEEE Transactions on*, vol. 1, no. 2, pp. 109-125, 1993.
- [106] D. G. Thelen, "Adjustment of muscle mechanics model parameters to simulate dynamic contractions in older adults," *Journal of biomechanical engineering*, vol. 125, no. 1, pp. 70-77, 2003.
- [107] N. Zheng, G. S. Fleisig, R. F. Escamilla, and S. W. Barrentine, "An analytical model of the knee for estimation of internal forces during exercise," *Journal of Biomechanics*, vol. 31, no. 10, pp. 963-967, 1998.
- [108] T. S. Buchanan, D. G. Lloyd, K. Manal, and T. F. Besier, "Neuromusculoskeletal modeling: estimation of muscle forces and joint moments and movements from measurements of neural command," *Journal of applied biomechanics*, vol. 20, no. 4, pp. 367, 2004.
- [109] R. Raikova, and H. Aladjov, "The influence of the way the muscle force is modeled on the predicted results obtained by solving indeterminate problems for a fast elbow flexion," *Computer methods in biomechanics and biomedical engineering*, vol. 6, no. 3, pp. 181-196, 2003.
- [110] D. A. Kistemaker, A. J. K. Van Soest, and M. F. Bobbert, "A model of open-loop control of equilibrium position and stiffness of the human elbow joint," *Biological cybernetics*, vol. 96, no. 3, pp. 341-350, 2007.
- [111] C. Y. Scovil, and J. L. Ronsky, "Sensitivity of a Hill-based muscle model to perturbations in model parameters," *J Biomech*, vol. 39, no. 11, pp. 2055-63, 2006.
- [112] F. De Groote, A. Van Campen, I. Jonkers, and J. De Schutter, "Sensitivity of dynamic simulations of gait and dynamometer experiments to hill muscle model parameters of knee

- flexors and extensors," *J Biomech*, vol. 43, no. 10, pp. 1876-83, Jul 20, 2010.
- [113] C. Redl, M. Gfoehler, and M. G. Pandy, "Sensitivity of muscle force estimates to variations in muscle-tendon properties," *Hum Mov Sci*, vol. 26, no. 2, pp. 306-19, Apr, 2007.
- [114] B. A. Garner, and M. G. Pandy, "Estimation of Musculotendon Properties in the Human Upper Limb," *Annals of Biomedical Engineering*, vol. 31, no. 2, pp. 207-220, 2003.
- [115] S. L. Lehman, and L. W. Stark, "Three algorithms for interpreting models consisting of ordinary differential equations: Sensitivity coefficients, sensitivity functions, global optimization," *Mathematical Biosciences*, vol. 62, no. 1, pp. 107-122, 1982.
- [116] M. G. Pandy, "An analytical framework for quantifying muscular action during human movement," *Multiple muscle systems*, pp. 653-662: Springer, 1990.
- [117] J. M. Winters, and L. Stark, "Analysis of fundamental human movement patterns through the use of in-depth antagonistic muscle models," *Biomedical Engineering, IEEE Transactions on*, no. 10, pp. 826-839, 1985.
- [118] W. Zangemeister, A. Arlt, and S. Lehman, "Sensitivity functions of a human head movement model," *Medical engineering & physics*, vol. 16, no. 2, pp. 163-170, 1994.
- [119] Z. Zi, "Sensitivity analysis approaches applied to systems biology models," *IET Syst Biol*, vol. 5, no. 6, pp. 336-6, Nov, 2011.
- [120] F. C. Anderson, and M. G. Pandy, "Storage and utilization of elastic strain energy during jumping," *Journal of biomechanics*, vol. 26, no. 12, pp. 1413-1427, 1993.
- [121] M. Bobbert, "Dependence of human squat jump performance on the series elastic compliance of the triceps surae: a simulation study," *Journal of Experimental Biology*, vol. 204, no. 3, pp. 533-542, 2001.
- [122] L. Out, T. G. Vrijkotte, A. J. van Soest, and M. F. Bobbert, "Influence of the parameters of a human triceps surae muscle model on the isometric torque-angle relationship," *Journal of biomechanical engineering*, vol. 118, no. 1, pp. 17-25, 1996.
- [123] C. N. Maganaris, "A predictive model of moment-angle characteristics in human skeletal muscle: application and validation in muscles across the ankle joint," *Journal of theoretical biology*, vol. 230, no. 1, pp. 89-98, 2004.
- [124] D. M. Corcos, G. L. Gottlieb, M. L. Latash, G. L. Almeida, and G. C. Agarwal, "Electromechanical delay: An experimental artifact," *Journal of Electromyography and Kinesiology*, vol. 2, no. 2, pp. 59-68, 1992.
- [125] J. W. L. Pau, "A physiological model driven neuromuscular interface for exoskeleton assisted rehabilitation," Mechanical Engineering, University of Auckland, 2013.
- [126] P. K. Artemiadis, and K. J. Kyriakopoulos, "EMG-based teleoperation of a robot arm using low-dimensional representation." pp. 489-495.
- [127] A. Smith, and E. E. Brown, "Myoelectric control techniques for a rehabilitation robot," *Applied Bionics and Biomechanics*, vol. 8, no. 1, pp. 21-37, 2011.
- [128] K. Kiguchi, T. D. Lalitharatne, and Y. Hayashi, "Estimation of Forearm Supination/Pronation Motion Based on EEG Signals to Control an Artificial Arm," *Journal of Advanced Mechanical Design, Systems, and Manufacturing*, vol. 7, no. 1, pp. 74-81, 2013.
- [129] P. Ibáñez-Gimeno, I. Galtés, X. Jordana, A. Malgosa, and J. Manyosa, "Biomechanics of forearm rotation: force and efficiency of pronator teres," *PloS one*, vol. 9, no. 2, pp. e90319, 2014.
- [130] F. Al Omari, and L. Guohai, "Analysis of extracted forearm sEMG signal using LDA, QDA, K-NN classification algorithms," *The Open Automation and Control Systems Journal*, vol. 6, pp. 108-116, 2014.
- [131] T. Nishimura, Y. Nomura, and R. Sakamoto, "A restrained-torque-based motion instructor: forearm flexion/extension-driving exoskeleton." pp. 86620J-86620J-7.
- [132] M. Gazzoni, N. Celadon, D. Mastrapasqua, M. Paleari, V. Margaria, and P. Ariano, "Quantifying forearm muscle activity during wrist and finger movements by means of

- multi-channel electromyography,” *PloS one*, vol. 9, no. 10, pp. e109943, 2014.
- [133] J. Tang, *Rao gu yuan duan gu zhe (in Chinese)*: Shanghai ke xue ji shu chu ban she, 2013.1.1.
- [134] F. A. Ekenstam, and C. G. Hagert, “Anatomical studies on the geometry and stability of the distal radio ulnar joint,” *Scandinavian journal of plastic and reconstructive surgery*, vol. 19, no. 1, pp. 17-25, 1985.
- [135] K. O. Matsuki, K. Matsuki, S. Mu, T. Sasho, K. Nakagawa, N. Ochiai, K. Takahashi, and S. A. Banks, “In vivo 3D kinematics of normal forearms: analysis of dynamic forearm rotation,” *Clinical biomechanics*, vol. 25, no. 10, pp. 979-983, 2010.
- [136] S. C. Tay, R. van Riet, T. Kazunari, M. F. Koff, K. K. Amrami, K.-N. An, and R. A. Berger, “A method for in-vivo kinematic analysis of the forearm,” *Journal of biomechanics*, vol. 41, no. 1, pp. 56-62, 2008.
- [137] S. C. Tay, R. Van Riet, T. Kazunari, K. K. Amrami, K.-N. An, and R. A. Berger, “In-vivo kinematic analysis of forearm rotation using helical axis analysis,” *Clinical Biomechanics*, vol. 25, no. 7, pp. 655-659, 2010.
- [138] T. Kataoka, H. Moritomo, S. Omokawa, A. Iida, T. Murase, and K. Sugamoto, “Ulnar variance: its relationship to ulnar foveal morphology and forearm kinematics,” *The Journal of hand surgery*, vol. 37, no. 4, pp. 729-735, 2012.
- [139] R. Hale, D. Dorman, and R. V. Gonzalez, “Individual muscle force parameters and fiber operating ranges for elbow flexion–extension and forearm pronation–supination,” *Journal of biomechanics*, vol. 44, no. 4, pp. 650-656, 2011.
- [140] Y. R. Chen, and J. B. Tang, “In vivo gliding and contact characteristics of the sigmoid notch and the ulna in forearm rotation,” *The Journal of hand surgery*, vol. 38, no. 8, pp. 1513-1519, 2013.
- [141] Y. R. Chen, and J. B. Tang, “Changes in contact site of the radiocarpal joint and lengths of the carpal ligaments in forearm rotation: an in vivo study,” *The Journal of hand surgery*, vol. 38, no. 4, pp. 712-720, 2013.
- [142] M. Yung, and R. P. Wells, “Changes in muscle geometry during forearm pronation and supination and their relationships to EMG cross-correlation measures,” *Journal of Electromyography and Kinesiology*, vol. 23, no. 3, pp. 664-672, 6//, 2013.
- [143] H. A. Rahman, Y. C. Fai, and E. S. L. Ming, “Analysis of Human Hand Kinematics: Forearm Pronation and Supination,” *Journal of Medical Imaging and Health Informatics*, vol. 4, no. 2, pp. 245-249, 2014.
- [144] S. L. Delp, F. C. Anderson, A. S. Arnold, P. Loan, A. Habib, C. T. John, E. Guendelman, and D. G. Thelen, “OpenSim: open-source software to create and analyze dynamic simulations of movement,” *IEEE transactions on bio-medical engineering*, vol. 54, no. 11, pp. 1940-1950, 2007.
- [145] T. Back, U. Hammel, and H. P. Schwefel, “Evolutionary computation: comments on the history and current state,” *IEEE Transactions on Evolutionary Computation*, vol. 1, no. 1, pp. 3-17, 1997.
- [146] S. Das, and P. N. Suganthan, “Differential Evolution: A Survey of the State-of-the-Art,” *IEEE Transactions on Evolutionary Computation*, vol. 15, no. 1, pp. 4-31, 2011.
- [147] K. Zielinski, D. Peters, and R. Laur, "Run time analysis regarding stopping criteria for differential evolution and particle swarm optimization."
- [148] H. S. Lo, “Exoskeleton Robot for Upper Limb Rehabilitation: Design Analysis and Control,” Mechanical Engineering, The University of Auckland, New Zealand, 2014.
- [149] P. De Leva, “Adjustments to Zatsiorsky-Seluyanov's segment inertia parameters,” *Journal of biomechanics*, vol. 29, no. 9, pp. 1223-1230, 1996.
- [150] " DC motors and drive systems by Maxon motor. Available: <http://www.maxonmotor.com>."
- [151] "ams. Available: <http://www.ams.com/eng>."
- [152] C. Carignan, J. Tang, and S. Roderick, "Development of an exoskeleton haptic interface for

- virtual task training." pp. 3697-3702.
- [153] R. A. R. C. Gopura, K. Kiguchi, and Y. Li, "SUEFUL-7: A 7DOF upper-limb exoskeleton robot with muscle-model-oriented EMG-based control." pp. 1126-1131.
- [154] J. C. Perry, "Design and development of a 7 degree-of-freedom powered exoskeleton for the upper limb," University of Washington, 2006.
- [155] S. Kousidou, N. Tsagarakis, C. Smith, and D. Caldwell, "Task-orientated biofeedback system for the rehabilitation of the upper limb." pp. 376-384.
- [156] T. Nef, M. Mihelj, and R. Riener, "ARMin: a robot for patient-cooperative arm therapy," *Medical & biological engineering & computing*, vol. 45, no. 9, pp. 887-900, 2007.
- [157] M. H. Rahman, M. Saad, J. P. Kenné and P. S. Archambault, "Modeling and control of a 7DOF exoskeleton robot for arm movements." pp. 245-250.
- [158] M. H. Rahman, K. Kiguchi, M. M. Rahman, and M. Sasaki, "Robotic exoskeleton for rehabilitation and motion assist." pp. 241-246.
- [159] M. Lee, J. Son, J. Kim, and Y. Kim, "Development and assessment of an EMG-based exoskeleton system." pp. 648-650.
- [160] M. Baklouti, E. Monacelli, V. Guitteny, and S. Couvet, "Intelligent assistive exoskeleton with vision based interface." pp. 123-135.
- [161] K. Kiguchi, and Y. Hayashi, "An EMG-Based Control for an Upper-Limb Power-Assist Exoskeleton Robot," *IEEE Transactions on Systems, Man, and Cybernetics, Part B (Cybernetics)*, vol. 42, no. 4, pp. 1064-1071, 2012.
- [162] M. F. Eilenberg, H. Geyer, and H. Herr, "Control of a powered ankle-foot prosthesis based on a neuromuscular model," *IEEE Transactions on Neural Systems and Rehabilitation Engineering*, vol. 18, no. 2, pp. 164-173, 2010.
- [163] E. Cavallaro, J. Rosen, J. C. Perry, S. Burns, and B. Hannaford, "Hill-based model as a myoprocessor for a neural controlled powered exoskeleton arm-parameters optimization." pp. 4514-4519.
- [164] T. S. Buchanan, S. L. Delp, and J. Solbeck, "Muscular resistance to varus and valgus loads at the elbow," *Journal of biomechanical engineering*, vol. 120, no. 5, pp. 634-639, 1998.
- [165] J. W. L. Pau, T. S. W. Chen, S. S. Q. Xie, and A. J. Pullan, "A neuromuscular interface for the elbow joint." pp. 214-219.